



PhD-FSTM-2024-059
The Faculty of Science, Technology and Medicine

DISSERTATION

Defence held on 02/08/2024 in Esch-sur-Alzette

to obtain the degree of

DOCTEUR DE L'UNIVERSITÉ DU LUXEMBOURG
EN SCIENCES DE L'INGÉNIEUR

by

Alfredo ROMERO GUZMÁN
Born on 7 April 1993 in Guanajuato (Mexico)

DEMOUNTABLE AND REUSABLE
STEEL-TIMBER COMPOSITE (STC) BEAMS

Dissertation defence committee

Prof. Dr.-Ing. Christoph Odenbreit, Dissertation Supervisor

Professor, University of Luxembourg, Faculty of Science Technology and Medicine

Prof. Dr. Numa Joy Bertola, Chairman

Professor, University of Luxembourg, Faculty of Science Technology and Medicine

Prof. Dr. Hervé Degée, Vice-chairman

Professor, University of Hasselt, Faculty of Engineering Technology

Dr. François Hanus

Business Manager, ArcelorMittal, Stelligence Fabrication Centre

Dr. Jie Yang

Research Engineer, ArcelorMittal, Global Research and Development

ACKNOWLEDGEMENTS

This thesis is the result of my work over nearly four years at the ArcelorMittal Chair of Steel Construction at the University of Luxembourg. Throughout this journey, I have received support from many individuals and industry partners who have contributed to the success of this research project.

I would like to extend my deepest gratitude to Fonds National de la Recherche Luxembourg (FNR) and the Luxembourg-based company Prefalux for providing the funding for this research project "Prefa-SeTi: Steel-Timber Composite Beams", through a PhD Industrial Fellowship (Grant No. 15695062). In particular, I thank *Mr. Laurent Nilles* for his support and insightful feedback, and *Simon Griffaton* and *Tim Kroon* for their support in the timber works.

To ArcelorMittal and Metsä Wood, thank you for your support for this project. Special thanks to *Omer Anwaar*, *Baas Meuwisen*, *Xavier Colin*, *Jussi Bjorman*, and *Cedric Lecomte* for your support and contributions.

I would like to express my sincere gratitude to *Professor Christoph Odenbreit*, my supervisor. His support and guidance have been essential throughout my academic journey. I am thankful for the opportunity to undertake this amazing research project, for the resources he provided, and for his encouragement to participate in courses and conferences.

I would also like to acknowledge my CET and Jury members, *Prof. Christoph Odenbreit*, *Prof. Numa Bertola*, *Prof. Hervé Degée*, *Dr. François Hanus*, *Dr. Jie Yang* and *Mr. Laurent Nilles* for their valuable feedback and support throughout this project, and for reviewing this thesis.

To the laboratory team, *Gilbert Klein*, *Marc Seil*, *Ed Weyer*, *Mehdi Saeidi*, *Cyrille Inglebert*, *Ken Adam*, *Vicente Reis*, *Claude Colle*, and *Ralph Reiter*, thank you for your support, technical assistance, and feedback, which were crucial for the experimental work.

I would like to thank my colleagues and former colleagues, *Valentino Vigneri*, *András Kozma*, *Jie Yang*, *Rigels Metolli*, *Shahin Sayyareh*, *Adil Ahmad*, *Teodora Bogdan*, *Rohola Rahnavard*, *Adriano Silva de Carvalho*, and *Esmael Ahmadzade Beiraki*, for your support and engaging discussions that have made this journey enriching and enjoyable.

I would like to thank all the students who contributed to this research project, in particular: *Melis Pelivani*, and *Gabriel Ibosiola*. Your company during long working days in the laboratory, your interest and eagerness to learn were always a great motivation.

Most of all, I am thankful beyond words to my family, especially my parents, my sister, and my beloved *Sher*. Everything I have achieved is thanks to your unwavering support and encouragement. To my beloved *Sher*, thank you for always being there for me, through good and bad days, for joining this adventure with me, and for your endless patience and love. Your presence and support have been my greatest strength and motivation.

Esch-sur-Alzette, June 2024

Alfredo Romero Guzmán

ABSTRACT

The construction sector significantly impacts the environment due to high resource consumption, waste production, and carbon emissions. To address these challenges, this research aligns with the European Green Deal's objective of achieving carbon neutrality by developing and studying an innovative steel-timber composite (STC) flooring system, which embodies the principles of the circular economy. The main objectives of this study were to design a demountable and reusable STC flooring system, to develop novel shear connections that enable the reuse of structural components, and to establish analytical procedures to estimate the bending capacity of STC beams.

Steel-timber composite structures represent a relatively new structural system with limited research available and no established codes or guidelines specifically addressing their design and implementation. Additionally, there is no record of shear connections for steel-timber composite structures designed for demountability and reuse. This pioneering research has made significant progress in developing and assessing an STC flooring system and its shear connections. The STC flooring system consists of downstanding I-shaped hot-rolled steel beams and timber slabs made of laminated veneer lumber (LVL). The LVL slabs are connected to the top flange of the steel beams using novel shear connectors that enable demountability and reuse of the structural components.

To achieve the objectives of this research project, experimental, numerical, and analytical investigations were conducted. Experimental tests included material characterization of LVL, push-out tests on the novel shear connections, full-scale bending tests on the STC beams, and vibration tests. Numerical models were developed using ABAQUS software to simulate the behavior of the STC beams and extend the findings of the experimental tests. Analytical procedures, including a strain-based procedure and a simplified procedure, were proposed to estimate the capacity of the STC beams. Additionally, an analytical procedure based on the γ -method was proposed to estimate their bending stiffness and elastic moment resistance.

The findings of this study indicate that the novel shear connections contributed to achieve composite action and enabled the demountability and reuse of the STC beams without compromising structural integrity when loads remained within service limits. The STC beams demonstrated significant stiffness as well as load-bearing and deformation capacities. The tested beams showed improvements in stiffness of approximately 80% and in capacity of at least 40% compared to a reference identical steel-timber beam with no composite action. The proposed analytical procedures provided accurate estimates of bending stiffness, and elastic and ultimate moment resistance. Vibration tests showed that the natural frequencies of the STC beams were above the excitation frequencies typical of walking and crowd activities, indicating a low risk of resonance.

CONTENTS

Acknowledgements	iii
Abstract	v
Nomenclature	xiii
1 Introduction	1
1.1 Motivation and background	1
1.2 Objectives	3
1.3 Thesis outline	4
1.4 Limitations	6
2 State of the art	9
2.1 Laminated Veneer Lumber (LVL)	9
2.1.1 General	9
2.1.2 Relevant publications	10
2.2 Shear connections for STC beams and flooring systems	12
2.2.1 General	12
2.2.2 Relevant publications	12
2.2.3 Overview of shear connections presented in the literature	15
2.3 Steel-timber composite (STC) beams and flooring systems	18
2.3.1 General	18
2.3.2 Relevant publications	18
3 Demountable steel-timber composite (STC) flooring system	21
3.1 General	21
3.2 The demountable STC flooring system concept	22
3.3 Developed shear connections	24
3.3.1 General	24
3.3.2 Shear connection devices	26
3.3.3 Removable components	27
ARTICLE 1	29
4 Experimental investigation on laminated veneer lumber (LVL)	31
4.1 Introduction	31
4.2 Material - Laminated Veneer Lumber (LVL)	32

4.3	Tests overview	33
4.4	Methods.	35
4.4.1	General	35
4.4.2	Compression tests	35
4.4.3	Tension tests	36
4.4.4	Shear tests.	39
4.4.5	Bending tests	40
4.5	Results and discussion	41
4.5.1	Compression tests	41
4.5.2	Tension tests	42
4.5.3	Shear tests.	43
4.5.4	Bending tests	45
4.5.5	Derived mechanical properties	47
4.5.6	Summary of derived mechanical properties	52
4.5.7	Mean stress-strain curves for compression and tension.	54
ARTICLE 2		55
5	Experimental push-out tests on the developed shear connections	57
5.1	Introduction	57
5.2	Overview of the experimental testing campaign	57
5.3	Materials	58
5.3.1	Laminated veneer lumber (LVL)	58
5.3.2	Steel profiles	59
5.3.3	Shear connection devices and round steel plates	59
5.3.4	Geka connectors	60
5.3.5	Screws	60
5.3.6	Bolts, washers and nuts	61
5.3.7	Direct tension indicators (DTI)	61
5.4	Bolt preload calibration	61
5.5	Specimen details	64
5.6	Test setup and instrumentation	65
5.7	Loading procedure	66
5.8	Results and discussion	67
5.8.1	Load-slip response	67
5.8.2	Failure mode	73
ARTICLE 3		77
6	Experimental full-scale STC beam tests	79
6.1	Introduction	79
6.2	Overview of the experimental testing campaign	79

6.3	Materials	80
6.3.1	Laminated veneer lumber	80
6.3.2	Steel beams	80
6.3.3	Shear connection devices and round plates	80
6.3.4	Screws	81
6.3.5	Bolts, washers and nuts	81
6.3.6	Direct tension indicators.	81
6.3.7	Mortar	81
6.4	Specimen details	82
6.5	Assembly process.	84
6.6	Test setup and instrumentation	87
6.7	Loading procedure	89
6.8	Results and discussion	90
6.8.1	Load-deflection of the STC beams	90
6.8.2	Slope of the elastic branch in the load-deflection curve	94
6.8.3	Slip measurements and shear connectors response	94
6.8.4	Strains in the timber slabs and effective width	95
6.8.5	Strain distribution through the depth of the STC beam	98
6.8.6	Gap opening measurements.	99
6.8.7	Beam's bending stiffness	100
6.8.8	Failure mode	104
7	Numerical investigations on STC beams	107
7.1	Introduction	107
7.2	Modelling strategy	107
7.2.1	General	107
7.2.2	Material properties	108
7.2.3	Shear connection.	111
7.2.4	Contact definitions	111
7.2.5	Boundary conditions.	112
7.2.6	Loading	113
7.2.7	Mesh.	113
7.3	Comparison of experimental and numerical results.	114
7.3.1	Comparison of moment/load vs. midspan deflection curves	114
7.3.2	Comparison of slip measurements through the beam.	115
7.4	Influence of parameters on the mechanical response of STC beams.	116
7.4.1	General	116
7.4.2	Influence of the steel grade of the steel beam	117
7.4.3	Influence of the transversal gaps	118
7.4.4	Influence of the connectors' spacing and the degree of shear connection	119

8 Analytical determination of the bending capacity of STC beams	121
8.1 Introduction	121
8.2 Considerations for STC beams	123
8.3 Strain-based procedure	124
8.4 Material constitutive laws	126
8.4.1 Steel	126
8.4.2 Timber.	127
8.5 Shear connection cases	128
8.5.1 General	128
8.5.2 Full-rigid shear connection	129
8.5.3 No shear connection	130
8.5.4 Partial shear connection	130
8.6 Degree of of shear connection in STC beams.	130
8.7 Effective shear resistance of steel-to-timber connections.	131
8.7.1 General	131
8.7.2 Idealisation of the load-slip response of steel-to-timber connections	133
8.7.3 Idealisation of the load-slip response of the developed connections	134
8.7.4 Definition of effective shear resistance of connectors	135
8.8 Algorithm to transform a load-slip curve into an effective shear resistance	136
8.8.1 General	136
8.8.2 Considerations for the algorithm	138
8.8.3 Algorithm's steps	139
8.9 Estimation of the bending capacity of STC beams considering the section's resistance and the effective shear resistance of the connectors	141
8.10 Comparison of experimental results and strain-based moment resistance values	143
8.10.1 General	143
8.10.2 Comparison of results	145
8.11 Simplified analytical procedure	146
8.11.1 General	146
8.11.2 Material assumptions	147
8.11.3 Overview of cases considered	150
8.11.4 Bending capacity of STC beams with full-rigid shear connection.	151
8.11.5 Bending capacity of STC beams with no shear connection	155
8.11.6 Bending capacity of STC beams with partial shear connection	156
8.11.7 Bending capacity of an STC cross-section at a gap.	160
8.11.8 Comparison of results	165
8.12 Procedure to estimate the bending capacity of STC beams in the elastic range	166
8.12.1 General	166
8.12.2 Stresses in the cross-section in the elastic range	167
8.12.3 Bending capacity in the elastic range	167
8.12.4 Comparison of results	168

8.13 Summary of proposed analytical procedures and their effectiveness	169
8.13.1 Proposed analytical procedures	169
8.13.2 Effectiveness of the proposed analytical procedures.	170
9 Vibration tests	173
9.1 Introduction	173
9.2 Experimental tests	174
9.2.1 General	174
9.2.2 STC beam specimens.	174
9.2.3 Test setup and instrumentation	175
9.2.4 Testing procedure	176
9.2.5 Results.	177
9.3 Analytical estimation of the natural frequency of STC beams.	179
9.3.1 Analytical formulation	179
9.3.2 Comparison of experimental results and analytical predictions	179
9.4 Estimation of the natural frequencies and mode shapes with numerical models . .	180
9.4.1 General	180
9.4.2 Comparison of experimental and numerical results	181
10 Design considerations	183
10.1 Introduction	183
10.2 Materials	183
10.2.1 Steel	183
10.2.2 Timber.	184
10.3 Shear connection.	184
10.3.1 Shear connection resistance.	184
10.3.2 Shear connection stiffness	185
10.4 Cross-section resistance	185
10.4.1 General	185
10.4.2 Critical cross-sections	185
10.4.3 Analytical estimation of the cross-section's moment resistance	186
10.5 Bending stiffness and deflections	186
10.5.1 Bending stiffness	186
10.5.2 Deflections	186
10.6 Vibration	186
10.6.1 Fundamental frequency	186
10.6.2 Vibration assessment and acceptance criteria	187
11 Conclusions and Outlook	189
11.1 Introduction	189
11.2 Conclusions.	189
11.2.1 Experimental investigations on LVL.	189

11.2.2 Novel shear connections for demountable STC beams	190
11.2.3 Full-scale STC beam tests	192
11.2.4 Numerical investigations on STC beams	193
11.2.5 Analytical determination of the bending capacity of STC beams	195
11.2.6 Vibration behaviour of STC beams	195
11.3 Outlook	196
List of Publications	199
Bibliography	201
Annex	215
A Analytical strain-based procedure	217
A.1 Moment resistance for full-rigid shear connection	217
A.2 Moment resistance for no shear connection	219
A.3 Moment resistance for partial shear connection.	221

NOMENCLATURE

ABBREVIATIONS

5-p	5-percentile
BT	Beam test
CFRP	Carbon fiber reinforced polymer
CFS	Cold-formed steel
CG	Centroid of a cross-section
CLT	Cross-laminated timber
CV	Coefficient of variation
DTI	Direct tension indicator
EMA	Experimental modal analysis
ETA	European technical approval
FE	Finite element
FFT	Fast Fourier transform
FRF	Frequency response functions
Glulam	Glued laminated timber
HRC	High resistance calibrated
L	Longitudinal direction of timber
LVDT	Linear variable displacement transducer
LVL	Laminated veneer lumber
MoE	Modulus of elasticity
NA	Neutral axis
PNA	Plastic neutral axis
POT	Push-out test

PTFE	Polytetrafluoroethylene, also known as teflon
R	Radial direction of timber
REDUCE	Reuse and Demountability Using steel structures and the Circular Economy
RFCS	Research fund for coal and steel
RMSE	Root mean square error
SCC	Steel-concrete composite
SCT	Shear connection type
SLS	Serviceability limit state
STC	Steel-timber composite
T	Tangential direction of timber
TCC	Timber-concrete composite
TTC	Timber-timber composite
ULS	Ultimate limit state

LATIN UPPER CASE LETTERS

$(EI)_{ef}$	Effective bending stiffness
$(EI)_{exp}$	Experimentally obtained bending stiffness
$(EI)_{K_0}$	Bending stiffness of steel-timber beams with no shear connection
$(EI)_{K_\infty}$	Bending stiffness of STC beams with full-rigid shear connection
$(EI)_s$	Bending stiffness of the bare steel section
A	Area
A_s	Stress area of the bolt
C_1	Parameter to calculate quad-linear stress-strain relationship of steel
E	Modulus of elasticity
$E_{c,1}$	Modulus of elasticity of timber in compression in the longitudinal direction
$E_{c,2}$	Modulus of elasticity of timber in compression in the tangential direction
$E_{c,3}$	Modulus of elasticity of timber in compression in the radial direction

E_{cm}	Mean modulus of elasticity of mortar
E_c	Modulus of elasticity of timber in compression
$E_{m,1}$	Global modulus of elasticity in bending for flatwise bending in the longitudinal direction
$E_{m,2}$	Global modulus of elasticity in bending for flatwise bending in the tangential direction
E_m	Global modulus of elasticity in bending
E_{sh}	Slope of the hardening branch in the stress-strain relationship
$E_{t,1}$	Modulus of elasticity of timber in tension in the longitudinal direction
$E_{t,2}$	Modulus of elasticity of timber in tension in the tangential direction
$E_{t,3}$	Modulus of elasticity of timber in tension in the radial direction
E_t	Modulus of elasticity of timber in tension
F	Force; load
$F_2 - F_1$	Increment of load between points 1 and 2
F_{max}	Maximum load
$F_{p,C}$	Minimum preload of bolted assemblies
G	Shear modulus
$G_{v,12}$	Shear modulus in the TR-plane with force in the tangential direction
$G_{v,13}$	Shear modulus in the RT-plane with force in the radial direction
$G_{v,21}$	Shear modulus in the LR-plane with force in the longitudinal direction
$G_{v,23}$	Shear modulus in the RL-plane with force in the radial direction
$G_{v,31}$	Shear modulus in the LT-plane with force in the longitudinal direction
$G_{v,32}$	Shear modulus in the TL-plane with force in the tangential direction
I	Moment of inertia, second moment of area
K	Connector stiffness
K_1	Stiffness of the initial branch of the load-slip curve
K_2	Stiffness of the bearing branch of the load-slip curves of the push-out tests

K_{SLS}	Mean slip modulus for SLS verifications
L	Span length (distance between supports)
M	Bending moment
M_{Ed}	Design bending moment
$M_{el,exp}$	Elastic moment from the experimental tests
$M_{max,exp}$	Maximum moment from the experimental tests
$M_{R,el}$	Elastic moment resistance
$M_{R,\eta=0}$	Moment resistance for no shear connection
$M_{R,\eta=1}$	Moment resistance for full-rigid shear connection
$M_{R,\eta}$	Moment resistance for partial shear connection
$M_{R, steel}$	Moment resistance of the steel section
$M_{R, timber}$	Moment resistance of the timber section
$M_{Rd,el}$	Design value of the elastic moment resistance of a composite section
M_{Rd}	Design value of the moment resistance of a composite section
M_R	Moment resistance
M_{sw}	Bending moment at midspan due to self-weight
$M_{y,k}$	Characteristic yield moment of screws and bolts
N	Normal force
N_i	Normal force i
$N_{timber,\eta=1}$	Resultant normal force in the timber section for full-rigid shear connection
N_{timber}	Resultant normal force in the timber section
P	Force; load
P_R	Shear connector's resistance
P_x	Load associated to a slip with a value of x
$P_{15\ mm}$	Load corresponding to a slip of 15 mm
$P_{6\ mm}$	Load corresponding to a slip of 6 mm
P_μ	Slip resistance

P_{est}	Estimated maximum load
P_i	Shear force transferred by connector i
P_{max}	Maximum load
$P_{R, eff}$	Connector's effective shear resistance
P_{Rd}	Design shear resistance of a single connector
P_{Rk}	Characteristic shear resistance of a single connector
R^2	Correlation coefficient
R_{ij}	Yield stress ratio
S	Spacing of connectors, determined by the sum of connectors per unit length
V	Shear force
$W_{i,el}$	Elastic section modulus of section i
$W_{i,pl}$	Plastic section modulus of section i

LATIN LOWER CASE LETTERS

a	Distance between a loading position and the nearest support; in the γ -method is the distance between centroids of the sections
a_i	Distance between the centroid of section i to the elastic neutral axis of the composite section
b	Width of the cross-section
b_v	Width of the glued face of the specimen in shear tests
b_{bf}	Width of the bottom flange of the steel profile
b_{eff}	Effective width of the slab
b_{slab}	Slab width
b_{tf}	Width of the top flange of the steel profile
f_u	Ultimate strength
f_y	Yielding strength
$f_{c,0,d}$	Design strength for compression parallel to the grain
$f_{c,0,k}$	Characteristic strength for compression parallel to the grain

$f_{c,1,lim}$	Compressive strength limit of timber in the longitudinal direction
$f_{c,1}$	Compressive strength of timber in the longitudinal direction
$f_{c,2}$	Compressive strength of timber in the tangential direction
$f_{c,3}$	Compressive strength of timber in the radial direction
$f_{c,lim}$	Compressive strength limit of timber
$f_{C_1\varepsilon_u}$	Stress at the beginning of the fourth branch in the quad-linear stress-strain relationship of steel
f_{cm}	Mean compressive strength of mortar
f_c	Compressive strength of timber
f_d	Design value of a strength parameter
f_i	Natural frequency for mode i
f_k	Characteristic value of a strength parameter
$f_{m,1}$	Bending strength of timber in flatwise bending in the longitudinal direction
$f_{m,2}$	Bending strength of timber in flatwise bending in the tangential direction
f_m	Bending strength of timber
$f_{n,exp}$	Natural frequency obtained experimentally for the first bending mode
$f_{n,FE}$	Natural frequency obtained numerically for the first bending mode
f_n	Natural frequency for the first bending mode
$f_{s,lim}$	Strength limit of steel
f_{sh}	Hardening strength of steel
$f_{t,1,lim}$	Tensile strength limit of timber in the longitudinal direction
$f_{t,1}$	Tensile strength of timber in the longitudinal direction
$f_{t,2}$	Tensile strength of timber in the tangential direction
$f_{t,3}$	Tensile strength of timber in the radial direction
$f_{t,k}$	Characteristic tensile strength of screws and bolts
f_t	Tensile strength of timber
f_{ub}	Ultimate strength of the bolt material

$f_{v,12}$	Shear strength in the TR-plane with force in the tangential direction
$f_{v,13}$	Shear strength in the RT-plane with force in the radial direction
$f_{v,21}$	Shear strength in the LR-plane with force in the longitudinal direction
$f_{v,23}$	Shear strength in the RL-plane with force in the radial direction
$f_{v,31}$	Shear strength in the LT-plane with force in the longitudinal direction
$f_{v,32}$	Shear strength in the TL-plane with force in the tangential direction
f_v	Shear strength of timber
$f_{y,0}$	Reference yielding strength
$f_{y,d}$	Design yield strength
h_0	Initial height of the specimen
$h_{G,2}$	Position of the centroid in section 2, measured from its bottom fibre
$h_{N,1}$	Position of the neutral axis in section 1, measured from its bottom fibre
$h_{w,t}$	Height of the top portion of the web in compression
h_w	Height of the web of the steel profile
h	Height of the cross-section
k_{el}	Slope of the elastic branch in the load-deflection curve
k_{mod}	Modification factor accounting for the effect of the load duration and the moisture content of timber
l_c	Initial gauge length in compression tests
l_t	Initial gauge length in tension tests
l_v	Length of the specimen in shear tests
l	Span; distance between two supports
m	Mass
q	Uniformly distributed load, load per unit length
s_i	Slip at shear connector i
t	Time
t_{bf}	Thickness of the bottom flange of the steel profile

$t_{tf,t}$	Thickness of the top portion of the top flange in compression
t_{tf}	Thickness of the top flange of the steel profile
t_v	Thickness of a specimen in shear tests
t_w	Thickness of the web of the steel profile
u	Deformation
$u_2 - u_1$	Increment of deformation corresponding to $F_2 - F_1$
w	Deflection; midspan deflection
$w_2 - w_1$	Increment of midspan deflection corresponding to $F_2 - F_1$
w_{el}	Elastic midspan deflection
w_{lim}	Deflection limit
w_{max}	Maximum deflection
x	Relative displacement between parallel steel plates of shear tests
$x_2 - x_1$	Increment of relative displacement between the parallel steel plates of shear tests
z_i	Lever arm i

GREEK UPPER CASE LETTERS

$\Delta\gamma$	Increment of shear strains
$\Delta\tau$	Increment of shear stresses
$\Delta\varepsilon$	Increment of strain in the iterations of the strain-based procedure

GREEK LOWER CASE LETTERS

α_v	Inclination of the specimen with respect to the vertical direction
β	Reduction factor applied to the compressive strength of timber
δ	Slip
δ_R	Slip associated to the resistance of the connector (P_R)
δ_u	Slip associated to the ultimate load of the connector (P_u)
δ_y	Slip associated to the yielding of the connector
η	Degree of shear connection

η_{EI}	Efficiency of the composite action in terms of the bending stiffness
γ	Shear strain
γ_{M0}	Partial safety factor applied to structural steel
γ_M	Partial safety factor for material property
γ_V	Partial safety factor for shear connectors
κ	Curvature of a beam
ν	Poisson's ratio
σ	Stress
σ_1	Stress at the bottom fibre of section 1
$\sigma_{i,b}$	Stress at the bottom fibre of section i
$\sigma_{i,t}$	Stress at the top fibre of section i
$\sigma_{m,i}$	Stress due to bending at the top or bottom fibre of section i
$\sigma_{N,i}$	Stress due to normal force at the top or bottom fibre of section i
τ	Shear stress
ε	Strain
$\varepsilon_{c,1,el}$	Strain at the proportional limit for timber in compression in the longitudinal direction
$\varepsilon_{c,1,lim}$	Strain limit of timber in compression in the longitudinal direction
$\varepsilon_{c,1,u}$	Ultimate strain for timber in compression in the longitudinal direction
$\varepsilon_{c,1}$	Strain corresponding to the compressive strength of timber in the longitudinal direction
$\varepsilon_{s,lim}$	Strain limit for steel
ε_{sh}	Hardening strain
$\varepsilon_{t,1,lim}$	Strain limit of timber in tension in the longitudinal direction
$\varepsilon_{t,1}$	Strain corresponding to the tensile strength of timber in the longitudinal direction
ε_u	Ultimate strain
$\varepsilon_{xx,max}$	Maximum absolute strain in the longitudinal direction

ε_{xx} Strains in the longitudinal direction

ξ_i Modal damping ratio for mode i

OTHER

$\int \varepsilon_{xx} dy$ Integral of the strain distribution measured at the top of the timber slab

\varnothing Diameter

1

INTRODUCTION

1.1. MOTIVATION AND BACKGROUND

The construction sector plays an important role in the global economy but also exerts substantial environmental impact due to its resource consumption and waste production. It consumes a significant portion of global raw materials and is responsible for an equally considerable percentage of global waste output [1, 2]. These factors contribute to the depletion of non-renewable resources and increase the environmental footprint of built environments. In light of these challenges, there is a rising movement to steer construction practices toward a more sustainable and environmentally responsible model—the circular economy [3].

This transition is increasingly driven by rigorous policy requirements. Initiatives such as the European Green Deal [4] aim to cut carbon emissions across all sectors to net-zero by 2050, aligning with the broader Sustainable Development Goals [5] of the United Nations. These goals emphasize the optimization of resource use, which is crucial as the global population rises and demands more residential, commercial, and office space. Projections suggest that by 2050, the global population may require significantly expanded built environments, intensifying the demand on resources and requiring innovative construction practices that minimize environmental impact [6].

One of the main barriers to adopting a circular economy within the sector is the prevalent construction practices and regulatory codes, which are currently not aligned with circular principles. Moreover, conventional construction methods are often linear: materials are used, and structures are built without systematic consideration for end-of-life reuse or recycling. There is an urgent need to rethink the conventional construction methods and to adapt the design codes to better support the disassembly and subsequent reuse of building structures.

Innovations in material science and engineering have begun to address these issues. Notably, advancements in steel-concrete composite (SCC) structures have led to the development of shear connections that facilitate demountability and reuse [7, 8], which are essential features for circular economy models. In addition to recent advancements in composite construction, timber has gained attention as a sustainable material, acting as a significant carbon sink. The use of timber has the potential to reduce the construction sector's carbon footprint, with en-

engineered timber in buildings and constructions providing long-term carbon storage [9]. The efforts to incorporate the use of timber in construction have led to the recent developments on steel-timber composite (STC) systems [10], which combine the strength and ductility of steel with the environmental benefits of timber. These systems use engineered timber products such as Cross-Laminated Timber (CLT), glued laminated timber (glulam), and Laminated Veneer Lumber (LVL) connected to steel beams to enhance material efficiency and structural integrity through composite action. STC flooring systems consist of a steel beam in the tension zone, a timber slab in the compression zone, and shear connection between the two components.

The practical advantages of the STC structural systems are significant and include: (i) enhanced strength and stiffness compared to hybrid non-composite systems and pure-timber floors, leading to (ii) the possibility to create larger open spaces; (iii) lighter construction compared to other structural solutions (e.g. reinforced concrete and steel-concrete composite floors), which results in (iv) benefits for the foundations, column sizes and the response of the building to lateral and dynamic actions; (v) potential reductions in construction time and costs due to the feasibility of prefabrication and modularisation, (vi) lower embodied carbon, and (vii) the potential for disassembly and reuse of structural components.

The environmental benefits of STC systems can be amplified when they are designed for disassembly and reuse. Demountable systems facilitate the recovery and reuse of structural elements, thus extending their lifecycle, minimizing waste, and reducing the demand for raw materials and energy associated with manufacturing new components. Furthermore, designing for disassembly and reuse of all structural components contributes to transitioning the construction sector towards a circular economy. Additionally, the environmental benefits of these structures can be further enhanced with the use of steel produced with recycled steel. Besides the environmental benefits of demountable and reusable systems, there are also potential economic advantages, for instance, the costs associated with material sourcing and waste processing can be reduced or eliminated. Moreover, demountable structures can be modified, expanded, or repurposed in response to changing needs or functions, consequently enhancing their investment value over time.

Although there is some research on STC structures, to date, there is no standard or guideline addressing STC beams and flooring systems. Furthermore, research on demountable and reusable STC beams and flooring systems is not present in the literature.

In composite structures, the shear connection is a key element that keeps the elements together and transfers shear forces to ensure effective composite action. The disassembly potential of STC beams largely depends on the shear connections, while existing connections in STC systems allow for disassembly, they often fall short when it comes to facilitating reuse, particularly due to damage to timber during assembly and disassembly that can compromise structural integrity. This requires the development of connections specifically designed for reuse to maintain the longevity of materials and reduce waste.

The "Prefa-SeTi: Steel-Timber Composite Beams" research project aimed to address these challenges by developing three novel shear connections for STC flooring systems that enable demountability and reuse of the structural components while preserving the integrity through-

out multiple use cycles. In this project an STC flooring system consisting of downstanding I-shaped hot-rolled sections and LVL slabs was developed and tested. Additionally, analytical procedures to estimate the bending capacity of the STC beams have been proposed. This thesis presents the findings of the research project "Prefa-SeTi", aiming to contribute to the broader goal of sustainable construction practices that align with the principles of the circular economy.

The research project "Prefa-SeTi" builds on findings from the RFCS-funded project "RE-DUCE" (Reuse and Demountability Using steel structures and the Circular Economy) [11], which investigated demountable and reusable steel-concrete composite flooring systems and their shear connections. "Prefa-SeTi" was funded by Fonds National de la Recherche Luxembourg and the Luxembourg based company Prefalux SA through a PhD Industrial Fellowship (Grant No. 15695062), additionally it received support from ArcelorMittal and Metsä Wood.

1.2. OBJECTIVES

The overarching aim of this research project is to develop and study a demountable and reusable STC flooring system and shear connections that enable reuse of the structural components. This research intends to provide a sustainable alternative to conventional flooring systems such as pure timber floors, existing non-reusable steel-timber composite floors, and carbon-intensive options like reinforced concrete and SCC slabs. The specific objectives are:

1. **Conceptualization of the STC Flooring System:** Designing the conceptual framework of the STC flooring system, which includes selecting appropriate materials and determining optimal layout and grid patterns to support demountability and reusability.
2. **Development of Innovative Shear Connections:** Engineering and refining shear connections to overcome the limitations of existing steel-to-timber connections, which do not support the reuse of structural components. These connections are designed to allow for easy disassembly and minimal damage to timber, ensuring structural integrity during the reuse phase.
3. **Experimental Testing Campaigns:** Conducting three testing campaigns:
 - i. **Timber Material Characterization Tests** to assess the mechanical properties of LVL made from Scandinavian Spruce, chosen for its low variability in mechanical properties and suitability as a flooring slab.
 - ii. **Push-Out Tests on Shear Connections** to evaluate the load-slip behaviour and load-bearing capacity of the novel shear connections developed.
 - iii. **Full-Scale STC Beam Tests** to investigate the flexural and vibration behaviour of the STC beams implementing two of the developed shear connectors, focusing on load-deformation responses, bending capacity, slip distribution, shear lag effects in the timber slab, and the modal parameters of the beams.
4. **Numerical Investigations:** Developing 3D finite element models that extend the findings of the full-scale bending tests to enhance the understanding and application of the

experimental data.

5. **Analytical Investigations:** Proposing analytical procedures to estimate the bending stiffness and capacity of the STC beams, and conducting analytical investigations using these procedures to compare the estimations with experimental results, thereby validating the proposed procedures.

1.3. THESIS OUTLINE

This thesis is organized into eleven chapters, beginning with a comprehensive introduction that outlines the motivations and objectives of the research. Following this, the state of the art is reviewed, providing a contextual framework for the research contributions. The concept of the developed STC flooring system, along with the innovative demountable shear connections, is then explained. Subsequently, the experimental campaigns are presented, followed by numerical and analytical investigations. The vibration tests are introduced, and finally, the conclusions and outlook are presented.

Structured as a cumulative dissertation, this research is grounded in three articles that have been published or submitted to peer-reviewed journals. These articles form the core of Chapters 4, 5, and 6, detailing the experimental and research efforts supporting this study. While each article stands as an independent chapter contributing to the thesis, the collective state of the art is integrated into a single comprehensive chapter to avoid redundancy and enhance coherence.

Below is a detailed overview of each chapter, highlighting the journey from the literature review and conceptualization of the demountable and reusable STC flooring system through to experimental investigations, numerical and analytical evaluations, and closing with final conclusions and outlook.

Chapter 1: Introduction

Introduces the context and rationale for investigating demountable and reusable STC flooring systems. It outlines the specific objectives of the thesis, including the development and testing of innovative shear connections and the STC flooring system. Additionally, the structure of the thesis document is described.

Chapter 2: State of the art

Presents the current state of research in three main areas: (i) laminated veneer lumber, (ii) shear connections for STC systems, and (iii) STC beams and flooring systems. This chapter synthesizes relevant literature on the development and mechanical performance of LVL, existing shear connection technologies for STC beams, and the current research status on composite beams.

Chapter 3: Demountable steel-timber composite (STC) flooring system

Details the design and components of the STC flooring system, including the three developed shear connection systems. The chapter elaborates on the components and features of these connections and the flooring system.

Article 1**Chapter 4: Experimental investigation on laminated veneer lumber (LVL)**

Describes the experimental procedures and results from investigations conducted to determine the mechanical properties of crossband LVL used in the STC flooring system.

Article 2**Chapter 5: Experimental push-out tests on the developed shear connections**

Describes the push-out tests experimental campaign conducted on the developed shear connections. This chapter details the specimens, test setup, loading conditions, results, and the analysis of the results.

Article 3**Chapter 6: Experimental full-scale STC beam tests**

Presents the full-scale STC beam tests, describing the specimen preparation, test setup, assembly details, testing procedures, results and the analysis of the results.

Chapter 7: Numerical modelling of the STC beams

Outlines the finite element modelling strategy for simulating the behaviour of STC beams and includes a parametric study to extend the findings of the experimental investigations.

Chapter 8: Analytical determination of the bending capacity of STC beams

Introduces a strain-based method and a simplified procedure to estimate the bending capacity of STC beams, with analytical results being compared to experimental findings.

Chapter 9: Vibration tests

Presents the vibration tests on the two full-scale STC beam specimens, detailing the testing procedures, results, and comparisons with analytical and numerical findings.

Chapter 10: Design considerations

Due to the lack of established standards and guidelines for design, this chapter explores preliminary design considerations for demountable and reusable STC beams and flooring systems focusing on bending capacity, bending stiffness, elastic analyses, and vibration performance.

Chapter 11: Conclusions and Outlook

Summarizes the research findings, discusses the implications of these outcomes, and identifies potential areas for future research directions to advance the development and application of the STC flooring systems and the shear connections proposed in this study.

As of the submission date, the status of the articles that comprise the core of this thesis is as follows:

Article 1: Presented in: Chapter 4

Article title: Experimental investigation on Strength and Stiffness Properties of Laminated Veneer Lumber (LVL)

Journal: Materials (ISSN: [1996-1944](#))

Status: Published (DOI: [10.3390/ma16227194](#))

Article 2: Presented in: Chapter 5

Article title: Experimental investigation on novel shear connections for demountable steel-timber composite (STC) beams and flooring systems

Journal: Engineering structures (ISSN: [1873-7323](#))

Status: Published (DOI: [10.1016/j.engstruct.2024.117620](#))

Article 3: Presented in: Chapter 6

Article title: Innovative Demountable Steel-Timber Composite (STC) Beams: Experimental Full-Scale Bending Tests

Journal: Engineering structures (ISSN: [1873-7323](#))

Status: Published (DOI: [10.1016/j.engstruct.2024.118599](#))

1.4. LIMITATIONS

This research project focused on developing and testing a demountable and reusable STC flooring system and the shear connections to enable easy assembly, demountability and reuse of the structural components, and while the findings provide valuable insights, they are subject to some limitations.

Firstly, the study was limited to a specific type of engineered timber—crossband LVL made of Scandinavian Spruce wood with a thickness of 144 mm. The push-out tests and full-scale beam tests were conducted exclusively using this material. As such, the applicability of the results to other thicknesses, timber species, or engineered timber product is not established.

Furthermore, the shear connections developed and tested were of a fixed size. The load-slip behaviour of steel-to-timber connections, is known to be influenced by the size of the connection. Consequently, the results presented here are applicable only to the specific connection dimensions tested and cannot be generalized to other sizes without further investigation.

Additionally, the orientation of the grain in the LVL panels was aligned with the direction of the load in the push-out tests and with the longitudinal direction of the beam in the beam tests. Studies on steel-to-timber connections have shown that the orientation of the grain relative to the load and the bending direction influence the response of the connection and the flexural behaviour of the beams. Therefore, the results of this study cannot be directly extrapolated to other scenarios where these parameters vary.

The STC beams were tested under conditions of sagging bending and were simply supported. This study did not investigate different bending and support conditions, which could influence the behaviour of the beams.

The numerical models and the proposed analytical procedures were validated with the findings of this investigation. Therefore, their applicability to different configurations and materials needs to be assessed.

These limitations underscore the need for caution in extending the conclusions of this study beyond the tested configurations and suggest areas for future research to broaden the applicability of the findings.

2

STATE OF THE ART

2.1. LAMINATED VENEER LUMBER (LVL)

2.1.1. GENERAL

LVL is an engineered wood product created by bonding together thin wood veneers, typically with a thickness of 3-4 mm, to form panels of various dimensions and configurations (see Figure 2.1). Engineered for superior strength and stiffness, LVL's composite structure involves pressing and bonding veneer layers using phenolic adhesive. This construction effectively mitigates many of the natural defects found in solid wood [12], resulting in a highly uniform material with minimized property variations. This attribute distinguishes LVL from conventional timber products.



Figure 2.1: LVL panels and beam, picture from "LVL Europe Handbook" [13].

LVL has garnered significant attention due to its capacity to leverage the inherent strength and durability of wood, while also mitigating some of the limitations associated with solid timber size and natural defects. Moreover, LVL production efficiently utilizes small-diameter logs and lower-grade timber that might otherwise be discarded as waste [14, 15].

The maximum width (measured in the tangential direction) that can be produced is 2500 mm, and the maximum lengths range from 18-25 m depending on the production line. There are two standard types of layups: (i) a layup in which the veneer layers are oriented with their grain running parallel to each other, known as LVL-P; and (ii) a layup in which approximately 20% of the veneer layers have their grain running perpendicular to the grain of the other veneers, which is known as LVL-C.

The mechanical properties required for design purposes are typically provided by the manufacturer, as they are dependent on factors such as the specific timber species, layout, and production process. Reference values commonly used for structural design can be found in sources such as the Finnish Woodworking Industries LVL Handbook [13] and the technical information given by suppliers like Metsä Wood [16]. These documents typically report strength values as characteristic values and stiffness values as mean values. Nevertheless, technical information provided by suppliers generally lacks experimental values and details regarding the load-deformation behaviour of LVL. This gap in information is also evident in the existing literature.

As the construction industry faces growing scrutiny for its environmental impact [17], engineered wood products such as CLT and LVL have emerged as a sustainable alternative to conventional materials like concrete and steel [18, 19, 20, 21]. The appeal of LVL extends to its suitability for a wide range of structural applications, from beams and columns to slabs and shear walls. Moreover, investigations have been done to implement its use as slabs in conjunction with steel structural beams as STC beams [22, 23, 24, 25]. In Europe, LVL manufactured from Spruce wood sourced from Scandinavian countries stands out as one of the most prevalent LVL products [13].

2.1.2. RELEVANT PUBLICATIONS

LVL has emerged as a cornerstone of modern construction, rooted in the mid-20th century alongside the development of plywood [26]. The development of LVL as a product as we know it today, began in the 1970s with the development of "press-lam" wood based veneer beams [27]. Initially conceived as a response to the limitations of solid timber and seeking to provide technology for more efficient use of the wood resource. LVL represented a breakthrough in engineered wood products, offering superior strength and dimensional stability.

Within the product's development efforts at the United States Forest Products Laboratory, Schaffer et al. [14] demonstrated its superior mechanical performance when compared to solid wood due to the dispersion of natural imperfections in its layered structure. Additionally, it was found that in elements with constant thickness, the variation of mechanical properties was less scattered in the elements with more layers (i.e. with thinner layers), meaning that the scatter in properties reduced as the number of layers increased as illustrated in Figure 2.2. The first commercial solution for manufacturing LVL was developed by Al Troutner, and in 1975 the Finnish company Metsäliiton Teollisuus Oy (today known as Metsä Wood) developed the first LVL production line in Europe [13].

The research reported in the literature related to LVL is mostly linked to the study of the

effects of different parameters in the mechanical properties of LVL such as the jointing method [28], wood age (e.g. juvenile, mature) [29, 30, 31], veneer thickness [14, 31, 32, 33], orientation of the veneers [34], type of adhesive [35, 36], log pre-treatment [37], veneer quality [38], lathe checks [39, 40, 41, 42], special treatments [43, 44], and pressure during production [45, 46, 47, 48]. Nevertheless, the literature lacks comprehensive information of full mechanical characterisation of the commercially available products.

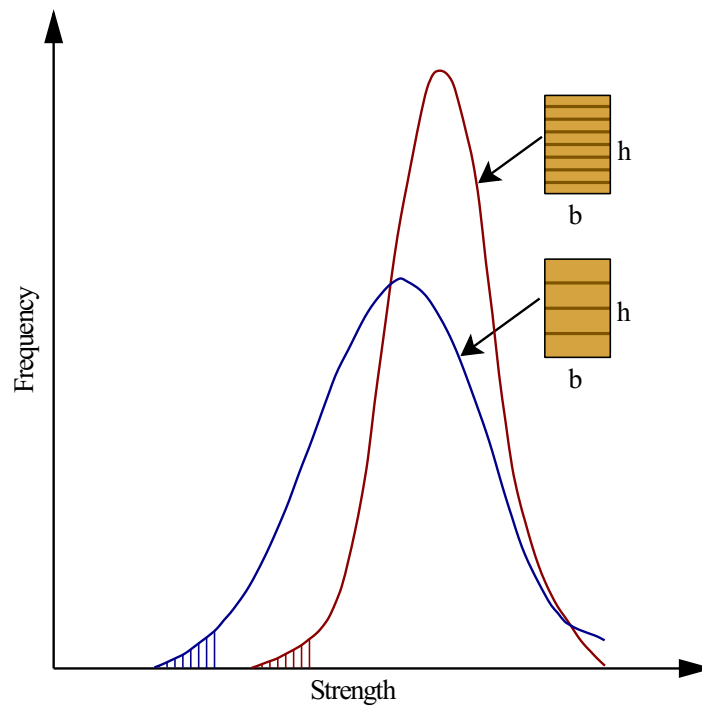


Figure 2.2: Schematic representation of the effect of the number of layers on the normal distribution of the experimentally obtained mechanical properties of laminated products with constant cross-section [14, 49].

There are some investigations on the mechanical properties and behaviour of LVL, however, none of them deal with LVL-C made from Scandinavian Spruce wood. Chybinski and Polus [50] conducted compression, tension and bending tests of LVL-P (LVL with the grain of all veneers oriented in the same direction) panels made of Spruce and Scots pine, moreover, they built 2D and 3D finite element models and implemented the properties obtained in their tests, showing good agreement with the experimental observations. A comprehensive investigation on the strength and stiffness properties of Radiata pine LVL was presented by Van Beerschoten [51]. Ardalany et al. [52, 53] studied the fracture energy, toughness, as well as the strength in tension perpendicular to the grain of LVL crafted from Radiata pine. Similarly, Franke and Quenneville [54] analysed experimentally the fracture behaviour of Radiata pine LVL.

Other studies related to LVL focused on the assessment of LVL with certain variations in its standard structure and/or layup and its response under certain conditions. For instance, Bal [55] determined some physical and mechanical properties of LVL reinforced with wooven fibers. Sokolovic et al. [56] assessed the bending strength of flexural properties of LVL rein-

forced with woven carbon fibers. Bakalarz [57] studied the bending response of LVL beams reinforced with carbon fiber reinforced polymer (CFRP).

While there are studies that have focused on the mechanical characterization of certain LVL products and on the enhancement of its mechanical response, it is noteworthy that none of them have specifically assessed the strength and stiffness properties of crossband LVL derived from Scandinavian Spruce wood, as far as the author of this contribution is aware.

2.2. SHEAR CONNECTIONS FOR STC BEAMS AND FLOORING SYSTEMS

2.2.1. GENERAL

Shear connections are essential components of composite structures, ensuring the integrity and effective composite action. The structural behaviour of STC systems heavily relies on the load-slip behaviour of connections attaching timber slabs to steel beams.

Understanding the behaviour of steel-to-timber shear connections is crucial for determining their capacity and deformation characteristics. This enables the development of connectors that effectively transfer shear forces and ensure composite action in STC beams.

With the increasing interest in STC beams and flooring systems, research on shear connections for steel-timber flooring systems has expanded in recent years. Investigations into shear connections for flooring system applications, as documented in the literature, have focused on their development and assessment, including various push-out tests and analytical and numerical analyses.

2.2.2. RELEVANT PUBLICATIONS

Shear connections for STC beams implementing screws, bolts, C-type connectors, epoxy adhesives, steel plates (both punched and embedded in the timber), combinations of these methods, and mechanical connectors embedded in grout pockets, have been the focus of dedicated research efforts. These studies, which include both static and cyclic push-out tests as well as numerical simulations and long term tests, have provided comprehensive insights into the connections for STC beams.

In 2000, Moore [58] presented the design of a 12-storey apartment building consisting of a structural steel gravity and lateral load resisting system and timber floors connected to steel beams. The beams were connected to the timber floors with screws. Although, this is one of the first reported contributions addressing steel-timber floors and their shear connections, no details were included concerning the mechanical performance of the connections.

Asiz and Smith [59] performed push-out tests of CLT panels connected to steel beams by means of screws to determine their load-slip response. The results showed that the load-slip response was influenced by the orientation of the panel and the length of the connector. Larger ultimate loads and stiffness were observed for longer connectors and when the grain of the thicker layers of the CLT plates were aligned with the direction of the load. They concluded that the capacity and the load-deformation behaviour of the connections was adequate for use in flooring systems.

Loss et al. [60, 61] did static and cyclic push-out tests to study the mechanical behaviour of steel beam to CLT panels connections, including connections with screws, bolts, c-type connectors, glue, combinations of these connectors, and steel plates embedded in timber with epoxy resin. Most connections exhibited large deformations and none of them had a brittle failure before reaching a deformation of at least 10 mm. Concerning stiffness, peak load and deformation capacity the values varied within a broad range for all the connections, however, the connections implementing steel plates embedded in the timber and filled with epoxy resin showed the largest peak forces and stiffnesses, followed by threaded rods reinforced either with geka connectors or with screws, and the least performing connections were those using vertical screws only. Based on the results, two connections (i.e. inclined screws and plates embedded in epoxy resin) were selected for their implementation in STC floors due to their simplicity and ease of installation, as well as good load-bearing and deformation capacities.

Hassanieh et al. [22, 62, 63, 64, 65] did static push-out tests to study steel-to-timber (i.e. LVL and CLT) connections using bolts, screws only, glue at the interface with screws, screws with punched metal plates, and bolts embedded in grout pockets. The parameters analysed in the experiments, which have influence on the stiffness and the load-bearing response of the connections were mainly: (i) the size and strength of the screws and bolts, (ii) the orientation of the grain with respect to the load direction, (iii) the use of adhesives at the steel-timber interface, (iv) the reinforcing nail plate and, (v) size of the grout pocket. Results indicate that the orientation of the grain of the panels significantly influences the response and capacity of the connections. Screws and bolts showed good deformation and bearing capacity, their capacity was enhanced with the implementation of punched metal plates, and the connections with glue exhibited high stiffness and load-bearing capacities but were associated to brittle failure with limited deformation capacity. The bolts in grout pockets showed the largest load-bearing capacity. Furthermore, numerical models were developed to reproduce the push-out tests and conduct parametric studies to investigate the influence of different parameters on the response of the connections.

Yang et al. [66] carried out static push-out tests on connections of steel beams and glulam plates using bolts and screws. The bearing capacity, yield characteristics and failure modes were investigated together with the effect of the type, size and spacing of the connectors as well as the thickness of the glulam plates. The bearing capacity results obtained in the tests were compared to values from codes (i.e. GB/T 50005-2017 [67], NDS-2018 [68] and Eurocode 5 [69]). Connections with screws showed the largest stiffness but bolted connections exhibited better ductility and load-bearing capacity. Additionally, the results showed that the analytical models from Eurocode 5 [69] models produced reasonable predictions of the bearing capacity.

Wang et al. [70] assessed steel-to-glulam connections with inclined screws using special taper washers. The load-slip behaviour and failure modes were analysed for screws with different sizes and inclinations (i.e. 0°, 30°, 45° with respect to the vertical), moreover, the influence of the use of custom taper washers for inclined screws was assessed. The results show that longer screws increase the embedded depth in the timber, leading to greater peak loads. In addition, inclined screws performed better in terms of peak load but when there were no tap

washers there was significant loss in stiffness compared to vertical screws. However, this drop in shear stiffness was mitigated by using taper washers. Overall, the inclined screws with tap washers had better load-bearing capacity and stiffness than vertical screws due to the use of longer screws that increase the embedment depth.

Zhao et al. [71] investigated connections with screws with a portion of the tip embedded in grout pockets. The aim of the grout pocket at the tip was to actively control the failure mode of the screws and induce two plastic hinges in the screws. The results indicate that the stiffness and strength of these connections is improved when compared to connections with only screws and no grout pocket.

Gao et al. [72] executed static push-out tests to investigate the response of steel-to-timber connections with bolts and screws. Bolts had the best strength and stiffness, and it was determined that the strength and stiffness of the connections increase with increasing thickness of the timber.

Moritani et al. [73] conducted tests to analyse connections between cold-formed steel (CFS) beams and CLT panels. Five connectors were studied, including screws, bolts and bolts with T-nuts and threaded inserts. The connections exhibited good deformation capacity, bolted connections with T-nuts, and connections with both, threaded inserts and T-nuts, had the best performance in terms of strength.

Chybinski and Polus [74, 75] studied bolted connections and connections with screws reinforced with C-type connectors (i.e. bulldog and geka) used to connect LVL and aluminium beams. The load-bearing behaviour of connections with and without reinforcing toothed plate connectors was compared. Connectors type C2 (i.e. bulldog) were used to reinforce the connections with bolts and screws, additionally, connectors type C11 (i.e. geka) were implemented in connections with screws. In all the configurations, the toothed connectors were placed at the aluminium-timber interface. It was concluded that bulldog and geka connectors improve the strength of the connections but have negligible effects on their stiffness. Similarly, Zhou et al. [76] assessed aluminium-to-timber (i.e. glulam) connections with bolts and screws, their load-slip behaviour and capacity was similar to connections implementing steel beams.

Zhang and Ling [77] conducted a study on shear studs embedded in grout pockets, employing finite element models to simulate double symmetric push-out tests that connected CLT panels to steel beams. Their 3D finite element model was calibrated using experimentally obtained results. The investigation explored into various parameters affecting the connector response, including the shape of the pocket (i.e., rectangular-straight and rectangular-tapered), pocket size, shear stud size and grade, orientation of the grain of the outer layers, and CLT panel thickness. The findings revealed that the yielding point and maximum loads increased with larger connector diameters. Higher steel grades were associated with slightly larger maximum loads. Models with outer layers parallel to the grain demonstrated higher loads. Moreover, as the angle of the tapered pocket increased, the capacity of the connections decreased. Panel thickness showed minimal influence on connection capacity.

Böhm et al. [78] studied steel-to-timber connections with inclined screws and shear studs embedded in grout to connect CLT panels and steel beams. The screws were set at a skew angle

of 45° relative to the vertical axis, and their orientation across various skew angles relative to the horizontal plane was investigated to assess their impact on the behaviour and load-bearing capacity of the connection. It was discovered that the load-bearing capacity decreases as the skew angle in the horizontal plane increases. Conversely, the capacity is significantly enhanced with an increase in the length of the inclined screws.

Cyclic loading tests on steel-to-CLT connections for floors have been performed by Ataei et al. [79, 80] to investigate the failure mode, ductility, energy dissipation capacity, equivalent viscous damping and strength impairment. The connections with screws and bolts previously assessed by Hassanieh et al. [22, 62, 63, 64, 65] through monotonic push-out tests, were tested in this study under a low-cycle high-amplitude loading regime. The parameters analysed include the size and type of the connectors (i.e. coach screws, dog screws and bolts) as well as the orientation of the grain of the CLT panels with respect to the load direction. According to the results, these connections have high ductility and energy dissipating capacity, most connections were able to sustain slip values larger than the minimum requirements established in design codes (e.g. EN 1998-1 [81]). Furthermore, a hysteretic analytical model was proposed for these connections and calibrated against test results.

The long-term behaviour of STC shear connections under sustained load was studied experimentally and numerically by Chiniforush et al. [82]. Connections with coach screws, dog screws, bolts and bolts in grout pockets were investigated by means of push-out tests in which a sustained load was applied over a period of 16 months in conditions classified as Service Class 2 according to EN-1995-1 [69]. The parameters monitored over the testing period were the slip, the relative humidity, and the load, which was re-adjusted to keep the load within the range of $\pm 4\%$ of the target load. The results were used to calibrate a long-term rheological model to predict the slip and the creep coefficient over a service life of 50 years. It was determined that the bolts in grout pocket have the lowest creep coefficient of 0.6, whereas the bolted connection showed the highest creep coefficient of 3.9.

2.2.3. OVERVIEW OF SHEAR CONNECTIONS PRESENTED IN THE LITERATURE

The shear connections for STC beams and flooring systems presented in the literature include the following main configurations (see Figure 2.3):

- (a) Screws (coach screws, dog screws, self-tapping, universal) [22, 58, 62, 63, 66, 72, 73, 76] (Figure 2.3a).
- (b) Inclined screws with or without taper washers [70] (Figure 2.3b).
- (c) Inclined screws with respect to both the vertical and the horizontal plane [78] (Figure 2.3c).
- (d) Screws with epoxy glue at the steel-timber interface [22, 62] (Figure 2.3d).
- (e) Screws with geka connectors at the steel-timber interface [75] (Figure 2.3e).
- (f) Screws with bulldog connectors at the steel timber interface [75] (Figure 2.3f).

- (g) Screws with their tip embedded in grout, with mortar or epoxy resin as grout [71] (Figure 2.3g).
- (h) Screws with punched metal plates [22] (Figure 2.3h).
- (i) Screws installed in strip plates welded along the top flange of the beam [60] (Figure 2.3i).
- (j) Inclined screws installed in steel plates or C-shaped profiles welded to the top flange of the beam [60] (Figure 2.3j).
- (k) Threaded rod welded to beam with a rectangular steel plate on top of the timber slab fixed with screws [60] (Figure 2.3k).
- (l) Threaded rod welded to beam with a steel disc with flared holes and inclined screws (with or without epoxy resin filling in the hole) [60] (Figure 2.3l).
- (m) Threaded rod welded to beam with a C-shape profile on top of the slab and inclined screws (with or without epoxy resin filling in the hole) [60] (Figure 2.3m).
- (n) Threaded rod welded to beam with one geka connector [60] (Figure 2.3n).
- (o) Threaded rod welded to beam with two geka connectors [60] (Figure 2.3o).
- (p) Threaded rod (partially or fully threaded) welded to beam and hole filled with epoxy resin [60] (Figure 2.3p).
- (q) Rod and perforated plate welded to beam and filled with epoxy resin [60] (Figure 2.3q).
- (r) Plate welded to steel beam and hole filled with epoxy resin, variants of this connection include: partially perforated plate, fully perforated plate, striated plate, and plate with welded thin steel elements [60] (Figure 2.3r).
- (s) Steel tube welded to beam and hole filled with epoxy resin [60] (Figure 2.3s).
- (t) Bolts [22, 62, 66, 72, 73, 74, 76] (Figure 2.3t).
- (u) Bolts with threaded insert and T-nut insert, variations of this connection include: bolt with both threaded insert and T-nut insert, bolt with only threaded insert, and bolt with only T-nut insert [73] (Figure 2.3u).
- (v) Bolts embedded in grout pockets with walls of the pockets at straight angles [63] (Figure 2.3v).
- (w) Bolts embedded in tapered grout pockets (i.e. walls of the pockets with a certain inclination) [77] (Figure 2.3w).
- (x) Shear studs embedded in grout pockets, the pocket with circular shape and inclined walls [78] (Figure 2.3x).

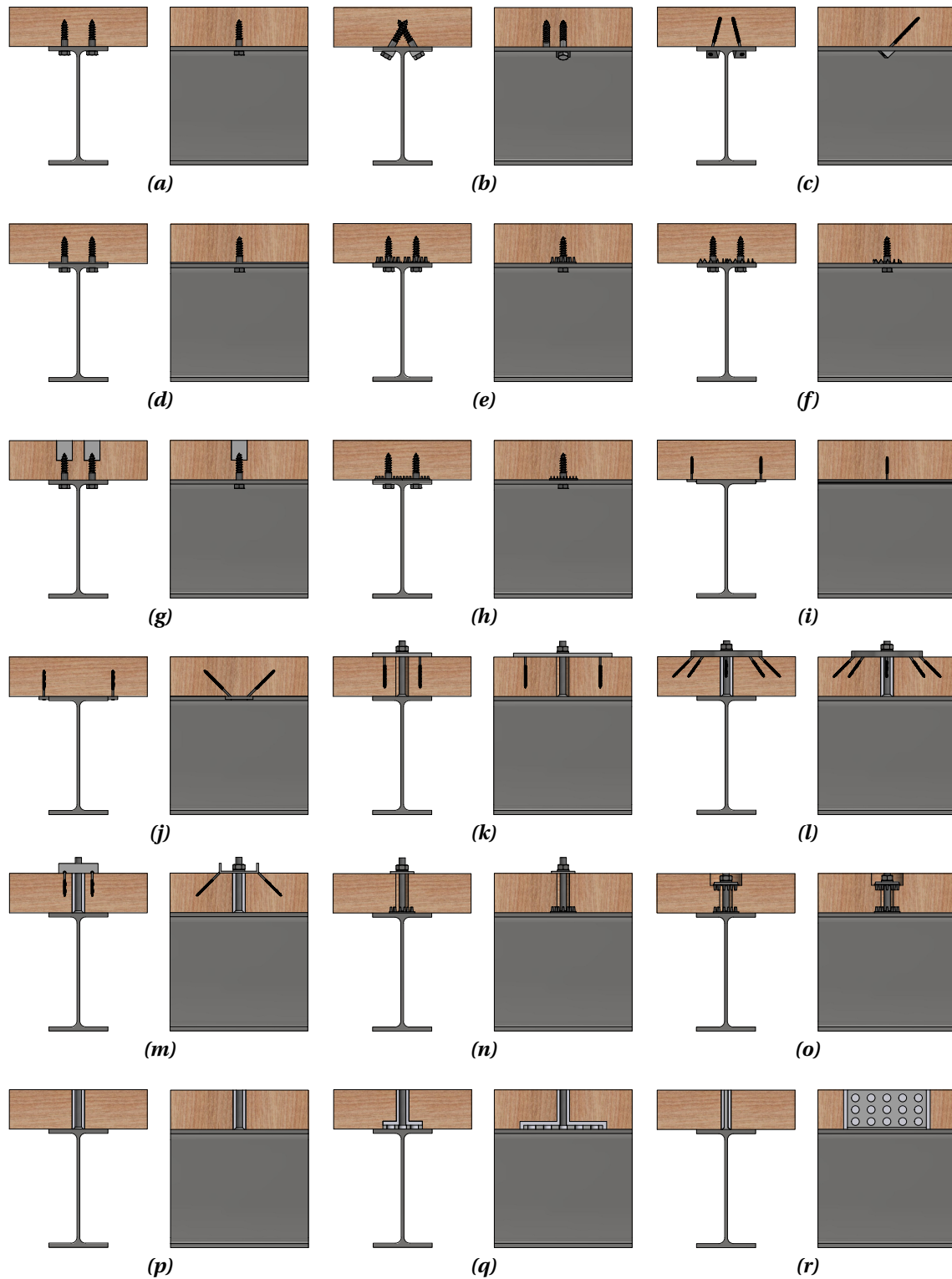


Figure 2.3: Shear connections for STC beams and flooring system presented in the literature.

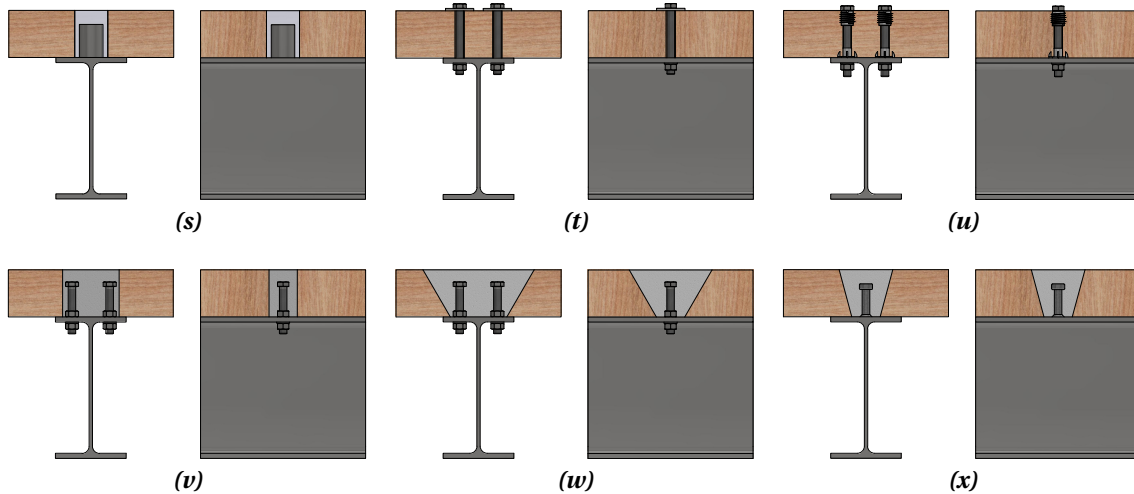


Figure 2.3: Shear connections for STC beams and flooring system presented in the literature (cont.).

2.3. STEEL-TIMBER COMPOSITE (STC) BEAMS AND FLOORING SYSTEMS

2.3.1. GENERAL

The available research of steel-timber composite beams includes full scale beam tests of beams with I-shape hot-rolled steel profiles and with U-shape cold-formed steel profiles. Bending tests, for short-term and long-term loading conditions, have been performed in specimens implementing CLT, LVL, and glulam slabs to determine the load-deformation behaviour, the capacity of the system and the shear connection performance.

2.3.2. RELEVANT PUBLICATIONS

Current research on STC beams and flooring systems, which includes both bending tests and numerical simulations, has largely been centred around steel beams connected to CLT slabs, primarily using screws as shear connectors. To date, only a limited number of 7 bending tests have been reported in the literature on STC beams that implement LVL slabs, 29 bending tests on STC beams that implement CLT slabs, and 8 that implement glulam slabs. Furthermore, these studies typically involved timber slabs of narrow width connected to hot-rolled steel beams, without investigating the shear lag effect. The literature lacks studies addressing shear lag effects in these configurations, as well as on defining an effective width for the analytical determination of the bending capacity of STC beams.

Asiz and Smith [83] studied numerically the response to seismic and wind loads of medium-rise and high-rise buildings with steel frame and CLT floors, the drifts were compared with those obtained for buildings with the same steel frame but with concrete floors, results indicate that the drifts are significantly smaller for buildings with timber slabs.

Hassanieh et al. [23, 84] carried fourteen 4-point bending tests on STC beams with LVL (seven tests) and CLT (seven tests) slabs implementing bolts, screws, and screws with glue. It was determined that the stiffness of beams with bolted connectors was higher than the stiffness

of beams with screws. In general, the beams showed ductile behaviour, except the STC beams with screws and glue, which were associated to brittle failure. Furthermore, from these bending tests, only two of these implemented bolted connections, one STC beam with LVL slab and one with CLT slab. In these two tests, the full preload of the bolt was not reached, and damages were observed in the LVL due to compression of washers against the slab exerted by the preload of the bolt.

Loss and Davison [85] conducted 6-point bending tests on modular prefabricated STC floor components consisting of CFS beams connected to CLT panels, implementing two types of connections: inclined screws (three tests) and steel plates embedded in timber with epoxy resin (three tests). The beams were tested under (i) simply supported conditions and (ii) restraining the rotation of the supports. It was observed that both tested systems — inclined screws and steel plates — performed similarly in terms of bending capacity and initial stiffness. Furthermore, the study found that restraining the rotation of the supports resulted in increased load-bearing capacity and stiffness of the floor components. A similar STC floor component combining steel plates embedded in timber and vertical screws was tested in 6-point bending and a numerical model was developed to replicate the test [86]. The results demonstrated adequate stiffness and bending capacity of the STC floor module, and a high level of composite action.

Zhao et al. [87] used screws, alone and with their tips anchored in pockets filled with either mortar or epoxy resin, to connect glulam slabs to hot-rolled I-shaped steel beams. They conducted 4-point bending tests to analyse the flexural response of the STC beams with a length of 4 m. The test results showed that the connections involving screws with their tips anchored in mortar-filled pockets or epoxy resin demonstrated increased stiffness and strength compared to those using screws alone. The study concluded that mortar was more effective than epoxy resin in enhancing bending stiffness and strength.

Böhm et al. [88] carried out fifteen 4-point bending tests on STC beams with CLT slabs and I-shaped hot-rolled steel profiles, analysing spans of 8.1 m and 10.8 m, connected with inclined screws and shear studs in grout pockets. Results showed adequate deformation capacities of the STC beams, suggesting that their design is likely to be governed by serviceability limitations (e.g. deflection and vibration) rather than bending capacity. The beams implementing screws showed larger stiffness than the beams with shear studs in grout pockets, and screws were more effective to limit slip. Furthermore, in the beams with shear studs in grout pockets there was a significant loss of stiffness due to the mortar cracking at about 30% of the maximum load.

STC beams have been also studied analytically [85, 89, 90, 91, 92], the analysing methods consist on the implementation of the γ -method [69, 93], the use of the elastic theory of layered beams and full plastic analyses with rectangular stress blocks similar to Eurocode 4 [94] procedure for SCC beams. Results have been compared with experimental and numerical results, showing good agreement for most cases. However, it remains unclear which effective width has to be considered in the analyses of beams with wider timber slabs than those tested and reported in the literature.

Research has also focused on the load-deformation behaviour and capacity of STC joints,

using tests and numerical models to develop analytical formulations to estimate their capacity [95, 96, 97, 98, 99, 100, 101, 102, 103, 104]. Long-term effects under sustained loads have been examined experimentally and numerically on STC joints, as well as on STC beams [105, 106, 107, 108]. Additionally, experimental and numerical modal analyses, as well as human-induced vibration tests, have been conducted to assess vibrations in STC beams and slabs [88, 109, 110, 111, 112, 113, 114, 115, 116, 117, 118]. The diaphragm behaviour has been analysed through experimental and numerical methods [61, 119, 120, 121]. Investigations into the sustainability potential have also been conducted [18, 20].

3

DEMOUNTABLE STEEL-TIMBER COMPOSITE (STC) FLOORING SYSTEM

3.1. GENERAL

In light of the pressing need for sustainable alternatives to conventional construction practices, STC structures have emerged as an efficient and sustainable solution. Their ecological advantages can be further enhanced by designing them for demountability and reusability. Thus, enabling the recovery and subsequent reuse of structural elements, extending their life cycle and reducing waste.

The potential for demountability and reusability in STC systems is primarily influenced by the type of shear connection used to connect steel beams and timber slabs. Conventional connectors (e.g. bolts and screws) can facilitate the disassembly of components but are less suitable for reuse due to potential timber damage, which can compromise the integrity and load-bearing capacity of the connection upon reassembly.

This issue highlights a critical challenge in the development of STC flooring systems: ensuring that connections allow disassembly and safeguard the structural components against damage to enable future reuse. Despite the clear need for such solutions, there are no connection systems that fulfil the criteria of demountability and reusability specifically for STC flooring systems. This reveals a gap in knowledge in steel-to-timber connections and emphasizes the need for innovative approaches in the design of STC systems.

Addressing this need, this research project introduces an innovative concept for a demountable and reusable STC flooring system, its details are presented in Section 3.2. Furthermore, three novel shear connection systems have been developed and tested. These shear connections have been designed to support both the disassembly and subsequent reuse of structural elements without compromising their structural integrity. Detailed information about these connections is provided in Section 3.3.

3.2. THE DEMOUNTABLE STC FLOORING SYSTEM CONCEPT

The flooring system concept developed within the frame of the research project "Prefa-SeTi: Steel-Timber Composite Beams" is shown in Figure 3.1. It consists of downstanding I-shaped hot rolled steel profiles with LVL panels on top, connected using novel demountable shear connections (see Section 3.3).

3

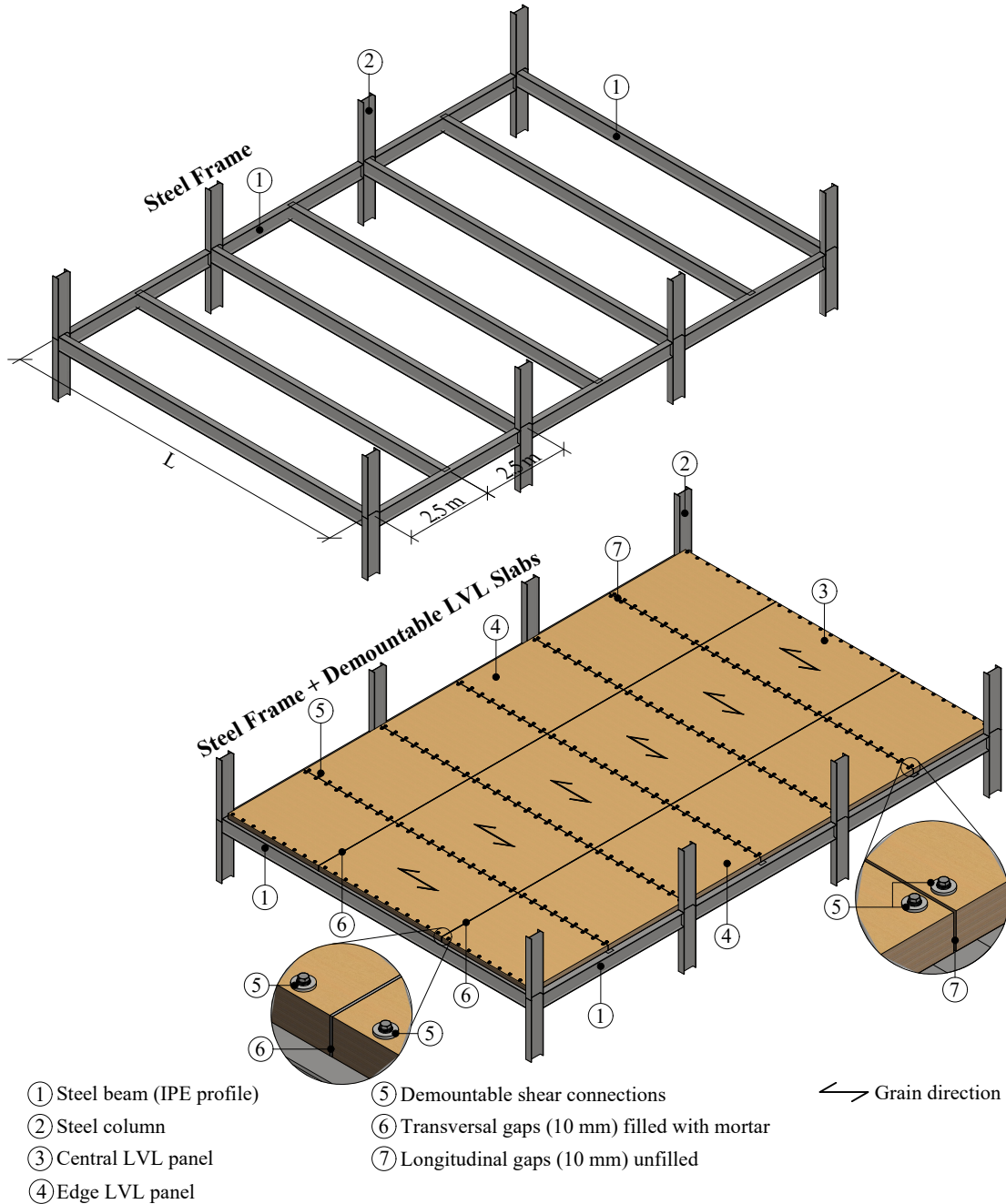


Figure 3.1: Demountable steel-timber composite (STC) flooring system.

In this system, LVL was selected for its low variability in mechanical properties and enhanced mechanical performance, leading to greater mean and characteristic strength values, and to smaller partial safety factors. The grain orientation of the LVL panels aligns with the

beams' longitudinal direction to maximize the strength and stiffness of the STC beams.

Crossband LVL panels (LVL-C, Kerto-Q [122]), which have approximately 20% of crossband veneers, was chosen for its superior strength and stiffness in the tangential direction, important features to minimise slab deflection between steel beams. Additionally, as the connections have been placed close to the edge of the panels, the cross banded veneers provide reinforcement against splitting failure, a common issue in engineered timber products with thicker layers and/or with the grain of all layers aligned to the load direction such as glulam and CLT [70, 123].

The size limitations of LVL panels are primarily dictated by the manufacturers. As such, the maximum available width (measured in the tangential direction) is capped at 2.5 m, while maximum lengths can vary between 18 and 25 m. This constraint is due to the production processes employed by manufacturers, which currently do not accommodate wider panels. Consequently, the width of the panels in this flooring system has been standardized at 2.5 m to maximise the spacing between steel beams.

The panels' length in the longitudinal direction is variable, it depends on span needs, and it is influenced by transport, installation, and construction tolerances. For long spans a practical solution is to divide the panels along the span into three portions (i.e., edge panels and a central panel), as depicted in Figure 3.1. This provides tolerances and facilitates transport and installation, which can be critical for long spans.

In the proposed STC flooring system, a 10 mm gap between adjacent panels necessary for construction tolerances is present. The transversal gaps (perpendicular to the grain direction) are to be filled with mortar to enable compression transfer and to activate the shear connectors in the edge panels.

This flooring system is promising for modularization, standardization, and off-site serial production, making it ideal for prefabrication in standard sizes and modules. Hence, it could greatly enhance construction efficiency and labor productivity.

The composite nature of the system offers enhanced strength and stiffness, facilitating the creation of large open spaces. Its easy disassembly allows for straightforward reuse and adaptability for spatial changes and redesigns. Additionally, the ease of replacing and recycling degraded components contributes to its practicality.

STC floors, being lighter than reinforced concrete and steel-concrete composite slabs, provide advantages such as reduced foundation requirements, smaller columns, and improved seismic and lateral performance, leading to lower material use. The incorporation of timber in these floors also reduces the structure's embodied carbon, which can be further decreased by using low-emission steels for the components of the frame system, like those produced with recycled steel and renewable energy sources (e.g. XCarb® steel [124]).

3.3. DEVELOPED SHEAR CONNECTIONS

3.3.1. GENERAL

Common shear connectors, including screws and bolts, as well as adhesives (e.g. epoxy adhesives), can be used to connect timber to steel beams. However, these connectors present certain drawbacks, especially when the objective is to facilitate easy disassembly and reuse of the components. These drawbacks are as follows:

- **Screws:** The process of drilling and unscrewing can potentially cause irreversible damage in the vicinity of the connector. A significant risk exists of over-tightening the screws, which can lead to damage in the wood. This typically occurs when using high-speed drilling equipment and/or when the tightening threshold is exceeded. The repetitive action of screw insertion and removal can weaken and damage the wood, reducing the capacity of the connection and compromising its integrity.
- **Bolts:** When bolts are aligned parallel to the radial direction of the wood, preloading the bolts can cause damage due to the inherently lower stiffness and strength of wood in this direction. As a result, bolts are often not fully preloaded to prevent such damage. Additionally, wood tends to relax after compression, which results in gradual loss of preload over time.
- **Adhesives:** The brittle nature of most adhesives, including epoxies, is a concern as it contrasts with the desired ductility in structural elements. Furthermore, the use of adhesives complicates the disassembly process. Adhesives are permanent and make the separation of components difficult without causing damage.

To overcome these drawbacks, three novel shear connections were developed and tested in this research project. These connections implement "shear connection devices" designed to enable disassembly, prevent timber crushing during bolt preloading, and facilitate the optimal preloading of high-strength bolts.

The novel shear connections have been designated as Shear Connection -Type 1 (SCT-1), -Type 2 (SCT-2), and -Type 3 (SCT-3). Drawings with the details of the connections are presented in Figure 3.2. Detailed descriptions of the shear connection devices and the removable components of these connections are provided in the subsequent two subsections.

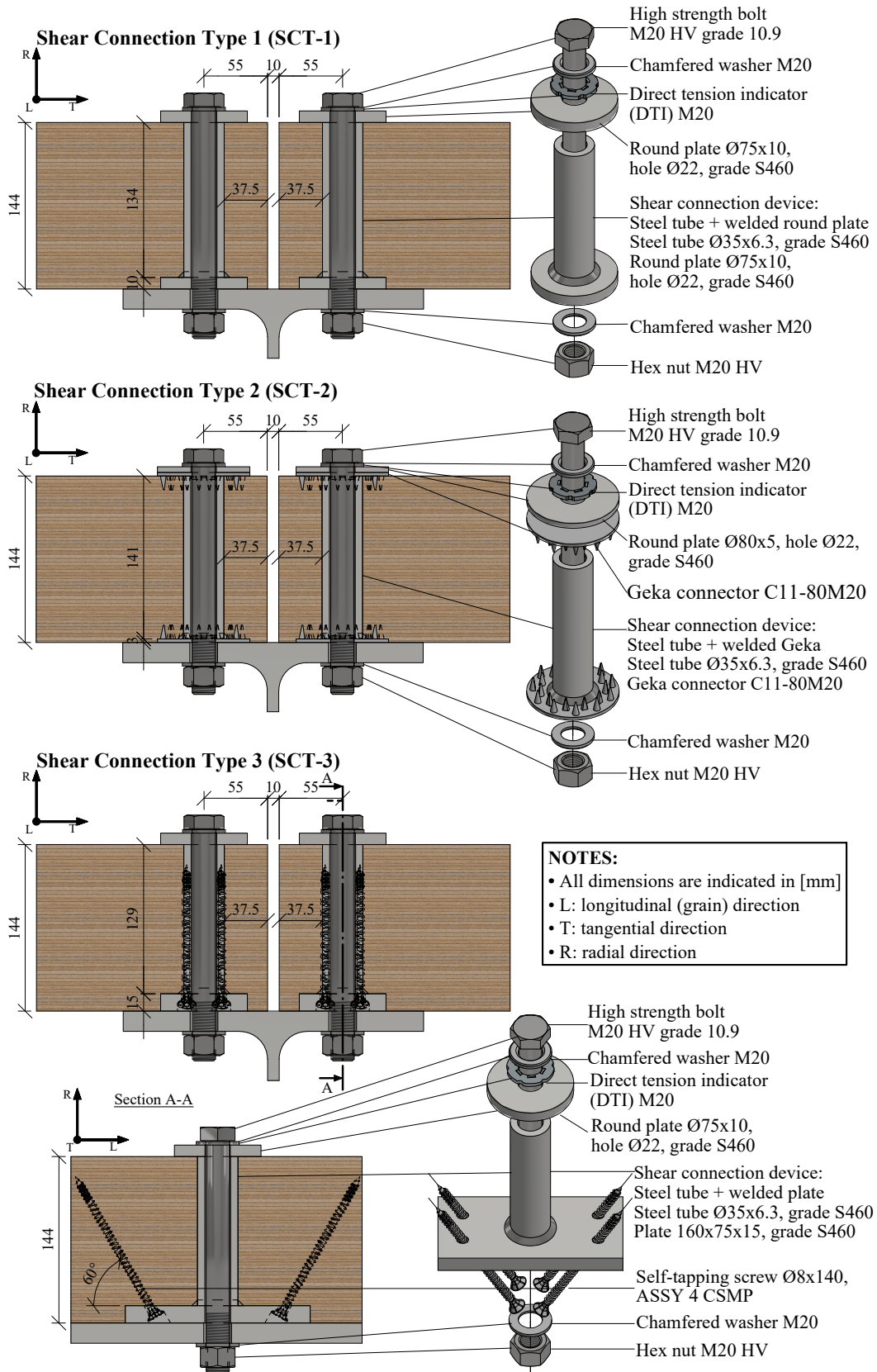


Figure 3.2: Shear connections for demountable STC flooring systems.

3.3.2. SHEAR CONNECTION DEVICES

The shear connection devices shown in Figure 3.3, are a fundamental feature of the connection systems developed in this research project. They consist of a steel tube made of grade S460 in compliance with EN 10025 [125]. The tube has an outer diameter of 35 mm and a wall thickness of 6.3 mm, with its base welded to a reinforcing steel element, which varies depending on the connection type as follows:

1. For SCT-1 it is a round steel plate (S460, EN 10025 [125]) with an outer diameter of 75 mm, a thickness of 10 mm, and an inner hole with a diameter of 22 mm.
2. For SCT-2 it incorporates a Geka connector for bolts M20 (C11-80M20) complying with EN 912 [126].
3. For SCT-3 it consists of a rectangular steel plate (S460, EN 10025 [125]) 160×75×15 mm with custom drills to allow the installation of timber screws Ø8×140 mm (Würth ASSY 4 CSMP, ETA-11/0190 [127]) with an inclination of 60° with respect to the horizontal.

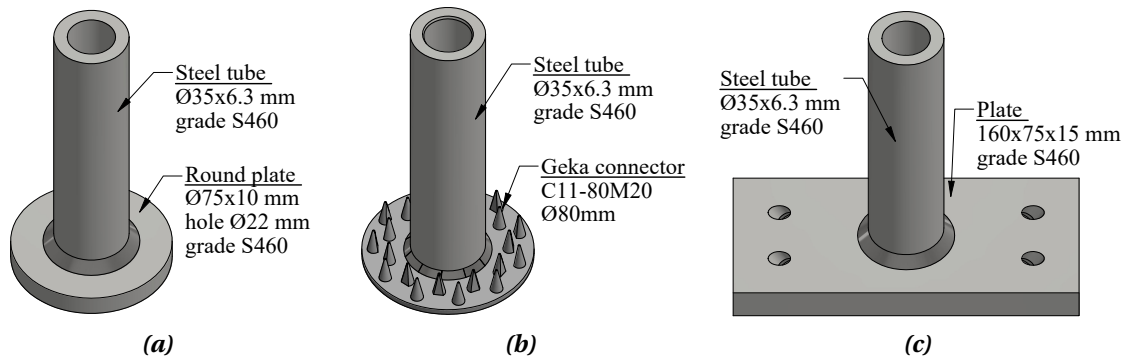


Figure 3.3: Shear connection devices for: (a) SCT-1, (b) SCT-2, and (c) SCT-3.

The shear connection devices are meant to be preinstalled in the timber slabs and remain as part of the slab during its life-span. The steel tubes must fit perfectly without clearances in holes drilled in the timber panels to ensure perfect contact of the connection device and the timber panel.

In these devices the tube serves three primary functions:

1. It accommodates a bolt that connects the timber panel to the steel beam.
2. It enables optimal preloading of the bolt, which is crucial because the tube takes all compression forces resulting from the bolt's preload, thus preventing compression stress and damage to the timber in the radial direction.
3. It enhances embedment strength. By increasing the contact area, stress is distributed over a larger surface, reducing the forces exerted on the timber.

Given the significant compression stress levels the tube undergoes from the bolt's preload, its design—specifically the steel grade and dimensions (i.e. wall thickness and inner diameter)—must be capable of withstanding the stresses induced by the bolt's preload. Therefore,

the selection of the tube's specifications is influenced by the bolt's size, its grade, and the desired preload.

For this research project, bolts M20 grade 10.9 [128] were selected, with the target preload determined in accordance with the specifications outlined in Eurocode 3 [129] and EN 1090-2 [130]. As a result, the tube was designed to meet these specific conditions.

3.3.3. REMOVABLE COMPONENTS

The connection system includes removable components, such as bolts, nuts, and washers, which do not constitute a permanent part of the panels. These can be removed as needed, whether for repairs or for reusing the timber panels. The removable components of SCT-1 and SCT-3 are common for both connection types, these components are as follows:

- i. A partially threaded high-strength HV bolt M20×210 mm grade 10.9.
- ii. A direct tension indicator (DTI) situated beneath the washer at the bolt head's face.
- iii. Two washers for HV bolts—one at the bolt head side and another at the nut side.
- iv. A nut for HV assemblies.
- v. A round steel plate with the same dimensions ($\varnothing 75 \times 10$ mm, hole $\varnothing 22$ mm) as the one welded to the tube's bottom side.

The removable components of SCT-2 include the components i to iv of SCT-1 and SCT-3 as well as two additional components, the components are listed below:

- i. A partially threaded high-strength HV bolt M20×210 mm grade 10.9.
- ii. A DTI situated beneath the washer at the bolt head's face.
- iii. Two washers for HV bolts—one at the bolt head side and another at the nut side.
- iv. A nut for HV assemblies.
- v. A round steel plate ($\varnothing 80 \times 5$ mm, hole $\varnothing 22$ mm).
- vi. A Geka connector with the same specifications (C11-80M20) as the one welded to the tube's bottom side.

Components i to iv (i.e., bolt, DTI, washers, and nut) are common to all three connection types and adhere to EN 14399 [128] standards for high-strength HV assemblies. The selection of HV bolts grade 10.9 is deliberate to prevent premature bolt failure due to bearing and shear.

ARTICLE 1

4

EXPERIMENTAL INVESTIGATION ON LAMINATED VENEER LUMBER (LVL)

4.1. INTRODUCTION

Despite LVL's increasing use in the construction industry, a comprehensive understanding of its mechanical behaviour, including testing procedures, stress-strain responses, and failure modes, remains crucial. The technical literature lacks comprehensive insights into these aspects. The mechanical properties of this engineered timber product (e.g. strength, stiffness, stress-strain response, fracture behaviour) are fundamentally important when it is used as load-bearing structural element in pure timber, steel-timber or timber-concrete structures. These mechanical properties are used to determine the bearing capacity of structural members, their load-deformation behaviour, and potential failure modes. Additionally, these properties are essential to develop numerical models of LVL members and structures (e.g. finite element modelling). Hence, to address the existing gap of knowledge concerning the mechanical characterisation of LVL-C made of Scandinavian Spruce wood, this research focuses on panels made from this wood species.

This chapter introduces a series of mechanical tests on LVL-C specimens, including compression, tension, shear, and bending, conducted to thoroughly assess the material's mechanical performance in the three orthogonal directions. It offers valuable insights into the material's testing procedures, and presents strength values, elasticity moduli, and shear moduli. Additionally, it details the observed stress-strain and load-deformation responses. The mechanical properties identified through this experimental investigation were subsequently used in analytical and numerical analyses to evaluate the performance of the STC demountable flooring system developed in this research project.

4.2. MATERIAL - LAMINATED VENEER LUMBER (LVL)

For this testing campaign the specimens were produced from LVL-C panels with a thickness of 51 mm made of Scandinavian Spruce wood (i.e. *Picea abies*) (see Figure 4.1). This product is commercialized by Metsä Wood under the brand name of Kerto-Q. It has 17 veneers in total, each veneer with a thickness of 3 mm, 3 of them are cross veneers distributed within the matrix of the section, hence, the layup is as follows: II-III-III-III-II, in which 'I' represents the veneers which grain aligns to the longitudinal direction of the timber element and '-' represents the cross veneers.

Due to its nature, timber is anisotropic, however, for engineering purposes it is considered as an orthotropic material. The three orthogonal directions are linked to the growth directions of the trees, longitudinally and transversely. The strongest and the stiffest direction is often referred as longitudinal direction, or grain direction, it follows the longitudinal growth of the tree. The other two directions are the radial and the tangential direction which follow the transversal growth of the tree. Figure 4.2 shows the definitions of the directions considered in this study for the LVL panels, the longitudinal (L), tangential (T) and radial (R) directions are defined as directions 1, 2 and 3 respectively.



Figure 4.1: Laminated veneer lumber (LVL) tested in this experimental investigation.

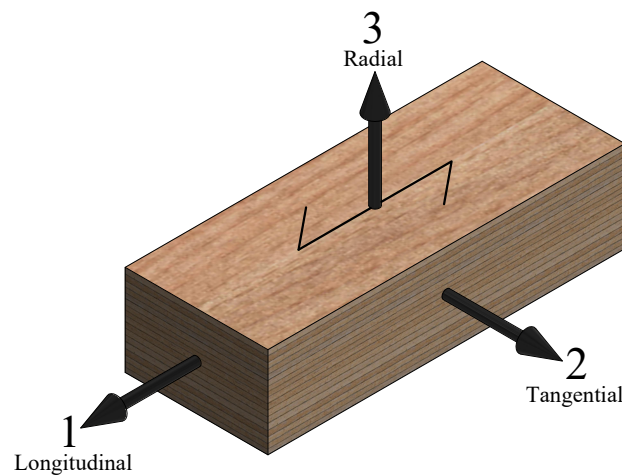


Figure 4.2: LVL directions considered in this investigation.

4.3. TESTS OVERVIEW

The testing campaign includes compression (C-), tension (T-), shear (S-) and bending (B-) tests to determine the stiffness and strength properties of crossband LVL in the three main orthogonal directions.

A nomenclature was defined to label the specimens and assign IDs to the different tests, this nomenclature (see Figure 4.3) consists of one letter followed by 2 digits separated by dashes, the letter refers to the type of test, the first digit, which is placed after the letter, refers to the direction, and the last digit refers to the specimen number within the sample. Thus, for instance the ID 'C-1-1' belongs to the compression tests (C-) in the longitudinal direction (1), specimen no. 1.

Following this nomenclature, an overview of the tests is presented in Figure 4.4. This figure includes, the schematic representations of the specimens' grain direction, the test IDs, the direction of the applied loads, and the number of specimens tested in this experimental campaign.

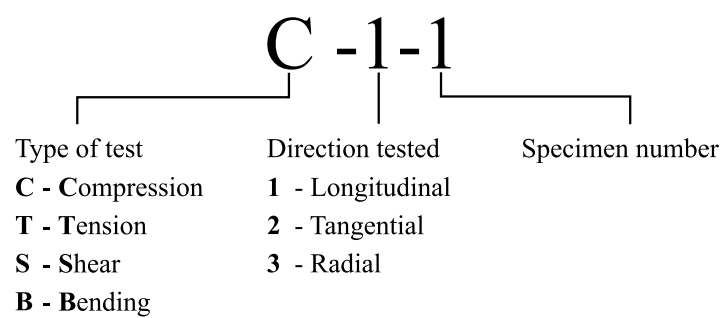


Figure 4.3: Nomenclature definition for test types and specimen identification.

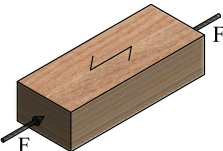
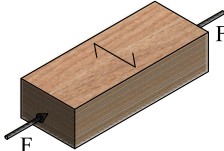
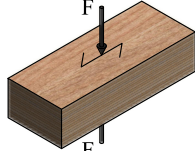
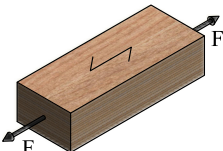
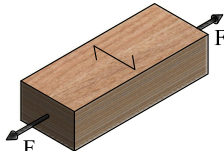
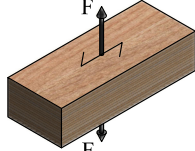
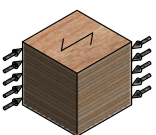
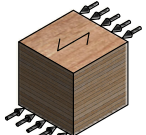
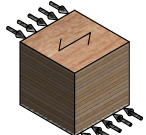
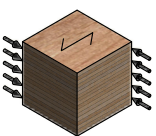
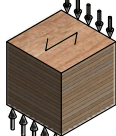
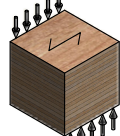
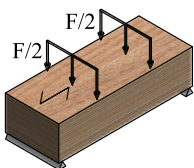
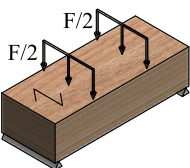
Compression	<p>A</p>  <p>Compression parallel to the grain (in the longitudinal direction) Test ID: C-1 Specimens tested: 9 Strength: $f_{c,1}$ Modulus of elasticity: $E_{c,1}$</p>	<p>B</p>  <p>Compression perpendicular to the grain (in the tangential direction) Test ID: C-2 Specimens tested: 6 Strength: $f_{c,2}$ Modulus of elasticity: $E_{c,2}$</p>	<p>C</p>  <p>Compression perpendicular to the grain (in the radial direction) Test ID: C-3 Specimens tested: 6 Strength: $f_{c,3}$ Modulus of elasticity: $E_{c,3}$</p>
	<p>D</p>  <p>Tension parallel to the grain (in the longitudinal direction) Test ID: T-1 Specimens tested: 6 Strength: $f_{t,1}$ Modulus of elasticity: $E_{t,1}$</p>	<p>E</p>  <p>Tension perpendicular to the grain (in the tangential direction) Test ID: T-2 Specimens tested: 6 Strength: $f_{t,2}$ Modulus of elasticity: $E_{t,2}$</p>	<p>F</p>  <p>Tension perpendicular to the grain (in the radial direction) Test ID: T-3 Specimens tested: 6 Strength: $f_{t,3}$ Modulus of elasticity: $E_{t,3}$</p>
	<p>G</p>  <p>Shear in the LR-plane with force in the longitudinal direction Test ID: S-1 Specimens tested: 6 Strength: $f_{v,21}$ Shear modulus: G_{21}</p>	<p>H</p>  <p>Shear in the LT-plane with force in the longitudinal direction Test ID: S-3 Specimens tested: 6 Strength: $f_{v,31}$ Shear modulus: G_{31}</p>	<p>I</p>  <p>Shear in the TL-plane with force in the tangential direction (rolling) Test ID: S-5 Specimens tested: 6 Strength: $f_{v,32}$ Shear modulus: G_{32}</p>
Shear	<p>J</p>  <p>Shear in the TR-plane with force in the tangential direction Test ID: S-2 Specimens tested: 6 Strength: $f_{v,12}$ Shear modulus: G_{12}</p>	<p>K</p>  <p>Shear in the RT-plane with force in the radial direction Test ID: S-4 Specimens tested: 6 Strength: $f_{v,13}$ Shear modulus: G_{13}</p>	<p>L</p>  <p>Shear in the RL-plane with force in the radial direction Test ID: S-6 Specimens tested: 6 Strength: $f_{v,23}$ Shear modulus: G_{23}</p>
	<p>M</p>  <p>Bending parallel to the grain (in the longitudinal direction) Test ID: B-1 Specimens tested: 4 Strength: $f_{m,1}$ Modulus of elasticity: $E_{m,1}$</p>	<p>N</p>  <p>Bending perpendicular to the grain (in the tangential direction) Test ID: B-2 Specimens tested: 4 Strength: $f_{m,2}$ Modulus of elasticity: $E_{m,2}$</p>	
Bending			

Figure 4.4: Overview of the tests carried-out in this experimental investigation.

4.4. METHODS

4.4.1. GENERAL

The tests were conducted in accordance with the standards EN 408 [131] and EN 789 [132], the strength and stiffness values were estimated following the procedures established in these standards. The coefficient of variation and the 5-percentiles (5-p) values were calculated according to EN 14358 [133].

All the tests were carried out at room temperature conditions. The moisture content of the LVL specimens was measured using a capacitive moisture sensor, and the air humidity and temperature were also measured using a digital sensor. Both sensors were from Ahlborn, the sensor FHA 696 MF for timber moisture and the sensor FHAD46-Cx for air humidity and temperature. The data logger ALMEMO 2590 was used to process the signals and read the values. The average measurements recorded were as follows: moisture content at 12%, air humidity at 46%, and room temperature at 23° C.

In accordance with standards EN 408 [131] and EN 789 [132] the loading procedures were as follows: (i) a monotonic load was applied to all specimens in displacement-controlled mode, and (ii) specific loading rates were defined for each test to ensure that specimen failure occurred within a specific time frame of 300 ± 120 seconds.

For the tension and shear tests custom apparatus were designed. For tension tests, the custom apparatus consist of clamping steel plates in which bolts were used to apply pressure on the specimen, in addition, glue was applied to prevent slip which could cause drops in forces during the tests. For shear tests, the custom apparatus consist of (i) a set of bearings that allow to introduce the loading to the specimen with an inclination of 14° with respect to the vertical, such that shear failure is induced through the specimen, and (ii) steel plates as recommended in EN 408 [131], these plates were glued to the specimen in two parallel faces. Further details of these devices have been included in the respective sections

Preliminary tests were conducted to validate the performance of the devices and to define a suitable glue for the tension and shear tests. Two types of glue were tested: (i) two-part epoxy glue (Würth ESK-50), and (ii) methylmethacrylate glue (Würth MAK 38). It was determined that the two-part epoxy glue exhibited superior resistance at the glued interface and a shorter curing time for this specific application. Consequently, the two-part epoxy glue (Würth ESK-50) was selected for use in both tensile and shear tests to effectively bond steel and LVL surfaces.

4.4.2. COMPRESSION TESTS

The compression tests were performed in the longitudinal (C-1), tangential (C-2) and radial (C-3) directions. The specimens' dimensions are shown in Figure 4.5. In the tests C-1 and C-2, a small preload of 5 kN and 2 kN respectively was applied to the specimens, then, the load was applied at a rate of 0.6 mm/min and 1.5 mm/min respectively. In the tests C-3 no preload was applied, the loading rate was set to 4 mm/min.

Nine specimens were tested in C-1 tests, and six specimens in C-2 and C-3 tests. In the C-1 tests, initially, six specimens were tested and these tests were stopped at a load drop of 70 kN.

However, after analysing the results of these initial tests, it was decided to test three additional specimens up to the point of fracture, to obtain more detailed information about fracture and the softening branch of the stress-strain curve in the longitudinal direction.

The test setup of the compression tests is shown in Figure 4.6. The tests C-1 and C-2 were done in a compression testing machine with a capacity of 4 MN and the tests C-3 were done in a compression testing machine with a capacity of 300 kN, both machines from TESTING Bluhm & Feuerherdt GmbH.

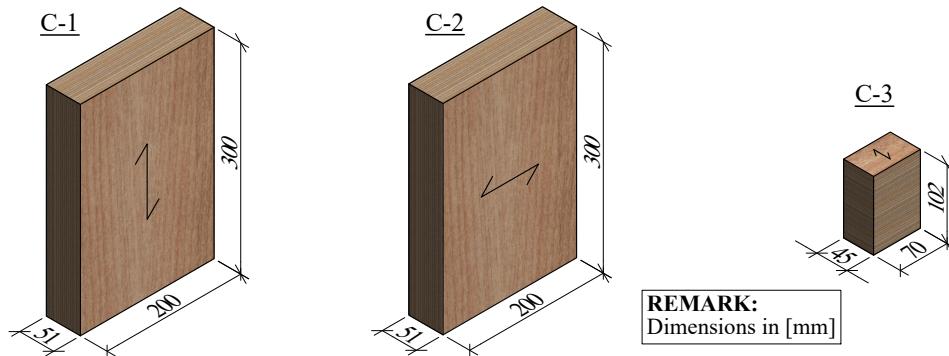


Figure 4.5: Dimensions of the specimens tested in compression.

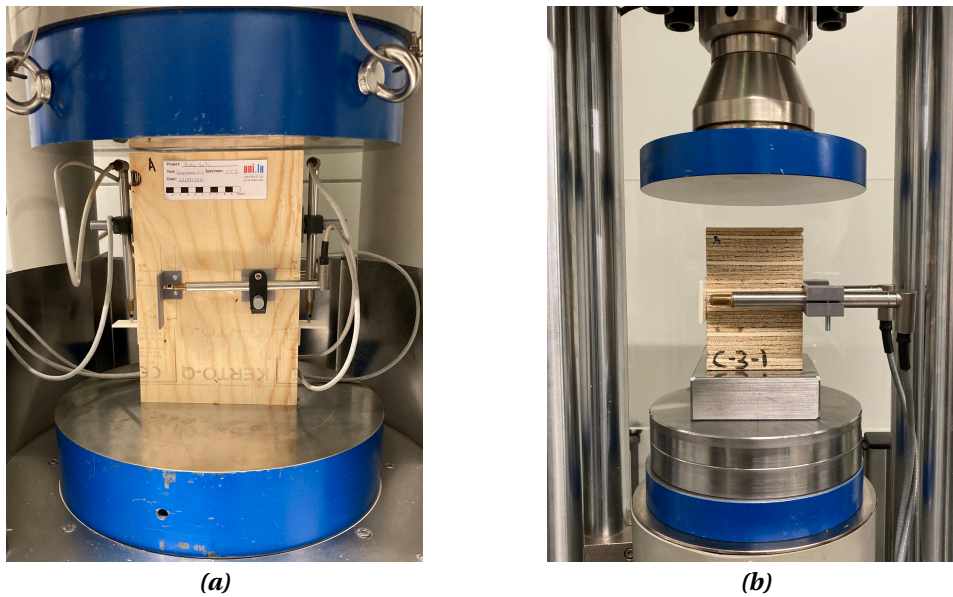


Figure 4.6: Test setups of: (a) compression tests C-1 and C-2, and (b) tests C-3.

4.4.3. TENSION TESTS

The tension tests were performed in the three orthogonal directions, longitudinal (T-1), tangential (T-2) and radial (T-3). Six identical specimens were tested for each direction. For tests T-1 and T-2 the specimens had a coupon shape to induce failure at the central part of the specimen and to measure the local displacements within a well-defined gauge length. The tests T-3 were done on rectangular prismatic specimens. The shapes and dimensions of the specimens tested in tension are shown in Figure 4.7. The tests were conducted in a universal machine for

compression and tension tests Form+Test UP 500 with a capacity of 100 kN.

Custom apparatus were designed and produced to carry out these tests. In the tests T-3 the load was transferred to the specimen through custom grips and steel blocks which were bonded to the specimen with a two-part epoxy glue (see Figure 4.8). The custom devices for the tests T-1 and T-2 (see Figure 4.9) consist of steel plates with a thickness of 20 mm with drilled holes to allow the installation of bolts in order to apply pressure and clamp the coupon-shape specimen from its tabs. To prevent slip and force drops due to slip of the specimen, a two-part epoxy glue was applied at the steel-timber interface of the custom gripping plates. Pictures of the tension tests setup are shown in Figure 4.10.

The load was applied at rates of 0.1 mm/min, 0.3 mm/min, and 0.2 mm/min, respectively for tests T-1, T-2 and T-3. Local displacements were measured with two LVDT sensors placed at parallel faces of the specimens. In the tests T-1 and T-2, local displacements were measured in the gage of the specimen within a length of 100 mm. In the tests T-3 the displacements were measured through the whole length of the specimen (i.e. 51 mm).

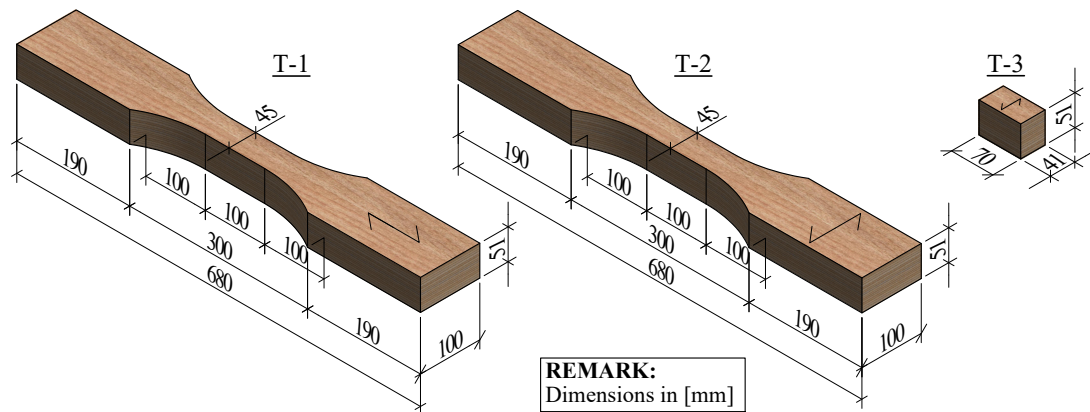


Figure 4.7: Dimensions of the specimens tested in tension.

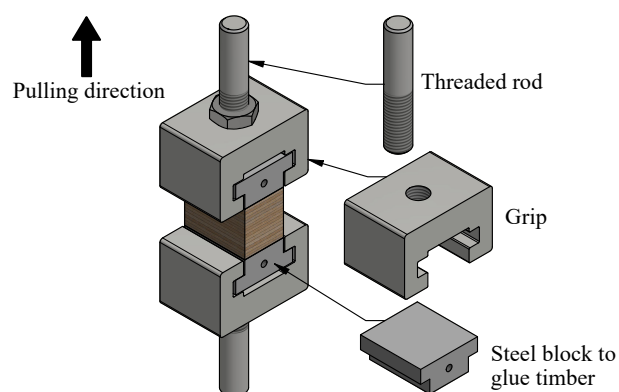


Figure 4.8: Custom devices for tension tests T-3.

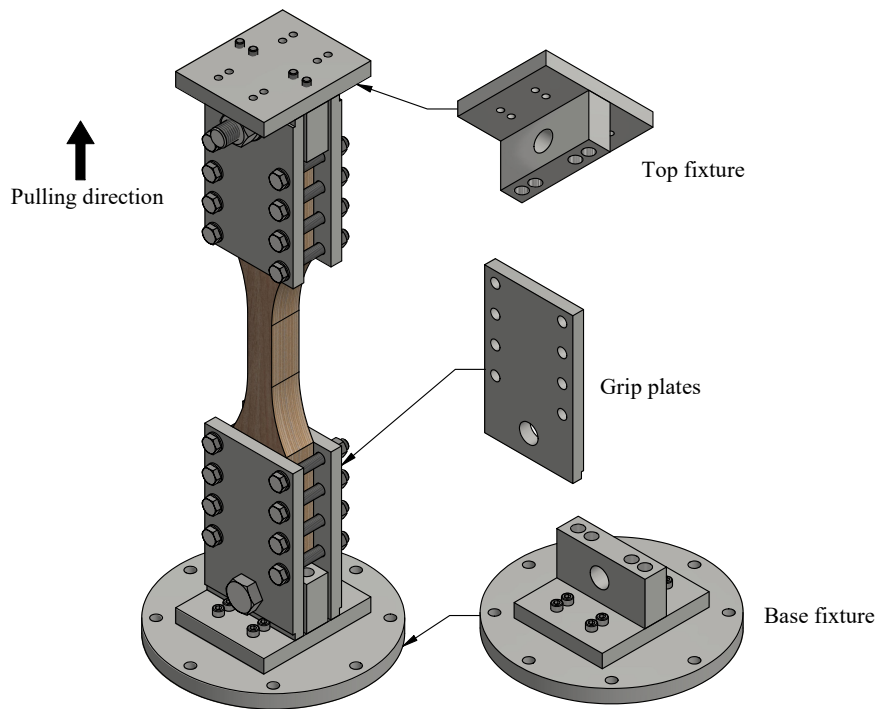
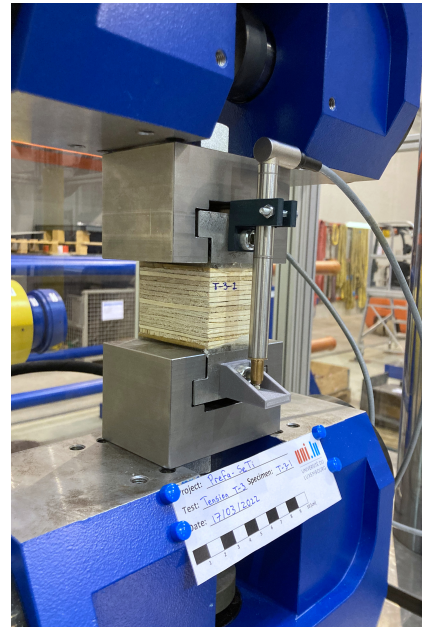


Figure 4.9: Custom devices for tension tests T-1 and T-2.



(a)



(b)

Figure 4.10: Test setups of: (a) tension tests T-1 and T-2, and (b) tests T-3.

4.4.4. SHEAR TESTS

Six different shear tests (i.e. S-1, S-2, S-3, S-4, S-5, S-6) were performed in the direction indicated in Figure 4.4. Six identical specimens were tested for each one of the directions, the dimensions of the specimens are shown in Figure 4.11. The specimens for tests S-4 and S-6 were formed by stacking and gluing 5 LVL cubic-shaped pieces with dimensions $51 \times 51 \times 51$ mm. The tests were conducted in a universal machine for compression and tension tests Form+Test UP 500 with a capacity of 100 kN.

Custom devices were designed and produced for these tests (see Figure 4.12). The top and bottom bearings have a channel which allows to place and remove a specimen at an inclination of 14° with respect to the vertical line of the applied load. Two steel plates ($275 \times 51 \times 10$ mm) with the shape recommended in EN 408 [131] were glued with two-part epoxy glue to the specimen in parallel faces of the specimen in the corresponding shear plane for each test. The differential displacement between the steel plates was measured with two LVDT sensors installed at parallel faces. The test setup is shown in Figure 4.13.

The loading rate for the tests S-1 and S-4 was set to 0.2 mm/min, for tests S-2 and S-3 it was set to 0.4 mm/min, for tests S-5 it was 0.5 mm/min, and for tests S-6 it was set to 0.6 mm/min.

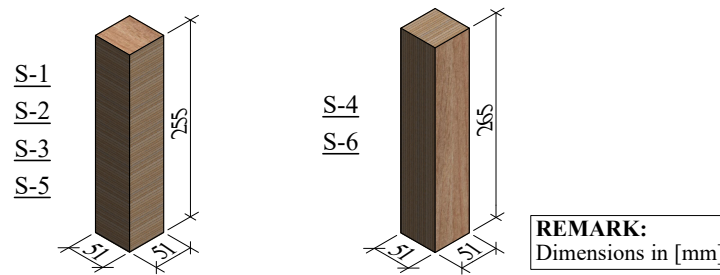


Figure 4.11: Dimensions of the specimens tested in shear.

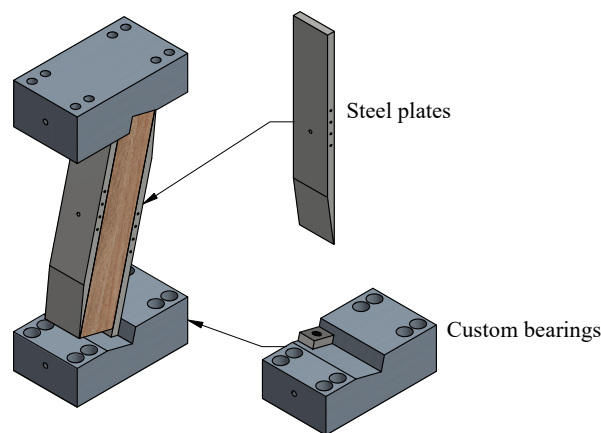


Figure 4.12: Custom devices for shear tests.

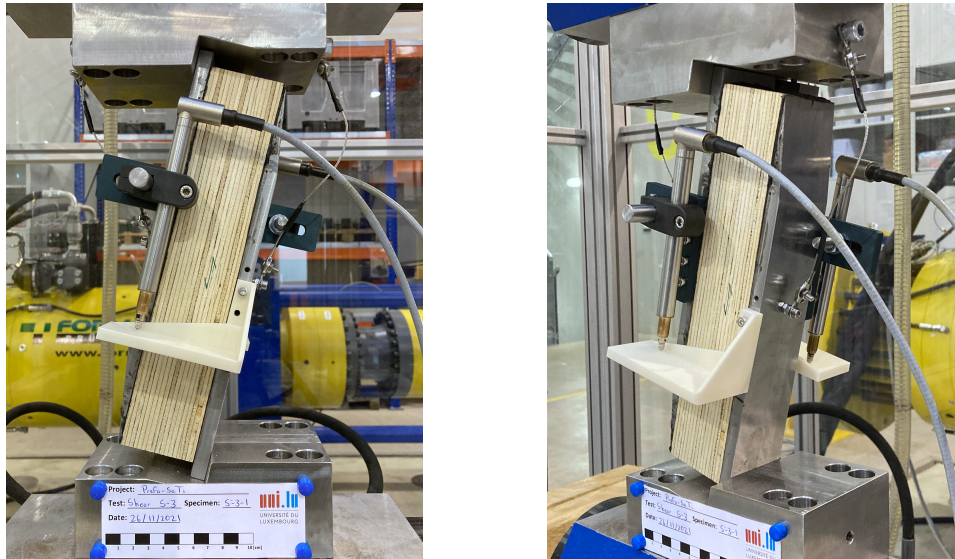


Figure 4.13: Shear tests setup.

4.4.5. BENDING TESTS

Simply supported panels were tested in 4-point bending. Two different bending tests were executed, flatwise bending parallel to the grain (B-1), and flatwise bending perpendicular to the grain (B-2). Four identical specimens with dimensions $1200 \times 150 \times 51$ mm (see Figure 4.14) were tested for each type of test. The load was applied at rates of 4.2 mm/min and 4.8 mm/min for tests B-1 and B-2 respectively. The deflection of the panels was measured at midspan at both sides of the panels. The tests were carried out in a machine for bending tests with a capacity of 300 kN from TESTING Bluhm & Feuerherdt GmbH. The positions of the loading points and the supports are depicted in Figure 4.15 and the test setup is illustrated in Figure 4.16.

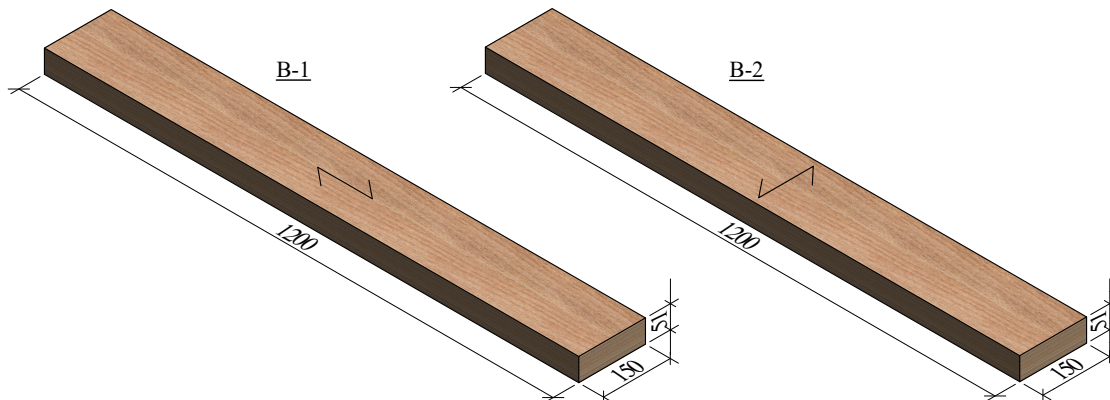


Figure 4.14: Dimensions of the specimens tested in 4-point bending.

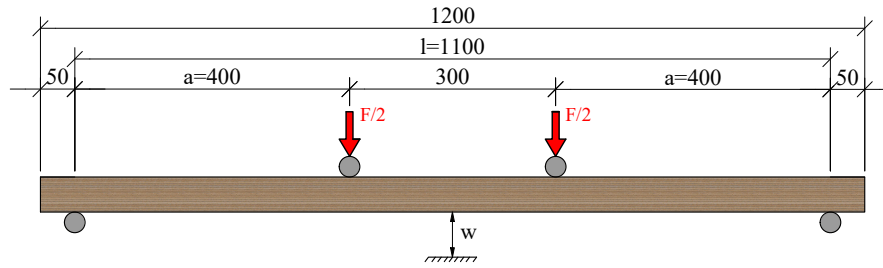


Figure 4.15: Elevation view of the positions of the loading points and the supports of the bending tests.

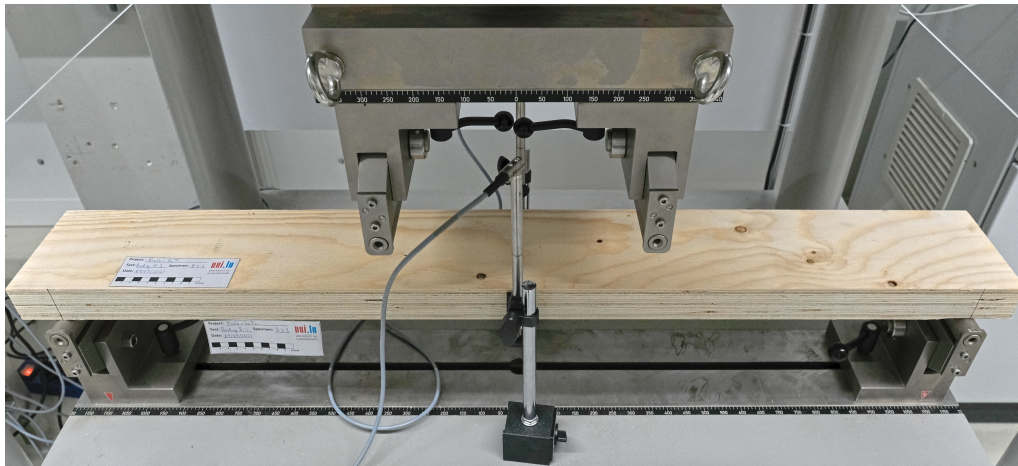


Figure 4.16: Test setup of the bending tests.

4.5. RESULTS AND DISCUSSION

4.5.1. COMPRESSION TESTS

The stress-strain curves of the compression tests in the three main orthogonal directions are depicted in Figure 4.17 and some of the tested specimens are illustrated in Figure 4.18. The response of the material in the longitudinal direction (tests C-1), was characterized by an initial linear monotonic increasing stress-strain relationship, followed by a non-linear response, after the peak a softening branch developed. Out of the nine specimens that were tested in C-1 tests, only three were brought to rupture. After reaching the peak load, crushing of the fibres at the mid-height of the specimen, followed by delamination and opening of the veneers was observed. In some specimens, shear failure was observed, these specimens showed an inclined crack of crushed veneers through their thickness, with an inclination of about 45°.

The specimens tested in the tangential direction (tests C-2), also exhibited an initial linear behaviour followed by a hardening branch and softening after the peak. The tests were stopped before reaching the rupture. In the radial direction (tests C-3), the tested specimens showed an initial linear behaviour followed by a hardening region of increasing stress with strain. In this direction LVL exhibited a large deformation capacity in compression.

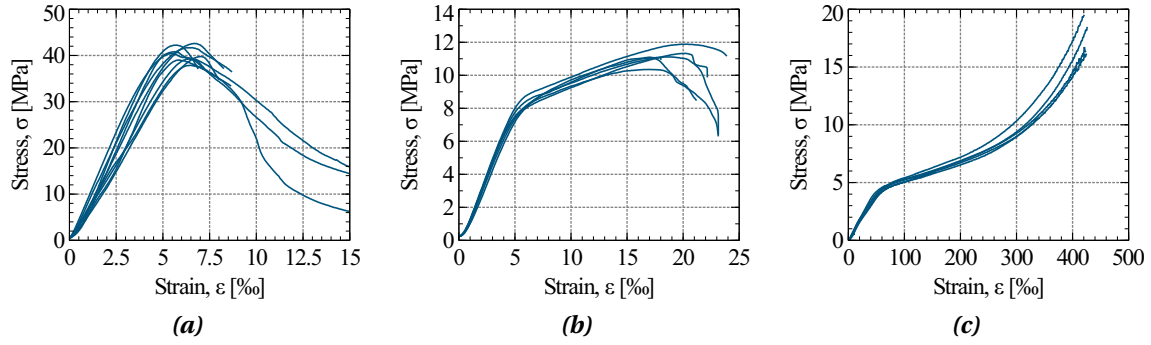


Figure 4.17: Stress-strain plots of the compression tests (a) C-1, (b) C-2, and (c) C-3.

4

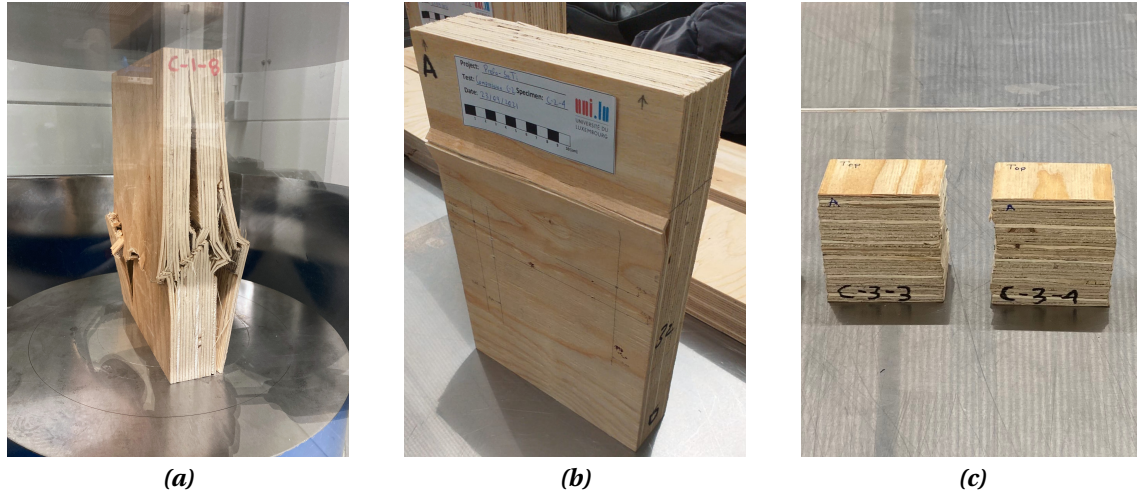


Figure 4.18: Pictures of specimens tested in compression (a) C-1, (b) C-2, and (c) C-3.

4.5.2. TENSION TESTS

The stress-strain plots for the tension tests conducted in the three main orthogonal directions are presented in Figure 4.19. In both the longitudinal (tests T-1) and tangential direction (tests T-2) tensile tests, the stress-strain curves exhibited an initial linear relationship, wherein stresses increased with strain. Subsequently, the specimens reached a maximum force, and failure of the veneers occurred. Following this peak, the stress-strain curve underwent a sharp turn, with stresses decreasing at varying rates across all specimens. Most of the specimens tested in the radial direction (tests T-3) displayed an initial linear stress-strain relationship, characterized by increasing stresses with strain. This was followed by a transition to non-linear behaviour, along with a rapid force drop immediately after reaching the peak load, indicating specimen failure.

Figure 4.20 depicts pictures of specimens tested in shear at the point of failure. In the case of specimens tested in the longitudinal direction (T-1), the veneers exhibited a gradual tension failure, occurring at various locations without localization to a specific section. Consequently, in some specimens, the post-peak load drop was relatively gradual, and in others, a brief hardening branch emerged after the load drop. In contrast, during the tensile tests conducted in the tangential direction (T-2), in some specimens the failure was concentrated in a specific section

due to the tension failure of the veneers. Furthermore, in the tensile tests conducted in the radial direction (T-3), the observed failure mode was in some cases localized at a well-defined horizontal plane. At this plane, the fibres of a specific wood layer were pulled apart. In other cases the tensile force induced shear failure through the veneers of the specimen.

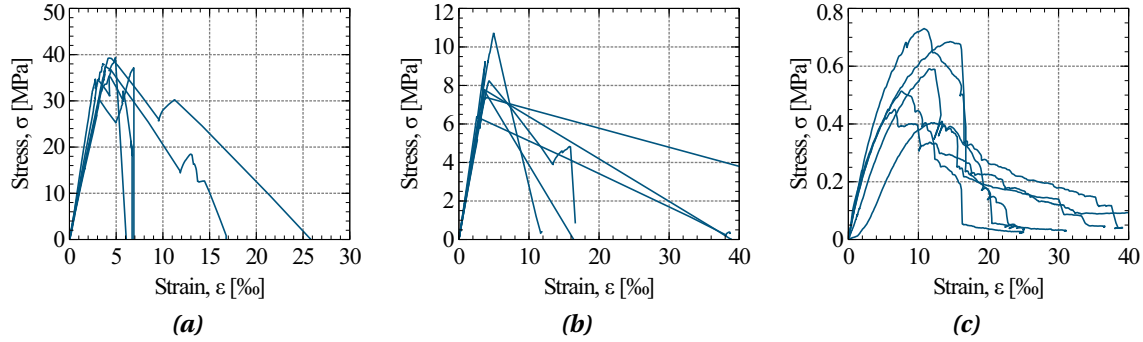


Figure 4.19: Stress-strain plots of the tension tests (a) T-1, (b) T-2, and (c) T-3.

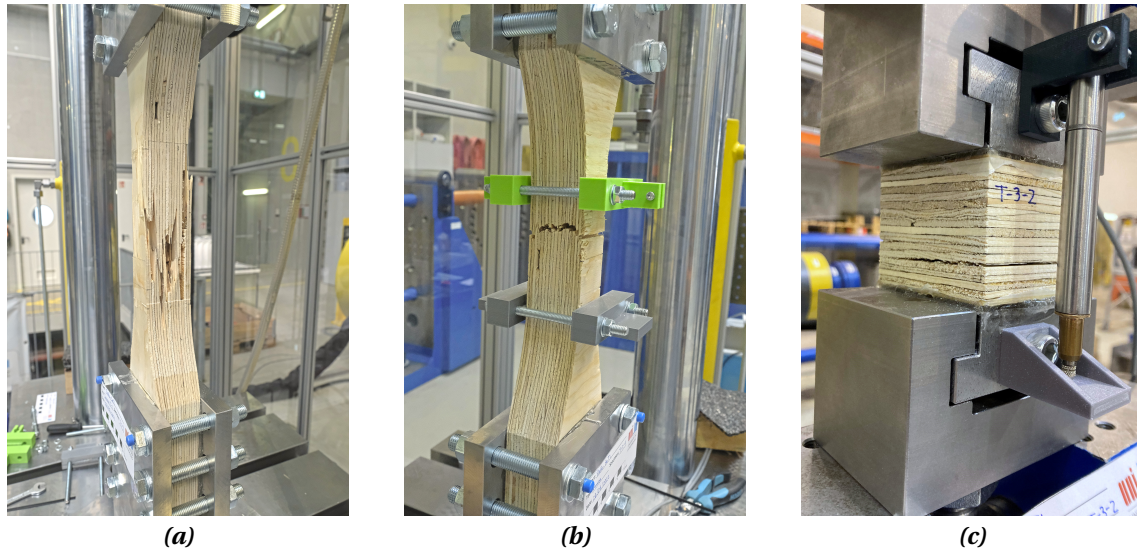


Figure 4.20: Pictures of specimens tested in tension (a) T-1, (b) T-2, and (c) T-3.

4.5.3. SHEAR TESTS

The shear stress vs. shear strain plots for the six types of shear tests conducted in this experimental study (see Figure 4.4) are presented in Figure 4.21. In each of the six defined types of shear tests (see Figure 4.4), six specimens were tested. Nevertheless, in the case of tests S-2, two of the specimens experienced failures at the bonding steel-timber interface. Similarly, in tests S-3, one specimen exhibited glue failure. Consequently, the results of these particular tests were excluded from the calculations and were not considered in the final analysis.

Generally, the stress-strain responses of the tested samples followed a similar pattern. There was an initial linear increase in stress with increasing strain, followed by a subsequent force drop that indicated specimen failure. Notably, in tests S-1 and S-2, following this force drop, a plateau phase was observed in which there was no further increase or decrease in load with

increasing strain.

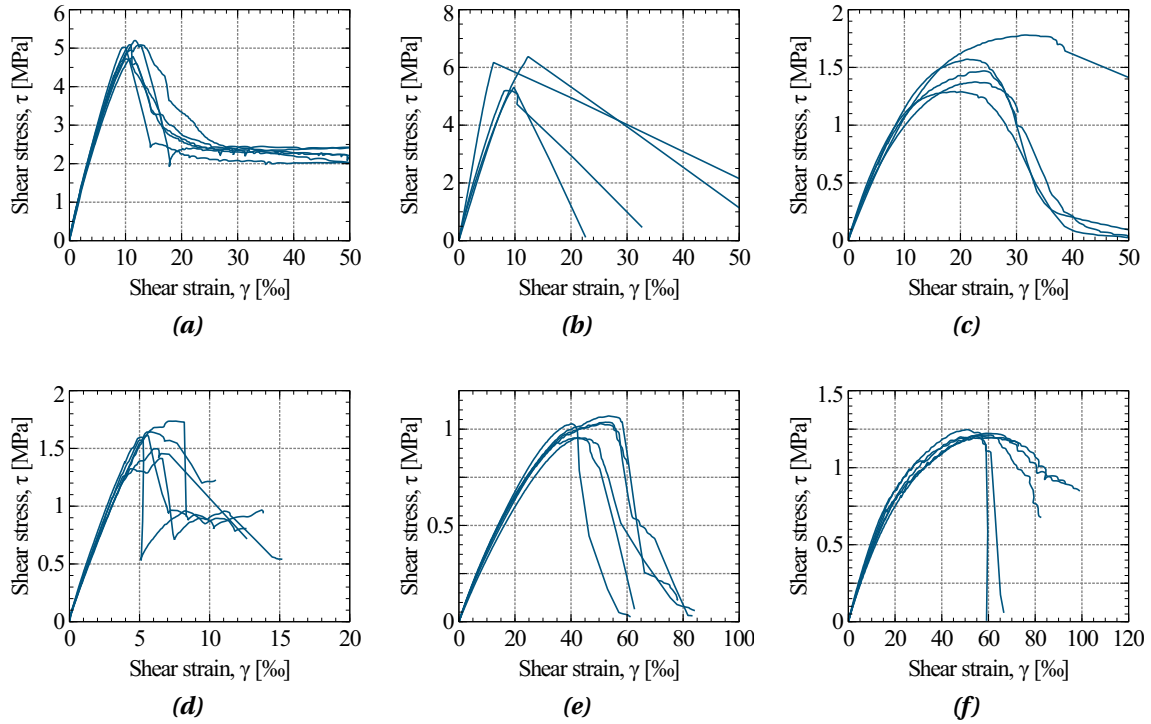


Figure 4.21: Stress vs. shear strain curves of the shear tests: (a) S-1, (b) S-2, (c) S-3, (d) S-4, (e) S-5, and (f) S-6.

Figure 4.22 presents pictures showcasing typical failure modes of the tested specimens. In the case of tests S-1, the specimens exhibited a vertical shear plane extending from the top to the bottom. However, this plane did not cut straight through the thickness of the specimen, resulting in the specimen remaining in one piece, with friction between the cut veneers preventing separation. In the tests S-2, the shearing planes were horizontal and followed the grain direction. The failure mode observed in the tests S-3 was localized to a single veneer in the vertical direction of the specimen, with shear failure occurring along that specific wood layer. For specimens in tests S-4, the failure occurred along a cutting plane aligned horizontally with one of the LVL layers. In the case of tests S-5, the failure crack due to the induced shear propagated from one corner on the top of the specimen to the opposite corner on the bottom. Lastly, in tests S-6, cracks appeared throughout the wood veneers of the specimen, resulting in gradual softening and eventual rupture through some of the layers.

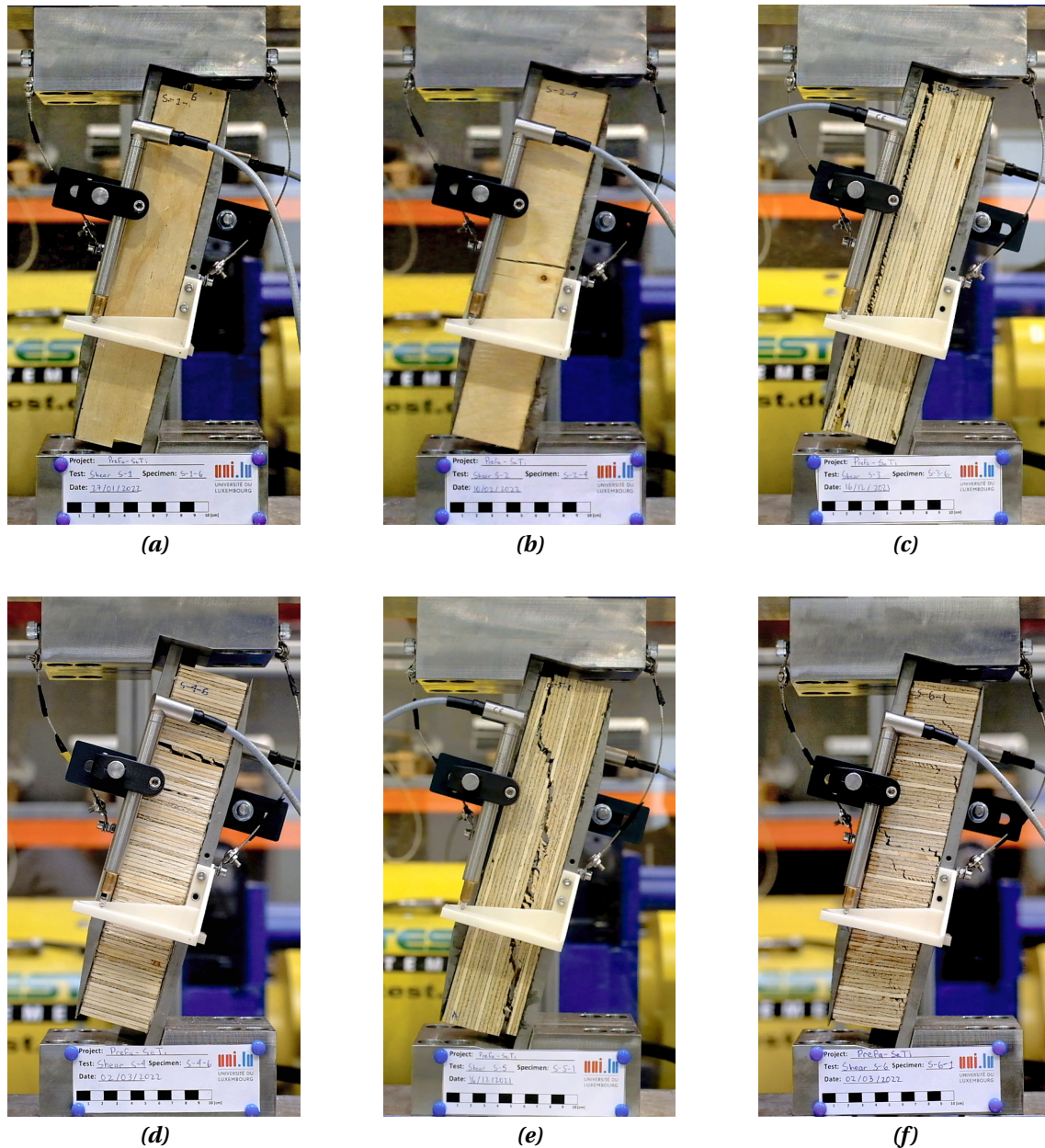


Figure 4.22: Pictures of specimens tested in shear: (a) S-1, (b) S-2, (c) S-3, (d) S-4, (e) S-5, and (f) S-6.

4.5.4. BENDING TESTS

The load-deflection curves (see Figure 4.23) for two types of bending tests are presented in this investigation: (i) bending flatwise parallel to the grain in the longitudinal direction (B-1 tests), and (ii) bending flatwise perpendicular to the grain in the tangential direction (B-2 tests). The peak loads achieved in these two types of tests differ significantly in magnitude, with B-1 tests reaching peak loads approximately five times greater than those observed in B-2 tests. Nevertheless, the specimens of both test types exhibited a similar load-slip response pattern. Initially, midspan deflection increased linearly up to the point of peak load, followed by a subsequent force drop attributed to the failure of some veneers.

In some specimens, following this initial drop, the panel exhibited the ability to carry additional load, resulting in a short branch where load increased in tandem with midspan deflection. Ultimately, a sudden load drop marked the failure of the specimen.

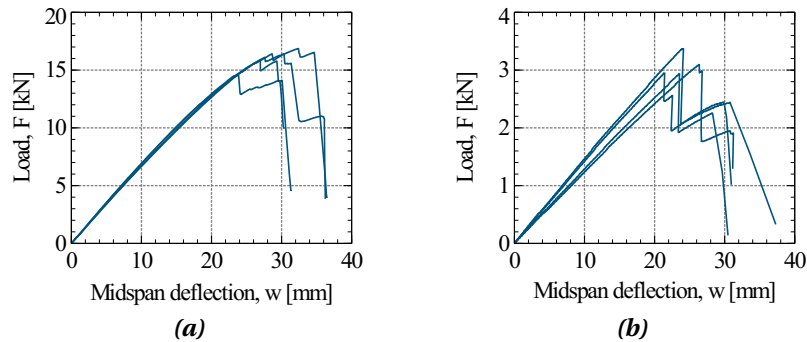


Figure 4.23: Load-deflection curves of bending tests (a) B-1 and (b) B-2.

Pictures of some of the tested specimens are presented in Figure 4.24. In the bending tests in the longitudinal direction B-1, gradual failure of the bottom fibres was observed occurring at different locations within the region of the points of load application. A similar failure mode was observed in the bending tests conducted in the tangential direction BT-2, where the failure initiated at the bottom fibres near one of the points of load application.

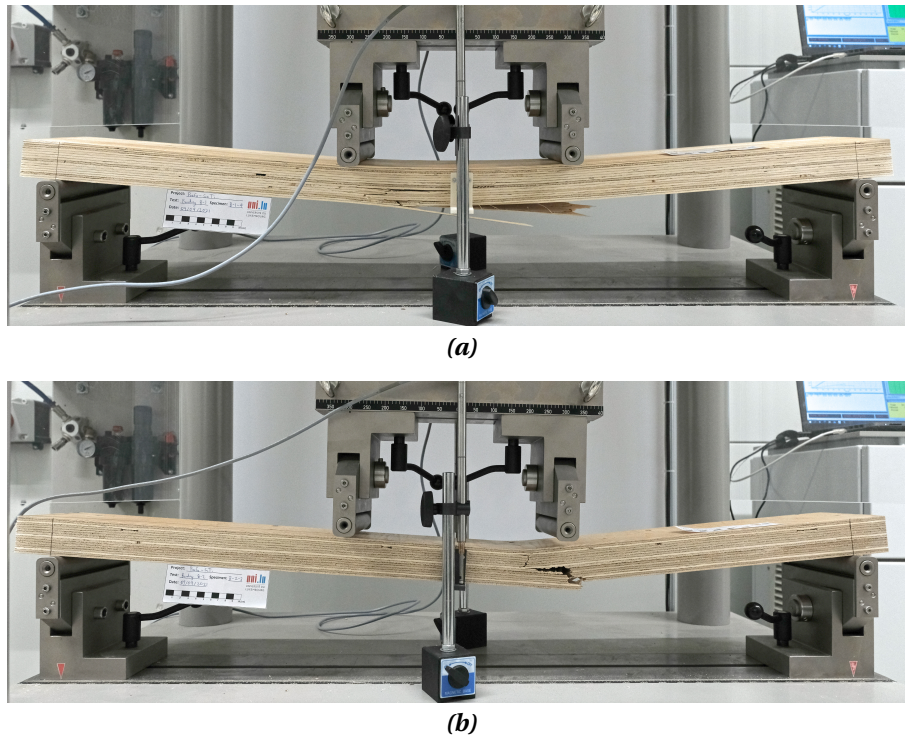


Figure 4.24: Load-deflection curves of bending tests (a) B-1 and (b) B-2.

4.5.5. DERIVED MECHANICAL PROPERTIES

COMPRESSION: STRENGTH AND MODULUS OF ELASTICITY

The calculation of the strength (f_c) and the modulus of elasticity (E_c) in compression tests was done according to the formulas in Equation 4.1 and Equation 4.2, as specified in EN 408 [131] and EN 789 [132]. Figure 4.25 illustrates the parameters considered in these formulas. Table 4.1 summarizes the derived strength and modulus of elasticity values in compression for the three tested orthogonal directions.

$$f_c = \frac{F_{max}}{A} \quad (4.1)$$

$$E_c = \frac{(F_2 - F_1)l_c}{(u_2 - u_1)A} \quad (4.2)$$

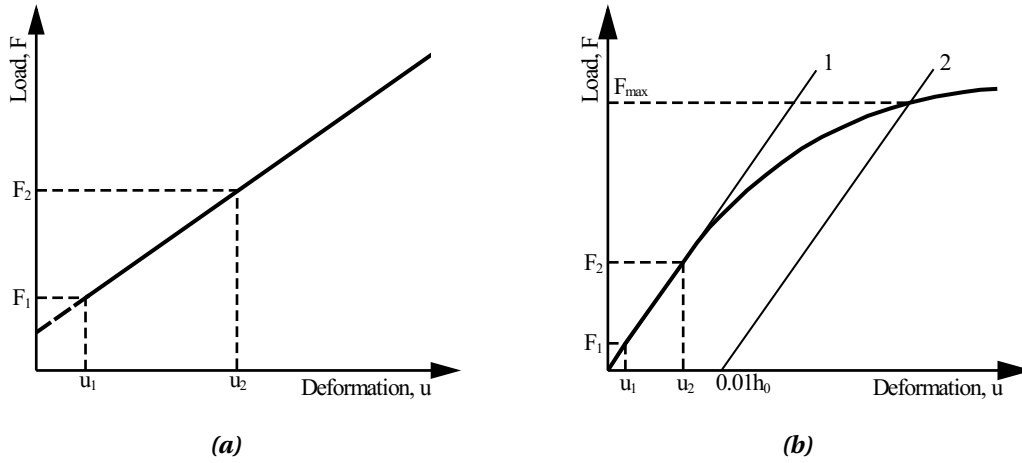


Figure 4.25: Plots illustrating the parameters of the formulas in Equation 4.1 and Equation 4.2 for: (a) compression tests C-1 and C-2, and (b) C-3.

The determination of the modulus of elasticity for compression tests (C-1 and C-2), was done by considering a load increment ($F_2 - F_1$) between 10% and 40% of the maximum applied load (F_{max}) as illustrated in Figure 4.25a.

In compression in the radial direction (C-3) the load-deformation curves differ from the typical curves obtained in C-1 and C-2 tests. In this case, the hardening branch increases monotonically and there is no clear turning point in which a maximum load is reached followed by softening and failure. Therefore, a different iterative procedure is defined for these tests according to EN 408 [131] as follows:

1. Using the test results plot the load-deformation curve in the form shown in Figure 4.25b.
2. Calculate F_1 ($0.1F_{max}$) and F_2 ($0.4F_{max}$) and determine where these values intersect the load-deformation curve.
3. Through these two points draw the straight line 1 as shown in Figure 4.25b.
4. Parallel to line 1, draw line 2 having its origin at load $F = 0$ and at a distance from it

equivalent to a deformation of $0.1h_0$ as shown in Figure 4.25b, where h_0 is the initial height of the specimen.

5. The intersection between line 2 and the curve of the test results is taken as F_{max} . If the value of F_{max} as determined is within 5% of the initially F_{max} value estimated in step 2, then that value may be used to determine the compressive strength; otherwise, repeat the procedure until a value of F_{max} within that tolerance is obtained.

Table 4.1: Derived strength and modulus of elasticity of LVL in compression.

Compression tests C-1			Compression tests C-2			Compression tests C-3		
ID	$f_{c,1}$ [MPa]	$E_{c,1}$ [MPa]	ID	$f_{c,2}$ [MPa]	$E_{c,2}$ [MPa]	ID	$f_{c,3}$ [MPa]	$E_{c,3}$ [MPa]
C-1-1	40.8	9 091.5	C-2-1	11.1	1 765.7	C-3-1	4.2	84.5
C-1-2	42.6	7 691.1	C-2-2	11.9	1 834.3	C-3-2	3.9	97.1
C-1-3	39.0	6 627.3	C-2-3	11.1	1 786.9	C-3-3	4.4	98.2
C-1-4	42.3	9 807.6	C-2-4	11.3	1 728.3	C-3-4	4.2	96.8
C-1-5	39.8	6 357.9	C-2-5	11.1	1 630.0	C-3-5	4.0	99.3
C-1-6	41.7	8 693.0	C-2-6	10.4	1 841.7	C-3-6	3.2	97.1
C-1-7	40.4	9 441.0	-	-	-	-	-	-
C-1-8	39.3	6 355.1	-	-	-	-	-	-
C-1-9	37.9	7 189.3	-	-	-	-	-	-
Mean	40.4	7 917.1	Mean	11.1	1 764.5	Mean	4.0	95.5
CV	3.9%	17.3%	CV	4.4%	4.4%	CV	10.6%	5.7%
5-p	36.1	10 626.5	5-p	9.8	1 737.9	5-p	3.0	93.8

TENSION: STRENGTH AND MODULUS OF ELASTICITY

The calculation of the the strength (f_t) and the modulus of elasticity (E_t) in tension tests was done according to the formulas in Equation 4.3 and Equation 4.4, as specified in EN 408 [131] and EN 789 [132]. Figure 4.26 illustrates the parameters considered in these formulas. Table 4.2 summarizes the derived strength and modulus of elasticity values in tension for the three tested orthogonal directions.

The determination of the modulus of elasticity for tension tests, was done by considering a load increment ($F_2 - F_1$) between 10% and 40% of the maximum applied load (F_{max}) as illustrated in Figure 4.26.

$$f_t = \frac{F_{max}}{A} \quad (4.3)$$

$$E_t = \frac{(F_2 - F_1)l_t}{(u_2 - u_1)A} \quad (4.4)$$

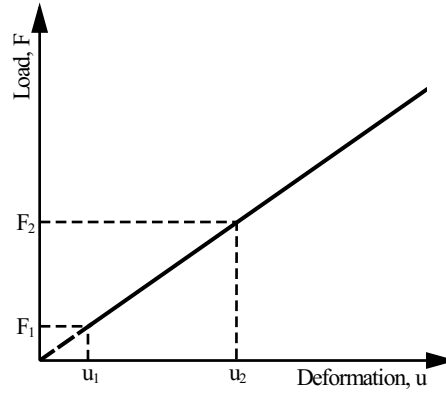


Figure 4.26: Plot illustrating the parameters of the formulas in Equation 4.3 and Equation 4.4 for tension tests.

Table 4.2: Derived strength and modulus of elasticity of LVL in tension.

Tension tests T-1			Tension tests T-2			Tension tests T-3		
ID	$f_{t,1}$ [MPa]	$E_{t,1}$ [MPa]	ID	$f_{t,2}$ [MPa]	$E_{t,2}$ [MPa]	ID	$f_{t,3}$ [MPa]	$E_{t,3}$ [MPa]
T-1-1	38.1	13 898.6	T-2-1	7.4	2 093.1	T-3-1	0.59	75.0
T-1-2	37.5	9 708.5	T-2-2	8.3	2 028.6	T-3-2	0.69	92.5
T-1-3	39.3	9 841.1	T-2-3	6.6	2 008.6	T-3-3	0.40	50.0
T-1-4	35.2	10 901.1	T-2-4	7.8	2 266.7	T-3-4	0.45	104.5
T-1-5	39.4	10 425.9	T-2-5	10.7	2 280.6	T-3-5	0.73	116.7
T-1-6	37.2	9 304.8	T-2-6	9.3	2 521.9	T-3-6	0.51	113.7
Mean	37.8	10 680.0	Mean	8.3	2 199.9	Mean	0.56	92.1
CV	4.1%	15.7%	CV	17.7%	8.9%	CV	23.0%	27.9%
5-p	34.1	10 174.8	5-p	5.5	2 140.8	5-p	0.31	84.3

SHEAR: STRENGTH AND SHEAR MODULUS

The calculation of the the shear strength (f_v) and the shear modulus (G) in shear tests was done according to the formulas in Equation 4.5 and Equation 4.6, as specified in EN 408 [131] and EN 789 [132]. Figure 4.27 illustrates the parameters considered in these formulas. Table 4.3 summarizes the derived shear strength and shear modulus values for the six shear planes tested in this investigation.

The determination of the modulus of elasticity for shear tests, was done by considering a load increment ($F_2 - F_1$) between 10% and 40% of the maximum applied load (F_{max}) as illustrated in Figure 4.27.

$$f_v = \frac{F_{max} \cdot \cos \alpha_v}{l_v \cdot b_v} \quad (4.5)$$

$$G = \frac{\Delta \tau}{\Delta \gamma} = \frac{(F_2 - F_1) \cdot \cos \alpha_v \cdot t_v}{l_v \cdot b_v \cdot (x_2 - x_1)} \quad (4.6)$$

The computation of the shear modulus from shear tests (S-1 to S-6) was done by considering a load increment ($F_2 - F_1$) between 10% and 40% of the maximum applied load (F_{max}) as illustrated in Figure 4.27.

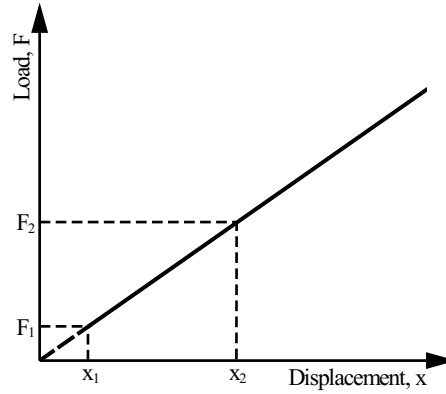


Figure 4.27: Plot illustrating the parameters of the formulas in Equation 4.5 and Equation 4.6 for shear tests.

Table 4.3: Derived shear strength and shear modulus of LVL.

Shear tests S-1			Shear tests S-2			Shear tests S-3		
ID	$f_{v,21}$ [MPa]	$G_{v,21}$ [MPa]	ID	$f_{v,12}$ [MPa]	G_{12} [MPa]	ID	$f_{v,31}$ [MPa]	G_{31} [MPa]
S-1-1	5.2	565.9	S-2-1	5.2	747.8	S-3-1	1.4	113.7
S-1-2	4.8	568.2	S-2-2	6.2	1 051.3	S-3-2	1.3	139.7
S-1-3	5.0	602.7	S-2-3	-	-	S-3-3	1.6	124.9
S-1-4	5.1	571.2	S-2-4	6.4	622.3	S-3-4	1.8	111.4
S-1-5	5.1	635.5	S-2-5	-	-	S-3-5	-	-
S-1-6	4.7	553.4	S-2-6	5.3	643.5	S-3-6	1.5	126.8
Mean	5.0	582.8	Mean	5.8	765.2	Mean	1.5	123.3
CV	3.8%	5.3%	CV	10.3%	25.9%	CV	12.7%	9.2%
5-p	4.4	573.6	5-p	4.2	691.2	5-p	1.0	119.5

Shear tests S-4			Shear tests S-5			Shear tests S-6		
ID	$f_{v,13}$ [MPa]	G_{13} [MPa]	ID	$f_{v,32}$ [MPa]	G_{32} [MPa]	ID	$f_{v,23}$ [MPa]	G_{23} [MPa]
S-4-1	1.6	324.4	S-5-1	1.03	34.5	S-6-1	1.20	41.0
S-4-2	1.6	348.6	S-5-2	1.04	35.0	S-6-2	1.25	51.0
S-4-3	1.4	347.5	S-5-3	0.95	33.5	S-6-3	1.21	47.3
S-4-4	1.6	377.7	S-5-4	1.07	35.5	S-6-4	1.21	43.8
S-4-5	1.5	336.0	S-5-5	1.03	35.8	S-6-5	1.20	48.8
S-4-6	1.7	323.7	S-5-6	0.96	31.3	S-6-6	1.22	44.7
Mean	1.6	343.0	Mean	1.01	34.3	Mean	1.21	49.1
CV	7.2%	5.9%	CV	4.6%	4.9%	CV	1.5%	7.9%
5-p	1.3	336.9	5-p	0.89	33.8	5-p	1.07	45.0

BENDING: STRENGTH AND GLOBAL MODULUS OF ELASTICITY

The calculation of the bending strength (f_m) and the global bending modulus of elasticity (E_m) in bending tests was done according to formulas 4.7 and 4.8, as specified in EN 408 [131] and EN 789 [132]. Figure 4.27 illustrates the parameters considered in these formulas. Table 4.4 summarizes the derived bending strength and global modulus of elasticity in bending values for the two types of bending included in this investigation.

$$f_m = \frac{3aF_{max}}{bh^2} \quad (4.7)$$

$$E_m = \frac{3al^2 - 4a^3}{2bh^3 \left(2 \cdot \frac{w_2 - w_1}{F_2 - F_1} - \frac{6a}{5Gbh} \right)} \quad (4.8)$$

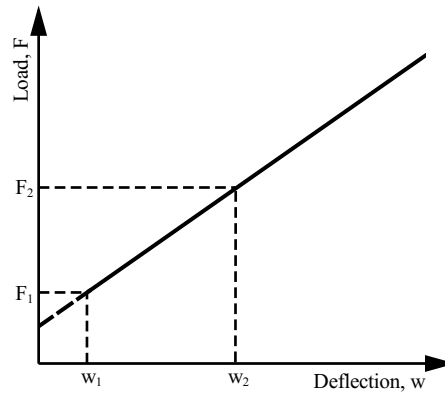


Figure 4.28: Plot illustrating the parameters of the formulas in Equation 4.7 and Equation 4.8 for bending tests.

Table 4.4: Derived bending strength and global modulus of elasticity in bending of LVL.

Bending tests B-1			Bending tests B-2		
ID	$f_{m,1}$ [MPa]	$E_{m,1}$ [MPa]	ID	$f_{m,2}$ [MPa]	$E_{m,2}$ [MPa]
B-1-1	44.9	10 390.8	B-2-1	9.0	1 894.6
B-1-2	48.8	9 989.0	B-2-2	10.4	2 157.7
B-1-3	51.9	10 308.9	B-2-3	9.1	2 128.0
B-1-4	50.5	10 086.2	B-2-4	9.5	1 839.6
Mean	49.0	10 193.7	Mean	9.5	2 005.0
CV	6.2%	1.8%	CV	6.5%	8.0%
5-p	40.8	10 003.1	5-p	7.8	1 944.7

4.5.6. SUMMARY OF DERIVED MECHANICAL PROPERTIES

A summary of the calculated strength and stiffness properties is summarized in Table 4.5 and Table 4.6 respectively. The values were computed according to EN 408 [131] and EN 789 [132].

Table 4.5: Summary of strength properties.

Strength property	Notation	From Figure 4.4	Strength [MPa]		CV [%]
			Mean	5-p	
Compression strength parallel to the grain, edgewise (in the longitudinal direction)	$f_{c,1}$	A	40.41	36.11	3.91
Compression strength perpendicular to the grain, edgewise (in the tangential direction)	$f_{c,2}$	B	11.14	9.83	4.44
Compression strength perpendicular to the grain, flatwise (in the radial direction)	$f_{c,3}$	C	3.99	2.99	10.64
Tension strength parallel to the grain, edgewise (in the longitudinal direction)	$f_{t,1}$	D	37.76	34.10	4.11
Tension strength perpendicular to the grain, edgewise (in the tangential direction)	$f_{t,2}$	E	8.33	5.47	17.68
Tension strength perpendicular to the grain, flatwise (in the radial direction)	$f_{t,3}$	F	0.56	0.31	23.04
Shear in the LR-plane with force in the longitudinal direction (edgewise shear parallel to the grain)	$f_{v,21}$	G	4.98	4.40	3.79
Shear in the LT-plane with force in the longitudinal direction (flatwise shear parallel to the grain)	$f_{v,31}$	H	1.50	1.03	12.69
Shear in the TL-plane with force in the tangential direction (flatwise shear perpendicular to the grain)	$f_{v,32}$	I	1.01	0.89	4.57
Shear in the TR-plane with force in the tangential direction (edgewise shear perpendicular to the grain)	$f_{v,12}$	J	5.76	4.16	10.28
Shear in the RT-plane with force in the radial direction (edgewise shear perpendicular to the grain)	$f_{v,13}$	K	1.58	1.32	7.17
Shear in the RL-plane with force in the radial direction (edgewise shear perpendicular to the grain)	$f_{v,23}$	L	1.21	1.07	1.51
Bending parallel to the grain in the longitudinal direction (flatwise bending parallel to the grain)	$f_{m,1}$	M	49.01	40.82	6.16
Bending perpendicular to the grain in the tangential direction (flatwise bending perpendicular to the grain)	$f_{m,2}$	N	9.51	7.83	6.53

The longitudinal direction of the LVL-C tested in this study, exhibited the best performance in terms of strength and stiffness for both tension and compression, followed by the tangential direction, and the radial direction which showed a very low stiffness and turned into non-linear plastic behaviour at quite small stresses. Similarly, the panels tested in bending performed the

best in the flatwise bending tests parallel to the grain, the bending strength and stiffness of the panels tested in flatwise bending perpendicular to the grain were about one fifth of the values obtained in the bending parallel to the grain.

Table 4.6: Summary of stiffness properties.

Stiffness property	Notation	From Figure 4.4	Stiffness [MPa]		CV [%]
			Mean	5-p	
MoE in compression parallel to the grain, edgewise (in the longitudinal direction)	$E_{c,1}$	A	7 917.08	7 626.51	17.29
MoE in compression perpendicular to the grain, edgewise (in the tangential direction)	$E_{c,2}$	B	1 764.47	1 737.85	4.44
MoE in compression perpendicular to the grain, flatwise (in the radial direction)	$E_{c,3}$	C	95.49	93.83	5.74
MoE in tension parallel to the grain, edgewise (in the longitudinal direction)	$E_{t,1}$	D	10 680.01	10 174.84	15.67
MoE in tension perpendicular to the grain, edgewise (in the tangential direction)	$E_{t,2}$	E	2 199.90	2 140.77	8.91
MoE in tension perpendicular to the grain, flatwise (in the radial direction)	$E_{t,3}$	F	92.05	84.30	27.88
Shear modulus in the LR-plane with force in the longitudinal direction (edgewise shear parallel to the grain)	$G_{v,21}$	G	582.82	573.59	5.25
Shear modulus in the LT-plane with force in the longitudinal direction (flatwise shear parallel to the grain)	$G_{v,31}$	H	123.26	119.48	9.23
Shear modulus in the TL-plane with force in the tangential direction (flatwise shear perpendicular to the grain)	$G_{v,32}$	I	34.27	33.75	4.86
Shear modulus in the TR-plane with force in the tangential direction (edgewise shear perpendicular to the grain)	$G_{v,12}$	J	765.22	691.18	25.87
Shear modulus in the RT-plane with force in the radial direction (edgewise shear perpendicular to the grain)	$G_{v,13}$	K	342.96	336.90	5.86
Shear modulus in the RL-plane with force in the radial direction (edgewise shear perpendicular to the grain)	$G_{v,23}$	L	49.09	44.99	7.90
Global MoE in bending parallel to the grain in the longitudinal direction (flatwise bending parallel to the grain)	$E_{m,1}$	M	10 193.74	10 003.05	1.84
Global MoE in bending perpendicular to the grain in the tangential direction (flatwise bending perpendicular to the grain)	$E_{m,2}$	N	2 004.94	1 944.65	8.04

4.5.7. MEAN STRESS-STRAIN CURVES FOR COMPRESSION AND TENSION

To compare the magnitude of the stresses and the stress-strain response in compression and tension in the three orthogonal directions, Figure 4.29 shows the mean stress-strain curves of the compression and tensile tests in the longitudinal, tangential, and radial directions. These curves were constructed by averaging the stress values for equal strains. Therefore, the maximum values presented in the plot do not necessarily match the compressive or tensile strength values presented in Table 4.5. This discrepancy occurs because the maximum stress values, which are considered for the computation of the strength, are not always reached at the same strains. Nevertheless, there is no apparent large deviation.

This plot clearly shows that the strongest direction in both tension and compression is the longitudinal direction, followed by the radial direction. Timber in the radial direction can withstand large deformations, but its strength in this direction is negligible compared to the strength in the longitudinal direction.

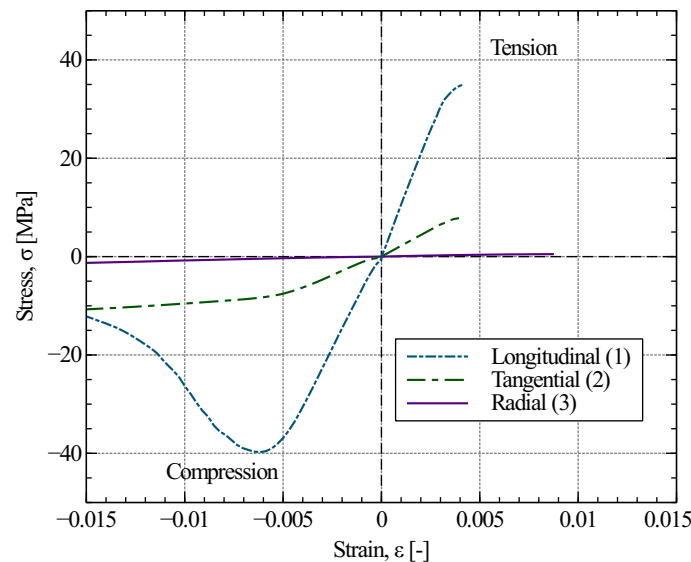


Figure 4.29: Mean curves for compression and tension in the three orthogonal directions.

ARTICLE 2

5

EXPERIMENTAL PUSH-OUT TESTS ON THE DEVELOPED SHEAR CONNECTIONS

5.1. INTRODUCTION

Shear connections constitute a critical component of composite structures, ensuring the integrity and effectiveness of composite action. The connectors maintain the components together, reduce their relative slip, transfer the shear forces, and enhance the overall stiffness and strength of the system.

The three demountable connections developed in this research project allow for disassembly and prevent crushing of the timber in the radial direction while optimal preloads of high-strength bolts can be attained. A detailed description of the connections is presented in Chapter 3, Section 3.3.

The load-bearing behaviour of the newly developed connections was investigated experimentally through push-out tests with a double-symmetric test setup, implementing LVL plates connected to HEB steel profiles. Three identical specimens were tested to assess each connection type, hence, a total of nine push-out tests were carried out. This chapter presents the details of the experimental campaign as well as the results and the discussion of the tests results.

5.2. OVERVIEW OF THE EXPERIMENTAL TESTING CAMPAIGN

The evaluation of the connections' performance involved a series of push-out tests aimed at assessing the load-slip characteristics of the three types of demountable shear connectors and determining their respective failure modes. The test setup was designed following the guidelines outlined in Eurocode 4 (EN 1994–1-1) [94] for push-out tests of steel-concrete connections, leading to the execution of double-symmetric push-out tests.

The experimental testing campaign consists of three series of push-out tests (POT), with each series corresponding to one shear connection type. Each series comprises three identical specimens, an overview of the tests is shown in Table 5.1. Specifically, POT1 covers connection type 1, POT2 tests connection type 2, and POT3 examines connection type 3.

Table 5.1: Overview of push-out tests carried out in this investigation.

Test series	Shear Connection	Test IDs	Specimen IDs
Push-out test series 1	Type 1 (SCT-1)	POT1	POT1-1
			POT1-2
			POT1-3
Push-out test series 2	Type 2 (SCT-2)	POT2	POT2-1
			POT2-2
			POT2-3
Push-out test series 3	Type 3 (SCT-3)	POT3	POT3-1
			POT3-2
			POT3-3

5

5.3. MATERIALS

5.3.1. LAMINATED VENEER LUMBER (LVL)

LVL is an engineered wood product formed by bonding and layering 3 mm thick wood veneers, creating wood panels with various dimensions and layups. Two standard layups are distinguished [13]: LVL-P, where veneer layers run parallel to each other, and LVL-C, with approximately 20% of veneer layers oriented perpendicular to the grain.

In this experimental investigation, crossband LVL-C from MetsäWood (i.e. Kerto-Q) [134] with a thickness of 144 mm were used to produce the timber plates (650×300×144 mm) of the push-out tests specimens. The layup of the panels consists of 48 veneers with a thickness of 3 mm as follows: II-IIIII-III-III-IIIII-II-IIIII-III-III-IIIII-II, where 'I' represents the veneers with the grain aligned in the longitudinal direction and '-' represents the cross veneers (i.e. veneers with the grain placed perpendicular to the grain of the 'I' veneers), Figure 5.1 shows the layup of the LVL used for the push-out tests. This LVL product is crafted with Scandinavian Spruce (i.e. Picea abies) wood. The cross veneers in the LVL matrix enhance the strength and stiffness of the timber elements in the direction perpendicular to the grain.

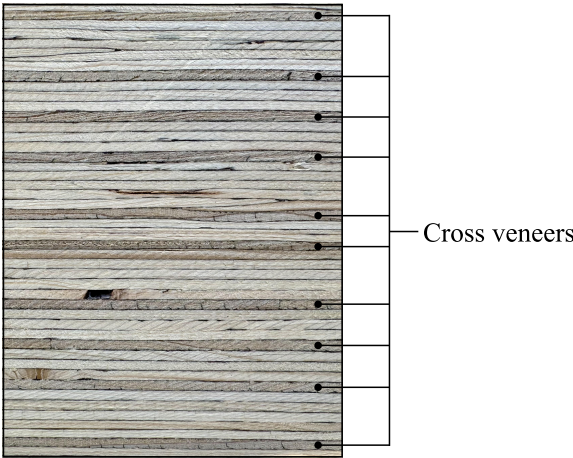


Figure 5.1: Layup of the crossband LVL with a thickness of 144 mm.

LVL and CLT are among the most suitable engineered wood products for steel-timber composite flooring applications. However, LVL was chosen for this study due to its low variability in properties, enhanced strength and stiffness, and efficient utilization of smaller diameter logs and low-grade timber. Additionally, since the shear connections were positioned near the timber's edge, which is susceptible to splitting failure, the cross veneers reinforce this region, preventing such failure.

The strength and stiffness properties of the LVL were obtained experimentally, the results are presented in Chapter 4, in Section 4.5. The mean density of these LVL panels is 510 kg/m^3 . Before the preparation of the plates for the assembly of the specimens the LVL panels were stored indoors at room temperature. The average moisture content of the LVL plates was 12%, it was measured using a capacitive moisture sensor from Ahlborn (sensor ID: FHA 696 MF) and data logger ALMEMO 2590.

5.3.2. STEEL PROFILES

The steel profiles used for the push-out test specimens were crafted from an I-shaped European hot-rolled section HEB 260 with steel grade S355 in accordance with EN 10025 [125], without coating or painting. The length of the steel profile was 700 mm in all the specimens. A capping steel plate S355 was welded to one end of the steel profile to transfer the load from the jack to the specimen. Eight coupon shape specimens were tested in tension, and were conducted according to EN ISO 6892-1 [135] in order to determine the mechanical properties of the structural steel S355 of the steel profiles. A mean yield strength of 399 MPa with a CV of 1.7%, a mean ultimate strength of 512 MPa with a CV of 1.7%, and a mean modulus of elasticity of 207 GPa with a CV of 1.9%, were obtained.

5.3.3. SHEAR CONNECTION DEVICES AND ROUND STEEL PLATES

The shear connection devices described in section 2 are depicted in Figure 5.2, they consist of a steel tube grade S460 according to EN 10025 [125] with an external diameter of 35 mm and a wall thickness of 6.3 mm. These tubes were welded to steel elements that differed based on the shear connection type. For SCT-1, a round steel plate was employed, while SCT-3 featured a rectangular plate, both made from steel grade S460. SCT-2 incorporated a Geka connector welded to the tube. None of these steel tubes or plates had coatings or paint.

Round steel plates, made of S460 steel, were placed beneath the bolt head and below standard washers to prevent uplift of the timber panels. SCT-1 and SCT-3 featured round plates with an outer diameter of 75 mm and a thickness of 10 mm, while SCT-2 utilized round plates with an outer diameter of 80 mm and a thickness of 5 mm. Four coupon shape specimens were tested in tension, and were conducted according to EN ISO 6892-1 [135] in order to determine the mechanical properties of the steel S460 of the shear connection devices. A mean yield strength of 526 MPa with a CV of 0.2%, a mean ultimate strength of 581 MPa with a CV of 0.3%, and a mean modulus of elasticity of 203 GPa with a CV of 1.6%, were obtained.



Figure 5.2: Components of the shear connections.

5.3.4. GEKA CONNECTORS

Connectors type C11 (i.e. Geka connectors) for bolts M20 (C11–80M20) complying with EN 912 [126] were used in shear connection type 2 (SCT-2), these connectors are shown in Figure 5.2. One Geka connector was welded to the steel tubes described in Section 5.3.3 and another connector was placed underneath the bolt head and the round steel plate. The Geka connectors were made of galvanized cast iron, they had an outer diameter of 80 mm, a hole with a diameter of 21 mm, and a total height (teeth and plate) of 15 mm.

5.3.5. SCREWS

Universal partial-thread screws (see Figure 5.2) were installed only in shear connection type 3 (SCT-3). The screws fix the shear connection device to the timber and make the connection more robust, they help to reduce slip and prevent crushing of wood at early loading stages. These universal partial-thread screws (ASSY 4 CSMP) made of stainless steel from Würth (ETA 11/0190) [127] with a diameter of 8 mm and a length of 140 mm were installed with an inclination of 60° with respect to the horizontal. According to the European technical approval (ETA) of the product (ETA 11/0190) [127], the characteristic tensile strength ($f_{t,k}$) is 21.5 kN and the characteristic yield moment ($M_{y,k}$) is 23 N·m.

5.3.6. BOLTS, WASHERS AND NUTS

High-strength partially threaded bolts M20 10.9 HV according to EN 14399 [128] (see Figure 5.2), with a diameter of 20 mm and a length of 210 mm, were used in the three shear connections. The tensile mechanical properties of the bolts were determined through tensile tests carried out on four coupon specimens

A flat washer with chamfer for high strength fittings and hot dip galvanisation in accordance with EN 14399 [128] was positioned under the head of the bolt and another washer was placed under the nut, the washers are shown in Figure 5.2. The washer has an outer diameter of 37 mm, an inner diameter of 21 mm and a thickness of 4 mm. The hexagon nuts (see Figure 5.2) used in the assemblies comply with EN 14399 [128], and were made with hot-dip galvanised steel class 10Z, the nuts had a height of 16 mm.

5.3.7. DIRECT TENSION INDICATORS (DTI)

The direct tension indicators (DTI) (see Figure 5.2) made of galvanized steel and manufactured by Turna-Sure, were placed under the washer at the bolt head side to ensure the minimum preload requirement was met. Before preloading the bolt, the protrusions of the DTI leave a gap between the DTI and the element placed next to it (e.g. washer, nut, bolt head), during the preloading the gap reduces (see Figure 5.3c), this gap is checked with a feeler gauge which has a calibrated thickness. The minimum preload has been reached when the minimum number of feeler gauge refusals as defined in EN 14399-9 [128] is observed.

5.4. BOLT PRELOAD CALIBRATION

In accordance to Eurocode 3 [129] and EN 1090-2 [130] the bolts were preloaded at 70% of its ultimate strength. The minimum preload of bolted assemblies ($F_{p,C}$) is estimated according to Equation 5.1:

$$F_{p,C} = 0.7 f_{ub} A_s \quad (5.1)$$

This level of preload is required for slip resistant connections and for all other preloaded connections unless a lower level of preload is specified. In all the connection assemblies of this research project, the target was to achieve the minimum preload specified above (i.e. 70% of the ultimate strength of the bolt). Therefore, the required preload $F_{p,C}$ for the M20 10.9 bolts used in this investigation's connection assemblies was 172 kN.

There are different methods to ensure the minimum required preload for slip resistant connections is attained: (i) torque method, (ii) combined method, (iii) HRC method, and (iv) direct tension indicator method (DTI method). Some details of these methods are as follows:

- i. **Torque method:** the bolted assembly is tightened using a calibrated torque wrench.
- ii. **Combined method:** this method consists of two steps, in the first tightening step the torque wrench is set at 75% of the required torque moment, in the second step a specified rotation is applied to the nut or the bolt head (preferably the nut), the rotation values

depend on the bolt diameter and grade, reference values are given in EN 1090-2-2018 [130].

- iii. **HRC method:** the high resistance calibrated (HRC) bolts are tightened using a specific shear wrench equipped with two co-axial sockets, which react by torque one against the other.
- iv. **DTI method:** this method requires the use of special washers called direct tension indicators in accordance with EN 14399-9 [128]. These indicators work as springs, they have protrusions that deform while the preload is being applied to the bolt, the preload is achieved when a certain gap in the protrusions is achieved.

In this study, the DTI method and the combined method (i.e. torque + nut rotation) were implemented to ensure that the minimum preload of the bolted assemblies was reached.

To identify a suitable torquing procedure, tests were conducted on a connection assembly of SCT-1. The test setup shown in Figure 5.3, consists of all elements of SCT-1, however, the shear connection device (i.e. the tube welded to a round plate) was shortened in order to accommodate a load-cell washer, which was placed between the shear connection device and the flange of the beam to measure the applied force while tightening the nut. The load cell used to measure the preload of the bolts in the tests was an HBM washer load cell 1-KMR/300KN (see Figure 5.3b). The bolts, nuts and washers were used as delivered and no lubricants were applied to any part of the assembly.

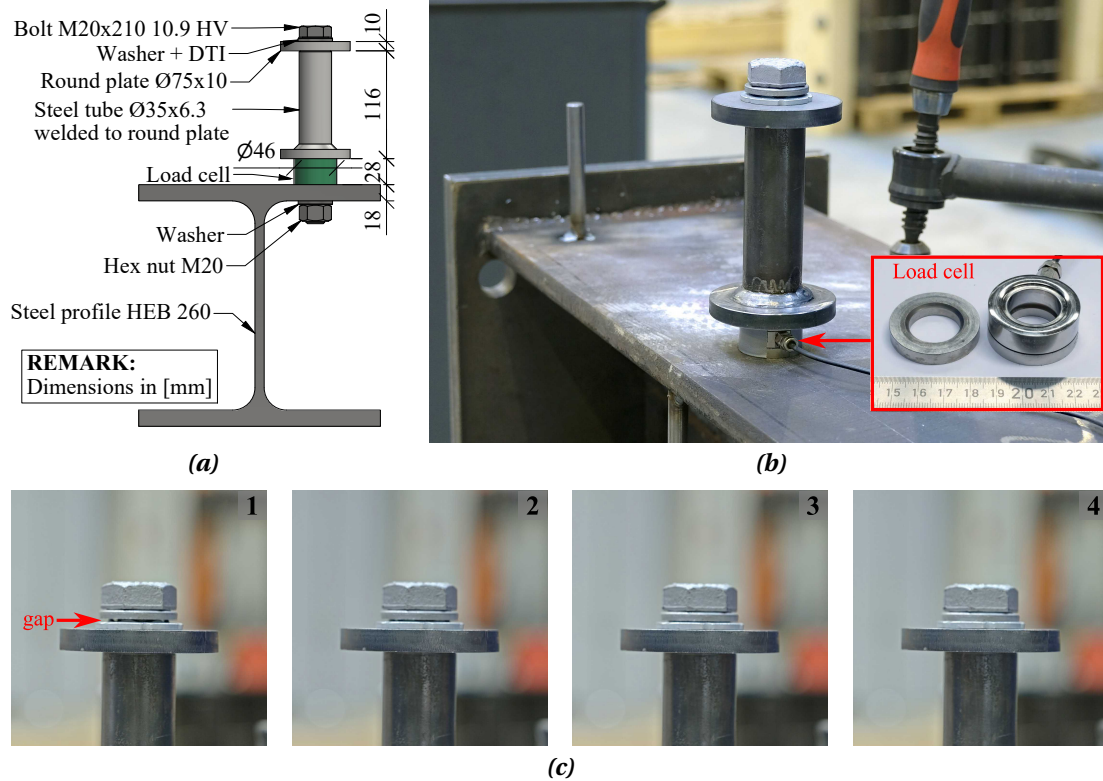


Figure 5.3: Preload calibration tests: (a) test setup components; (b) test setup picture and washer load cell; (c) set of pictures showing the DTI's gap closing as the nut is tightened.

The tightening procedure followed during these tests involved the following steps:

1. Initially, the nut was tightened with a torque wrench with the torque cut-out set to 240 N·m, during this step and subsequent steps, the bolt head was secured with a wrench to prevent its rotation;
2. After the initial torquing step, the preload was applied gradually by increasing the torque cut-out of the torque wrench;
3. The torque cut-out value, the nut rotation, and the force readings from the washer load cell were recorded for each torque cut-out increment;
4. The test was finished when a load between 170 kN and 190 kN was reached.

This procedure was repeated for five new bolts. Additionally, the gap between the DTI and the washer was measured with a feeler gauge to determine the number of refusals, as defined in EN 14399-9 [128].

The data collected during the preload tests was used to construct the plots displayed in Figure 5.4. The two plots show the values from an initial point at which a torque of 240 N·m was applied, meaning that, for a nut rotation of 0° as indicated in the plot of Figure 5.4b, a torque of 240 N·m had already been applied. The correlation between force and torque was 70.4%, and the correlation between force and nut rotation was 92.9%. Since the correlation between force and nut rotation was significantly stronger, the full torque-based method was discarded, and a combined torque+nut rotation method for tightening the bolts of this testing campaign was defined as follows: (i) an initial torque of 240 N·m was applied, then (ii) the nut was turned 260° to ensure the required preload. Once the specified rotation of the nut was reached, the gap of the DTI was measured with a feeler gauge to verify the number of refusals.

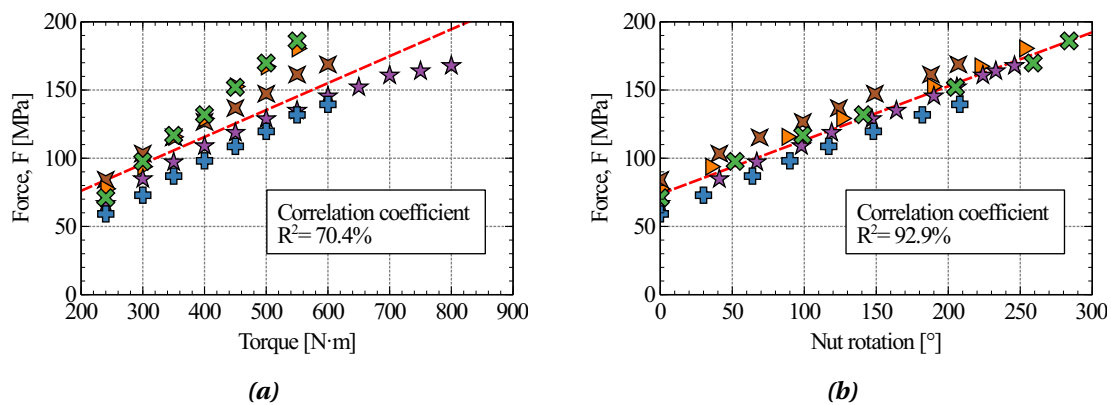


Figure 5.4: Results of preload calibration tests: (a) force vs. torque, and (b) force vs. nut rotation.

5.5. SPECIMEN DETAILS

According to the literature presented in Chapter 2, the double symmetric push-out test setup is the preferred testing setup to determine the mechanical properties of steel-to-timber connections. In this investigation, the specimen's arrangement and its components sizes were defined following the recommendations for push-out tests established in Eurocode 4 [94] for steel-concrete composites.

All the POT specimens of this testing campaign shared basic components, materials, dimensions and connections arrangement, the difference between them lies only in the shear connection, which is different for each test series. Hence, the POT specimens have the following main components (see Figure 5.5 and Figure 5.6):

- i. A hot rolled steel section HEB 260 with steel grade S355 as described in Section 5.3.2, the holes drilled in the flanges for the bolts had a diameter of 24 mm, oversized holes with a diameter of 24 mm instead of 22 mm have been chosen to give tolerances during the assembly of the STC slabs and because the target of the connections is to be used in demountable and reusable flooring systems where tolerances are important.
- ii. Four LVL plates with dimensions $650 \times 300 \times 144$ mm, two plates were connected to each flange of the steel profile leaving a gap of 10 mm between adjacent timber plates, the orientation of the grain was parallel to the application of the load, the holes to accommodate the shear connection devices had exactly the diameter of the steel tubes ($\varnothing 35$ mm) so that there was no gap.
- iii. A total of eight shear connectors to attach the timber plates to the steel profile, two rows of connectors were placed on each flange of the beam with a longitudinal spacing of 250 mm and transversal spacing of 120 mm.

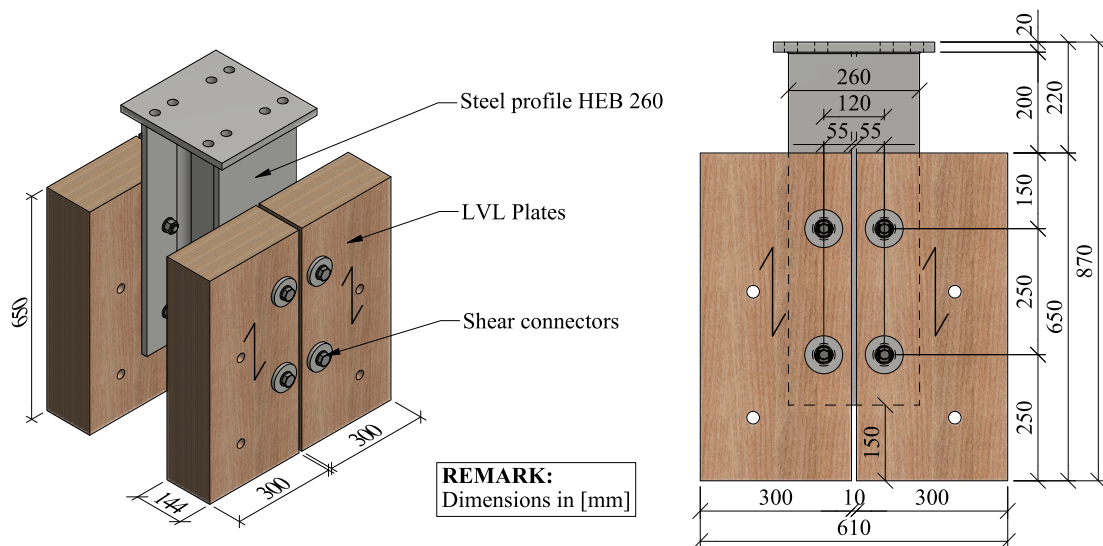


Figure 5.5: Main components and dimensions of the push-out test specimen.

The timber plates were cut and drilled in the Luxembourg's based company Prefalux using a Hundegger Robot-Drive machine, the connection devices were also installed at Prefalux, and then brought to the University's workshop to finalize the assembly of the POT specimens.

The assembly of the specimens was carried out at the University of Luxembourg, during this process, the shear connections introduced in this research project demonstrated ease of installation and facilitated the overall component assembly process.



Figure 5.6: Pictures of a push-out test specimen.

5.6. TEST SETUP AND INSTRUMENTATION

The testing setup is depicted in Figure 5.7 and Figure 5.8, it consists of the specimen with the components described in Section 5.5, sensors to measure displacements, and additional elements to secure the specimen and restrain the displacement of the LVL plates.

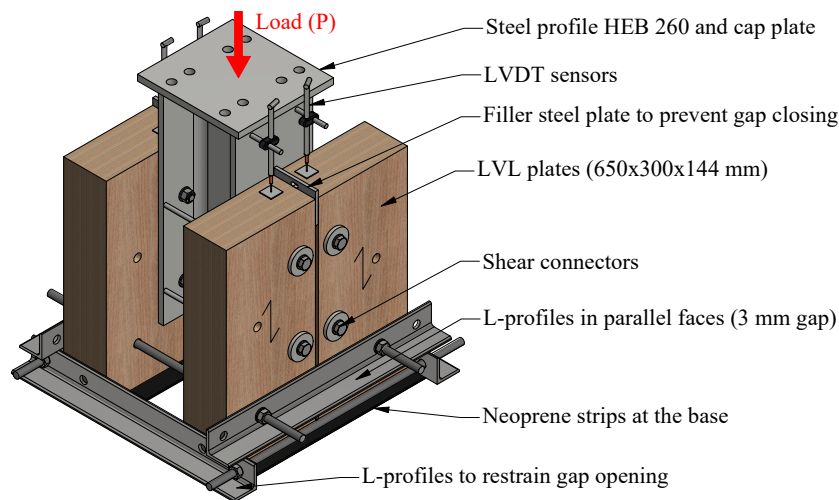


Figure 5.7: Push-out test setup components.

LVDT sensors were installed in the specimen to measure the relative displacement (i.e. slip) between the steel profile and each one of the four LVL plates. To prevent the gap between adjacent plates from closing, steel plates were placed in the gap. Additionally, steel L-profiles fixed with threaded rods were positioned at the lower part of the specimen on two sides of the specimen to prevent the gap from opening. Similar steel L-profiles, also fixed with threaded rods, were used to prevent components from separating once the connection was lost, in this case, a gap of 3 mm was left between the L-profiles and the timber plates.

The specimen was placed on a steel block covered by neoprene strips. The load was applied vertically using the test portal PP 4000 HK-2DH from Form+Test, with a capacity of 4000 kN.

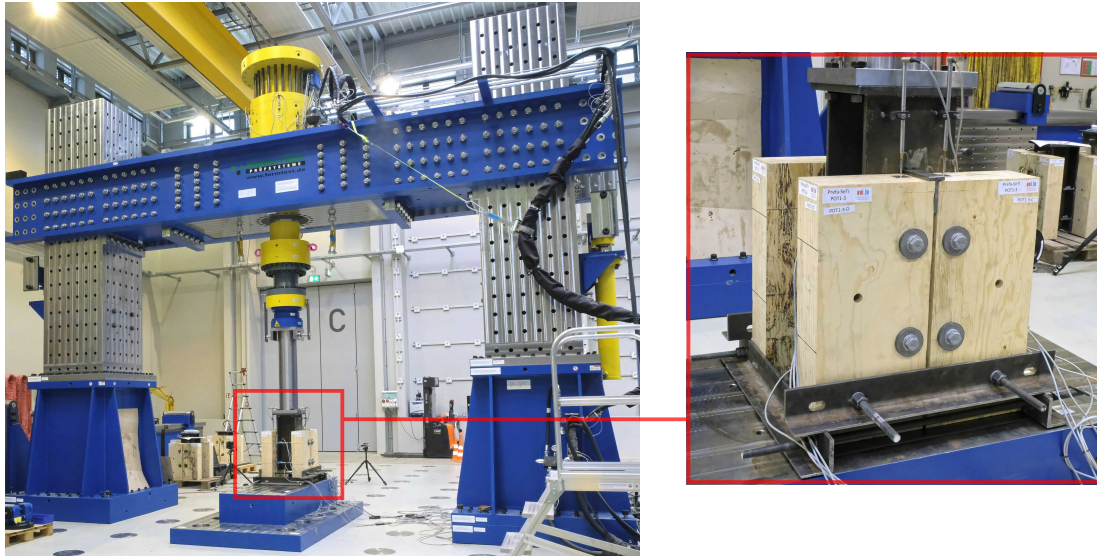


Figure 5.8: Pictures of the push-out test setup.

5.7. LOADING PROCEDURE

The time history of the load applied in the push-out tests is illustrated in Figure 5.9. Due to the lack of testing standards targeting steel-timber composite structures, the loading protocol implemented in this study considers the loading procedure for push-out tests of Eurocode 4 (EN 1994-1-1) [94] presented in Annex B and the loading protocol of EN 26891 [136].

The loading procedure had two main phases, in the first phase the loading was carried out in force control mode, and in the second phase the loading was in displacement control mode. In the first phase the specimen was loaded up to 480 kN which is about 40% of the estimated maximum load (P_{est}), then unloaded to 60 kN ($\sim 0.05P_{est}$), similar to what is established in the initial loading-unloading phase of EN 26891 [136]. After this initial step, 25 loading-unloading cycles within 60 kN and 480 kN were applied at a frequency of 1 cycle per minute, this was done as it is recommended in Eurocode 4 for push-out tests of SCC connections.

After the 25TH cycle, the system was switched to displacement control. Then, subsequent loading-unloading steps were carried out at 660 kN, 840 kN, 1020 kN and 1200 kN. After loading the specimen up to each one of these load levels there was a waiting period of five minutes, followed by unloading to 60 kN, when this load was reached there was a waiting period, which

was of 30 seconds after the loading step at 660 kN and of five minutes in all subsequent steps.

In the last loading step, after loading at 1200 kN and unloading at 60 kN, the specimen was either loaded up to failure of the connections or stopped when the maximum available deformation of the testing setup (~140 mm) was reached.

Only one push-out test specimen of each type of shear connection was tested up to a displacement of about 40–45 mm, when this slip was reached the test was halted to later do cuttings of these specimens and observe the state of the connections at this level of deformation. This approach was applied to specimens POT1–1, POT2–3 and POT3–3. The other two specimens of each series were tested until the shear connectors fractured or stopped when the maximum available deformation of the testing setup was reached.

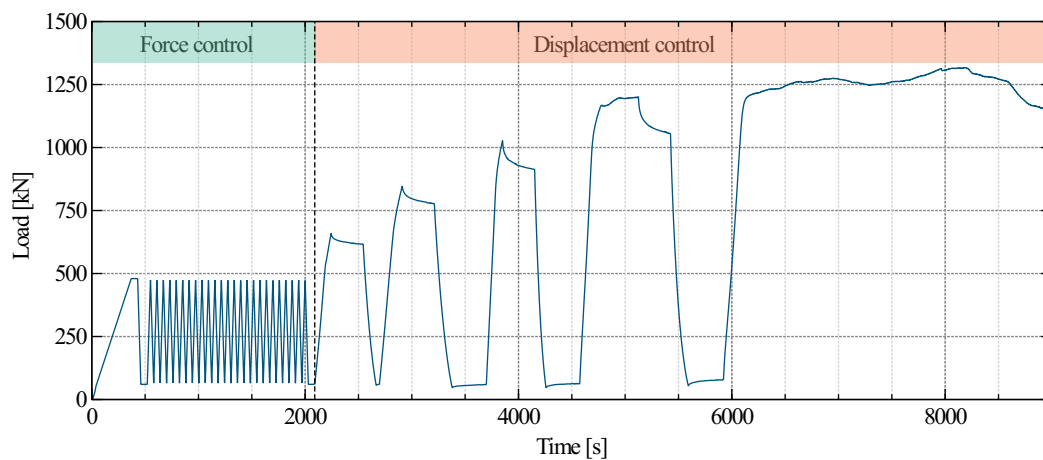


Figure 5.9: Time history of the applied load.

5.8. RESULTS AND DISCUSSION

5.8.1. LOAD-SLIP RESPONSE

LOAD BEARING MECHANISM AND SEQUENCE

The load-slip ($P-\delta$) response of the three types of shear connectors exhibited nonlinearity with significant deformation capacity. Despite differences in the magnitude of loads and bearing stiffness, the load-slip patterns were similar among the three types of shear connections and can be described as follows (see Figure 5.10):

1. An initial stiff response due to the friction provided by the preload of the bolt (i.e. slip resistance), which ends when the slip resistance is overcome. The preload increases the friction between the surface of the steel beam flange and the shear connection device, nevertheless, there is a small displacement which can be attributed to a combination of both, a relative displacement between the flange and the shear connection device, and initial embedment of the shear connection device in the timber.
2. When the slip resistance was overcome, and due to the clearance between the bolt and the hole in the flange of the beam, the sliding friction mechanism came into effect until the flange and the bolt were in full contact.

3. When contact between the bolt and top flange of the beam occurred, the load was transferred via shear in the bolt and respective bearing pressure at the contact point in the top flange. Due to the pressure of the bolt on the shear connection device there was embedment of the shear connection device in the wood, resulting in a nonlinear, monotonically increasing response.
4. In the next branch the stiffness of the system reduced considerably due to yielding of the connection, there was bearing and shear of the bolt as well as embedment of the shear connection in the timber, this branch also exhibited a monotonically increasing response.

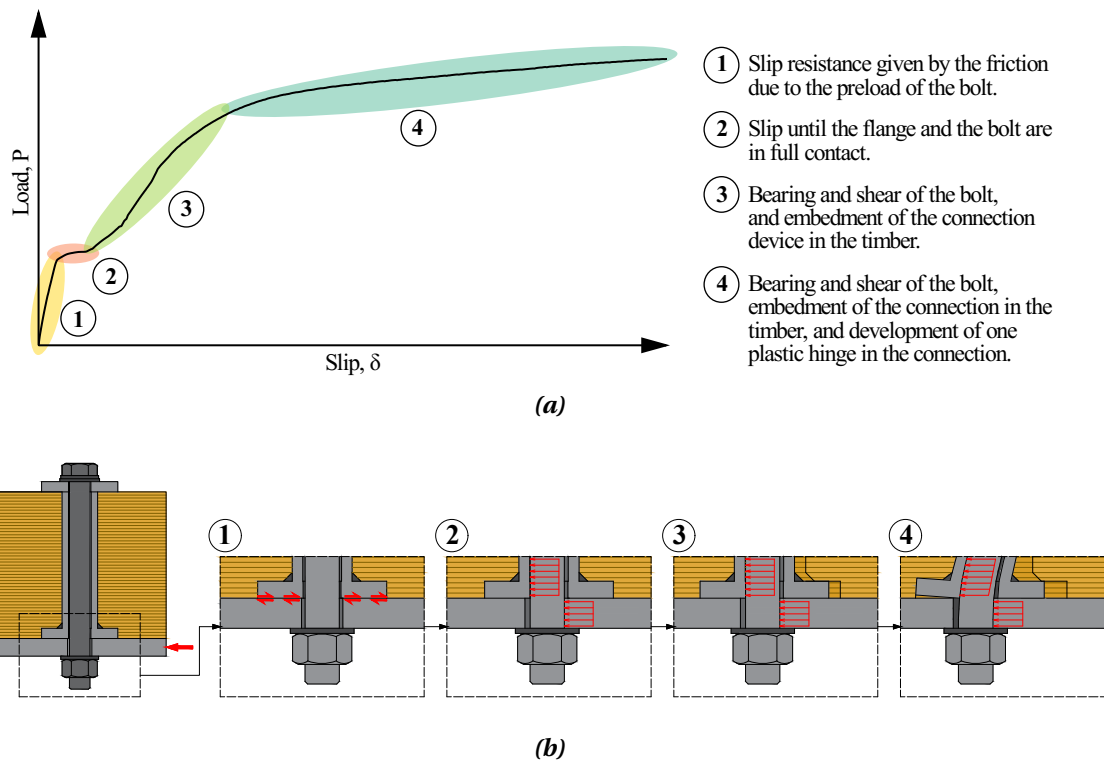


Figure 5.10: Load bearing sequence: (a) generalized load-slip curve; (b) schematic representation of the main stages of the load bearing sequence.

CHARACTERISTICS OF THE LOAD-SLIP CURVES

The detailed load-slip curves of the three test series are shown in Figure 5.11, and a comparison of the mean curves is depicted in Figure 5.12. Table 5.2 gives a summary of different parameters calculated for the curves, these parameters are illustrated in Figure 5.13. The load-slip curves of each specimen were obtained by averaging the slip recorded by the four LVDTs on the top side of the specimen, then the load applied to the specimen was divided by eight, which is the number of connectors in each specimen. In this way the load-slip curves presented in Figure 5.11 display the average load taken by each connector and the respective average slip.

The mean curves of each test series (Figure 5.12) were obtained as the average of the force values for constant slip values. The results of the tests show that the connection type, the po-

sition of the bolt inside the hole, and the bolt preload have relevant influence on the load-slip response.

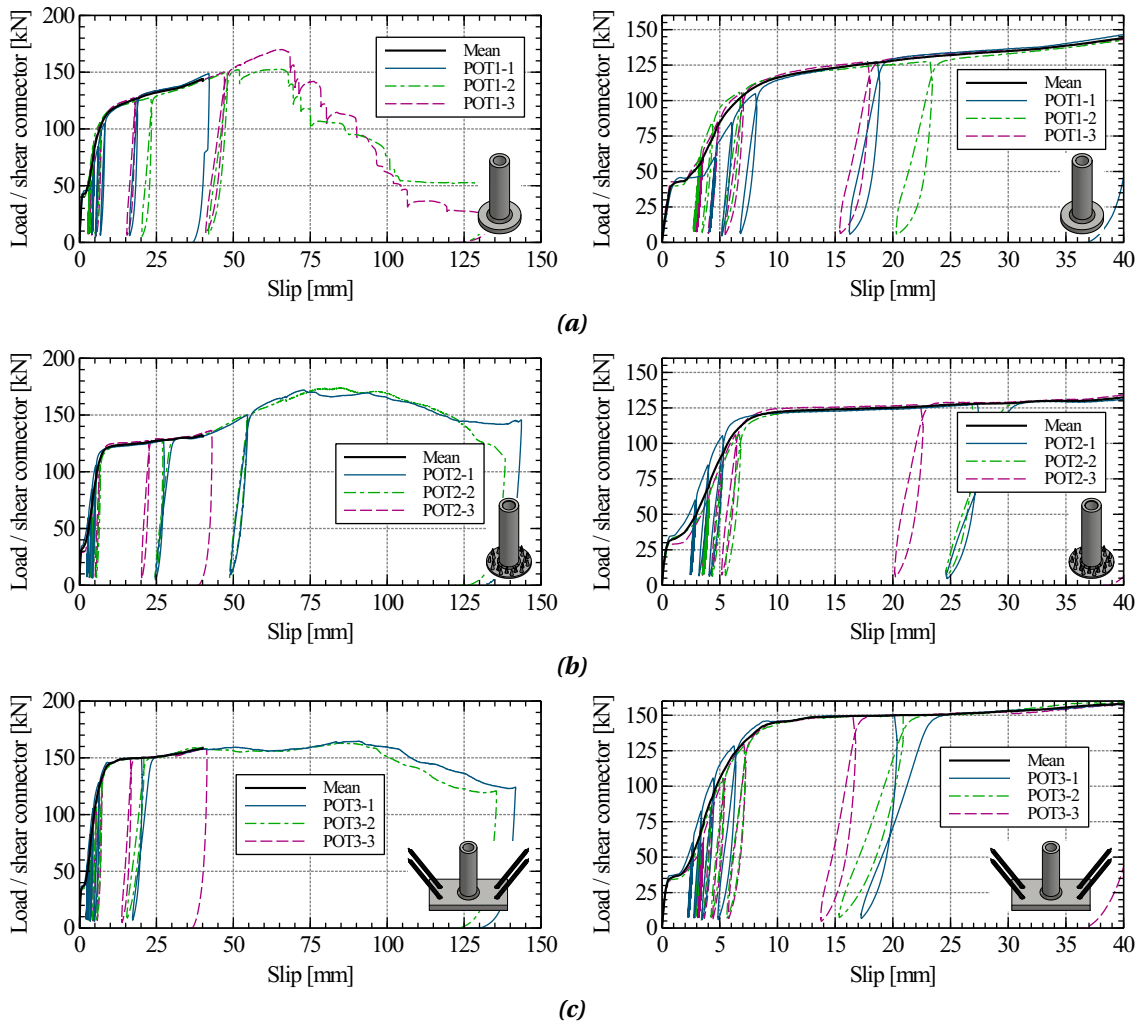


Figure 5.11: Load-slip curves of the test series: (a) POT1 for SCT-1, (b) POT2 for SCT-2, and (c) POT3 for SCT-3.

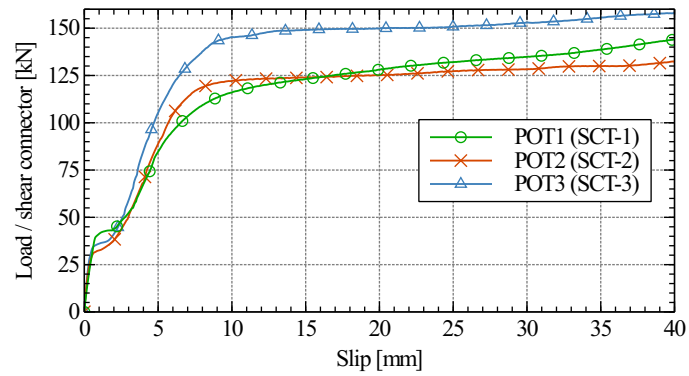


Figure 5.12: Mean load-slip curves of the three push-out test series.

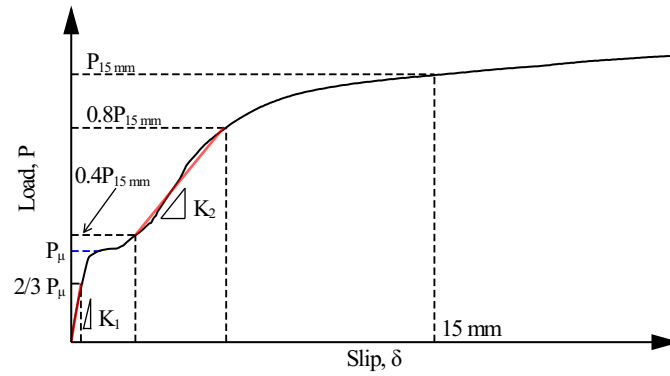


Figure 5.13: Parameters derived from the load slip curves.

Table 5.2: Summary of parameters derived from the load-slip curves of the push-out tests according to Figure 5.13.

Part A							
Series	Specimen	P_{μ} [kN]		$P_{6\text{ mm}}$ [kN]		$P_{15\text{ mm}}$ [kN]	
		Test	Mean ¹	Test	Mean ¹	Test	Mean ¹
POT1	POT1-1	46.2	43.3 (6.9)	84.6	95.7 (10.1)	122.9	124.9 (1.5)
	POT1-2	40.3		102.4		125.3	
	POT1-3	43.3		100.0		126.6	
POT2	POT2-1	34.9	32.9 (8.7)	113.8	104.4 (7.9)	122.8	124.0 (1.1)
	POT2-2	34.3		98.3		123.8	
	POT2-3	29.6		101.3		125.5	
POT3	POT3-1	37.5	36.8 (5.6)	126.5	120.2 (4.6)	149.6	149.1 (0.4)
	POT3-2	34.5		116.6		148.4	
	POT3-3	38.4		117.5		149.2	
Part B							
Series	Specimen	P_{max} [kN]		K_1 [kN/mm]		K_2 [kN/mm]	
		Test	Mean ^a	Test	Mean ^a	Test	Mean ^a
POT1	POT1-1	-	161.4 (7.6)	49.7	61.9 (17.5)	15.1	16.4 (11.9)
	POT1-2	152.7		65.5		18.7	
	POT1-3	170.1		70.4		15.5	
POT2	POT2-1	172.0	173.1 (0.9)	86.2	82.8 (21.5)	21.5	20.4 (6.4)
	POT2-2	174.2		63.5		18.9	
	POT2-3	-		98.7		20.7	
POT3	POT3-1	164.7	163.8 (0.7)	92.6	87.9 (5.7)	24.5	23.5 (6.6)
	POT3-2	163.0		88.5		21.7	
	POT3-3	-		82.6		24.3	

^a The values in parentheses indicate the coefficient of variation.

SLIP RESISTANCE AND INITIAL STIFFNESS

The bolts preloading procedure explained in Section 5.4 was developed to ensure consistent preload and slip resistance in the test specimens with the same type of shear connection. Hence, the first branch of the load-slip curve exhibits a high stiffness due to the friction between the shear connection device and the flange of the steel beam, which is enhanced by the preload of the bolts.

The average slip resistances (P_μ) obtained in each test series were 43.3 kN, 32.9 kN, and 36.8 kN for SCT-1, SCT-2, and SCT-3 respectively, with a CV of 6.9%, 8.7% and 5.6%, respectively for each shear connection type. The stiffness (K_1) of the initial branch of the load-slip curve was estimated as the slope of a secant line intersecting the curve at $2/3P_\mu$, the average values obtained respectively for each shear connection type were 61.9 kN/mm, 82.8 kN/mm and 87.9 kN/mm with coefficients of variation of 17.5%, 21.5% and 5.7%.

INFLUENCE OF THE POSITION OF THE BOLT IN THE HOLE

The diameter of the bolt in the three types of shear connection was 20 mm and the diameter of the holes in the flanges was 24 mm in all the specimens, this means that the bolt could have a clearance within the hole of up to 4 mm, hence, the initial slip before the contact between the bolt and the flange of the beam (i.e. before the bolt starts to work in bearing and shear) could be up to 4 mm.

During the assembly of the specimens the intention was to place the bolt at the center of the hole, this was achieved in most of the specimens, which in general showed a slip of about 2 mm at the end of the second branch of the load-slip curves (branch 2 from Figure 5.10b), however, the specimen POT2-1 and POT2-2 had a very small initial slip (~1 mm) in the bolt hole before starting the bearing branch, and the specimen POT1-1 showed almost 4 mm of initial slip in the bolt hole. This demonstrates the influence of the position of the bolt inside the hole of the flange on the load-slip response, which causes a horizontal shift of the bearing branch (branch 3 from Figure 5.10b) in the load-slip curves, hence, depending on the position of the bolt, this bearing branch starts to develop within the range of 0 to 4 mm of slip.

LOADS REACHED AT 6 MM SLIP

It is expected that the connections work at slip values smaller than 6 mm, this is to avoid damages of the connections and in the timber. This is in line with the assumptions made in Eurocode 4 [94] for shear connections of steel-concrete composite structures, in which the connectors are required to have a slip capacity of at least 6 mm, so that beams reach their capacity when a slip of about 6 mm occurs. Hence, the loads corresponding to a slip of 6 mm ($P_{6\text{ mm}}$) were also obtained for each test. The average loads for each type of shear connection were 95.7 kN, 104.4 kN and 120.2 kN for SCT-1, SCT-2 and SCT-3 respectively, with their corresponding coefficients of variation of 10.1%, 7.9% and 4.6%.

LOADS REACHED AT 15 MM SLIP

According to EN 26891 [136] the load reached at 15 mm ($P_{15\text{ mm}}$) shall be recorded as the maximum load in the tests of steel-to-timber connections. In the push-out tests carried-out in this

investigation, the connections reached the maximum loads at slip values which exceed considerably the 15 mm limit established in EN 26891 [136]. Nevertheless, the parameter $P_{15 \text{ mm}}$ has been included in this analysis as a reference value.

It was observed that regardless of the initial slip before the bearing branch, the load-slip curves reach values of the same order of magnitude at a slip of 15 mm, this is a point at which they nearly converge. The load corresponding to this slip was taken as a reference for comparison of the different types of connections and for the definition of the lower and upper bounds for the evaluation of the stiffness of the bearing branch.

The average loads $P_{15 \text{ mm}}$ for each type of shear connection were 124.9 kN, 124.0 kN and 149.1 kN for SCT-1, SCT-2 and SCT-3 respectively, with their corresponding coefficients of variation of 1.5%, 1.1% and 0.4%, which validates the near-convergence of curves at this point. SCT-1 and SCT-2 reached similar load levels, whereas the load reached by SCT-3 were about 20% higher. This confirms that the implementation of screws to reinforce the connections can significantly increase the load-carrying capacity of the connections.

STIFFNESS OF THE CONNECTION IN THE BEARING BRANCH

The stiffness (K_2) of the connection in the bearing branch (branch 3 from Figure 5.10b) was obtained through linear regression analyses. These regression analyses were done in a region enclosed by the points corresponding to $0.4P_{15 \text{ mm}}$ and $0.8P_{15 \text{ mm}}$. The average stiffness values obtained in each test series were 16.4 kN/mm, 20.4 kN/mm and 23.5 kN/mm, with a CV of 11.9%, 6.4% and 6.6% for SCT-1, SCT-2 and SCT-3 respectively. Moreover, in all the regression analyses, correlation coefficients (R^2) greater than 0.97 were obtained. The SCT-2 and SCT-3 had larger stiffness than SCT-1, this could be due to the use of Geka connectors in SCT-2 and inclined screws in SCT-3 along with a thicker plate. In terms of stiffness of the bearing branch K_2 , the SCT-3 had the best performance.

POST-YIELDING RESPONSE

In the bearing branch there was yielding of the connection, at this point the initial bearing stiffness reduced significantly and the branch 4 from Figure 5.10b developed. The yielding of the connection is owed to a combination of non-reversible timber crushing / embedment of the shear connection device, and plastic yield deformation of the bolt and the shear connection device. SCT-1 exhibited hardening from the yielding point, whereas in the SCT-2 and the SCT-3 this branch was close to a plateau between a slip of 10 mm and 35 mm. From a slip of 35 mm SCT-2 and SCT-3 displayed hardening, in SCT-3 hardening was very small, and the post-yielding branch was close to a plateau. This hardening was related to the densification of timber and hardening of the steel components of the connection (i.e. shear connection devices and bolt).

For the specimens that were tested up to rupture of the connectors or up to the maximum available deformation of the testing setup, the maximum loads (P_{max}) were obtained from the load-slip data. The average values for SCT-1, SCT-2 and SCT-3 were 161.4 kN, 173.1 kN, and 163.8 kN respectively. After reaching this peak load, these specimens of SCT-2 and SCT-3 exhibited a post-peak softening branch, while the specimens of SCT-1 experienced rupture of the bolts.

5.8.2. FAILURE MODE

The three types of shear connection showed a similar failure mode as shown in Figure 5.14. In these connections, there was timber crushing due to embedment of the shear connection device and one plastic hinge developed in the steel components at the steel-timber interface.

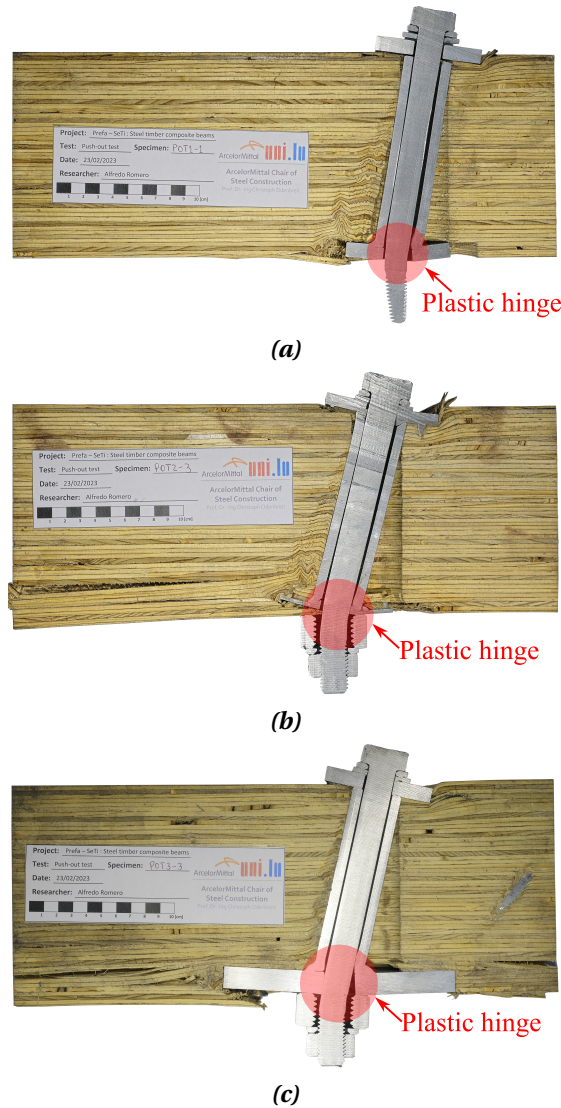


Figure 5.14: Cuttings of shear connections from tests that were stopped at 40-45 mm slip: (a) SCT-1, (b) SCT-2, and (c) SCT-3.

In the specimens that were not tested up to rupture (i.e. POT1-1, POT2-3 and POT3-3), pictures shown in Figure 5.14 (connections' cuttings) and Figure 5.15 (specimens), it can be noticed that there was rotation of the connection and embedment of the steel tube in the timber as well as little but noticeable embedment of the round steel plate—placed under the bolt head—in the timber plate surface.

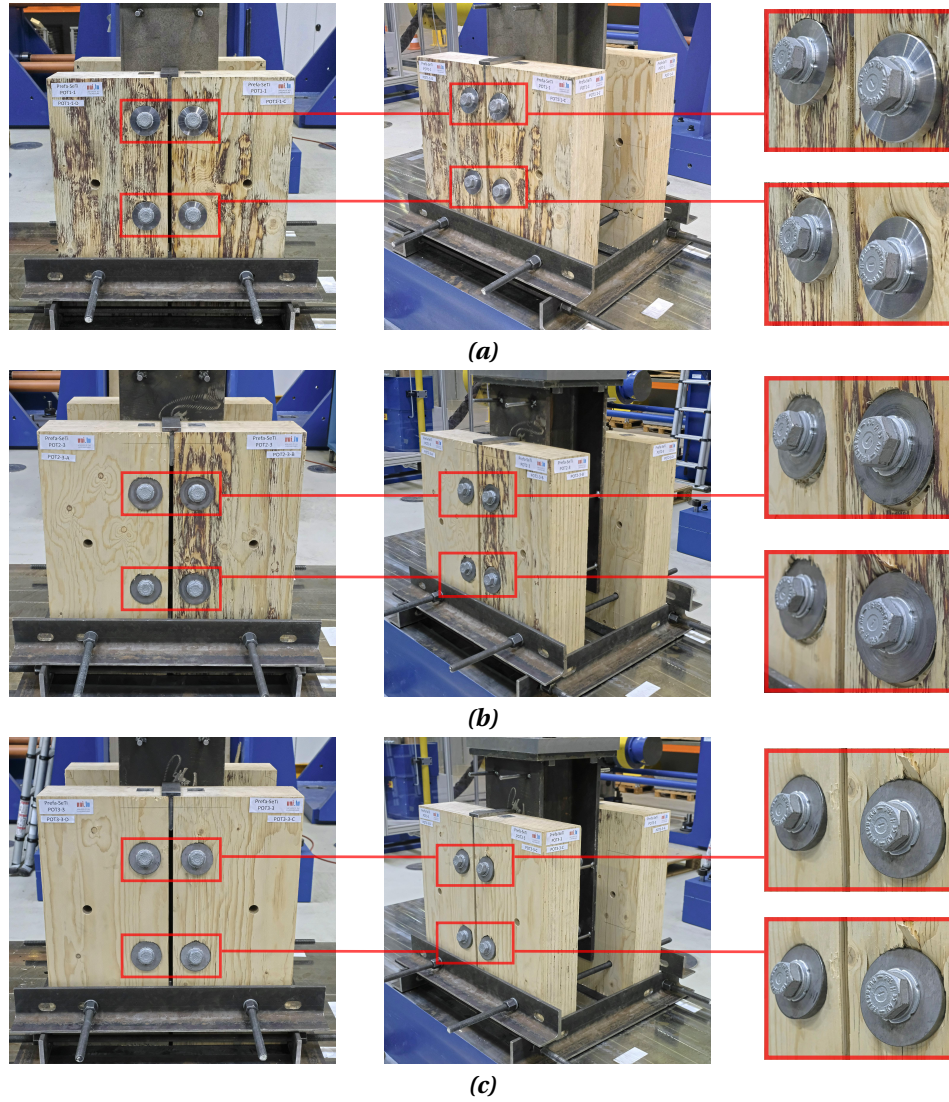


Figure 5.15: Pictures of the specimens tested up to a slip of 40–45 mm: (a) SCT-1, (b) SCT-2, and (c) SCT-3.

The three connections exhibited a large deformation capacity post-yielding. In the case of SCT-1, the post peak behaviour was characterized by softening followed by rupture of the bolts which did not fail simultaneously, this can be seen in the load-slip plots of SCT-1 (see Figure 5.11), the failure of each bolt caused a sudden drop in the post-peak branch, hence, this branch has several load drops. One of the bolts that experienced rupture is depicted in Figure 5.16a.

The SCT-2 and SCT-3 were stopped when the maximum available deformation of the testing setup was reached (i.e. ~140 mm), up to this point there was no rupture of the bolts, nevertheless, in both cases a softening branch post-peak was observed.

At large deformations (e.g. ~140 mm), in the specimens tested up to rupture, the head of the connections was fully embedded in the timber as depicted in Figure 5.16. In the specimens of SCT-1 (Figure 5.16a) the round plate placed under the bolt head was embedded in the surface of the timber plates. Additionally, in some timber plates with SCT-1, downwards pulling of the wood was observed at their top side. Similarly, in specimens of SCT-2 (see Figure 5.16b) the

Geka and the round plate placed under the head of the bolt was fully embedded but, in this case, the downwards pulling of veneers at the top of the timber plates was more evident, this is related to the anchoring effect of the Geka teeth which pull downwards the veneers near the surface of the timber plates. The SCT-3 (see Figure 5.16c), exhibited a similar but more visible downwards pulling effect, which is larger at the veneers located near the face next to the flange of the steel profile, this is due to the pulling effect of the inclined screws placed in that side of the timber plate.

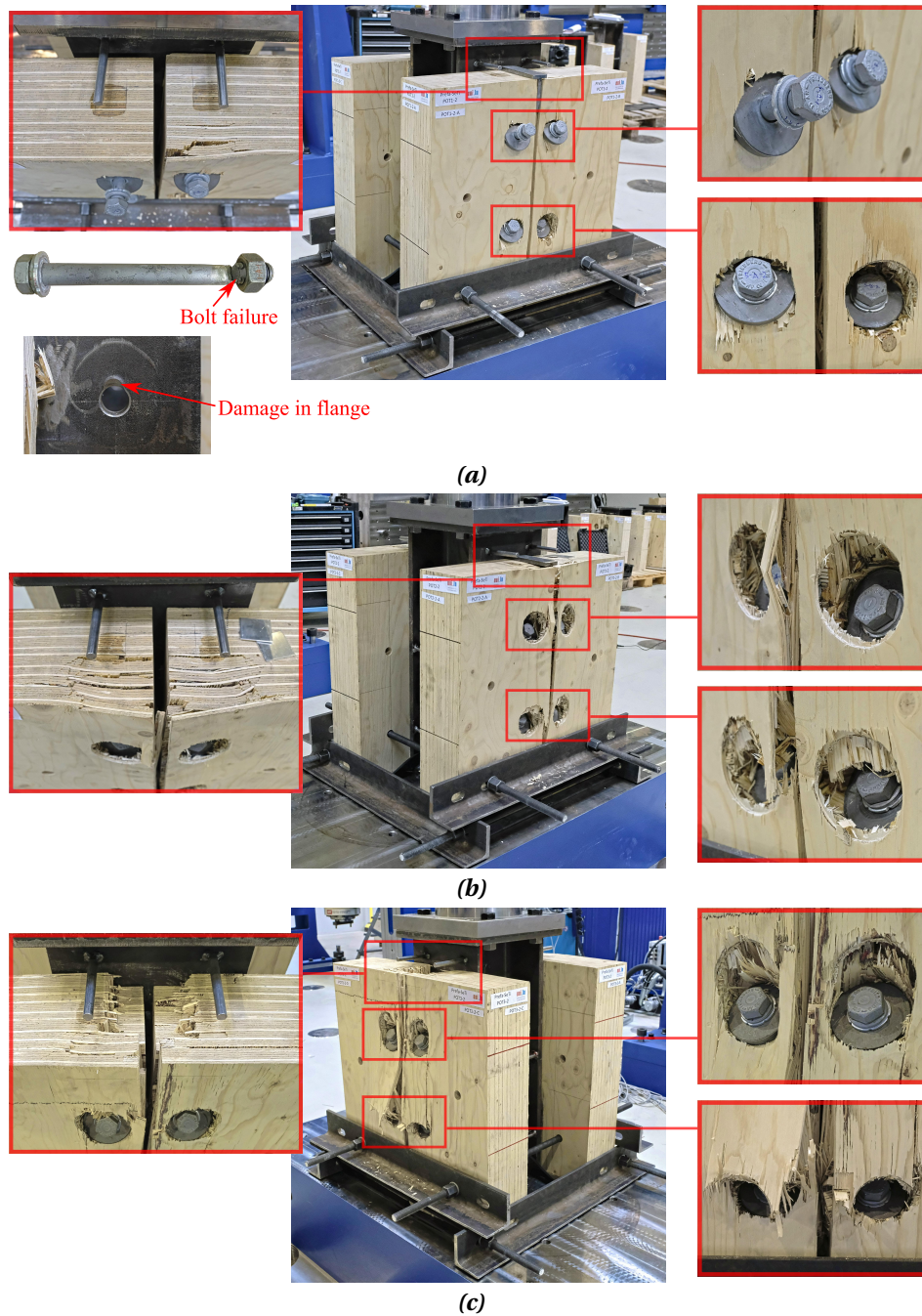


Figure 5.16: Pictures and details of specimens tested up to bolt rupture for (a) SCT-1, and up to the maximum available deformation (~140 mm) of the testing setup for (b) SCT-2 and (c) SCT-3.

ARTICLE 3

6

EXPERIMENTAL FULL-SCALE STC BEAM TESTS

6.1. INTRODUCTION

The newly developed shear connections (see Chapter 3, Section 3.3) have been tested through push-out tests (see Chapter 5) to assess their load-deformation behaviour and capacity. However, to fully realize their application in STC beams, it is crucial to investigate their behaviour in actual STC beams and their performance under full-scale bending conditions. Therefore, this research project included an experimental investigation of two simply supported STC beams with the novel demountable connectors, subjected to six-point bending, both with a span of 10 m and a slab width of 2.51 m. This chapter outlines the testing methodology, and presents the results along with their corresponding discussions.

6.2. OVERVIEW OF THE EXPERIMENTAL TESTING CAMPAIGN

The flexural response of the STC beams was investigated through experimental six-point bending tests on full-scale specimens in simply supported conditions. Two full-scale STC beams were tested: beam test 1 (BT-1) and beam test 2 (BT-2), both specimens consisted of a down-standing I-shaped hot-rolled steel profile (IPE 400) and LVL slabs on top with a thickness of 144 mm, connected using shear connectors that enable demountability and reuse (see Chapter 3, Section 3.3). Table 6.1 presents an overview of the beam tests carried out in this investigation.

The two STC beam specimens were identical in terms of geometry, materials, and shear connections' arrangement. The difference was the type of shear connection used, BT-1 implemented SCT-1, and BT-2 implemented SCT-3. SCT-1 was chosen due to its simplicity and ease of fabrication compared to SCT-2, whereas SCT-3 was chosen due to its enhanced performance and load-bearing capacity demonstrated in the push-out tests (see Chapter 5).

The two specimens had a total length of 10.6 m, a span (L) of 10 m, and a slab width (b_{slab}) of 2.51 m (see Figure 6.1). The tests were conducted at room temperature and under relative humidity conditions, both parameters were monitored with a sensor ALMEMO FHAD 46-C41, the mean values were 22°C and 41.1%, respectively. The moisture content of the LVL slabs was measured using a capacitive moisture sensor ALMEMO FHA 696 MF, the mean value was 12.9%.

Table 6.1: Overview of beam tests carried out in this investigation.

Test	Test ID	Shear connection	Span [m]	Slab width [m]	No. of Specimens
Beam test 1	BT-1	Type 1 (SCT-1)	10	2.51	1
Beam test 2	BT-2	Type 3 (SCT-3)	10	2.51	1

6.3. MATERIALS

6.3.1. LAMINATED VENEER LUMBER

The slab panels of the two STC beams were made with crossband LVL-C from MetsäWood (i.e. Kerto-Q) [134] with a thickness of 144 mm. It is the same engineered timber product used in the push out tests and the same layup, it consists of 48 veneers with a thickness of 3 mm as follows: II-IIII-III-III-IIII-II-IIII-III-III-IIII-II, where “I” represents the longitudinal veneers with their grain aligned in the longitudinal direction, and “-” represents the cross veneers with their grain perpendicular to the grain of the “I” veneers. Figure 5.1 shows the layup of the LVL used for both the push-out tests and the beam tests. This LVL product is crafted with Scandinavian Spruce (i.e. *Picea abies*) wood. The cross veneers in the LVL matrix enhance the strength and stiffness of the timber elements in the direction perpendicular to the grain.

6.3.2. STEEL BEAMS

The steel beams used in the two STC beams were hot-rolled IPE 400 with steel grade S355 in accordance with EN 10025 [125], without coating or painting. The length of the steel profile was 10.6 m in the two specimens. Stiffeners were welded at different locations of the beam and extension legs were welded at the supports, these elements were also produced with steel plates grade S355.

Eight coupon shape specimens were tested in tension, and the tests were conducted according to EN ISO 6892-1 [135] in order to determine the mechanical properties of the structural steel S355. A mean yield strength of 399 MPa with a CV of 1.7%, a mean ultimate strength of 512 MPa with a CV of 1.7%, and a mean modulus of elasticity of 207 GPa with a CV of 1.9%, were obtained.

6.3.3. SHEAR CONNECTION DEVICES AND ROUND PLATES

The shear connection devices of SCT-1 and SCT-3, as outlined in Chapter 3 in Section 3.3, consist of a steel tube grade S460 according to EN 10025 [125] with an external diameter of 35 mm and a wall thickness of 6.3 mm. These tubes were welded to steel elements that differed based on the shear connection type. For SCT-1, a round steel plate was employed, while SCT-3 featured a rectangular plate, both made from steel grade S460.

Round steel plates, made of S460 steel, were placed beneath the bolt head and below standard washers to prevent uplift of the timber panels. SCT-1 and SCT-3 featured round plates

with an outer diameter of 75 mm and a thickness of 10 mm.

Four coupon shape specimens were tested in tension, and were conducted according to EN ISO 6892-1 [135] in order to determine the mechanical properties of the steel S460 of the shear connection devices. A mean yield strength of 526 MPa with a CV of 0.2%, a mean ultimate strength of 581 MPa with a CV of 0.3%, and a mean modulus of elasticity of 203 GPa with a CV of 1.6%, were obtained.

6.3.4. SCREWS

Universal partial-thread screws (see Figure 5.2) were installed in shear connection type 3 (SCT-3) of BT-2. These universal partial-thread screws (ASSY 4 CSMP) made of stainless steel from Würth (ETA 11/0190) [127] with a diameter of 8 mm and a length of 140 mm were installed with an inclination of 60° with respect to the horizontal. According to the ETA of the product (ETA 11/0190) [127], the characteristic tensile strength ($f_{t,k}$) is 21.5 kN and the characteristic yield moment ($M_{y,k}$) is 23 N·m.

6.3.5. BOLTS, WASHERS AND NUTS

High-strength partially threaded bolts M20 10.9 HV according to EN 14399 [128] (see Figure 5.2), with a diameter of 20 mm and a length of 210 mm, were used in the shear connections of the specimens of BT-1 and BT-2. The tensile mechanical properties of the bolts were determined through tensile tests carried out on four coupon specimens.

A flat washer with chamfer for high strength fittings and hot dip galvanisation in accordance with EN 14399 [128] was positioned under the head of the bolt and another washer was placed under the nut, the washers are shown in Figure 5.2. The washer has an outer diameter of 37 mm, an inner diameter of 21 mm and a thickness of 4 mm. The hexagon nuts (see Figure 5.2) used in the assemblies comply with EN 14399 [128], and were made with hot-dip galvanised steel class 10Z, the nuts had a height of 16 mm.

6.3.6. DIRECT TENSION INDICATORS

The direct tension indicators (DTI) (see Figure 5.2) made of galvanized steel and manufactured by Turna-Sure, were placed under the washer at the bolt head side to ensure the minimum preload requirement was met, this was done by following the procedure established in EN 14399-9 [128].

6.3.7. MORTAR

High strength mortar (PAGEL V1/30 HF [137]) was used to fill the transversal gaps between adjacent panels. This enables the effective transfer of compressive forces from the central panels to the edge panels, consequently activating the connectors installed in the edge panels. This mortar reaches a compressive strength of at least 70 MPa in 24 hours according to the technical specifications of the supplier [137].

6.4. SPECIMEN DETAILS

The dimensions and details of the specimens are depicted in Figure 6.1 and Figure 6.2. The two STC beam specimens of this testing campaign consist of a downstanding steel profile IPE 400 S355 in accordance with EN 10025 [125] with a length of 10.6 m (Figure 6.2, part 3), and six crossband LVL (LVL-C, Kerto-Q [134]) panels with a thickness of 144 mm, the two central panels (Figure 6.2, part 2) have dimensions $4040 \times 1250 \times 144$ mm, and the four edge panels (Figure 6.2, part 1) have dimensions $3270 \times 1250 \times 144$ mm. The panels were placed on top of the steel beam and connected with the novel shear connectors introduced in Chapter 3, Section 3.3.

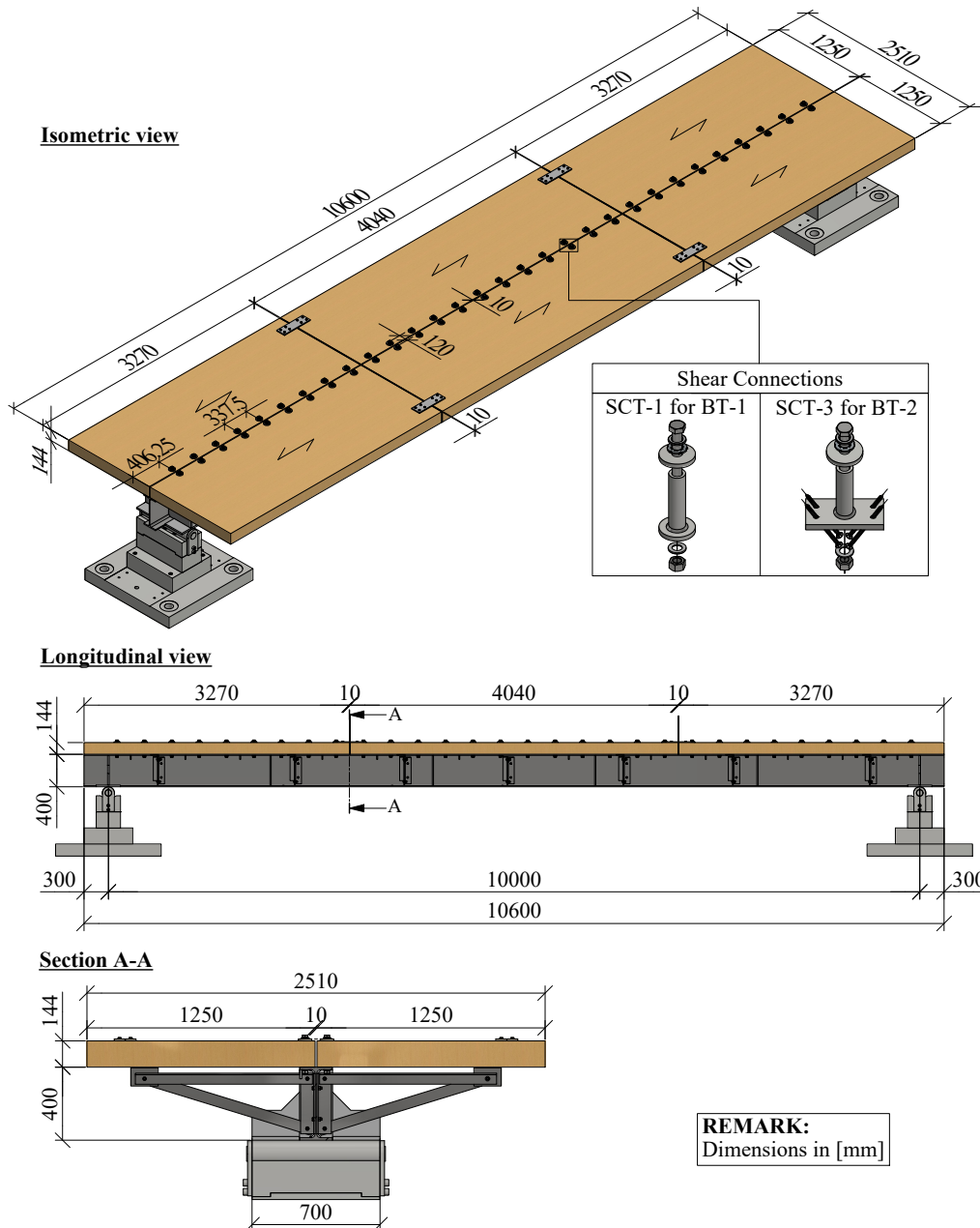


Figure 6.1: Dimensions of the tested specimens.

Stiffeners (Figure 6.2, part 11) were welded to the steel beam at the points where the load was applied, and at the two supports, stiffeners and extensions of the base to the two sides of the beam (Figure 6.2, part 4) were welded to the steel beam to provide stability. The holes drilled in the flanges of the steel beams had a diameter of 24 mm, allowing for up to 4 mm of clearance for the M20 bolts used in the connection.

Between adjacent panels there was a gap of 10 mm, the transversal gaps (Figure 6.2, part 9) were filled with high strength mortar (PAGEL V1/30 HF [137]) to transfer compression forces and activate the connectors of the edge panels. A plastic film was used to avoid moisture in the LVL panels due to the mortar pouring and prevent bonding between mortar and timber. The longitudinal gap remained unfilled, however, one steel plate (200×150×10 mm) was placed at the longitudinal gap in each end of the beam (Figure 6.2, part 5) to prevent its closure during the test at large deformations.

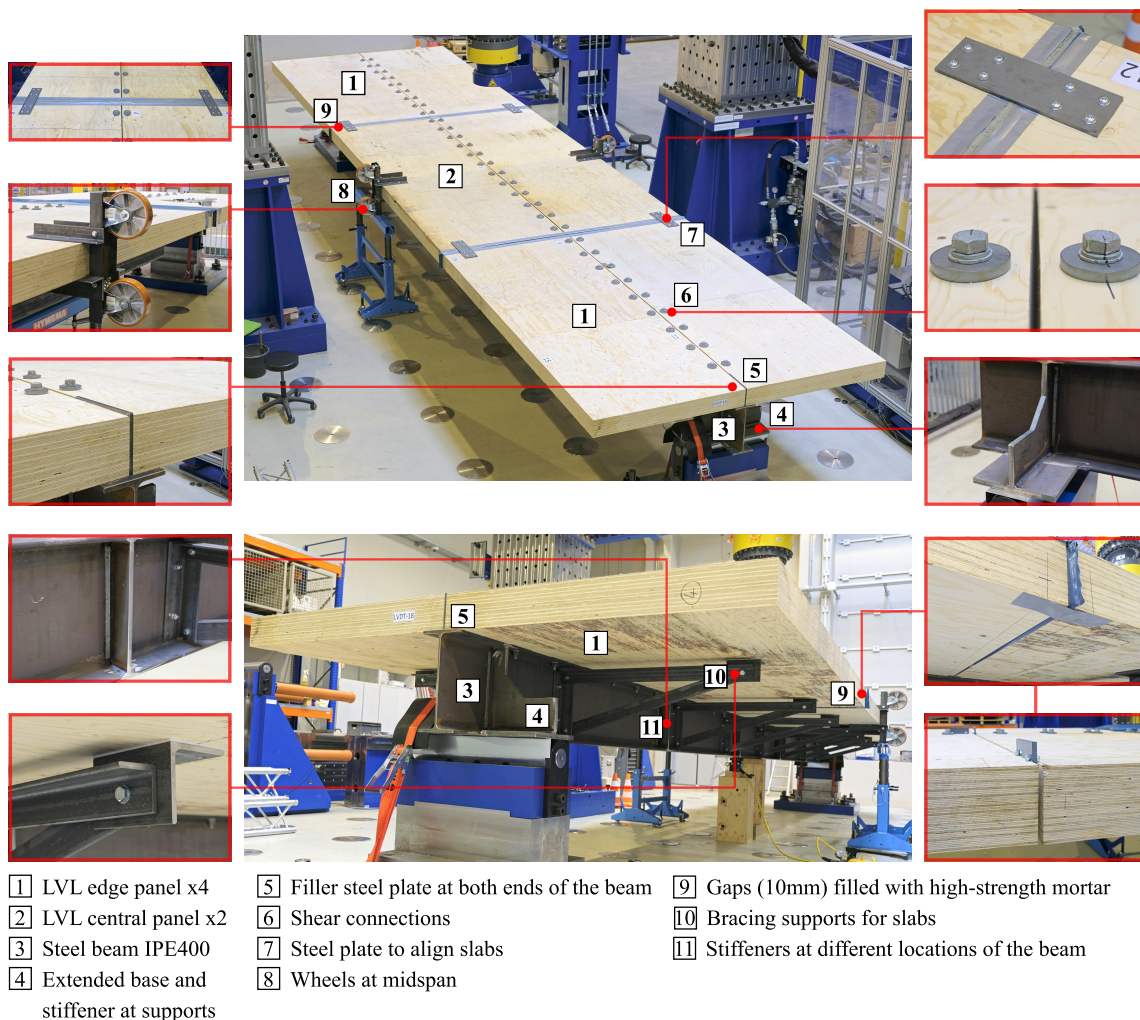


Figure 6.2: Components of the STC beam specimens.

Steel plates (400×120×10 mm) were used to ensure the horizontal alignment of adjacent panels at the transversal gaps, four plates were screwed near the edges of the slabs (Figure 6.2, part 7). It is important to note that these plates are only necessary for testing purposes. In the

actual flooring system, the LVL slabs will rest directly on the steel beams, ensuring automatic horizontal alignment without the need for these plates.

Two rows of shear connectors, spaced 120 mm transversally and 337.5 mm longitudinally, were installed in the specimens (Figure 6.2, part 6). The SCT-1 connectors were implemented in BT-1, while SCT-3 connectors were implemented in BT-2. Both types of connections incorporated bolts M20 grade 10.9, in accordance with Eurocode 3 [129] and EN 1090-2 [130], these bolts were preloaded to 70% of their ultimate strength.

The required preload for the bolts M20 grade 10.9 used in this study's connection assemblies was 172 kN. To ensure this minimum preload was reached, one DTI was placed under the washer adjacent to the bolt head. A consistent preload was achieved through a defined tightening procedure, established after testing eight SCT-1 connection assemblies instrumented with a load cell, following a testing approach outlined in Chapter 5, Section 5.4. The tightening procedure involved: (i) initially applying a torque of 400 N·m to the bolt head using a torque wrench while holding the nut to prevent its rotation with another wrench, followed by (ii) a 180-degree rotation of the bolt head using a pneumatic wrench. This approach, involving bolt head rotation, was preferred over the typical nut rotation for ease and practicality as working under the slab to tighten the nut is more difficult and requires more effort.

Braces were fixed to the steel beam (Figure 6.2, part 4) to support the panels and prevent stresses on the connections and panels due to the cantilever effect caused by the panels' free edges. These braces were not connected to the panels, ensuring they did not contribute to stiffness and strength. To minimize friction between the steel supports and timber panels, 3 mm thick PTFE plates were used. It is important to note that these braces are only necessary for testing purposes and will not be included in the actual flooring system.

6.5. ASSEMBLY PROCESS

The assembly process of the STC beam specimens is crucial for understanding the actual flooring system's assembly and identifying potential improvements in efficiency, cost, and execution time. Preliminary works on the components must be conducted offsite to minimize on-site execution times and errors, thereby ensuring the highest possible quality. This means all elements must be prepared offsite to be ready for installation, facilitating their subsequent connection to other components onsite. This subsection describes the preliminary works and the assembly process of the two specimens, which was the same for both, the specimen of BT-1 and the specimen of BT-2.

Prior to the assembly, the steel beams' drillings for the bolts were done, and the stiffeners and the extended bases at the supports were welded in a dedicated area for this purpose in the laboratory hall. The cutting and drilling works of the panels were executed in a specialized workshop, the connection devices were also installed in the timber panels before starting the assembly of the specimens, pictures of these processes are shown in Figure 6.3.

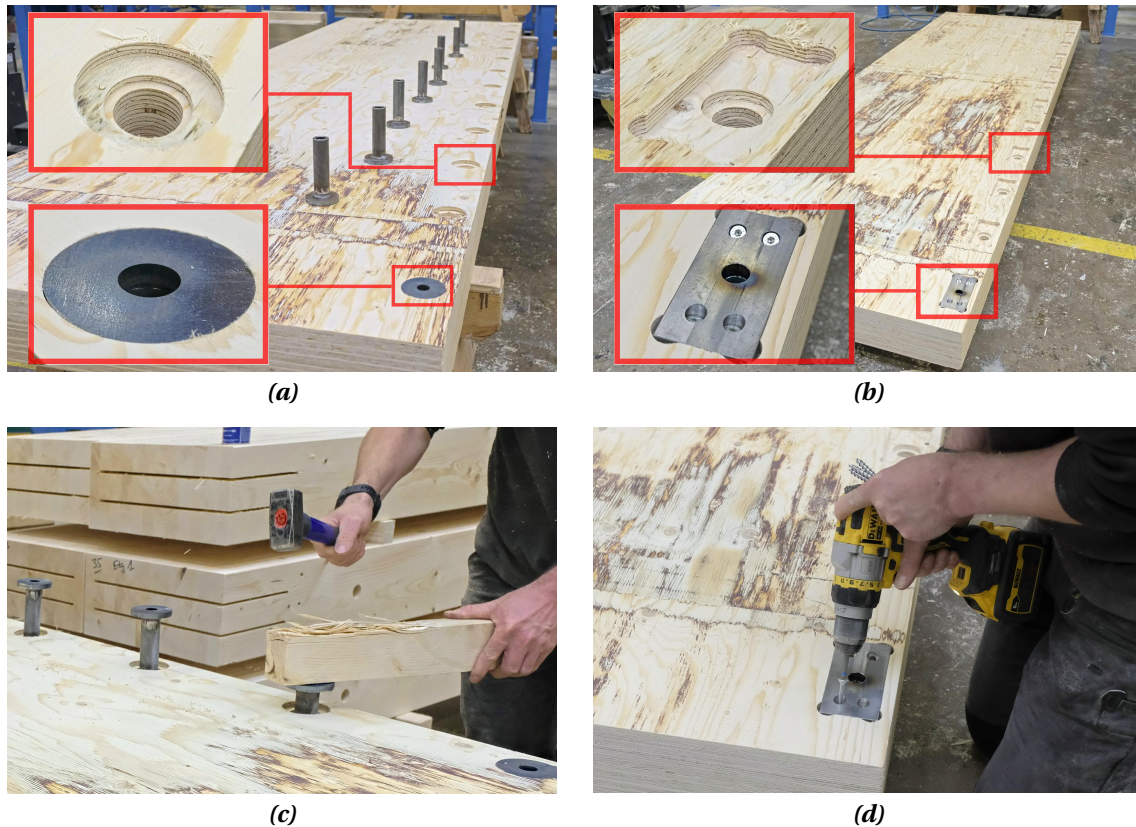


Figure 6.3: Pictures of the preliminary woodworks: drill details of the two types of connection (a) SCT-1 and (b) SCT-3, and installation of the shear connection devices of (c) SCT-1 and (d) SCT-3.

The assembly process was the same for the two STC beam specimens, pictures of the process are shown in Figure 6.4. The procedure for assembling both STC beam specimens consists of the following main steps:

- (a) Initially, the IPE 400 steel beam was moved to the strong floor in the laboratory hall and positioned on two supports (Figure 6.4a).
- (b) During assembly, ratchet straps secured the specimen to these supports, and were later removed just before starting the test (Figure 6.4b).
- (c) The supporting braces were connected to the beam's web with bolts, ensuring alignment of the support arm with the beam's top flange surface (Figure 6.4c).
- (d) Subsequently, LVL panels were sequentially placed on the top flange of the steel beam. At this stage, bolts were inserted but not tightened (Figure 6.4d).
- (e) After positioning all timber panels, the bolts were installed and tightened (Figure 6.4e).
- (f) Wheels were installed at midspan to guide vertical movement of the specimen during testing, their displacement is guided by a channel steel section attached to the portal frame (Figure 6.4f).
- (g) Next, the timber was protected with plastic film at the gaps, then, the mortar was poured

using manual tools to ensure even distribution and removal of air pockets (Figure 6.4g).

- (h) Finally, steel plates were placed at the gaps and near the panel edges to ensure horizontal alignment of the timber slabs (Figure 6.4h).



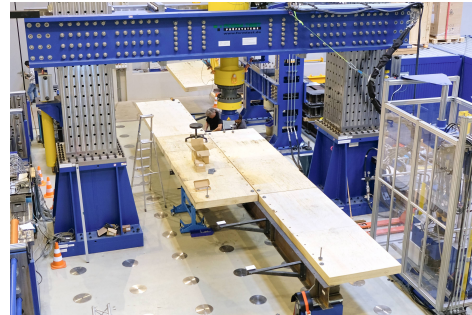
(a)



(b)



(c)



(d)



(e)



(f)



(g)



(h)

Figure 6.4: Pictures showing the assembly steps: (a) positioning of steel beam; (b) installation of ratchet straps; (c) installation of supporting braces; (d) placement of LVL panels; (e) preloading of bolts; (f) installation of wheels at midspan; (g) filling transversal gaps with mortar; (h) placement of steel plates to achieve horizontal alignment of slabs.

6.6. TEST SETUP AND INSTRUMENTATION

The test setup and the instrumentation of the steel beams is depicted in Figure 6.5. The instrumentation layout is illustrated in Figure 6.6. The tests were carried out at the Laboratory of Engineering Structures of the University of Luxembourg in a Test portal PP 4000 HK-2DH (Form+Test) equipped with a hydraulic jack to apply the load vertically, it has a capacity of 4 MN.

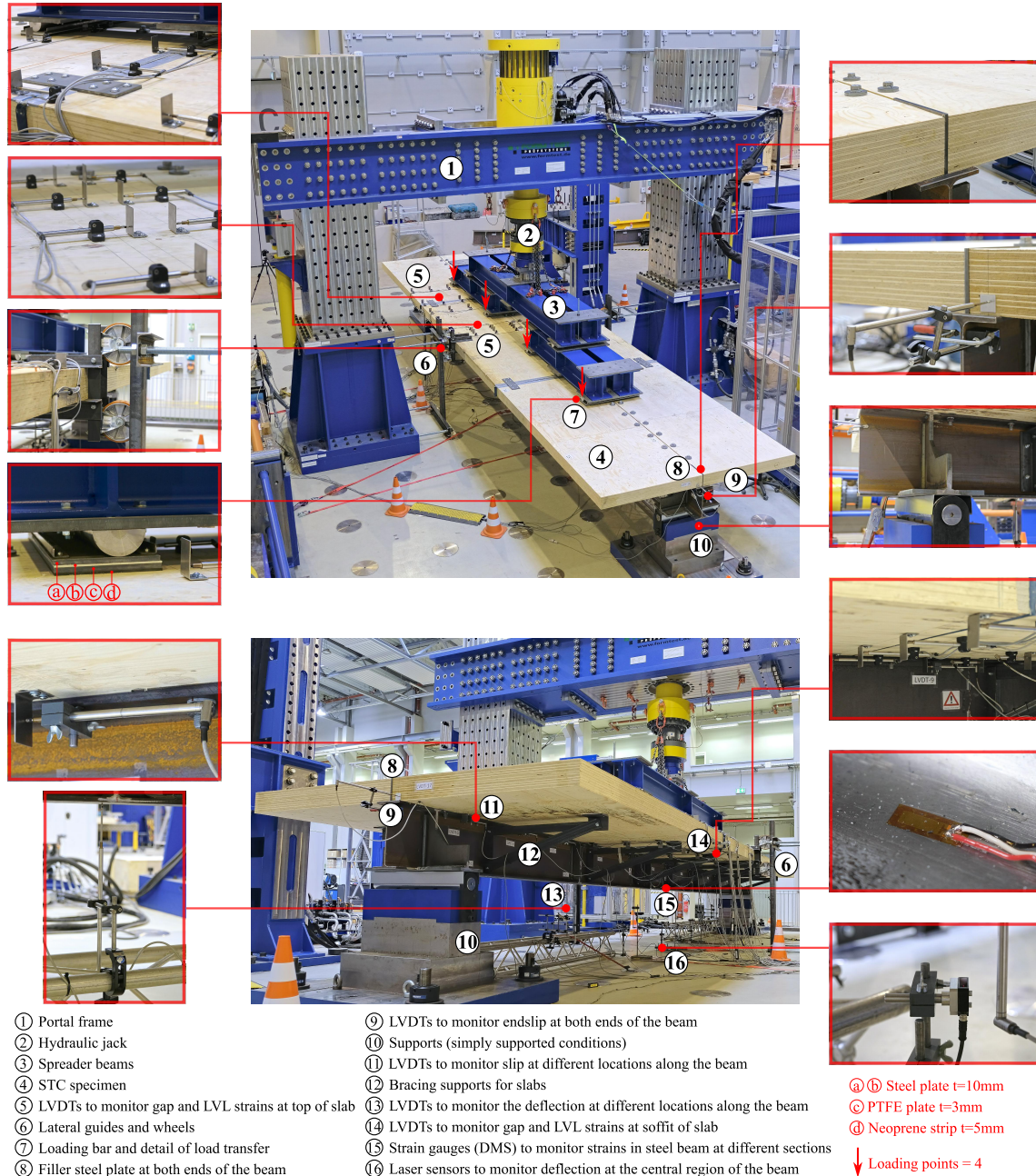


Figure 6.5: Test setup and instrumentation of the STC beams.

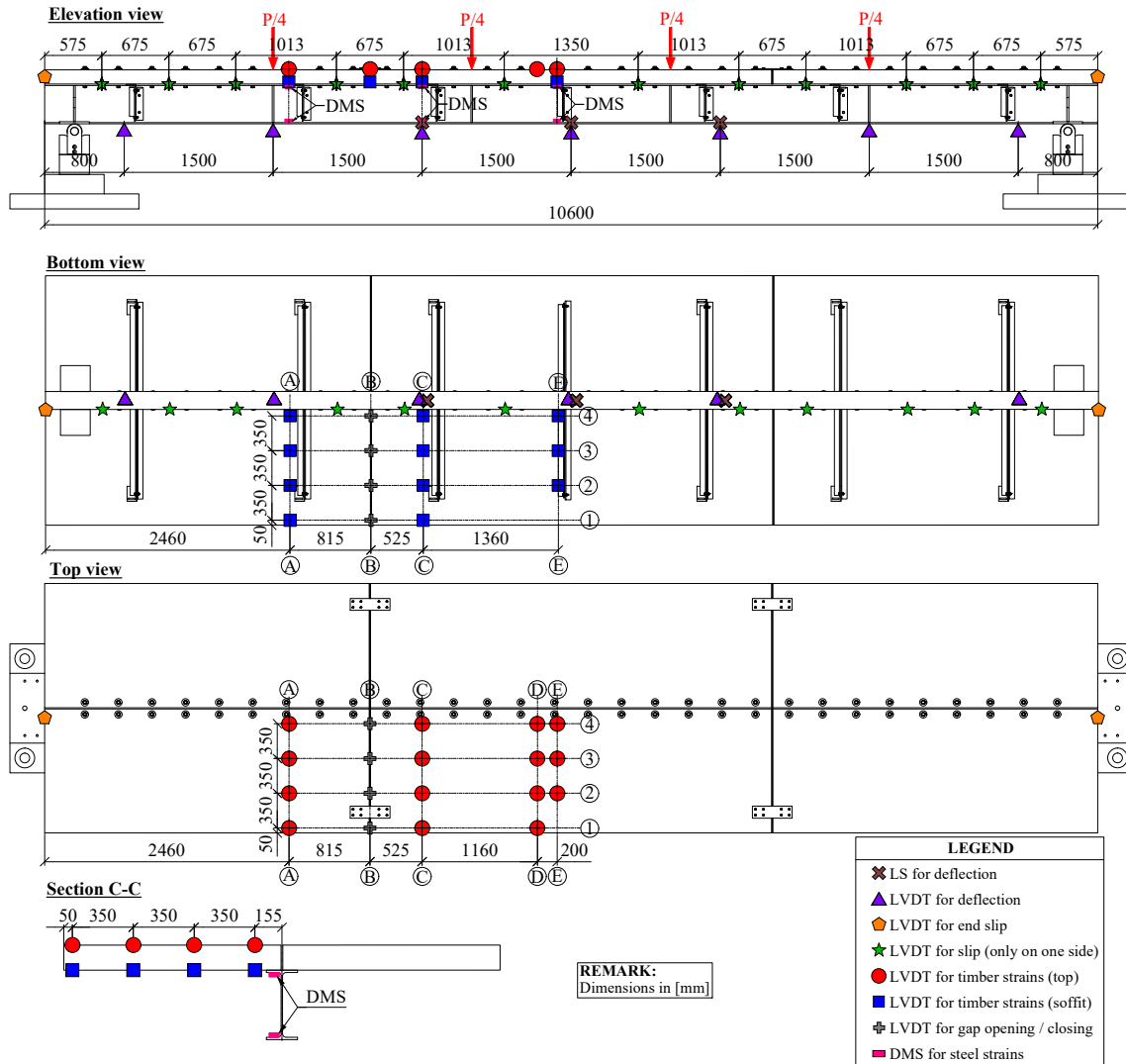


Figure 6.6: Test setup and instrumentation of the STC beams.

The two STC beam specimens were simply supported at two points and the load was transferred to the beam with spreader beams that apply the load at four points through rollers with a length of 800 mm. These rollers rest on a set of plates (see Figure 6.5, part 7), from top (next to the rollers) to bottom (next to the LVL slabs), as follows: a steel plate (800×200×10 mm), a PTFE plate (800×200×3 mm), a steel plate (800×200×10 mm), and a neoprene strip (800×200×5 mm).

The instrumentation of the STC beam consisted of strain gauges (DMS) installed in the steel beam, linear variable differential transformers (LVDTs) and laser sensors that were placed at different locations to monitor relevant displacements. At different sections of the LVL slabs, LVDTs were placed at the top and at the soffit, to monitor local deformations and to later obtain strains. The endsip at both ends of the beam was monitored with LVDTs. Similarly, the slip along the beam was monitored at different locations along the beam with LVDTs installed at the edge of the top flange of the steel beam. LVDTs and laser sensors were placed under the STC beam, on the strong floor to monitor the deflection of the beam at the bottom flange of the

steel beam and at different locations along the beam. In addition, the strains in the steel beam were monitored using strain gauges that were installed in three sections of the steel beam at the inner faces of the top and bottom flanges of the beam.

6.7. LOADING PROCEDURE

In these simply supported beams tested in 6-point bending, the load was applied symmetrically at four points on the top surface of the LVL slabs using a spreader beam to transfer the load, the details are shown in Figure 6.7. In this testing campaign the 6-point bending test setup was established to impose conditions on the STC beams comparable to that induced by a uniformly distributed load as it is the standard situation for structural analyses. The loading strips at each loading point were 800 mm long in the transversal direction, the distance from the support to the first loading point was 2 m, similarly, the distance between the four loading points was 2 m.

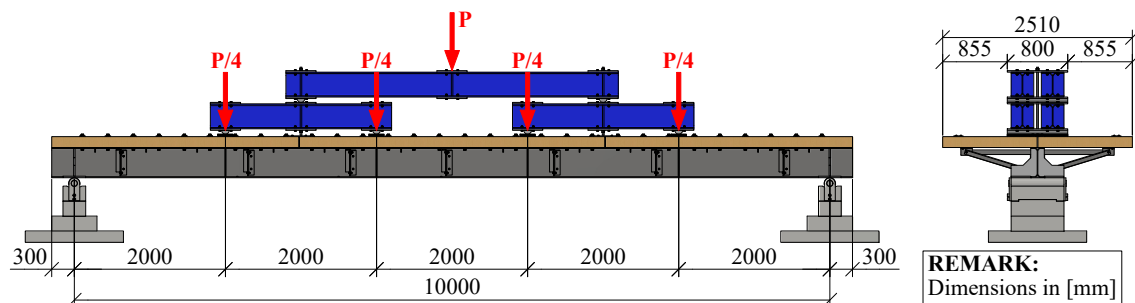


Figure 6.7: Details of the load introduction.

Due to the lack of testing standards targeting specifically STC structures, the loading procedure implemented in this study was based on the loading procedures established in EN 26891 [136] and Eurocode 4, Annex B [94]. The loading procedure presented schematically in Figure 6.8, shows that the specimens were initially loaded to around 40% of the estimated maximum load (P_{est}) and unloaded to 10% of P_{est} as established in the initial loading-unloading cycle of EN 26891 [136]. To assess the response of the STC system in the elastic range (e.g. serviceability conditions), 25 cycles within $0.1P_{est}$ and $0.4P_{est}$ were applied. Then, the specimen was gradually loaded in several incremental steps, the load values corresponding to the different load levels indicated in Figure 6.8 are presented in Table 6.2. In both tests the load was applied at a rate of 0.2 mm/s.

The loading procedure was similar for the two tested STC beams, however, in BT-1 the specimen was unloaded after reaching a load of 674 kN and a midspan deflection of ~400 mm because the maximum travel of the hydraulic jack was reached. In BT-2 this issue was addressed, an extension arm was added to the hydraulic jack to increase the travel range, nevertheless, BT-2 was stopped when the maximum midspan deflection for this test setup was reached (i.e. ~650 mm).

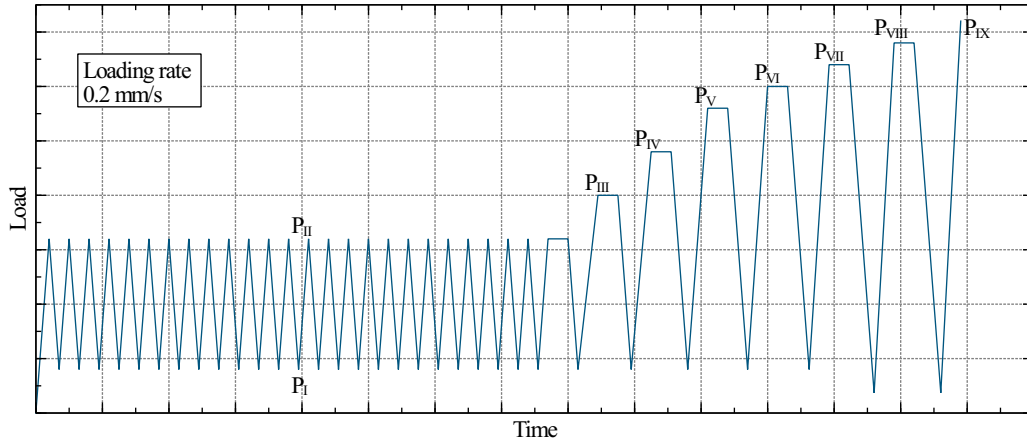


Figure 6.8: Schematic representation of the time history of the applied load.

6.8. RESULTS AND DISCUSSION

6.8.1. LOAD-DEFLECTION OF THE STC BEAMS

The moment-midspan deflection and load-midspan deflection curves obtained from BT-1 and BT-2 are presented in Figure 6.9a and Figure 6.10a, and the deflection along the beam, measured with LVDT and laser sensors, for different loading stages is shown in Figure 6.9b and Figure 6.10b. Additionally, the load and the corresponding midspan deflection values at different loading stages are presented in Table 6.2. Pictures showing an STC beam at different loading stages are depicted in Figure 6.11. In Figure 6.9a, Figure 6.10a and in Table 6.2, the moment (M) corresponds to the moment at midspan estimated considering an even distribution of forces at each of the four points where a load of $P/4$ was applied, and the force (P) corresponds to the total force applied to the specimen. Hence, the moment in $\text{kN}\cdot\text{m}$ was estimated as $M = 6 \cdot P \cdot L / 40$. The forces, the moment at midspan, and the deflections reported here do not include the effects of the self-weight which cause an additional bending moment at midspan (M_{sw}) of approximately $38 \text{ kN}\cdot\text{m}$.

In general, both beams exhibited similar response in terms of load-deflection. The response of the beam changed from linear to nonlinear at a load of about 400 kN (moment of $600 \text{ kN}\cdot\text{m}$) and a deflection of $\sim 60 \text{ mm}$, in both tests. This began around loading stage III, closely coinciding with the yielding of the bottom flange in the steel profile at the midspan section (section E), which occurred between loading stages III and IV. The yielding of the bottom flange was identified when the strain exceeded 1.9% . Additionally, when a load of about 600 kN (moment of $900 \text{ kN}\cdot\text{m}$) was reached, the load-deflection curve flattened significantly.

In BT-1, the maximum load reached was 674 kN (moment of $1011 \text{ kN}\cdot\text{m}$) while BT-2 reached a maximum load of 686 kN (moment of $1029 \text{ kN}\cdot\text{m}$). Remarkably, these values are nearly twice the plastic moment resistance of the IPE 400 (i.e. $521 \text{ kN}\cdot\text{m}$), which is calculated considering the actual properties of the steel profile, a yielding strength of 399 MPa (see Section 6.3.2).

In BT-2, after loading stage VIII, in the subsequent loading phase, a sudden drop of the load was observed. This drop was linked to mortar crushing in one of the gaps and delamination of

the LVL near this gap. The maximum deformations observed in the two tests were ~400 mm and ~650 mm, respectively for BT-1 and BT-2, which demonstrate the large deformation capacity of the tested STC beams. However, it is important to highlight that the termination of both tests was dictated by the maximum deformation capacity of the test setup, rather than the complete fracture of the specimens. Notably, the test BT-1 was stopped at a smaller deflection compared to BT-2, attributed to the latter having an extended range of the jack's travel due to an added arm extension, a modification not implemented in BT-1.

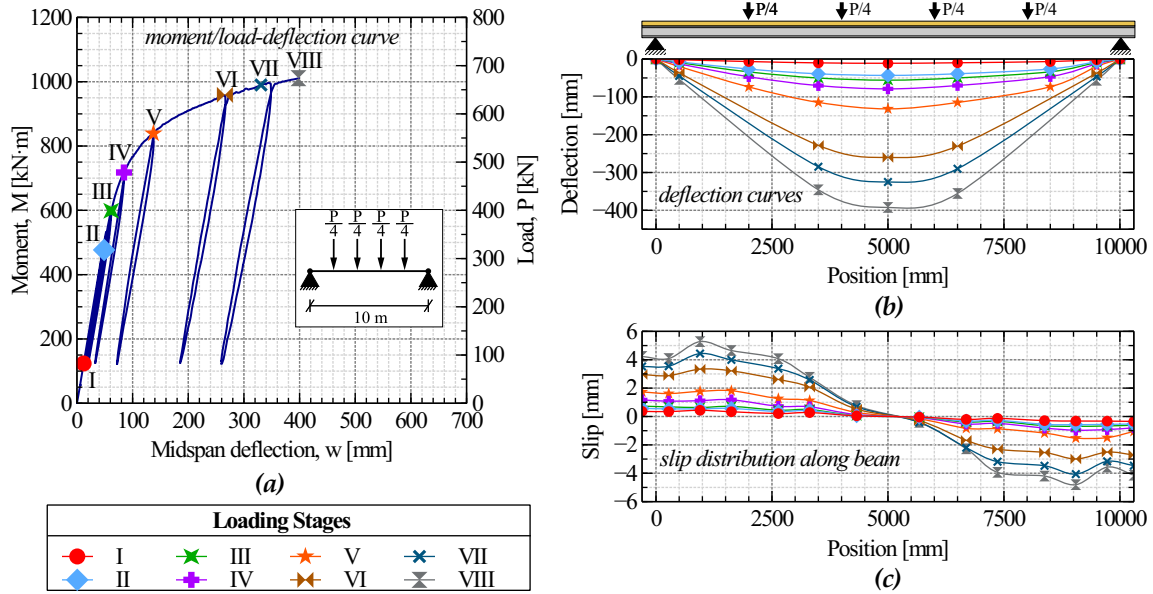


Figure 6.9: Load-deformation response of BT-1: (a) moment/load-deflection curve; (b) deflection curves; (c) slip distribution along beam.

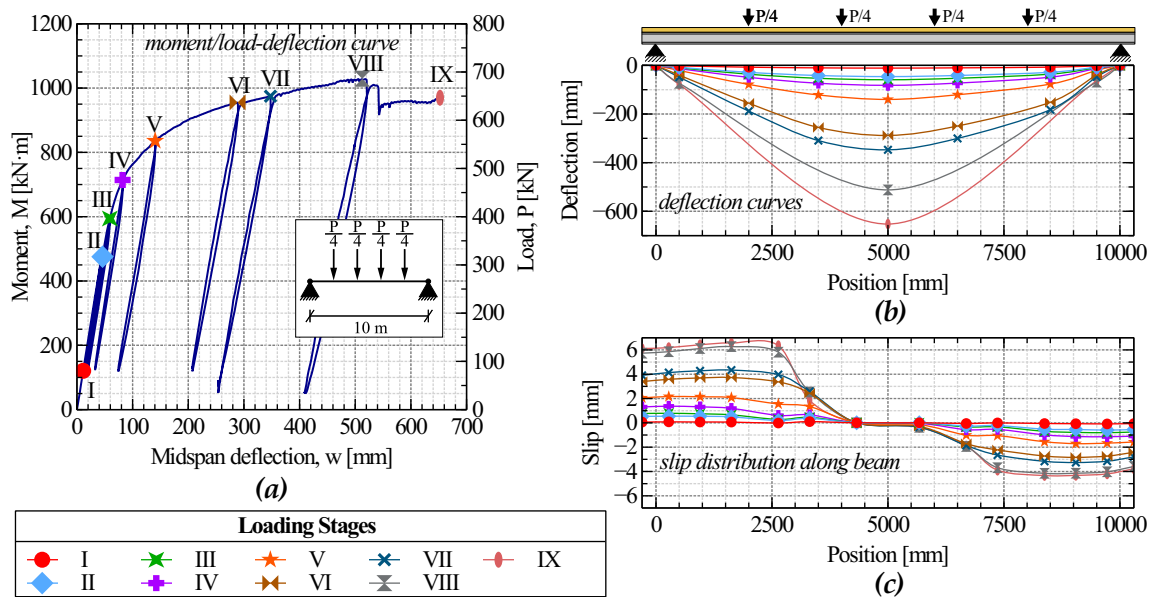


Figure 6.10: Load-deformation response of BT-2: (a) moment/load-deflection curve; (b) deflection curves; (c) slip distribution along beam.

Table 6.2: Parameters obtained at different loading stages.

Test	Loading Stage	Load	Moment	Midspan Deflection	Maximum Slip	Strains ^a					
						Section A		Section C		Section E	
		P [kN]	M [kN·m]	w [mm]	δ [mm]	ϵ_{timber} [‰]	ϵ_{steel} [‰]	ϵ_{timber} [‰]	ϵ_{steel} [‰]	ϵ_{timber} [‰]	ϵ_{steel} [‰]
BT-1	I	82.6	123.9	12.0	0.4	-0.18 (0.09)	-0.22 (0.26)	-0.12 (-0.07)	-0.32 (0.40)	-0.22 (-0.01)	-0.14 (0.40)
	II	317.9	476.8	48.8	0.6	-0.40 (0.07)	-0.51 (0.95)	-0.59 (-0.25)	-0.62 (1.29)	-0.71 (-0.09)	-0.30 (1.34)
	III	399.0	598.6	61.5	0.7	-0.43 (0.13)	-0.63 (1.18)	-0.79 (-0.30)	-0.75 (1.62)	-0.97 (-0.10)	-0.31 (1.35)
	IV	478.5	717.7	84.5	1.2	-0.44 (0.25)	-0.87 (1.45)	-1.06 (-0.28)	-0.92 (1.76)	-1.35 (-0.00)	-0.48 (3.23)
	V	559.4	839.0	137.4	1.8	-0.36 (0.26)	-1.00 (1.69)	-1.66 (-0.01)	-1.12 (2.28)	-2.16 (-0.39)	-0.40 (3.45)
	VI	639.4	959.2	265.8	3.3	-0.12 (0.17)	-1.07 (2.00)	-3.11 (1.64)	-1.13 (2.37)	-3.55 (1.11)	-0.28 (12.32)
	VII	659.9	989.9	330.7	4.4	-0.14 (0.15)	-1.10 (2.20)	-3.78 (2.35)	-1.13 (3.90)	-4.09 (1.50)	-0.33 (16.45)
	VIII	674.0	1011.0	398.0	5.3	-0.35 (0.15)	-1.17 (2.28)	-4.59 (3.06)	-1.39 (14.01)	-4.69 (1.74)	-0.27 (19.07)
BT-2	I	80.5	120.7	11.2	0.1	-0.06 (0.00)	-0.10 (0.24)	-0.14 (-0.08)	-0.15 (0.32)	-0.20 (-0.05)	-0.06 (0.32)
	II	317.0	475.5	44.2	0.6	-0.11 (0.07)	-0.40 (0.95)	-0.59 (-0.02)	-0.46 (1.26)	-0.66 (-0.13)	-0.21 (1.33)
	III	396.2	594.3	59.1	0.8	0.12 (0.24)	-0.51 (1.19)	-0.81 (-0.02)	-0.60 (1.64)	-0.92 (-0.16)	-0.29 (1.81)
	IV	476.1	714.2	82.0	1.4	0.13 (0.37)	-0.69 (1.45)	-1.07 (0.06)	-0.79 (3.25)	-1.27 (-0.08)	-0.34 (2.26)
	V	557.2	835.7	140.5	2.2	0.04 (0.35)	-0.69 (1.73)	-1.65 (0.33)	-1.01 (5.07)	-1.97 (0.33)	-0.28 (3.15)
	VI	636.8	955.3	288.6	3.7	-0.88 (0.22)	-0.42 (2.52)	-3.46 (1.13)	-1.04 (13.34)	-2.99 (1.21)	-0.28 (18.69)
	VII	649.7	974.6	347.7	4.3	-1.20 (0.26)	-0.32 (2.87)	-4.34 (1.43)	-1.11 (19.86)	-3.31 (1.53)	-0.14 (20.23)
	VIII	686.0	1029.0	512.6	6.3	-1.86 (0.46)	-0.20 (3.68)	-11.46 (2.39)	-1.03 (31.02)	-3.99 (2.17)	0.35 (20.40)
	IX	646.6	969.9	653.0	6.6	-1.67 (0.22)	-0.54 (4.06)	-16.12 (1.08)	-2.57 (44.33)	-3.96 (2.11)	0.10 (20.27)

^a The values in parentheses indicate the strain values at the bottom of the component and the values that are not in parenthesis correspond to the strain values at the top of the component.

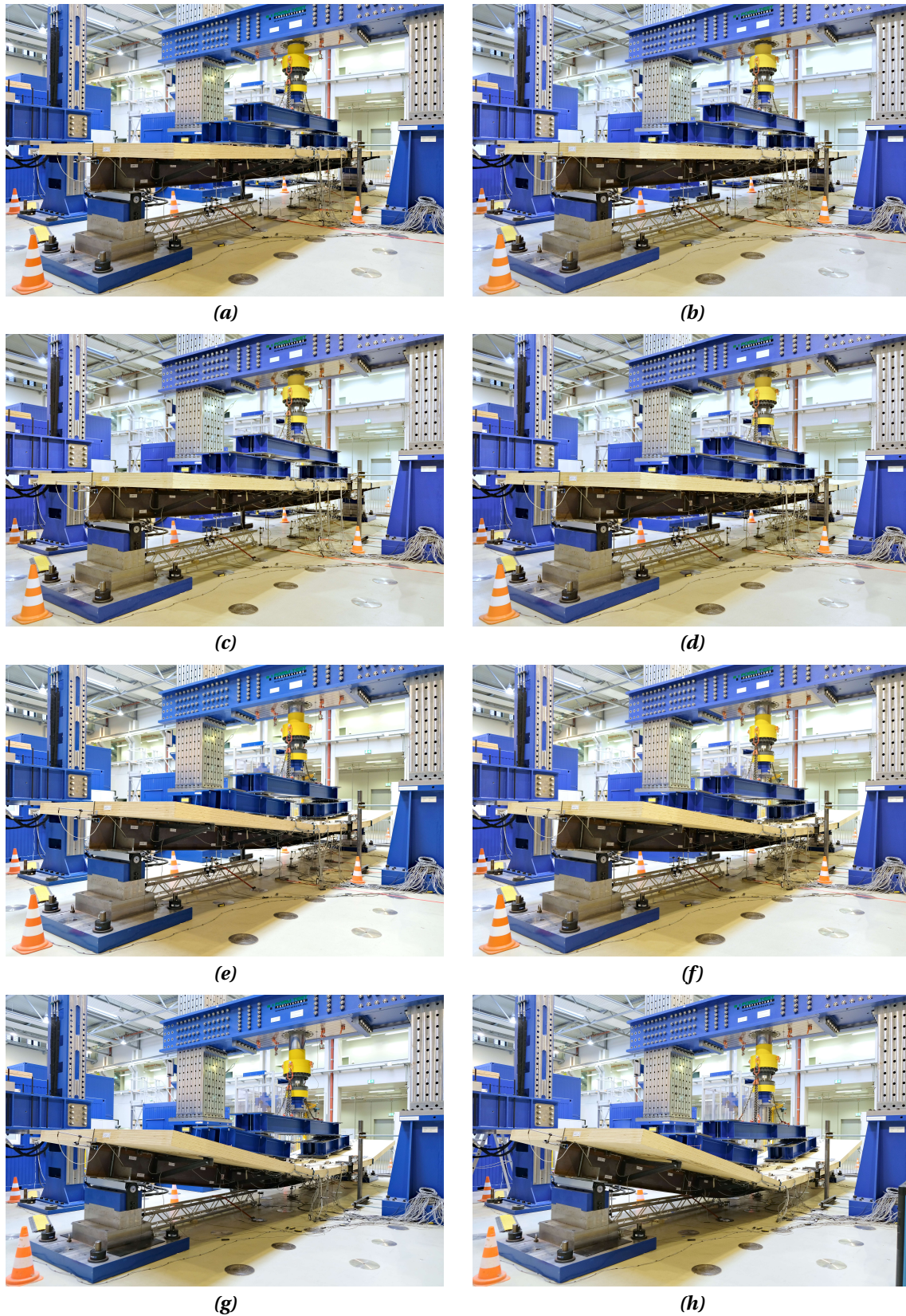


Figure 6.11: Pictures taken during the beam test at different loading stages: (a) Loading stage II; (b) loading stage III; (c) loading stage IV; (d) loading stage V; (e) loading stage VI; (f) loading stage VII; (g) loading stage VIII; (h) loading stage IX.

6.8.2. SLOPE OF THE ELASTIC BRANCH IN THE LOAD-DEFLECTION CURVE

The slope of the elastic branch in the load-deflection curve (k_{el}) values were 6.4 kN/mm for BT-1 and 7.2 kN/mm for BT-2. These values were calculated considering the forces and displacements corresponding to loading stages I and II, which are within the linear branch of the load-deflection curves. In the moment-midspan deflection curves in Figure 6.9a and Figure 6.10a it is evident that there was no loss of stiffness during the 25 loading-unloading cycles within the elastic range (i.e. service conditions). In the 25th loading cycle, the slope k_{el} values were recorded at 7.7 kN/mm for BT-1 and 8.0 kN/mm for BT-2.

6.8.3. SLIP MEASUREMENTS AND SHEAR CONNECTORS RESPONSE

The slip distribution along the beam was recorded with LVDTs placed in one side of the top flange of the steel beam (see Figure 6.6 and Figure 6.6). The slip distribution for different loading stages is illustrated in Figure 6.9c and Figure 6.10c for BT-1 and BT-2, respectively. In general, the largest slip values were observed in the last three connectors. However, in BT-1 the largest slip values were observed near the third shear connectors at both ends of the beam (see Figure 6.9c). Table 6.2 presents the maximum slip values obtained at different loading stages.

In BT-1 the slip distribution was almost symmetrical with respect to the midspan line with similar slip values in both halves of the beam, whereas in BT-2 the shape of the slip distribution was similar but the slip values were slightly larger in one half of the beam. The observed slip distributions in both beams align with the expected patterns, gradually increasing from the midspan towards the edges, and uninterrupted by the transversal gaps. This indicates that the mortar effectively transferred compression loads from the central to the edge panels, thereby activating the shear connectors of the edge panels.

In BT-1, at loading stage VIII the maximum slip values recorded in each half of the beam were 5.3 mm and 4.8 mm. In BT-2, at a similar load level in loading stage VIII, maximum slip values of 6.3 mm and 4.1 mm were recorded at each half of the beam. The difference of slip values observed in both halves of the beams is related to the alignment of the bolts in the holes of the beam, the half of the beam with smaller slip values indicates that the clearance between the bolts and the flange of the steel beam was smaller. Since the bolts have a diameter of 20 mm and the diameter of the holes is 24 mm the clearance can be any value within the range of 0 to 4 mm.

Within the elastic range (i.e. up to loading stage III) the maximum slip values were smaller than 1 mm in both beams. Since these values are relatively small compared to the deformation capacity of the connections observed in the push out tests (see Chapter 5), this showcases the reuse potential of the timber slabs when the loads acting on the beams remain within the elastic range (i.e. serviceability limit states). Moreover, even at the last loading stage, the most stressed connections remained undamaged, with an observed embedment of approximately 1 mm in the timber, demonstrating the connections' robustness.

6.8.4. STRAINS IN THE TIMBER SLABS AND EFFECTIVE WIDTH

STRAINS IN THE TIMBER SLABS

The strains were measured at sections A, C, D, and E (see Figure 6.6) of the slabs in the top and the soffit. The strains recorded in these sections for different loading stages are shown in Figure 6.12 for BT-1 and Figure 6.13 for BT-2.

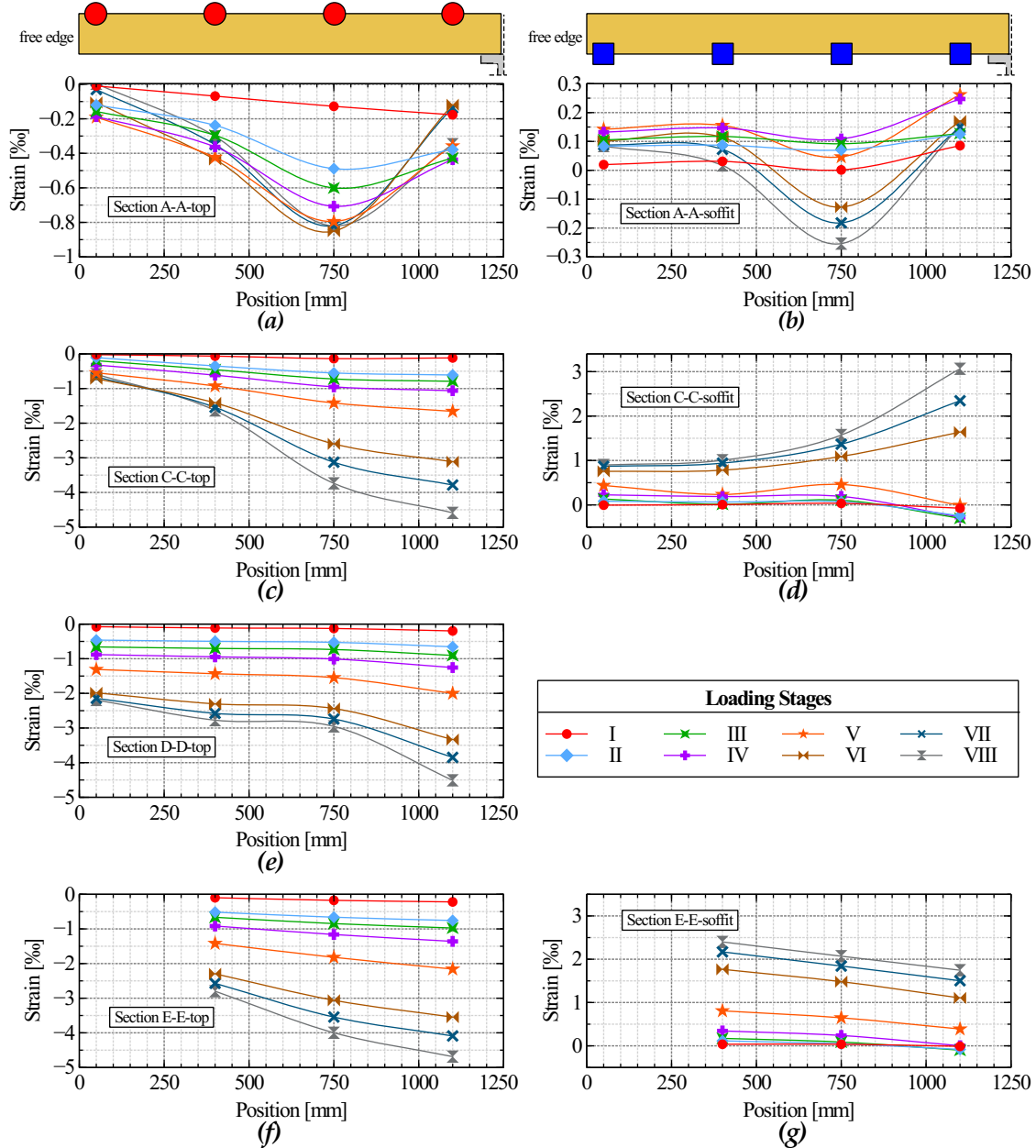


Figure 6.12: Strain measurements in the timber slab of BT-1: (a) section A-A at the top; (b) section A-A at the soffit; (c) section C-C at the top; (d) section C-C at the soffit; (e) section D-D at the top; (f) section E-E at the top; (g) section E-E at the soffit.

The results show that the strains distribution in the timber along the section is non-uniform. In the sections located in the central slab panel (Sections C, D and E) the strains are larger near

the longitudinal axis of the beam and decrease towards the free edge of the panels. This indicates the presence of shear lag effects which are to be considered when analyzing the resistance of the cross-section, because the width of the slab might not be fully utilized. Additionally, in sections C, D, and E negative strains were recorded in the sensors placed on the top surface of the slab indicating compression of the top fibers in the entire width of the timber slab. Analogously, in the sensors installed on the soffit of the slab, positive strain values were recorded, indicating tension of the bottom fibers in the entire width of the timber slab.

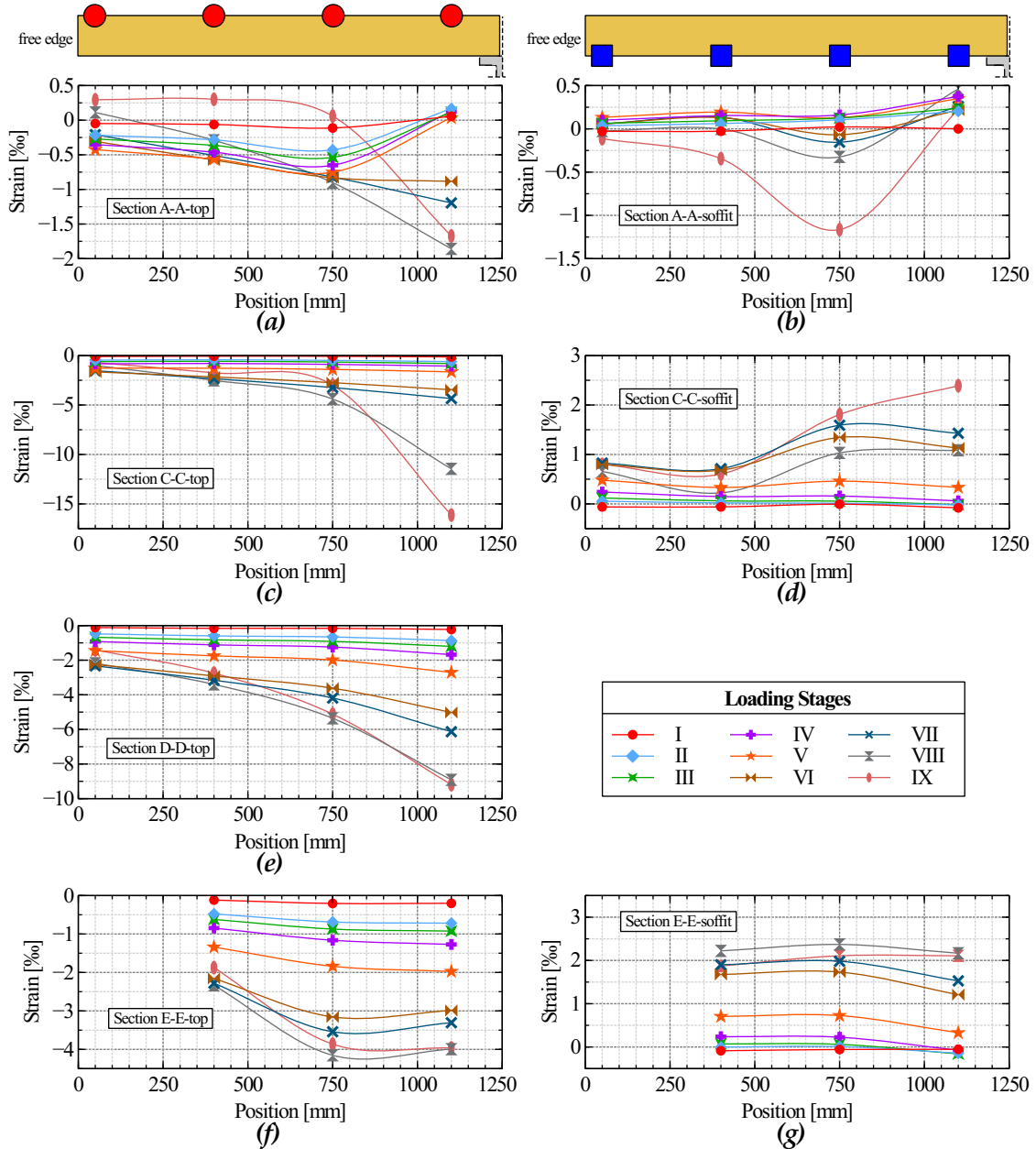


Figure 6.13: Strain measurements in the timber slab of BT-2: (a) section A-A at the top; (b) section A-A at the soffit; (c) section C-C at the top; (d) section C-C at the soffit; (e) section D-D at the top; (f) section E-E at the top; (g) section E-E at the soffit.

EFFECTIVE WIDTH

Due to shear deformations appearing in the plane of the timber slab and acting in the longitudinal direction of the steel beam, the slab does not deform uniformly throughout its entire width, therefore, the normal stresses lag from those appearing near the steel beam. The current Eurocode 5 [69] does not include a definition of the effective width for LVL or CLT in composite sections. For timber cross-sections combining LVL ribs and LVL panels, it is common practice to define the effective width as one tenth of the span length ($L/10$) [13] as indicated in Eurocode 5 [69] for plywood. Nevertheless, background supporting this assumption is lacking. Further to this, little has been mentioned in the literature concerning the definition of an effective width for STC beams. There are studies on the effective width of CLT slabs connected to timber beams, for instance Masoudnia et al. [138] proposed a formulation that depends on several parameters such as the thickness of the layers, the span, and the modulus of elasticity. Similarly, Kleinhenz et al. [139] found that the effective width of timber composite beams with CLT panels and glulam ribs is on average $0.15L$ or $L/6.67$. Concerning, composite cross-sections with LVL panels as slabs, nothing has been reported in the literature as far as the author of this contribution is aware.

Considering the measurements of strains at midspan in section E, at the top of the timber slab, an effective width was estimated according to equation 6.1:

$$b_{eff} = \frac{\int \varepsilon_{xx} dy}{\varepsilon_{xx, max}} \quad (6.1)$$

Strain measurements were taken only across half of the timber slab's width and at a limited number of points, leaving the strain values at certain locations (e.g. the edge, the center, the other half of the slab) unknown. The measured values were extrapolated, a symmetric distribution was assumed, and the links between measured points were treated as straight lines for calculation purposes. Figure 6.14 shows the strain distributions considered for BT-1 and BT-2 at section E. Based on the strains measured during the final loading stage, effective widths of 1881 mm for BT-1 and 1771 mm for BT-2 were determined, corresponding to an effective width of approximately $L/5.5$. Additionally, the effective width was determined for loading stage III, which corresponds approximately to the proportional limit of the STC beam, obtaining effective widths of 2002 mm for BT-1 and 2016 mm for BT-2.

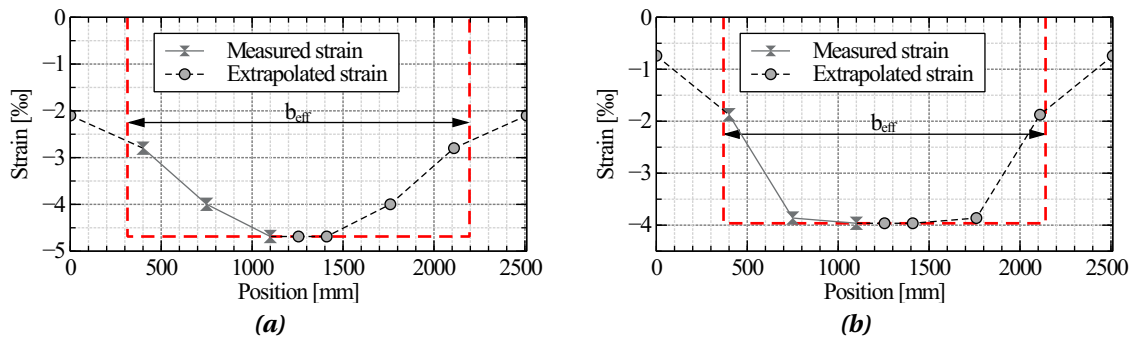


Figure 6.14: Strain distribution and effective width at the top of the slab in section E-E of the STC beams of (a) BT-1 and (b) BT-2.

6.8.5. STRAIN DISTRIBUTION THROUGH THE DEPTH OF THE STC BEAM

The strain distribution through the depth of the STC beam is shown in Figure 6.15 for BT-1 and Figure 6.16 for BT-2, in subfigures (a), (b) and (c) respectively for sections A, C and E. These plots were built considering the measurements of the sensors located at axis 4 (see Figure 6.6) for the strains in the LVL slab, and the measurements of the DMS sensors installed in the steel section. The values for different loading stages are presented in Table 6.2. The results show that most of the steel section was in tension during the test whereas the timber was almost in full compression in the initial loading stages and then as the deflection and curvature increased the timber started to take tension at the soffit and the compression increased at the top.

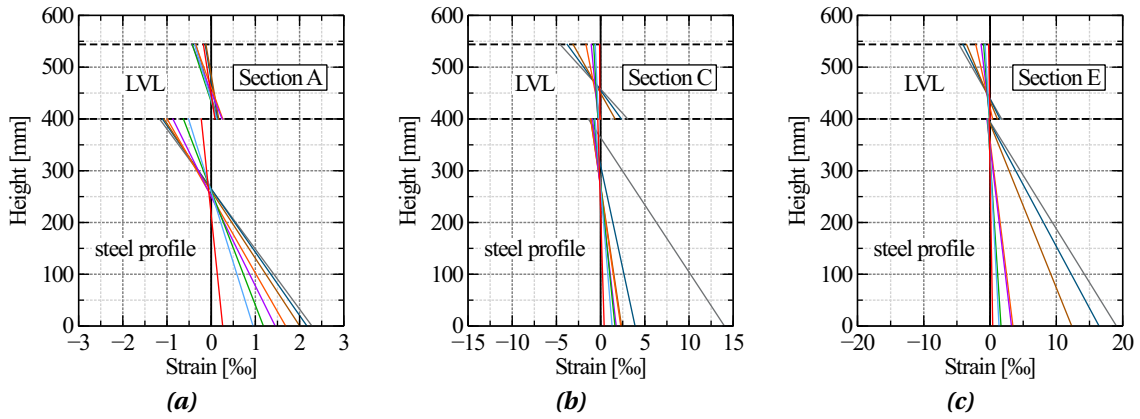


Figure 6.15: Strain distribution of BT-1 at (a) section A; (b) section C; and (c) section E.

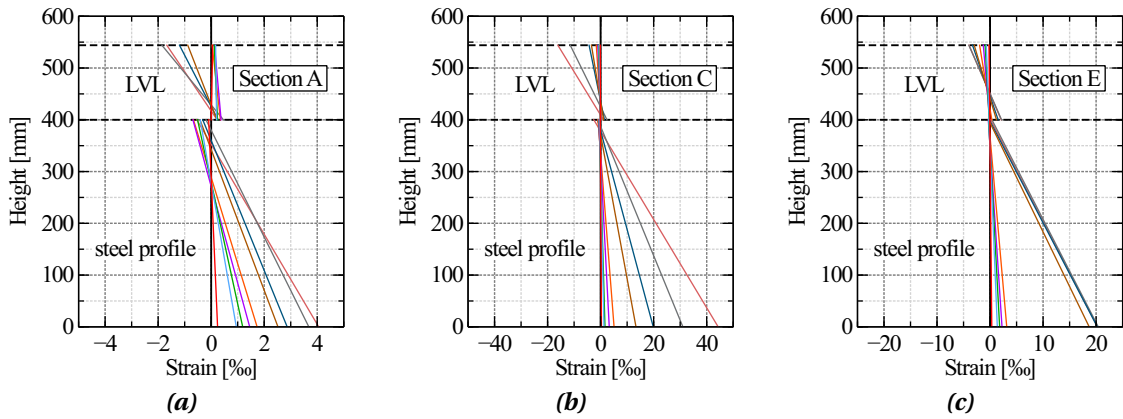


Figure 6.16: Strain distribution of BT-2 at (a) section A; (b) section C; and (c) section E.

Experimental results of the LVL showed that the proportional limit of the timber is reached at a strain of about 5‰, whereas the strain corresponding to the proportional limit of the steel S355 obtained experimentally is 1.9‰. According to this, the timber remained within the elastic range throughout the test and the steel beam surpassed its proportional limit at the bottom flange located in the midspan section at loading stage III. This is consistent with the transition from linear to nonlinear behaviour observed in the moment-midspan deflection curves shown in Figure 6.9 and Figure 6.10.

In BT-2 there was a redistribution of stresses which developed from loading stage VI onwards. From this loading stage the strains in the bottom flange of the steel beam increased significantly in subsequent loading stages at section C, from 13.3‰ in loading stage VI to 44.3‰ in loading stage IX, whereas in the midspan in section E, the strains in tension at the bottom flange of the steel beam increased from 18.7‰ in loading stage VI to 20.3‰ in loading stage IX. In fact, the strain distribution lines for the steel section, at Section E (midspan) as shown in Figure 6.16c and Table 6.2 for loading stages VII, VIII, and IX, overlap, indicating that there is no significant increase in stress within the steel profile at the midspan section. This suggests that there was a redistribution of stresses in which the regions near the transversal gaps filled with mortar became the most stressed regions of the beam.

According to these observations, when the the STC beams reach their capacity, the timber slab is capable of withstanding significant loads while remaining within the elastic range. In contrast, the steel beam may enter into plasticity, thereby enabling the use of its plastic capacity. Additionally, when analyzing the bending capacity of this STC beam, three critical sections must be considered: the midspan section and the two sections at the joints (transversal gaps).

6.8.6. GAP OPENING MEASUREMENTS

LVDT sensors were positioned at section B-B (see Figure 6.6) at the gap's location to monitor the opening of the gap at the soffit as the load increased. The measurements obtained at various loading stages are depicted in Figure 6.17. In the graphs, the horizontal axis represents half of the slab's width where the sensors were positioned; with position 0 mm at the slab's free edge and position 1250 mm at the center of the slab width.

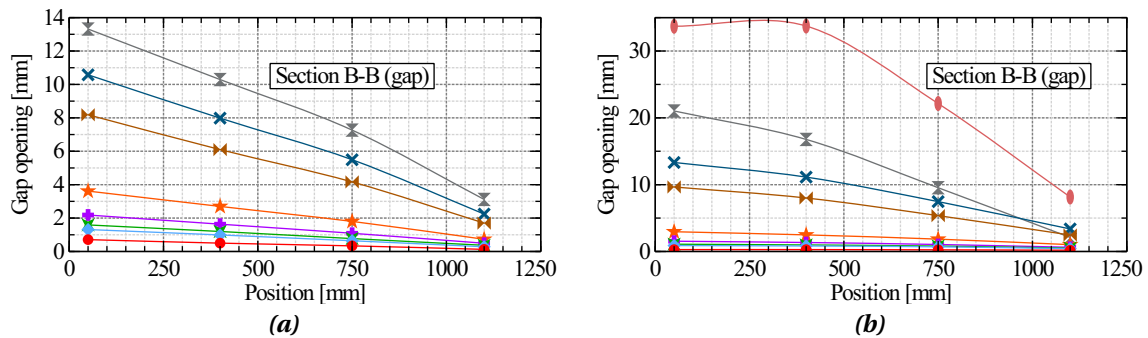


Figure 6.17: Gap opening measurements (section B-B) of (a) BT-1 and (b) BT-2.

For both beams, the gap openings were smaller near the center of the slab, close to the slab-to-beam connection, and gradually expanded towards the free edge, where larger displacements were observed. Up to loading stage V, the gap opening in both beams remained under 4 mm. Beyond this stage, the gap opening increased significantly. In BT-1, by the last loading stage (i.e. VIII), the gap opening was approximately 3 mm near the connection and approximately 13 mm near the free edge. In BT-2, at the final loading stage (i.e. loading stage IX), the gap opening was around 8 mm near the connection and approximately 34 mm towards the free edge.

6.8.7. BEAM'S BENDING STIFFNESS

The results of the tests revealed that maximum bending moments were reached at deflection values that are several times the deflections observed by the end of the linear-elastic branch of the moment-deflection curve. This indicates that the design of the demountable STC beams is likely to be governed by deformation limitations rather than their ultimate capacity.

The deflection of an STC beam depends on its effective bending stiffness $((EI)_{ef})$. It is an important parameter that can be used to determine the deflection of a beam within its linear-elastic range. The experimental bending stiffness $((EI)_{exp})$ of the STC beams was estimated for the load and deflections measured at loading stages I and III (see Figure 6.9 and Figure 6.10).

To simplify the calculations, an equivalent system with a uniformly distributed load has been considered. Since it was a six-point bending test with equidistant loads, and assuming equal magnitude for the 4 loads applied on top of the beam, the moment distribution can be approximated by an equivalent uniformly distributed load (q) according to Equation 6.2, where the load P is the total applied load in the system with 4 concentrated loads with a magnitude of $P/4$ for each load. Figure 6.18 shows the two equivalent systems, the two systems have equal moment at midspan and nearly identical moment distribution.

$$q = \frac{6 \cdot P}{5 \cdot L} \quad (6.2)$$

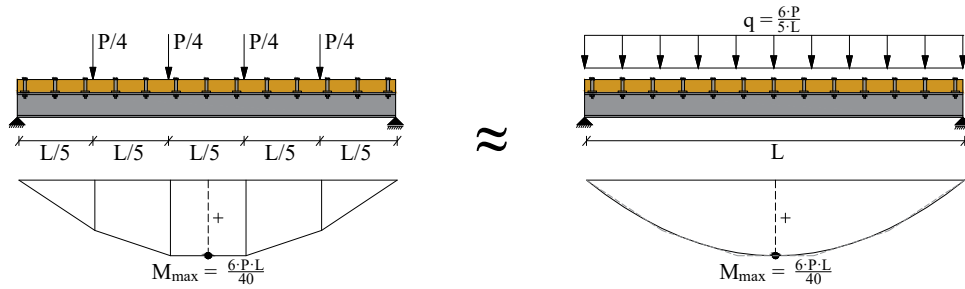


Figure 6.18: Equivalent systems and the respective bending moments resulting from four point loads $P/4$ as in the test setup and from a distributed load $q = \frac{6 \cdot P}{5 \cdot L}$

The deflection curve of a beam, also known as the elastic curve ($w(x)$), can be obtained by double integration of the curvature, which is represented by the second order differential equation presented in Equation 6.3.

$$\kappa(x) = \frac{d^2 w}{dx^2} = \frac{M(x)}{(EI)_{ef}} \quad (6.3)$$

After double integration of this equation for the moment function $M(x)$ corresponding to a uniformly distributed load $q(x)$, considering boundary conditions for a simply supported beam, and solving for $x = L/2$ to find the maximum elastic deflection (w_{el}), equation 6.4 is obtained. The experimental bending stiffness of the tested beams was obtained from this equation after solving for the bending stiffness as shown in equation 6.5. Thus, the experimental bending stiffness values for BT-1 were 107 552 kN·m at loading stage I and 101 372 kN·m at

loading stage III, and for BT-2 the bending stiffness values were 112 305 kN·m at loading stage I and 104 748 kN·m at loading stage III. The efficiency of the composite action in terms of the bending stiffness (η_{EI}) was estimated according to Equation 6.6, considering the experimental stiffness values for loading stage III. The η_{EI} values obtained for the tested beams, indicate an enhancement in stiffness of 76.1% for BT-1 and 82.6% for BT-2.

$$w_{el} = \frac{5 \cdot q \cdot L^4}{384(EI)_{ef}} \quad (6.4)$$

$$(EI)_{exp} = \frac{5 \cdot q \cdot L^4}{384w_{el}} \quad (6.5)$$

$$\eta_{EI} = \frac{EI_{exp} - EI_{K_0}}{EI_{K_\infty} - EI_{K_0}} \quad (6.6)$$

Möhler [93] studied the bending stiffness of composite beams with semi-rigid shear connections and proposed an analytical model to estimate $(EI)_{ef}$. The method was developed for simply supported beams subjected to loads giving a sinusoidal bending moment, because for that case the differential equation of partial composite action has a simple analytical solution. Nevertheless, this method can be used for loads giving a bending parabolic bending moment because the differences between the simplification and the exact solution of the differential equation are not significant.

Möhler's approach, also known as the " γ -method", has been included in Eurocode 5 [69] for timber composite members in bending. Although, the method was originally developed for timber-timber composite members (TTC), it has been used for other applications such as timber-concrete composite (TCC) beams for instance by Frangi et al. [140] and by Bathon et al. [141], and it has been also implemented for steel-timber composite beams by Loss et al. [85] and Aspila et al. [91], giving a good approximation to the experimental bending stiffness. Therefore, in this study the bending stiffness was calculated analytically with Möhler's approach, as specified in Annex B of Eurocode 5 [69]. Hence, $(EI)_{ef}$ was calculated according to Equations 6.7 to 6.10, with the definitions of the different parameters presented in Figure 6.20.

$$(EI)_{ef} = E_1 \cdot I_1 + E_2 \cdot I_2 + \gamma_1 \cdot E_1 \cdot A_1 \cdot a_1^2 + \gamma_2 \cdot E_2 \cdot A_2 \cdot a_2^2 \quad (6.7)$$

where:

$$\gamma_1 = \frac{1}{1 + \frac{\pi^2 \cdot E_1 \cdot A_1 \cdot S}{K \cdot L^2}} \quad (6.8)$$

$$\gamma_2 = 1 \quad (6.9)$$

$$a_2 = \frac{\gamma_1 \cdot E_1 \cdot A_1 \cdot (h_1 + h_2)}{2(\gamma_1 \cdot E_1 \cdot A_1 + \gamma_2 \cdot E_2 \cdot A_2)} \quad (6.10)$$

To estimate the bending stiffness of the tested beams with Möhler's approach, the connector's spacing S , was determined as the number of connectors per unit length. For comparison, the bending stiffness was estimated considering two different assumptions for the shear connection stiffness K (see Figure 6.19) as follows:

1. **Initial stiffness of the connector, K_1 :** If it is assumed that the shear connections have not reached the bearing branch, then, the stiffness of the connectors is their initial stiffness K_1 as estimated from the load-slip curves obtained in the push-out tests (see Section 5.8.1).
2. **Stiffness in the bearing branch, K_2 :** When it is assumed that the connectors are in full contact with the flanges and the timber, the stiffness of the connectors is governed by the embedment of the connection in the timber, as observed in the push-out tests for the bearing branch (K_2) (see Section 5.8.1).

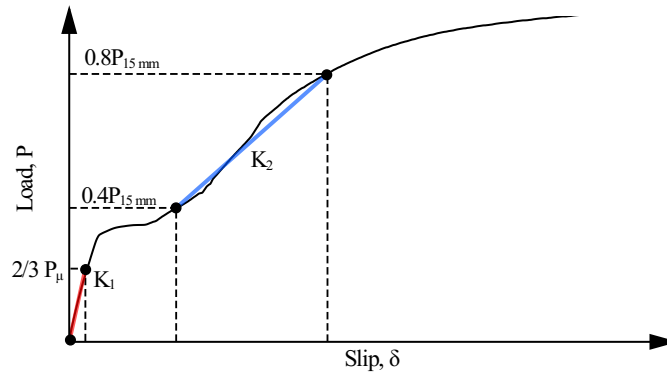


Figure 6.19: Shear connection stiffness values considered for the analytical estimation of the beams' bending stiffness.

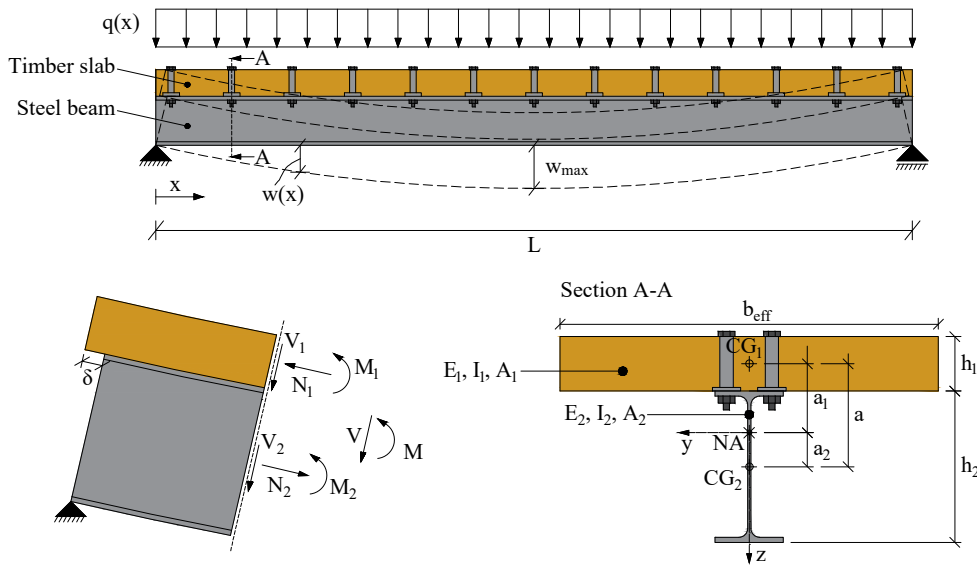


Figure 6.20: Idealisation of the steel-timber composite beam system and cross-section geometry definitions.

Table 6.3: Summary of analytical and experimental beam stiffness and deflections at midspan for the tested beams.

Beam test	Shear connection	Connector's stiffness		Beam's bending stiffness			Midspan deflection			
		Notation	Value [kN/mm]	$(EI)_{ef}^a$ [kN·m ²]	$(EI)_{exp}^b$ [kN·m ²]	$(EI)_{exp}^c$ [kN·m ²]	w_{el}^d [mm]	w_{el}^b [mm]	w_{el}^e [mm]	w_{el}^c [mm]
BT-1	SCT-1	K_1	61.9	108 536	107 552	101 372	11.9	12.0	57.4	61.5
		K_2	16.4	87 947			14.7		70.9	
		K_0	0.0	51 816			24.9		120.3	
		K_∞	∞	125 040			10.3		49.9	
BT-2	SCT-2	K_1	87.9	112 237	112 305	104 748	11.2	11.2	55.2	59.1
		K_2	23.5	94 260			13.3		65.7	
		K_0	0.0	51 816			24.3		119.5	
		K_∞	∞	125 040			10.1		49.5	

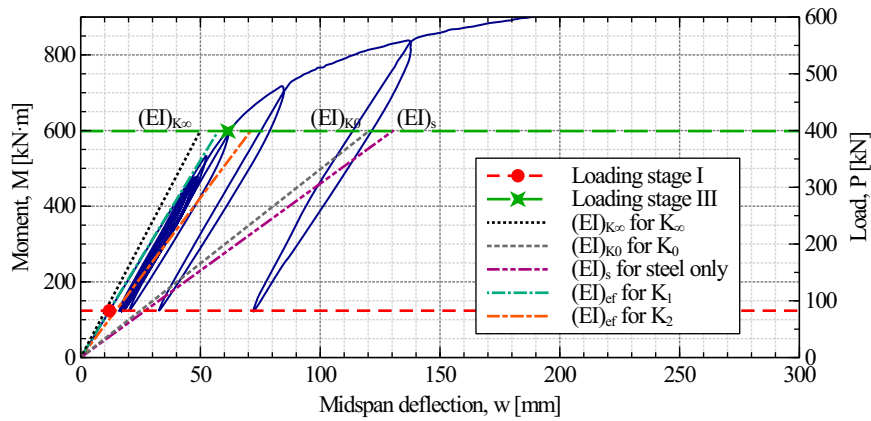
^a Analytically obtained bending stiffness based on the connector's stiffness.

^b Experimentally obtained values for loading stage I (i.e. beginning of the linear-elastic-branch).

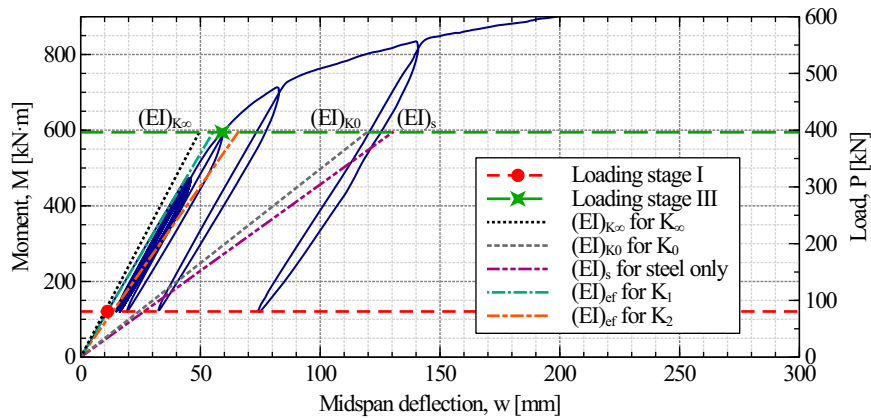
^c Experimentally obtained values for loading stage III (i.e. end of the linear-elastic branch).

^d Analytical prediction of the midspan deflection for loading stage I (i.e. beginning of the linear-elastic-branch).

^e Analytical prediction of the midspan deflection for loading stage III (i.e. end of the linear-elastic branch).



(a)



(b)

Figure 6.21: Moment-midspan deflection curves and beam stiffness for different shear connection scenarios for: (a) BT-1 and (b) BT-2.

A summary of the experimental and analytical bending stiffness values obtained for the tested beams is presented in Table 6.3 and represented graphically in Figure 6.21. From these results, it can be noticed that considering the initial stiffness of the connectors K_1 , leads to bending stiffness $(EI)_{ef}$ values which are in good agreement with the initial bending stiffness of the two beams, when the load at loading stage I is considered in the computation of $(EI)_{exp}$. According to the plots, this trend continues up to a load of 300 kN and a corresponding moment of 450 kN·m. However, when the calculations of $(EI)_{exp}$ are done considering the load reached at loading stage III, the bending stiffness $(EI)_{ef}$ calculated with the gamma method for K_1 overestimates the stiffness observed in the tests, leading to an underestimation of the midspan deflection.

When the stiffness of the bearing branch K_2 is considered to compute the bending stiffness $(EI)_{ef}$, the values underestimate the experimental bending stiffness $(EI)_{exp}$ for both beams, leading to midspan deflection values larger than the deflections measured in the tests. This indicates that, at this loading stage, the stiffness of the connectors might not be governed by the stiffness of the bearing branch K_2 as the connectors have reached very small slip values of less than 1 mm, and therefore, the bolts might not yet be working in bearing.

These results indicate that using Möhler's approach for the calculation of the bending stiffness of the tested STC beams gives reasonable results that are consistent with the experimental observations.

6.8.8. FAILURE MODE

In the specimen of BT-1 the steel beam plasticized and exhibited permanent deformations, however, no significant damages or local failures (e.g. buckling, fracture) were observed in the steel profile, and the midspan section exhibited the largest degree of plasticization. Although the deformation was large, the timber remained within the elastic range and there were no damages at the vicinity of the transversal gaps (see Figure 6.22c and Figure 6.22e), and the mortar did not fracture. This demonstrates that even at large deformations, the integrity of the mortar used to fill the gaps can be preserved. Furthermore, the most stressed shear connections remained undamaged, no noticeable damage was observed in the timber and in the holes of the beam flange (see Figure 6.23).

In the specimen of BT-2 the steel beam also plasticized, though to a larger degree as it underwent larger deformations. Similar to the specimen of BT-1, no significant damages or local failures were observed in the steel profile. The shear connection and the holes of the steel beam did not show damage (see Figure 6.23).

In BT-2 there was a redistribution of stresses leading to plasticization of the steel beams in the region near the transversal gaps, in which the recorded strains of the steel beam were larger than the strains in the midspan section in the last two loading stages. Additionally, the deformations and damages in the mortar and the timber close to the gap were larger, and the load drop observed after loading stage VIII was linked to crushing of the mortar in the transversal gap and delamination of the LVL (see Figure 6.22d and Figure 6.22f). Notwithstanding the large deformations underwent by this specimen and the delamination of some layers of timber, the

strains recorded in the timber revealed that the stresses remained within the elastic range.

These findings indicate that the failure of the tested STC beams is governed by plasticization of the steel section at midspan and at the joint sections where the slabs have a transversal discontinuity. The presence of these discontinuities (i.e. gaps filled with mortar) creates two additional critical sections where stresses tend to concentrate when certain load level is reached, due to the system's inability to transfer tensile forces through the gaps. The large deformations of the system and the concentration of the stresses at the gaps ultimately lead to the fracture of the mortar and delamination of the LVL slabs.

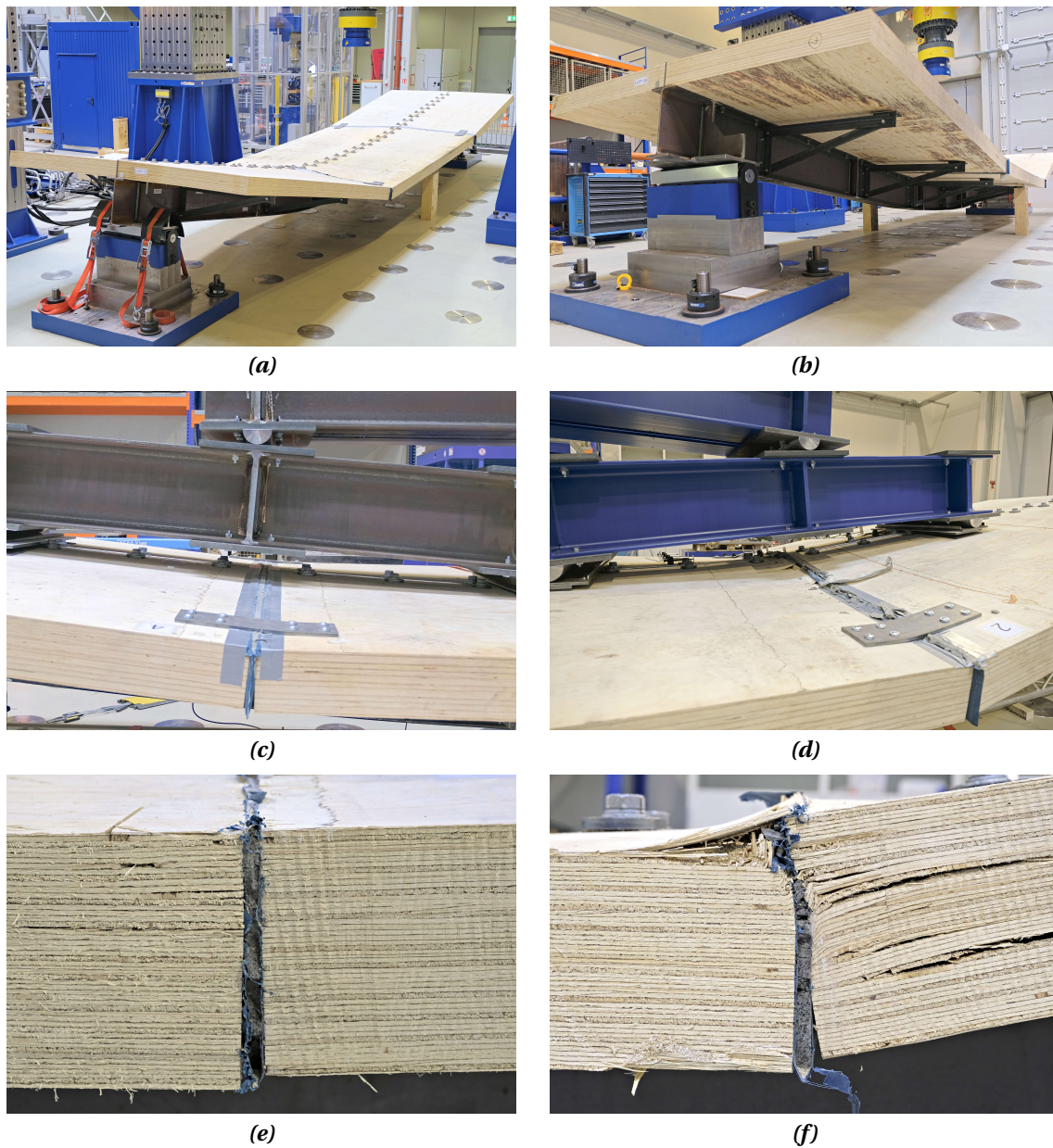


Figure 6.22: Pictures taken after the test: (a) beam specimen from top; (b) beam specimen from below; (c) undamaged panel-to-panel gap of BT-1; (d) damaged panel-to-panel gap of BT-2; (e) cutting of undamaged gap; (f) cutting of damaged gap.

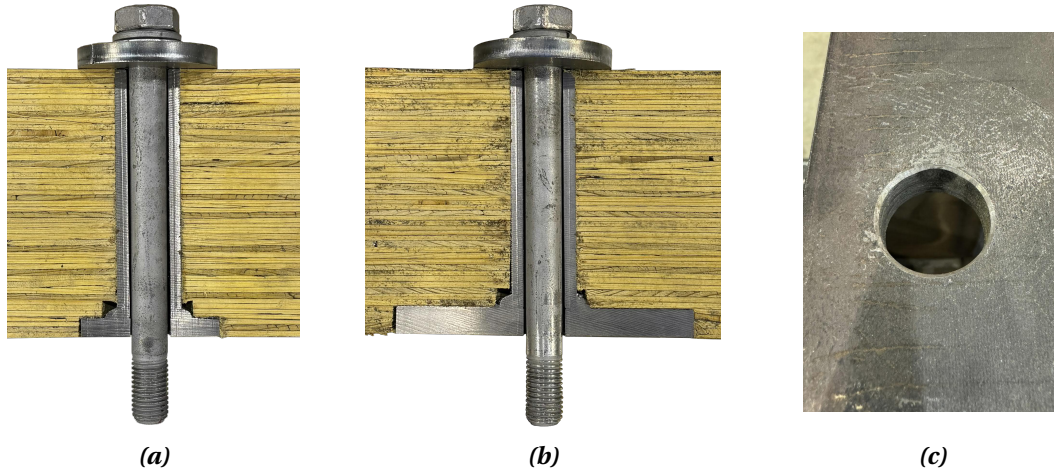


Figure 6.23: (a) Longitudinal cutting of the last connector (SCT-1) from BT-1; (b) longitudinal cutting of the last connector (SCT-3) from BT-2; (c) hole of a steel beam after the test.

7

NUMERICAL INVESTIGATIONS ON STC BEAMS

7.1. INTRODUCTION

Non-linear 3D finite element (FE) models of STC beams were developed using ABAQUS [142] to extend the findings of the experimental tests. The results of the numerical models were compared with the experimental results to validate the finite element models. Using these validated models, the influence of various parameters on the mechanical response of the STC beams was investigated. The parameters studied were: (i) the steel grade of the steel beam, (ii) the presence or absence of transversal gaps, including the effect of filling them, and (iii) the connectors' spacing and the degree of shear connection.

7.2. MODELLING STRATEGY

7.2.1. GENERAL

The 3D continuum finite element models were developed in the software ABAQUS [142] and the implicit static solver was used to compute the simulations. The modelling strategy outlined in this section refers to the models of the STC beams tested in the experimental investigation, which were developed to validate the numerical models. Therefore, the geometry of the STC beams, properties of materials, support conditions, and loading, correspond to those of the STC beams tested experimentally.

Simply supported beams in 6-point bending consisting of an LVL slab, steel beam, and two rows of shear connectors as described in Chapter 6, were modelled using 8-node brick elements with reduced integration (C3D8R) for the slab, the steel beam, steel plates and half-rods. The connectors were modelled as mesh-independent point-based fasteners.

The geometry and the features of the model are depicted in Figure 7.1, the dimensions are illustrated in Figure 6.1. The total length of the STC beams was set to 10.6 m, the distance between supports was set to 10 m. The steel beams were modelled as IPE 400 profiles steel grade S355, the stiffeners welded to the beam at the load introduction points and at the supports have been included in the model. The six LVL panels of the tested beams were modelled with properties of Kerto-Q LVL and the 10 mm gaps between them were included in the model. The

mortar of the transversal gaps was considered in the model. The overall width of the panels was 2.51 m. The load was applied as displacement at four points on top of the slab through half rods and steel plates. Two models have been developed for the validation of the finite element models, one for BT-1 implementing SCT-1, and another one for BT-2 implementing SCT-3.

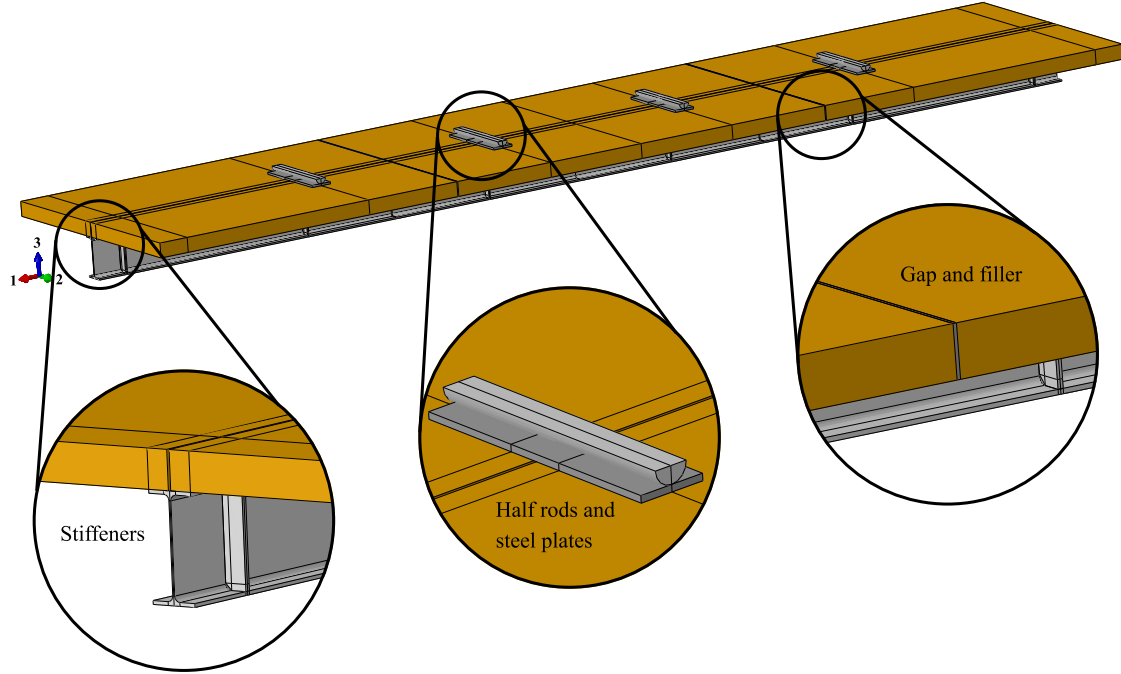


Figure 7.1: Assembly of the STC beam modelled in ABAQUS [142], and details of the components.

7.2.2. MATERIAL PROPERTIES

STEEL

The model incorporated the properties of the structural steel S355 obtained experimentally. A quad-linear stress-strain relationship as proposed by Yun and Gardner [143] was implemented in the FE model. The elasticity modulus E was set to 207 000 MPa, the yield strength f_y was set to 399 MPa, the ultimate strength f_u to 512 MPa, and the Poisson's ratio ν was set to 0.3. The quad-linear stress-strain relationship [143] is defined by the function presented in Equation 7.1, the ultimate strain (ϵ_u), the hardening strain (ϵ_{sh}), the parameter C_1 and the slope of the hardening branch (E_{sh}) are calculated according to Equations 7.2, 7.3, 7.4, and 7.5, respectively.

$$f(\epsilon) = \begin{cases} E \cdot \epsilon & \text{for } \epsilon \leq \epsilon_y \\ f_y & \text{for } \epsilon_y < \epsilon \leq \epsilon_{sh} \\ f_y + E_{sh}(\epsilon - \epsilon_{sh}) & \text{for } \epsilon_{sh} < \epsilon \leq C_1 \cdot \epsilon_u \\ f_{C_1 \epsilon_u} + \frac{f_u - f_{C_1 \epsilon_u}}{\epsilon_u - C_1 \cdot \epsilon_u} (\epsilon - C_1 \cdot \epsilon_u) & \text{for } C_1 \cdot \epsilon_u < \epsilon \leq \epsilon_u \end{cases} \quad (7.1)$$

$$\epsilon_u = 0.6 \left(1 - \frac{f_y}{f_u} \right), \text{ but } \epsilon_u \geq 0.06 \quad (7.2)$$

$$\varepsilon_{sh} = 0.1 \frac{f_y}{f_u} - 0.055, \text{ but } 0.015 \leq \varepsilon_{sh} \leq 0.03 \quad (7.3)$$

$$C_1 = \frac{\varepsilon_{sh} + 0.25(\varepsilon_u - \varepsilon_{sh})}{\varepsilon_u} \quad (7.4)$$

$$E_{sh} = \frac{f_u - f_y}{0.4(\varepsilon_u - \varepsilon_{sh})} \quad (7.5)$$

The values of the key parameters calculated from these expressions for the steel S355 tested experimentally are given in Table 7.1.

Table 7.1: Summary of mechanical properties and key parameters defining the quad-linear stress-strain relationship implemented in the FE model for steel S355.

Steel grade	E [MPa]	f_y [MPa]	f_u [MPa]	ε_y [%]	ε_{sh} [%]	ε_u [%]	E_{sh} [MPa]	C_1 [-]	ν [-]
S355	207 000	399	512	1.9	22.9	132.4	2 580	0.38	0.3

TIMBER - LVL

The grain direction of the LVL panels was considered as parallel to the longitudinal direction of the beam. The mechanical properties of Kerto-Q LVL [134], a cross-banded LVL product manufactured by Metsä Wood, were determined experimentally as shown in Chapter 3, mean values were incorporated in the FE model. The Poisson's ratios were obtained from Winter et al. [144].

The orthotropic material was modelled through engineering constants, the yield and plasticity were defined through Hill's criterion [145, 146]. This modelling approach was chosen as it has been used by other researchers to model steel-timber composite beams [86] with the results showing good agreement with the experimental tests. The mechanical properties implemented in the finite element model and the parameters to define Hill's yield function are summarized in Table 7.2.

Table 7.2: Summary of key properties and parameters implemented in the FE model for LVL.

Property	Units	LVL directions i and ij		
		1	2	3
E_i	[MPa]	7 920	1 765	1765
$f_{y,0}$	[MPa]	40.4		
$f_{y,i}$	[MPa]	40.4	11.1	11.1
		12	13	23
$f_{y,ij}$	[MPa]	5.8	1.6	1.6
G_{ij}	[MPa]	765	765	49
ν_{ij}	[-]	0.44	0.44	0.23

According to the results full-scale beam tests presented in Chapter 6, the stresses in LVL elements due to bending remained within the elastic range, even at the large deformations

observed in the last loading stages. Nevertheless, the behaviour of IVL beyond the elastic range was incorporated in the model, it was defined through Hill's yield criterion [145, 146] according to the potential function in Equation (7.6):

$$f(\sigma) = \sqrt{F(\sigma_{22} - \sigma_{33})^2 + G(\sigma_{33} - \sigma_{11})^2 + H(\sigma_{11} - \sigma_{22})^2 + 2L\sigma_{23}^2 + 2M\sigma_{31}^2 + 2N\sigma_{12}^2} \quad (7.6)$$

Where F , G , H , L , M , and N are constants defined in function of yield stress ratios (R_{ij}) as follows:

$$F = \frac{1}{2} \left(\frac{1}{R_{22}^2} + \frac{1}{R_{33}^2} - \frac{1}{R_{11}^2} \right) \quad (7.7)$$

$$G = \frac{1}{2} \left(\frac{1}{R_{33}^2} + \frac{1}{R_{11}^2} - \frac{1}{R_{22}^2} \right) \quad (7.8)$$

$$H = \frac{1}{2} \left(\frac{1}{R_{11}^2} + \frac{1}{R_{22}^2} - \frac{1}{R_{33}^2} \right) \quad (7.9)$$

$$L = \frac{3}{2R_{23}^2} \quad (7.10)$$

$$M = \frac{3}{2R_{13}^2} \quad (7.11)$$

$$N = \frac{3}{2R_{12}^2} \quad (7.12)$$

The six yield stress ratios (R_{11} , R_{22} , R_{33} , R_{12} , R_{13} , and R_{23}) are defined as follows:

$$R_{11} = \frac{f_{y,1}}{f_{y,0}} \quad (7.13)$$

$$R_{22} = \frac{f_{y,2}}{f_{y,0}} \quad (7.14)$$

$$R_{33} = \frac{f_{y,3}}{f_{y,0}} \quad (7.15)$$

$$R_{12} = \frac{\sqrt{3}f_{y,12}}{f_{y,0}} \quad (7.16)$$

$$R_{13} = \frac{\sqrt{3}f_{y,13}}{f_{y,0}} \quad (7.17)$$

$$R_{23} = \frac{\sqrt{3}f_{y,23}}{f_{y,0}} \quad (7.18)$$

MORTAR

The mortar used to fill the transversal gaps in the full-scale beam tests was considered in the FE model. During the tests, it was observed that mortar remains undamaged at large deformations. Its behaviour was modelled through a bi-linear elastic perfectly plastic stress strain relationship. The strength and stiffness values of the high-strength mortar Pagel V1/30HF were obtained from the technical specifications provided by the manufacturer. The strength (f_{cm}) was set to 100 MPa and the modulus of elasticity (E_{cm}) was set to 40 000 MPa.

7.2.3. SHEAR CONNECTION

The LVL panels were connected to the top flange of the steel beams by means of mesh independent point-based fasteners. These connectors couple the soffit of the timber slab to the surface of the top flange of the steel beam allowing only relative displacement along the longitudinal direction of the beam.

The fasteners were placed at predefined points along the top flange of the beam, two rows of equidistant connectors were modelled. The number of connectors of each row was set to 30, this gives a total of 60 connectors along the beam. The spacing between them in the longitudinal direction was set to 337.5 mm, the spacing between the two rows was set to 110 mm, and the distance from the edge to the first connector was set to 406.25 mm.

The load-slip behaviour of the connectors was defined by introducing the experimentally obtained mean load-slip curve of SCT-1 and SCT-3 (see Figure 7.2) for BT-1 and BT-2 respectively.

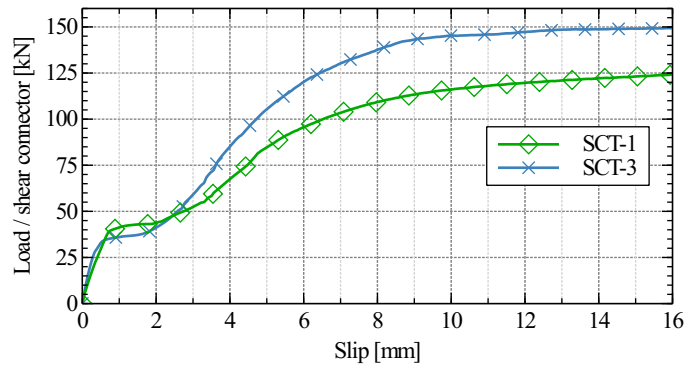


Figure 7.2: Mean load-slip curves of the shear connectors SCT-1 and SCT-3 implemented in the FE models.

7.2.4. CONTACT DEFINITIONS

The contact was defined through contact pairs as surface-to-surface contact with normal and tangential properties. Both properties were defined through a penalty factor. Normal contact was defined as hard contact with a penalty factor of 1.0 for all contact pairs. A penalty factor of 0.5 was assigned to the tangential behaviour of steel-to-steel contact, whereas a penalty factor of 0.3 was assigned to the tangential behaviour of steel-to-timber contact.

7.2.5. BOUNDARY CONDITIONS

The boundary conditions are depicted in Figure 7.3. Boundary conditions were applied to two reference points located in the surface of the bottom flange of the steel beam at 300 mm from the edges to simulate the support conditions. These points couple the nodes of a 20 mm strip defined at the surface of the bottom flange of the steel beam. At one end, the beam was restricted from translating in the three principal directions (i.e., RP-3: $U_1=0, U_2=0, U_3=0$), while at the other end, only the longitudinal displacement along the 1-axis was allowed (i.e., RP-4: $U_2=0, U_3=0$). The rotation around the 3-axis was unrestrained at both ends (i.e. RP-3 and RP-4) whereas the rotation around 1-axis and 2-axis was restrained (i.e., $UR_1=0, UR_2=0$).

Boundary conditions were applied to reference points that couple the top surfaces of the half-rods that transfer the load to the system (i.e. RP-1 and RP-2). These points were fixed for translation in the 1-axis and 2-axis directions and allowed to translate in the vertical direction 3 (i.e. $U_1=0, U_2=0$). Regarding the rotation restrictions of these points, they were restrained for rotations about 1-axis and 3-axis (i.e. $UR_1=0, UR_3=0$) and they were unrestrained for rotation about 2-axis so that when they moved downwards they followed the rotation of the beam surface.

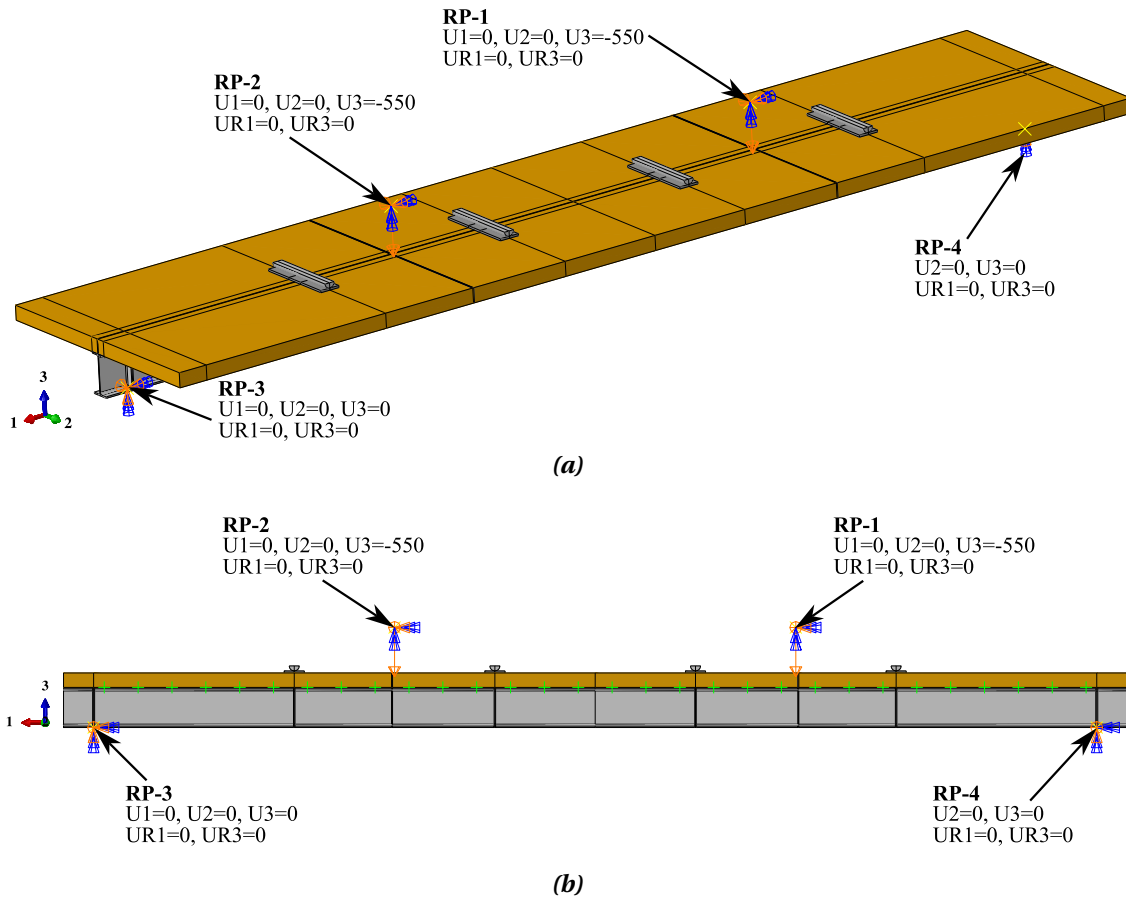


Figure 7.3: Boundary conditions of the STC beam FE model: (a) isometric view; and (b) elevation view.

7.2.6. LOADING

The loading was applied at 4 points on top of the STC beam through steel plates $800 \times 200 \times 20$ mm and half rods with a diameter of 100 mm and a length of 800 mm. The rods have been evenly spaced every 2000 mm. The top surfaces of the half-rods have been coupled to reference points (i.e. RP-1 and RP-2) as shown in Figure 7.4. These points were fixed for translation in the 1-axis and 2-axis directions and allowed to translate in the vertical direction 3, in this direction the displacement was set to 500 mm (i.e. $U_1=0$, $U_2=0$, $U_3=500$). Regarding the rotation restrictions of these points, they were restrained for rotations about 1-axis and 3-axis (i.e. $UR_1=0$, $UR_3=0$) and they were unrestrained for rotation about 2-axis so that when they moved downwards they followed the rotation of the beam surface.

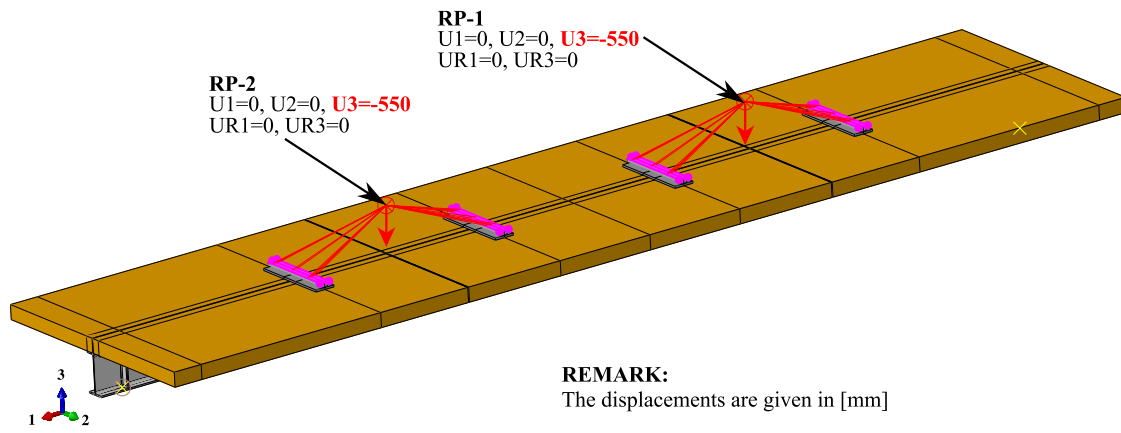


Figure 7.4: Loading conditions of the FE model of the STC beam.

7.2.7. MESH

The slab, the steel beam, steel plates, stiffeners and half-rods slab were meshed with using 8-node brick elements with reduced integration (C3D8R). A mesh sensitivity analysis was done to determine an efficient mesh size. This model consists of 123082 nodes and 85188 elements. The mesh of the 3D FE model is depicted in Figure 7.5.

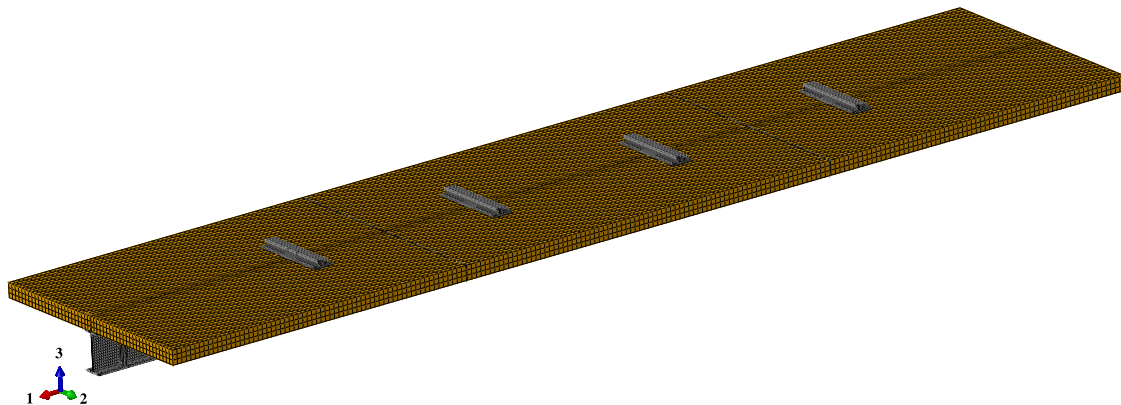


Figure 7.5: Mesh of the FE model of the STC beam.

7.3. COMPARISON OF EXPERIMENTAL AND NUMERICAL RESULTS

7.3.1. COMPARISON OF MOMENT/LOAD VS. MIDSPAN DEFLECTION CURVES

Figure 7.6 shows a comparison of the experimental and the numerical moment vs. midspan deflection curve for BT-1 in Figure 7.6a and BT-2 in Figure 7.6b. In the experimentally obtained moment vs. midspan deflection curves, the moment due to self weight and the corresponding deflection were not considered. To account for their effect in the numerical simulations, the moment due to self-weight (i.e. $M_{sw} = 38 \text{ kN}\cdot\text{m}$) and the corresponding numerically obtained midspan deflection were subtracted. The results show that for both tests, the FE model is in good agreement with the experimental results.

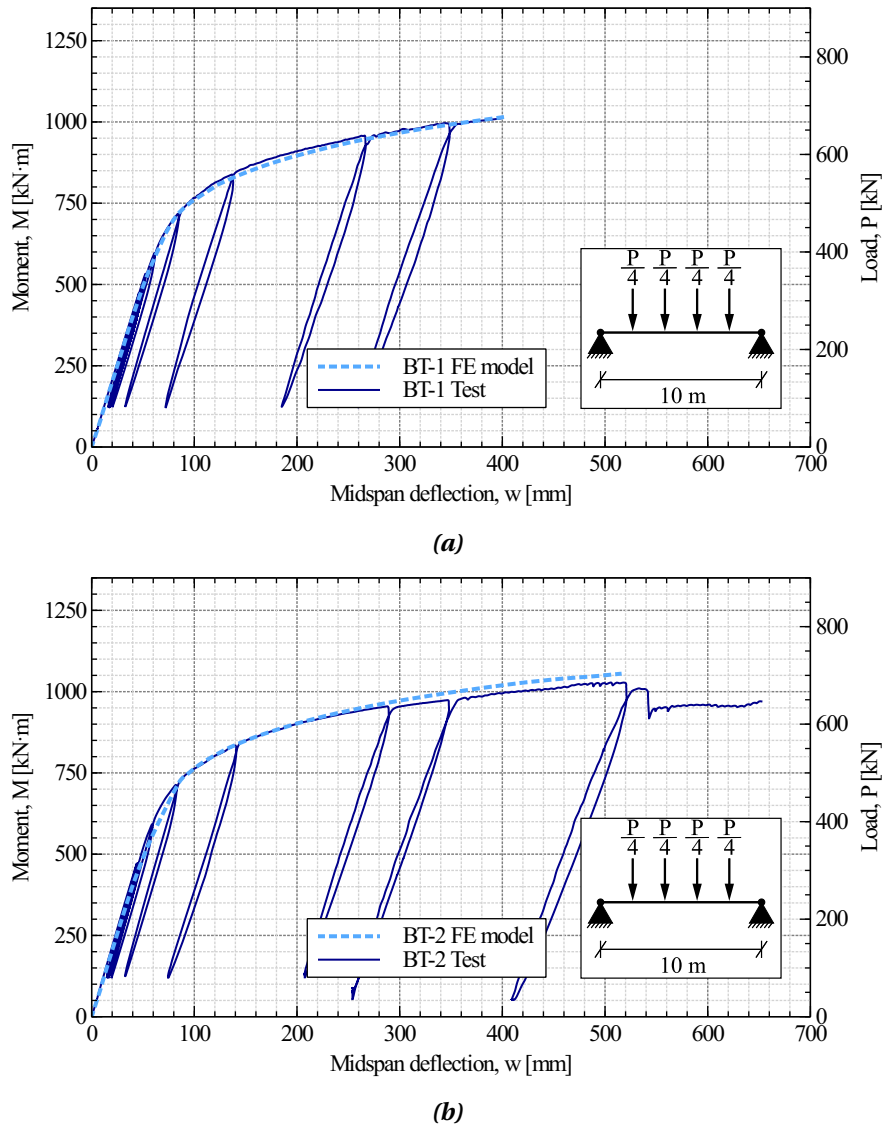


Figure 7.6: Experimental and numerical moment vs. midspan deflection curve for: (a) BT-1; and (b) BT-2.

7.3.2. COMPARISON OF SLIP MEASUREMENTS THROUGH THE BEAM

The slip was measured at different locations through the beam during the full-scale STC beam tests. In the finite element simulations the slip was measured at every connector. A comparison of these slip measurements is shown in Figure 7.7, for the last loading stage

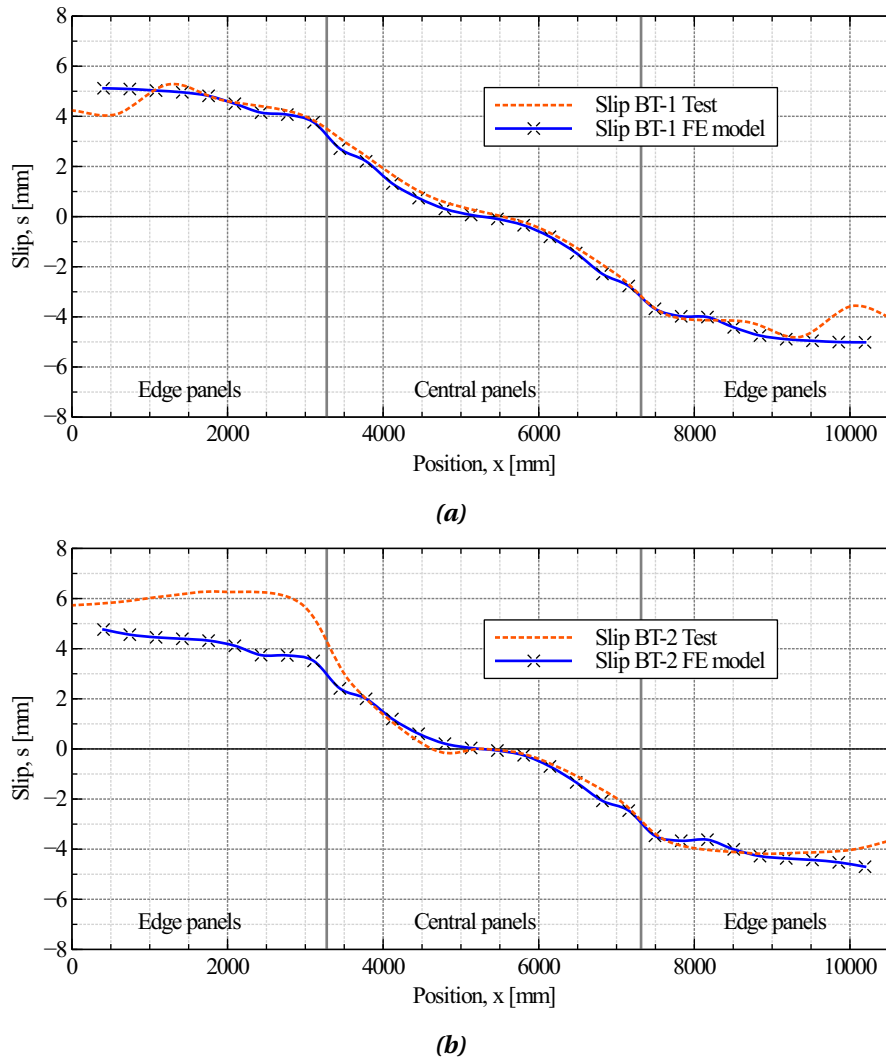


Figure 7.7: Experimental and numerical slip measurements for: (a) BT-1; and (b) BT-2.

The comparison of slip measurements depicted in Figure 7.7a for BT-1 shows good agreement. Both curves exhibit nearly symmetrical behaviour with respect to the midspan, suggesting similar bolt alignment along the beam. Conversely, in Figure 7.7b when comparing the slip measurements for BT-2, disparities in slip measurements are observed. Positive values are larger in the test, this difference between experimental and numerical results may be due to misalignment of bolts on the edge panels on that side of the STC beam, potentially leading to increased clearance and thus allowing for a larger travel of the bolts within the holes.

7.4. INFLUENCE OF PARAMETERS ON THE MECHANICAL RESPONSE OF STC BEAMS

7.4.1. GENERAL

To extend the results of the experimental full-scale beam tests and investigate the influence of various parameters on the response of the STC beams, the calibrated numerical models were used as the basis for numerical investigations.

The parameters investigated included: (i) the steel grade of the steel beam, (ii) the presence or absence of transversal gaps and the effect of filling them, and (iii) the connectors' spacing and the degree of shear connection. Table 7.3 summarizes the parameters investigated, and Figure 7.8 illustrates the nomenclature implemented to assign a unique label to each numerical model.

Table 7.3: Summary of parameters considered in the numerical investigations.

Parameter	Value	Abbreviation
Span (distance between supports)	10 m	10
Steel profile	IPE 400	IPE400
Steel grade	S355	S355
	S460	S460
Shear connection type	Shear connection type 1	SCT1
	Shear connection type 3	SCT3
Spacing of connectors or degree of shear connection	337.5 mm	S1
	515 mm	S2
	650 mm	S3
	1225 mm	S4
	Full-rigid shear connection	F
	No shear connection	N
Transversal gaps	With transversal gaps filled	GF
	With transversal gaps unfilled	GU
	Without transversal gaps	NG

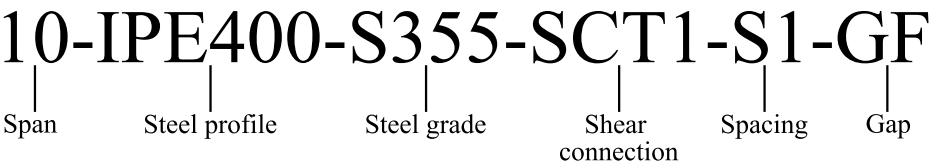


Figure 7.8: Nomenclature definition to assign a unique label to each numerical model.

7.4.2. INFLUENCE OF THE STEEL GRADE OF THE STEEL BEAM

The two beams tested in the full-scale beam tests had steel profiles made with steel grade S355. The influence of the steel grade of the steel beam was investigated by changing its properties in the numerical models to structural steel grade S460.

The yielding strength (f_y) and the modulus of elasticity (E) of this steel grade was obtained experimentally from tests on the components of the shear connection devices which were produced with structural steel S460 as mentioned in Chapter 5 in Section 5.3.3. Hence, the yielding strength implemented in the numerical models was 526 MPa and the modulus of elasticity was 203 GPa.

Figure 7.9 shows a comparison of the moment vs. midspan deflection curves obtained in the full-scale beam tests and the numerical simulations with steel profiles grade S460. These results show that the bending capacity increased significantly by implementing a profile with steel grade S460, an enhancement of the bending capacity of at least 25% was observed.

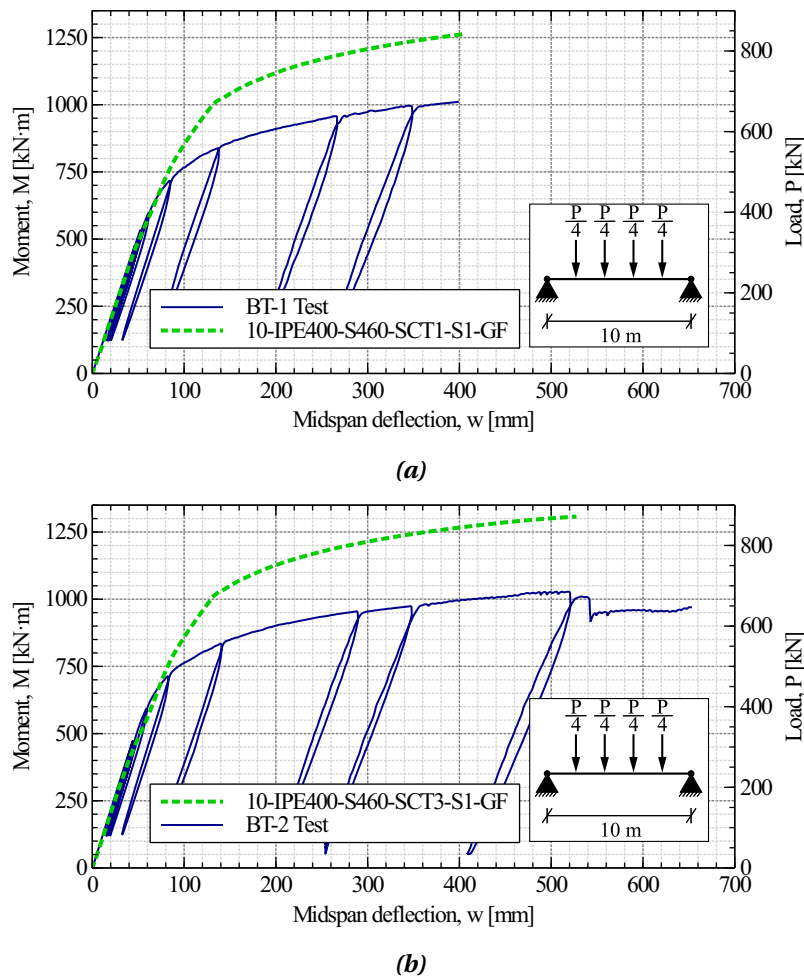


Figure 7.9: Moment vs. midspan deflection curves obtained in the tests and the numerical simulations for: (a) BT-1; and (b) BT-2.

7.4.3. INFLUENCE OF THE TRANSVERSAL GAPS

With the calibrated numerical models, the influence of the transversal gaps' presence/absence was investigated, along with the influence of filling and not filling the gap. Figure 7.10 shows the midspan deflection curves obtained experimentally and numerically.

As explained in Chapter 3 in Section 3.2, the STC flooring system along the span consists of 3 panels, one central panel covering approximately 40% of the span and two edge panels, each one covering 30% of the span. This facilitates the transport and installation of the panels, and provides construction tolerances. A gap of 10 mm between adjacent panels is present, it must be filled with high-strength mortar to enable the transfer of compressive forces and to activate the shear connectors in the edge panels. This segmentation generates transversal discontinuities between the central and the edge panels, which have an impact on the mechanical performance of the STC beams as observed in Figure 7.10.

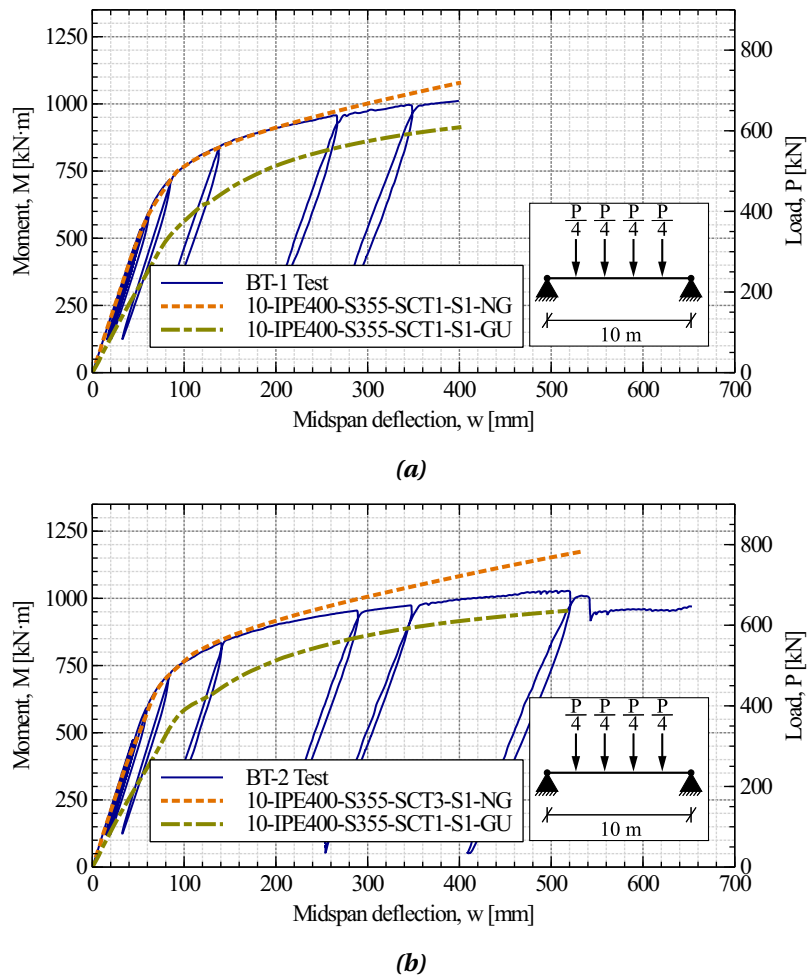


Figure 7.10: Moment vs. midspan deflection curves obtained in the tests and the numerical simulations for: (a) BT-1; and (b) BT-2.

From these results, the following can be concluded:

- Influence of the gap presence/absence when the gap is filled: The results indicate that there is no significant influence in the initial loading stages, which include the elastic branch and part of the post-yielding branch. Meaning that it has no significant impact in the initial bending stiffness of the STC beams. At a certain load, the responses diverge, suggesting that STC beams with continuous slabs have higher stiffness post-yielding at the last loading stages, thus, they have greater bending capacities.
- Influence of the gap filling: According to the results, the gap filling has a quite relevant impact on the response of the STC beams. Not filling the gap reduces their stiffness and their capacity considerably. These results highlight the importance of filling the gaps with a stiff material to ensure transfer of compression at all loading stages and activation of the shear connectors installed in the edge panels.

7.4.4. INFLUENCE OF THE CONNECTORS' SPACING AND THE DEGREE OF SHEAR CONNECTION

The effect of the degree of shear connection was investigated by modifying the spacing between the connectors and by modelling the cases of full-rigid shear connection and no shear connection. Figure 7.11, shows the experimentally and numerically obtained moment vs. midspan deflection curves.

In the beam tests BT-1 and BT-2, the spacing between connectors was 337.5 mm, with two rows, resulting in 60 connectors installed in each beam. Similarly, in the numerical models, two rows of equidistant connectors were considered. The spacings and number of connectors used in the models were 515 mm (40 connectors), 650 mm (32 connectors), and 1225 mm (18 connectors). Additionally, numerical models of beams with full-rigid shear connection and no shear connection were developed, and the moment vs. midspan deflection curves were included in the plots.

The results show that the tested beams have an initial bending stiffness similar to that of the beam with full-rigid shear connection, while the difference in stiffness and capacity between the tested beams and the beam with no shear connection is quite large. This demonstrates that composite action enabled by the shear connectors significantly improves the mechanical performance of STC beams.

When the spacing between connectors was increased, and therefore the number of connectors reduced, there was reduction of the initial bending stiffness and of the ultimate bending capacity. However, the impact on the loads reached at similar midspan deflections in the final loading stages was not as significant. In particular, the beam configurations with spacings of 515 mm and 650 mm were able to bear loads at a midspan deflection of 500 mm similar to those observed in the tested beams with a spacing of 337.5 mm. This is due to the specific load-slip response of the connectors. Fewer connectors result in larger slip values, but this also means that each connector transfers more shear forces. Consequently, even with fewer connectors, large compressive forces can be developed in the slab due to the connectors' large deformation

capacity and the high loads they can transfer at large deformations. The presence of more connectors is associated with increased initial bending stiffness and lower slip values. However, connectors at lower slip values transfer fewer shear forces, meaning that the increase in ultimate bending capacity provided by more connectors is not as significant as the improvement in initial bending stiffness and the reduction in slip.

For the beams with connectors spaced at 1225 mm (18 connectors), the bending stiffness and the maximum loads reached are lower than those for the cases with closer spacing and more connectors, but they are still quite large compared to the case of no shear connection. Thus, even with a relatively low number of connectors, it is possible to significantly improve the stiffness and capacity of the STC beams compared to beams with no shear connection.

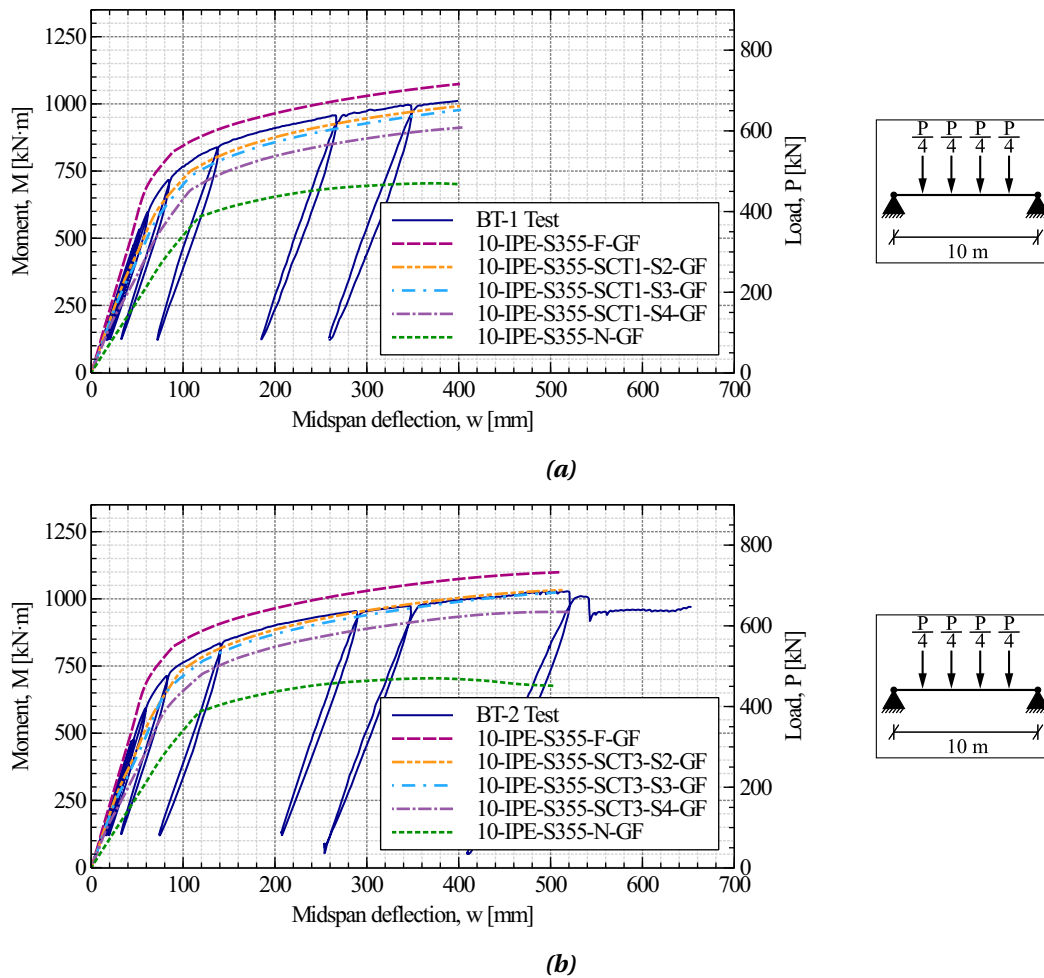


Figure 7.11: Moment vs. midspan deflection curves obtained in the tests and the numerical simulations for: (a) BT-1; and (b) BT-2.

8

ANALYTICAL DETERMINATION OF THE BENDING CAPACITY OF STC BEAMS

8.1. INTRODUCTION

Due to the lack of standardised design procedures and technical documentation, conventional steel-timber flooring systems are typically designed by either considering (i) the contribution of the steel beam alone or (ii) the sum of the moment resistance of the steel beam and the timber slab (i.e. additive moment resistance), but neglecting the additional bending capacity and bending stiffness provided by the composite action achieved by the shear connectors. Although these are conservative assumptions that are on the safety side, both approaches can lead to significant underestimation of the beams' bending capacity and to overestimation of their deformations, both critical aspects decisive when comparing different systems. These assumptions may result in uneconomical and/or unfeasible solutions.

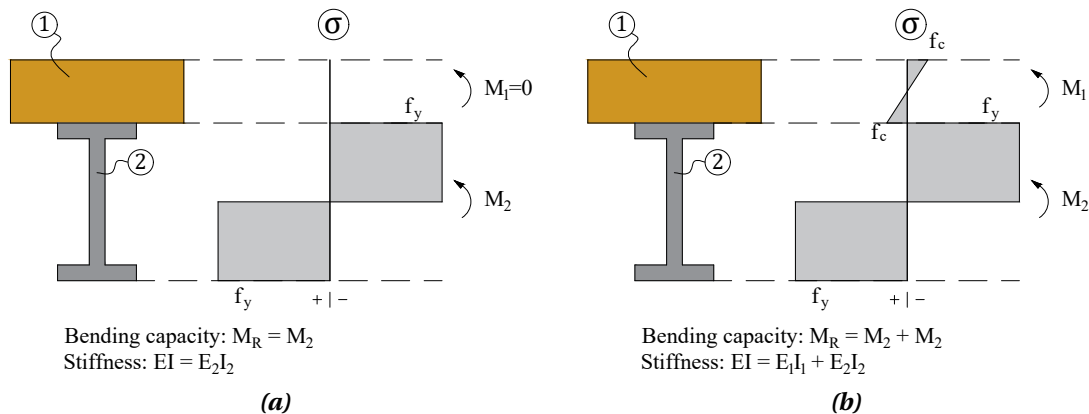


Figure 8.1: Typical considerations for the estimation of the bending capacity of steel-timber beams that neglect the effects of composite action: (a) steel beam only, and (b) steel beam + timber slab (shear connection neglected).

STC beams can be optimized by taking composite action into account. Indeed, their widespread implementation heavily depends on the availability of adequate analysing procedures. Devel-

oping such procedures is crucial for enabling designers to compare STC flooring solutions with other alternatives in terms of mechanical performance.

For STC beams, the calculation of the bending capacity cannot be done as in the case of SCC beams by assuming perfectly-plastic material constitutive laws for steel and concrete, with the tension of concrete neglected due to cracking (see Figure 8.2). Timber has a different behaviour, it can withstand considerable tensile stresses but it exhibits brittle failure when it reaches its tensile strength. Thus, neglecting the contribution of tension of timber to the capacity would not be appropriate. Furthermore, a fully elastic analysis, where both steel and timber remain within their elastic ranges, could lead to significant underestimations of the bending capacities. Tests have shown that STC beams reach their capacity when the steel beams have been plasticised, while the timber remains within the elastic range or reaches its tensile strength at its bottom fibre. Therefore, there is a need for procedures that consider these particularities of the two materials when working as a composite.

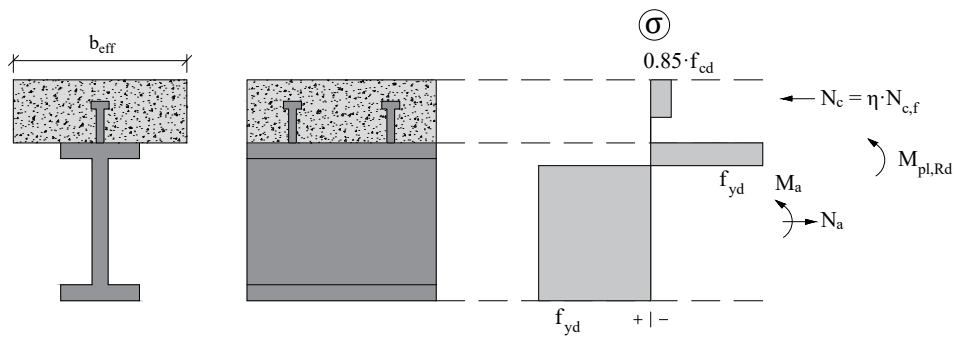


Figure 8.2: Example of a plastic stress distribution considered for the calculation of STC beams in sagging bending in which steel and concrete are idealised as perfectly-plastic and tension in concrete is neglected [94].

In order to address existing knowledge gaps in analysing approaches for STC beams, this study proposes two procedures to determine the ultimate capacity of STC cross-sections for any degree of shear connection (i.e. considering the composite action): (i) a strain-based procedure, and (ii) a simplified analytical procedure. Additionally, the γ -method established in Eurocode 5 [69] has been adapted for STC beams and it is proposed as a suitable method for the estimation of their bending stiffness and bending capacity within the elastic range.

The ultimate load of a beam is typically determined by the moment of resistance at the critical cross-section. Due to the nonlinearities associated to the materials response and the geometry of the section components, finding closed formulations for composite beams can be challenging. However, this can be overcome by implementing strain-based procedures. These approaches can accurately predict the cross-section resistance of composite beams with nonlinear materials and complex geometries.

Due to its robustness, this study proposes a strain-based procedure to predict the bending capacity of STC beams. Additionally, an algorithm to estimate the shear forces effectively transferred by the shear connectors is presented. The connectors developed in this investigation as well as other steel-to-timber connectors used in conventional STC flooring systems,

exhibit a load-slip response which cannot be directly idealised as either rigid or rigid-ductile. Consequently, their resistance cannot be assumed as the shear force effectively transferred by all the shear connectors placed within the shear length. The proposed approach transforms such load-slip curves into an idealised rigid-ductile (i.e. perfectly-plastic) load-slip response, which simplifies the computation of the shear forces transferred by the connectors.

The proposed strain-based procedure is an accurate analytical tool that predicts the moment resistance of an STC cross-section at any given state of stresses as it considers the exact strain distribution and non-linear material constitutive laws can be implemented. Nevertheless, its implementation might be a challenging and time-consuming task. Therefore, in this contribution simplified analytical procedures for elastic and ultimate limit state analyses are proposed considering assumptions that are based on the experimental observations and the results of the strain-based procedure.

Comparisons of the analytical predictions of the proposed procedures with the experimental and numerical results are presented, demonstrating good agreement. These comparisons highlight the procedures' capabilities to predict the bending capacity of the STC beams.

8.2. CONSIDERATIONS FOR STC BEAMS

The analytical procedures to predict the cross-section resistance of STC beams presented in this contribution were developed for steel-timber composite beams with downstanding I-shaped beams and timber slabs with material properties that can be considered homogeneous through its depth.

The shear lag effects in the timber slab in the transversal direction can be simplified considering an effective width. In this study effective widths of $L/5.5$ are considered for the ultimate limit state based on the findings of the experimental investigation presented in Section 6.8.4.

This method considers the following basic assumptions:

- i. Plane sections remain plane, meaning that sections of the beam which are plane before deformation remain plane after deformation. This implies that all strain is uniaxial and occurs only due to bending (i.e no shear strain).
- ii. It is assumed that there is no vertical separation of materials when composite beam is subject to bending (i.e. no uplift of the timber slab occurs).
- iii. Any section of the beam is not subjected to torsional moments.
- iv. Local or global buckling effects are not considered.
- v. The timber material of the slab and the steel material of the beam are assumed to be homogeneous.
- vi. The mechanical properties of the timber material in tension and compression are those corresponding to the timber in the X-axis (or 1-axis) direction, which is the longitudinal direction of the timber slab developed in this project.
- vii. For the steel profiles, when considering hot rolled I-shaped sections the radius at the

web-flanges interface are neglected. The components of the cross-section (i.e. timber slab, flanges of the beam and the web of the beam) are considered as rectangular shapes.

8.3. STRAIN-BASED PROCEDURE

Due to the non-linearity of the materials and the geometry of composite sections it is nearly impossible to find exact analytical solutions to determine the bending capacity of composite beams. One practical solution to overcome this, is the implementation of iterative strain-based approaches. Hence, in this chapter a strain-based approach developed to determine the ultimate capacity of STC beams subject to sagging moment is presented.

In this strain-based procedure (see Figure 8.3), the cross-section is divided in several horizontal layers (fibres). The strain distribution through the depth of the beam and the assumed material constitutive laws are the basis to determine the stresses in the cross-section at the different layers. Average stress and strain values are computed at each fibre and the strain distribution is modified until equilibrium of the internal normal forces in the section is reached. The moment resistance of the cross-section is then calculated for the equilibrium state. This general procedure can be applied to any cross-section regardless of the shape and materials. Its accuracy depends on the fiber size, the smaller the layers the better the accuracy.

In general, this procedure consists in the following main steps (see Figure 8.3):

1. The cross-section is divided in several horizontal layers (fibres).
2. The material constitutive laws are established.
3. Limit strains are defined for each material.
4. The strain distribution through the depth of the section is defined.
5. Based on the material constitutive laws, and considering average strains at every layer, the corresponding average stresses are determined.
6. The internal normal forces are estimated, their sum is computed, and equilibrium is checked.
7. The strain distribution is modified in each iteration until equilibrium of the internal forces in the cross-section is reached.
8. When equilibrium is reached, the moment resistance is calculated.

Details of the procedure are presented in Annex A. The strain-based procedure presented in this chapter was used to estimate the bending capacity of the tested beams and to compare with the numerical simulations as shown in Section 8.10.

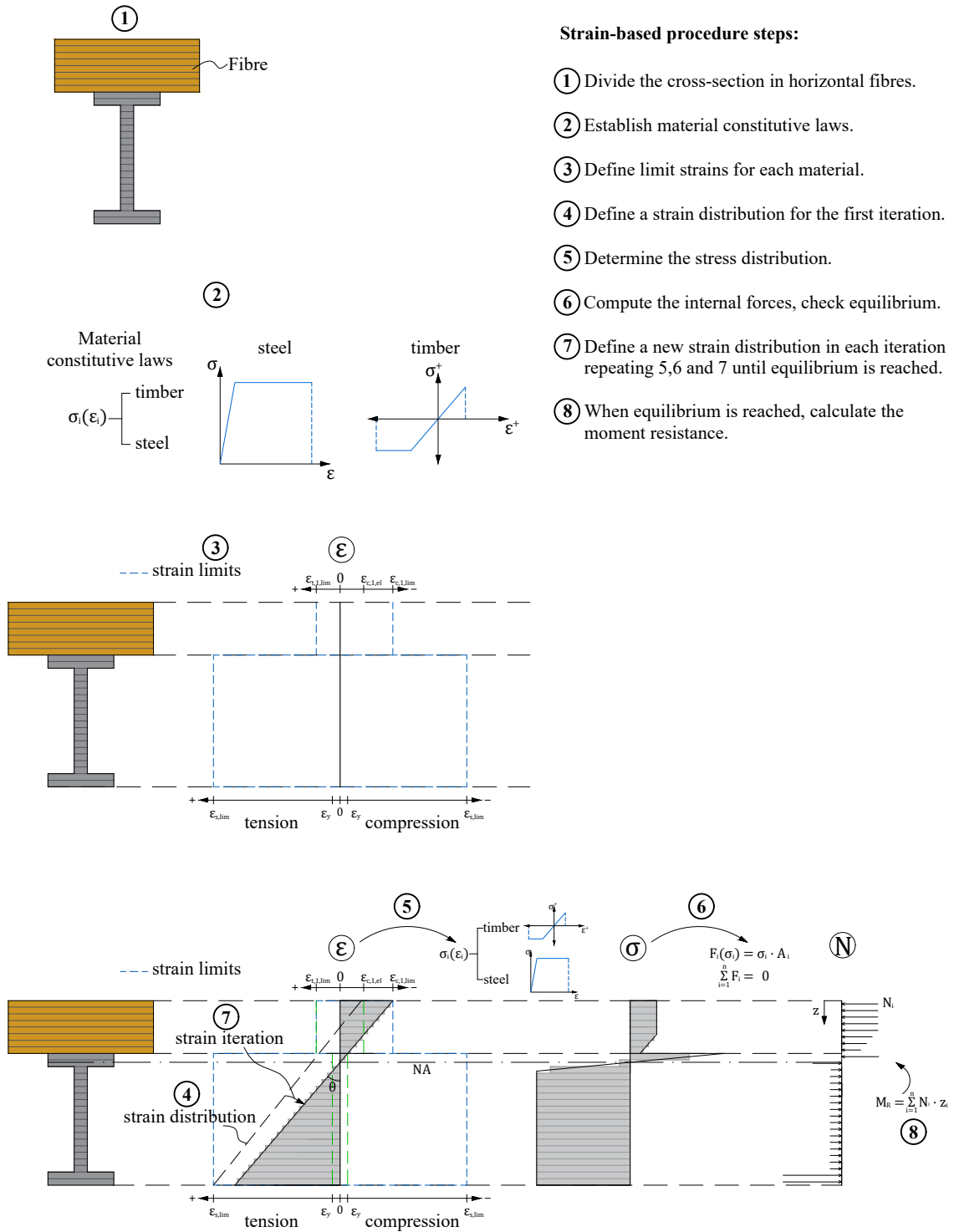


Figure 8.3: Schematic representation of the general strain-based procedure to determine the moment resistance of an STC beam cross-section.

8.4. MATERIAL CONSTITUTIVE LAWS

8.4.1. STEEL

The typical engineering stress-strain curve of hot-rolled carbon steel obtained in quasi-static tensile tests is shown in Figure 8.4a. The first branch is linear and corresponds to the elastic range, when the yielding point is reached, the curve turns into a region of plastic flow with near to constant stress, followed by a non-linear hardening branch, the peak stress is reached and then the curve turns into a descending branch.

According to EN-1993-1-1 [147], the elasticity (E) of hot-rolled carbon steel is 210 000 MPa. Other parameters such as yielding strain (ϵ_y) and strength (f_y), hardening strain (ϵ_{sh}) and strength (f_{sh}), and ultimate strain (ϵ_u) and strength (f_u), depend on the steel grade.

Accurate and simple representation of the full stress-strain curve is relevant for analytical and numerical analyses where large plastic strains are encountered. Common simplified models that represent the material response of hot-rolled carbon steels are: (i) linear elastic perfectly-plastic (Figure 8.4b); (ii) bi-linear elastic with linear hardening (Figure 8.4c); (iii) tri-linear (Figure 8.4d); (iv) quad-linear (Figure 8.4e); and (v) perfectly-plastic (Figure 8.4f).

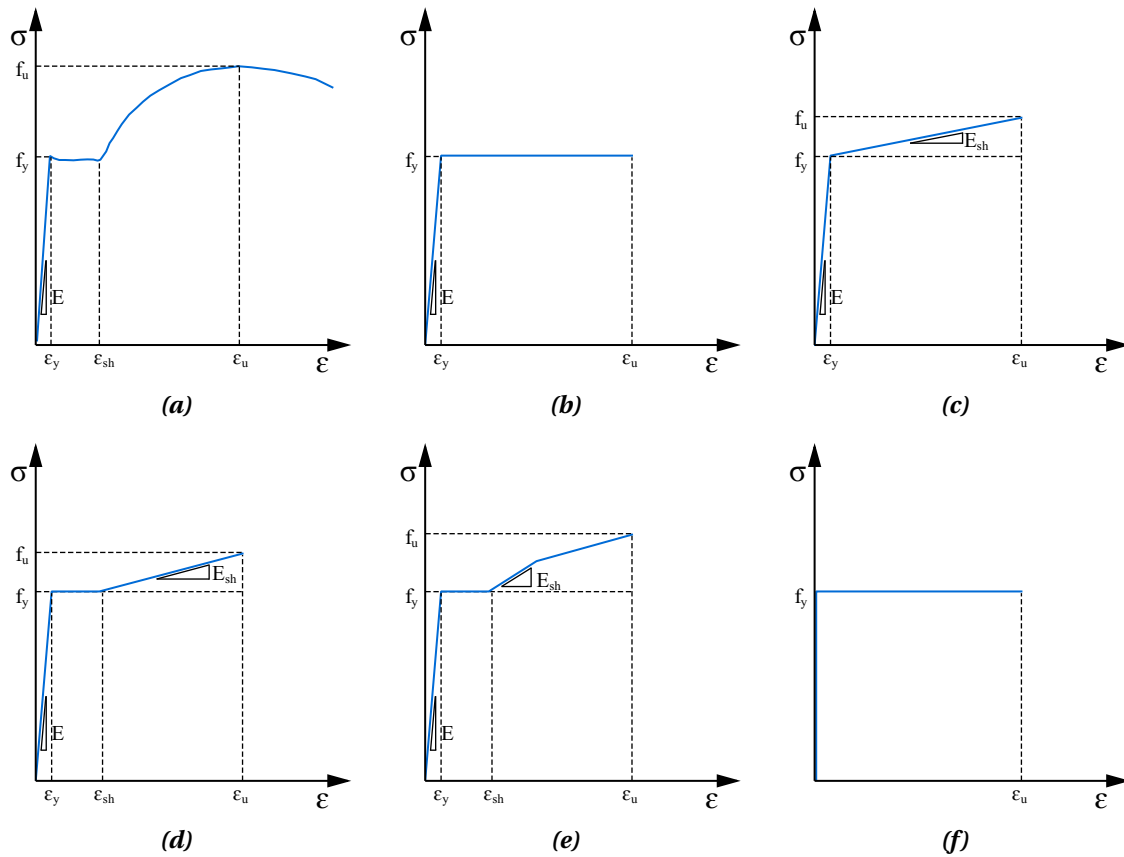


Figure 8.4: Material constitutive laws for hot-rolled carbon steel: (a) experimental engineering stress-strain relationship; (b) linear elastic perfectly-plastic; (c) bi-linear elastic with linear hardening; (d) tri-linear; (e) quad-linear; and (f) perfectly-plastic.

8.4.2. TIMBER

Timber is an anisotropic material commonly considered as orthotropic for engineering purposes. Its behaviour is different in the three orthogonal directions (i.e. longitudinal, tangential and radial). Typically, for the structural assessment of timber structures, the properties in tension and compression are considered as equal in strength and stiffness, and only the elastic range is considered. Nevertheless, timber engineered elements in compression and in bending can bear loads beyond the elastic range, in bending the fracture of the timber occurs in a brittle manner when fibers reach their tensile strength capacity.

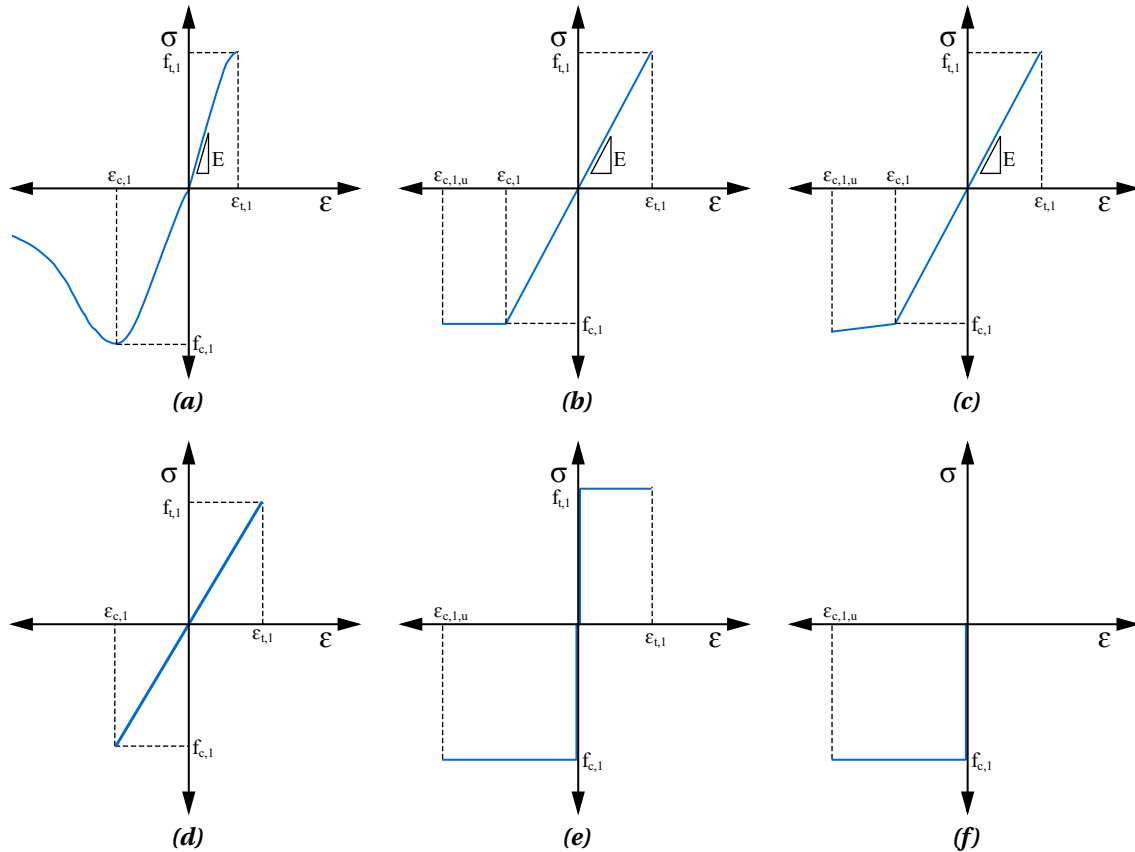


Figure 8.5: Material constitutive laws for timber in the longitudinal direction: (a) experimental stress-strain; (b) linear elastic perfectly-plastic; (c) bi-linear (or multi-linear) elastic with strain hardening; (d) linear elastic; (e) perfectly-plastic; and (f) perfectly-plastic without tension.

In uniaxial compression and tension in the longitudinal (grain) direction, the stress-strain relationship of LVL panels shown in Figure 8.5a is the typical curve observed in tests. In this curve, the LVL in tension is brittle and in compression it exhibits a ductile behaviour. The stress-strain relationship in compression and tension differs upon reaching the proportional limit. In tension, the proportional limit is linked to brittle rupture, whereas in compression after reaching the proportional limit, the curve turns into non-linear hardening, then reaching a peak point, followed by a softening branch.

The stress-strain relationship in tension can be idealized as linear-brittle, in compression it can be idealized through the following simplified models: (i) linear elastic perfectly-plastic

(Figure 8.5b); (ii) bi-linear (or multi-linear) elastic with strain hardening (Figure 8.5c); (iii) linear elastic (Figure 8.5d); (iv) perfectly-plastic (Figure 8.5e); and (v) perfectly-plastic without tension (Figure 8.5f). Due to the lower strength and stiffness of timber in the tangential direction compared to those in the longitudinal direction, the timber elements in bending are commonly oriented with their grain in the spanning direction. This allows to maximize the strength and minimize deflections.

8.5. SHEAR CONNECTION CASES

8.5.1. GENERAL

When a beam composed of two or more materials is subject to bending, the parts tend to deform at different rates and to develop different internal forces which depend on the mechanical properties of the materials and the shear connection characteristics. In STC beams there are three main cases in terms of mechanical behaviour that are of interest. These cases are related to the shear connection used to attach the elements and to transfer the shear forces caused by the interaction of the different mechanical properties of the components. The three cases are (see Figure 8.6): (i) full-rigid shear connection, (ii) no shear connection, and (iii) partial shear connection.

A full-rigid shear connection occurs when the shear connection is so strong that the ultimate load is determined by the maximum moments of resistance. The maximum load is reached when the optimum stress distribution occurs in the cross-sections of maximum bending moment. Adding more shear connectors will not increase the maximum load, as the maximum moments are normative. However, this represents an ideal case that is difficult to achieve in practice, as most shear connectors undergo deformations that cause slip at the steel-timber interface before they can bear any force. Conversely, using fewer shear connectors results in a smaller ultimate load, which depends on the number of connectors installed. This scenario is defined as a partial shear connection. The lower limit is reached when no shear connectors are used at all.

These cases affect both the bending capacity and the bending stiffness of the composite beams. Understanding these cases and their implications in terms of strains and stresses distribution through the depth of the cross-sections is crucial to implement both the strain-based procedure and the simplified procedure.

In the strain-based procedure outlined in this chapter, one of the objectives is to generate the moment resistance (M_R) vs. degree of shear connection (η) curve for a given cross-section of an STC beam, regardless of the characteristics of the shear connection. This can be constructed when the boundary values (i.e. full-rigid and partial shear connection) and intermediate values (partial shear connection) are determined. Once built, this curve can be used to estimate the bending capacity of an STC beam with any degree of shear connection. In contrast, the simplified procedure does not require to build up the full M_R vs. η curve. It offers a more direct approach to determine the capacity of an STC beam when the normal force that can be developed in the timber slab is known (i.e. total shear force effectively transferred by the

connectors). However, this method can also be used to create the full M_R vs. η curve for a given cross-section.

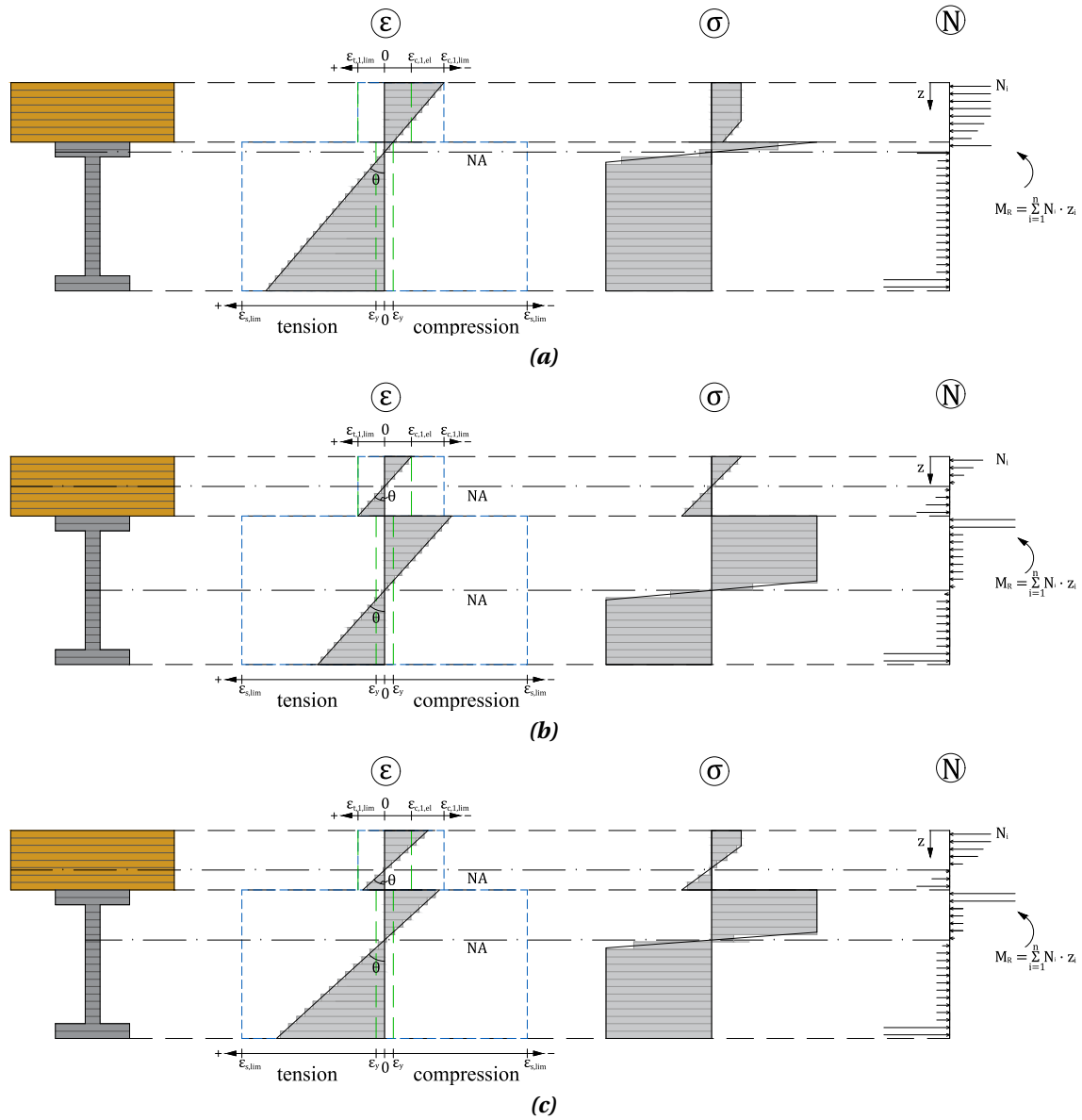


Figure 8.6: Shear connection cases: (a) full-rigid shear connection; (b) no-shear connection; (c) partial shear connection.

8.5.2. FULL-RIGID SHEAR CONNECTION

Full-rigid shear connection in an STC beam implies full interaction between the timber slab and the steel beam section. This means the shear connections fully transfer the shear forces developed at the interfaces between steel and timber, with slip at the steel-timber interface being zero or negligible. The entire section behaves as a monolithic element, maximizing the benefits of composite action. Consequently, this represents the upper bound of the M_R vs. η curve. In this case, the strain distribution across the cross-section is represented by a single straight line, indicating no slip between the timber slab and the steel beam (see Figure 8.6a).

8.5.3. NO SHEAR CONNECTION

When there is no shear connection but the timber slab and the steel beam are subjected to bending without separation (i.e. no uplift of the timber slab), there is no shear interaction between them, resulting in slip. Consequently, the bending capacity of the system is merely additive, meaning that the overall moment resistance (M_R) of the system equals the sum of their individual bending capacities, $M_{R, \text{timber}}$ and $M_{R, \text{steel}}$. This represents the lowest possible moment resistance for a composite beam and thus, it is the lower bound on the M_R vs. η curve. In this scenario, the strain distribution consists of two discontinuous straight lines with the same slope, as depicted in Figure 8.6b, ensuring compatibility of deformations. In general, for mass timber slabs, the contribution of the timber slab to the bending capacity cannot be neglected for this case, as it could lead to an important underestimation of the overall capacity of the beam.

8.5.4. PARTIAL SHEAR CONNECTION

In the case of partial shear connection, the degree of shear interaction between the timber slab and the steel beam is determined by the shear connectors. Their characteristics, such as stiffness, capacity, and arrangement along the length of the beam, dictate the amount of shear force that can be transferred between the timber slab and the steel beam, which is smaller compared to a full-rigid shear connection. Consequently, there is slip, and both the bending capacity and stiffness are less than those observed in a full-rigid shear connection. Therefore, the bending capacity of a beam with partial shear connection can range between that for rigid shear connection and no shear connection cases. Similarly to the case of no shear connection, the strain distribution consists of two discontinuous straight lines with the same slope to ensure compatibility of deformations, as shown in Figure 8.6c.

8.6. DEGREE OF OF SHEAR CONNECTION IN STC BEAMS

One fundamental question that arises with STC beams that have partial shear connection is how to determine their degree of shear connection, η . The degree of shear connection is a value that varies between 0 and 1 (i.e. $0 \leq \eta \leq 1$). A value of $\eta = 1$ indicates a full-rigid shear connection, $\eta = 0$ means no shear connection at all, and all the intermediate values $0 < \eta < 1$ represent partial shear connection.

Assuming that shear forces are transferred by n shear connectors placed within the shear length of the composite beam, the degree of shear connection can be defined as the ratio of the sum of the actual shear forces that can be transferred by the n shear connectors of the composite beam ($\sum_{i=1}^n P_i$) to the sum of the connectors' shear forces required to achieve full-rigid connection and monolithic behaviour ($(\sum_{i=1}^n P_i)_{\eta=1}$), as shown in Equation 8.1.

$$\eta = \frac{\sum_{i=1}^n P_i}{(\sum_{i=1}^n P_i)_{\eta=1}} \quad (8.1)$$

These forces are equal to the normal force that can be developed in the timber slab in the

case of partial shear connection (N_{timber}) and for full-rigid shear connection ($N_{timber, \eta=1}$), respectively (see Equation 8.2 and 8.3).

$$\sum_{i=1}^n P_i = N_{timber} \quad (8.2)$$

$$\left(\sum_{i=1}^n P_i \right)_{\eta=1} = N_{timber, \eta=1} \quad (8.3)$$

Therefore, the degree of shear connection in STC beams can be also estimated according to Equation 8.4.

$$\eta = \frac{N_{timber}}{N_{timber, \eta=1}} \quad (8.4)$$

This concept is straightforward, however, estimating the actual shear force that can be transferred by the shear connectors in a given composite beam might be challenging. This complexity arises because the shear force effectively transferred depends on the shear connections' mechanical properties, their arrangement along the beam, and the slip distribution throughout the beam. The task becomes particularly challenging when the connectors cannot be idealized as rigid-ductile (i.e., perfectly-plastic), as with the shear connections developed in this research project. In such cases, determining the transferred shear forces requires either experimental testing, complex numerical simulations, and/or analytical procedures.

8.7. EFFECTIVE SHEAR RESISTANCE OF STEEL-TO-TIMBER CONNECTIONS

8.7.1. GENERAL

The shear connectors significantly influence the structural behaviour of composite beams. The amount of shear forces that can be effectively transferred by each connector (P_i) is largely influenced by its specific load-slip response and the actual slip occurring in the composite beam under bending. It is important to note that slip varies along the length of a composite beam; it is more pronounced with some connectors and less with others, depending on their stiffness, specific load-slip response, and the number of connectors used. These are critical concepts that might be overlooked by standard procedures. For instance, according to Eurocode 5 [69], the shear forces transferred in a composite beam with multiple shear connectors is typically estimated by multiplying the shear resistance of each connector (P_R) by the number of connectors (n) (see Equation 8.5).

$$\sum_{i=1}^n P_i = P_R \cdot n \quad (8.5)$$

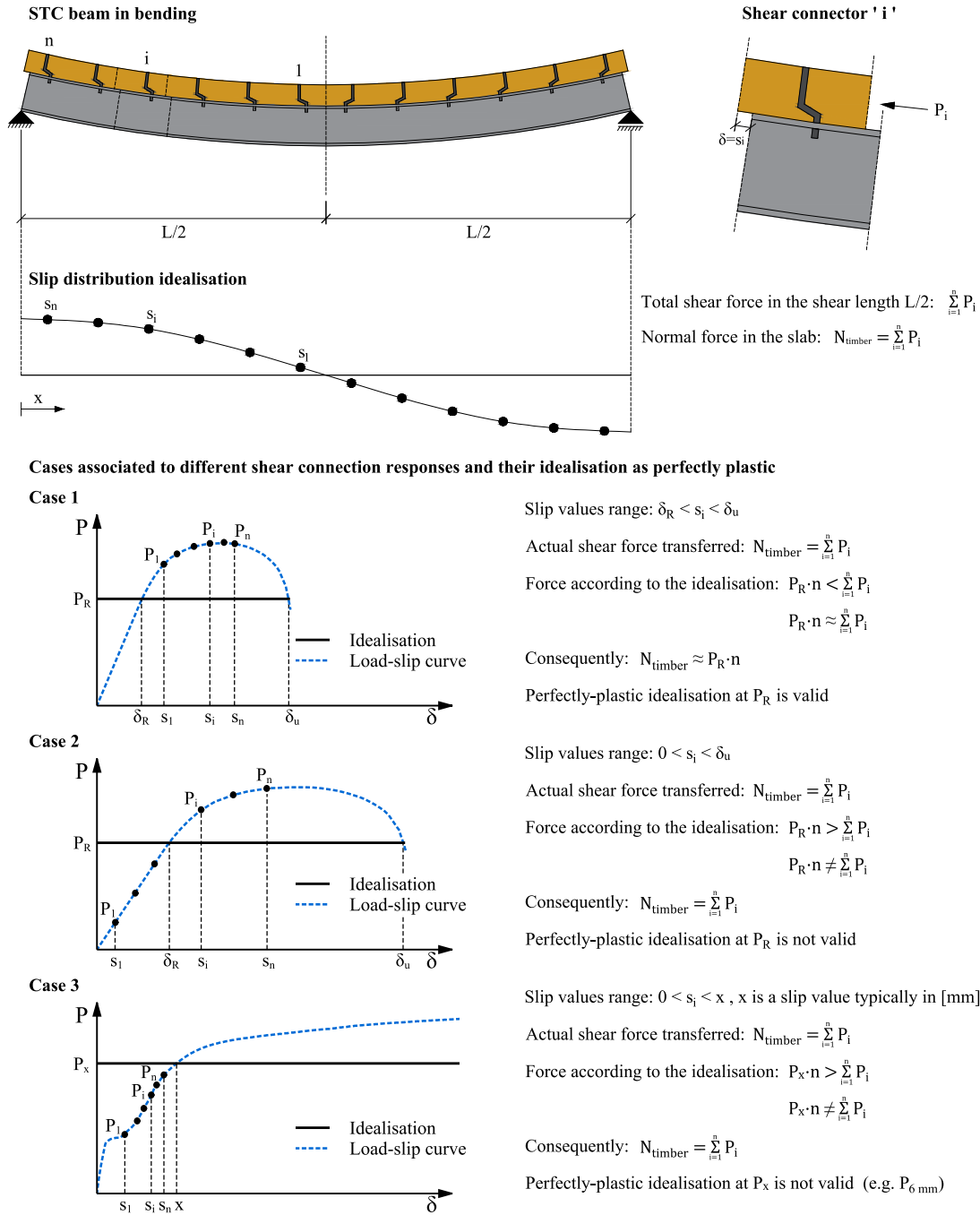


Figure 8.7: Schematic representation of the relationship between the slip of shear connectors in STC beams, their load-slip response and the shear force they transfer.

However, this approach relies on the assumption that, at the ultimate limit state, every shear connector can achieve slip values of at least the slip corresponding to the shear resistance (P_R) of the connection (i.e. the slip at δ_R). This implies that the connectors are idealised as rigid-ductile, meaning that each connector placed within the shear length transfers a constant force equal to their shear resistance P_R (see Figure 8.7, Case 1). Indeed, this idealisation simplifies the analysis of composite beams by eliminating the need to determine the slip distribution in the beam, thus reducing the estimation of the transferred shear forces to a single arithmetic

calculation. Unfortunately, the validity of this assumption must be carefully assessed to prevent unrealistic and unsafe estimations of the transferred shear forces, the normal force in the timber slab, and the bending capacity of the STC beam.

For STC beams, the assumption of a rigid-ductile connection might be adequate in some cases (see Figure 8.7, Case 1), but inappropriate in others (see Figure 8.7, Case 2 and 3). This is because certain connectors, such as those with low stiffness as well as the connectors developed in this study, reach their resistance load at relatively large slip values, which may be unachievable in some STC beams (see Figure 8.7, Case 2 and 3). Consequently, this assumption may not hold true, potentially leading to an overestimation of the total shear forces transferred by the connectors. This could result in an overestimation of the bending capacity of the STC beams, since the total shear force transferred by the connectors placed within the shear length is equal to the normal force that can be developed in the timber slab (see Equation 8.2).

This emphasizes the importance of understanding the relationship between the load-slip response of steel-to-timber connectors, their idealisation, and the actual expected slip in the STC beam where they are installed. Therefore, it is essential to consider appropriate assumptions for the shear connectors to ensure their compatibility with the beam's actual response and to prevent unrealistic estimations of the bending capacity of the STC beams.

8.7.2. IDEALISATION OF THE LOAD-SLIP RESPONSE OF STEEL-TO-TIMBER CONNECTIONS

The idealisation of the connection significantly impacts the estimation of a system's bending capacity and must be carefully chosen to avoid errors that could lead to unsafe solutions. The choice of idealisation for a connector depends not only on its load-slip response but also on the slip that the connector is expected to reach in the actual structural system. Some typical idealisations for steel-to-timber shear connections are as follows (see Figure 8.8):

- (a) **Rigid brittle:** Initial high stiffness and brittle failure.
- (b) **Rigid ductile (perfectly-plastic):** Initial high stiffness and plasticity.
- (c) **Semi-rigid brittle (linear elastic):** Lower stiffness and brittle failure.
- (d) **Semi-rigid ductile (linear elastic perfectly-plastic):** Lower stiffness and plasticity.

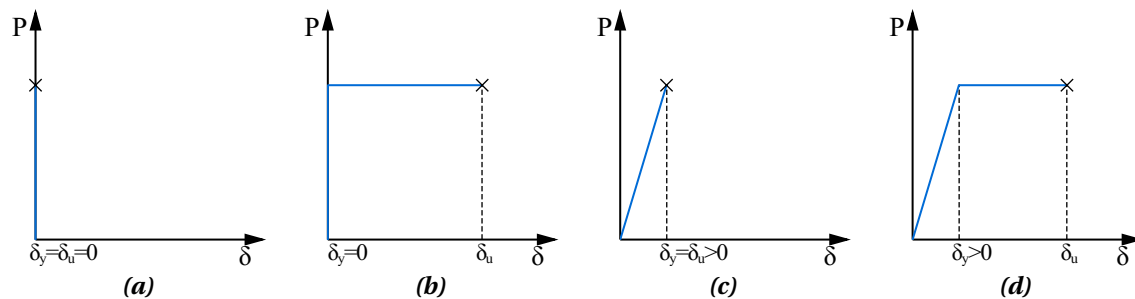


Figure 8.8: Idealisation of steel-to-timber connections: (a) rigid brittle; (b) rigid ductile; (c) semi-rigid brittle; and (d) semi-rigid ductile.

In general, connectors with sufficient deformation capacity can be idealised as perfectly-plastic, however, this is only feasible when it can be ensured that, at the ultimate limit state, the connectors are able to reach slip values of at least the slip corresponding to their shear resistance (P_R) or a threshold load (P_x). Threshold loads are typically associated to a slip of x mm, for example, the load at 6 mm slip, in which case $x = 6$ mm and, therefore, the load is denoted as P_6 mm. Thus, for connectors with sufficient deformation capacity, three main cases can be distinguished (see Figure 8.7):

1. **Case 1:** The connectors resistance at the ultimate limit state is defined at P_R and the corresponding slip is δ_R . In this case, all the connectors placed within the shear length can reach slip values of at least δ_R without failing (i.e. $\delta_R < s_i < \delta_u$). Consequently, the connectors can be idealised as perfectly-plastic at P_R . With this assumption, the estimation of the total shear forces transferred as $P_R \cdot n$ would yield conservative results for both the total shear forces and the bending capacity of the beam.
2. **Case 2:** The connectors' resistance at the ultimate limit state is again defined at P_R with the corresponding slip at δ_R . In this scenario, some connectors reach slip values larger than δ_R while others exhibit smaller slip values (i.e. $\delta_R < s_i < \delta_u$ for the former and $s_i < \delta_R$ for the latter). Consequently, the connectors may not be idealised as perfectly-plastic at P_R . Doing so could potentially lead to an overestimation of both the total shear forces transferred and the capacity of the beam.
3. **Case 3:** Here, the connectors' resistance at ultimate limit state is defined at P_x with the corresponding slip at $\delta = x$. None of the the connectors placed within the shear length of the beam reach the slip value $\delta = x$ associated to the threshold load P_x (i.e. $s_i < x$). A similar situation occurs when the connectors' resistance is defined at P_R with the corresponding slip at δ_R , and all the slip values reached by the connectors in the STC beam are smaller than δ_R . In these scenarios, the connectors may not be idealised as perfectly-plastic at P_R or P_x , respectively. This assumption would lead to an overestimation of both the total shear forces transferred and the bending capacity of the beam.

When it cannot be ensured that the connectors can reach the slip values associated to their shear resistance or the threshold load (e.g. Case 2 and Case 3). The shear force transferred by each connector can be either (i) estimated individually based on the slip distribution along the beam and the load-slip response specific to the connector, or (ii) an adequate threshold load may be defined in such a way that the idealisation as perfectly-plastic does not overestimate the actual shear forces transferred.

8.7.3. IDEALISATION OF THE LOAD-SLIP RESPONSE OF THE DEVELOPED CONNECTIONS

For some connectors, such as those developed in this investigation, the idealisation as perfectly-plastic may seem in principle not feasible due to their highly nonlinear behaviour and shear resistance associated with large slip values that are not achievable in the STC beam. For the beams tested in this investigation, the estimation of the shear forces transferred cannot be done

considering the full resistance of the connectors for three main reasons:

1. The load-slip curves obtained in the push-out tests (see Section 5.8.1) were highly non-linear, the curves flattened at slip values larger than 15 mm and peak loads were reached at even larger slip values.
2. According to the results of the beam tests, the slip distribution along the beam was not constant, indeed, the slip varied throughout the length of the beam (see Section 6.8).
3. The maximum recorded slip values at the final loading stages, observed near the ends of the beam, were relatively small, approximately 6 mm (see Section 6.8).

This indicates that the connectors transferred loads associated with slip values ranging from 0 to 6 mm (i.e. P_i for $0 < s_i < 6$ mm). Thus, assuming that every connector transfers a constant load (i.e. perfectly-plastic idealisation), for instance associated with a slip of 15 mm ($P_{15\text{ mm}}$) or 6 mm ($P_{6\text{ mm}}$), would be incorrect and lead to an overestimation of the total shear force transferred and the bending capacity of the beam. In this case, the estimation of the transferred shear forces may be computed individually for each connector. Nevertheless, due to the large deformation capacity of the connectors, they can be idealised as perfectly-plastic. However, the critical question remains: which threshold load can be considered as effectively transferred by each connector ($P_{R, eff}$) so that the sum of the actual forces is approximately equal to the number of connectors n multiplied by their effective shear resistance (i.e. $\sum_{i=1}^n P_i \approx n \cdot P_{R, eff}$), without overestimating the transferred forces, thus, ensuring that $n \cdot P_{R, eff} < \sum_{i=1}^n P_i$.

8.7.4. DEFINITION OF EFFECTIVE SHEAR RESISTANCE OF CONNECTORS

Regardless of the characteristics of the load-slip response of the shear connection, the most accurate approximation of the actual shear forces effectively transferred by the connectors is the sum of the actual shear forces calculated connector by connector, based on the actual slip each connector reaches in the composite beam (i.e. $\sum_{i=1}^n P_i$) and its specific load-slip curve. The average shear force transmitted by each connector along the beam is defined as the effective shear resistance ($P_{R, eff}$), as shown in Equation 8.6.

$$P_{R, eff} = \frac{\sum_{i=1}^n P_i}{n} \quad (8.6)$$

Since the product of the number of connectors and the effective shear resistance ($n \cdot P_{R, eff}$) is equal to the sum of the shear forces transferred by the shear connectors ($\sum_{i=1}^n P_i$), performing this calculation would be equivalent to idealise the connectors as perfectly-plastic transferring a constant force equal to $P_{R, eff}$. Thus, $P_{R, eff}$ enables the idealisation of the connector as perfectly-plastic. Based on this, the effective shear resistance of a shear connector ($P_{R, eff}$) is the average force transferred by the connectors placed within the shear length of a composite beam, that enables the idealisation of a connector as rigid-ductile (i.e. perfectly-plastic), thus, simplifying the procedure to estimate the compressive force that can be developed in the timber slab.

8.8. ALGORITHM TO TRANSFORM A LOAD-SLIP CURVE INTO AN EFFECTIVE SHEAR RESISTANCE

8.8.1. GENERAL

As illustrated in Figure 8.7, it is possible to determine the resultant normal force that can be developed in the timber slab (i.e. $N_{timber} = \sum_{i=1}^n P_i$) of a composite beam when the following is known: (i) the slip distribution along the beam, (ii) the load-slip curve of the given connector, and (iii) the shear connectors arrangement through the beam (i.e. the position of each connector in the beam). Therefore, it is necessary to estimate first the slip developed at each one of the shear connections, then, based on their slip value, the shear force transferred by the connector can be obtained from its load-slip curve. However, obtaining the exact slip values at each shear connector (i.e. slip distribution) of a composite beam is a complex task that requires either full-scale experimental investigations or advanced non-linear analyses with finite element software.

In the REDUCE project [11], demountable and reusable SCC beams and their shear connections were developed and investigated. Within this framework, Kozma [7, 148, 149] proposed an algorithm that transforms any arbitrary load-slip curve into an effective shear resistance ($P_{R, eff}$). This resistance can then be used to assess the internal normal force developed in the slab, estimate the degree of shear connection, and determine the bending capacity of the composite beams. This algorithm is suitable for composite beams whose connectors exhibit a load-slip response that complicates defining a threshold load to idealise them as perfectly-plastic, for instance highly nonlinear load-slip curves.

To proceed with this algorithm, the slip distribution through the composite beam must be known. This may be obtained from tests, FE simulations, or approximated by a specific function. The algorithm proposed by Kozma [7] has been adapted for STC beams in this research and may be used when connectors cannot be directly idealised as perfectly-plastic with the load associated to their shear resistance, such as the connectors presented in this investigation.

In practical terms, the algorithm's objectives are: (i) to simplify the procedure to determine the slip distribution through a composite beam, and (ii) to transform a connector's load-slip curve into a perfectly-plastic idealisation that is consistent with both the load-slip curve of the connector and the expected slip values in the STC beam (see Figure 8.9).

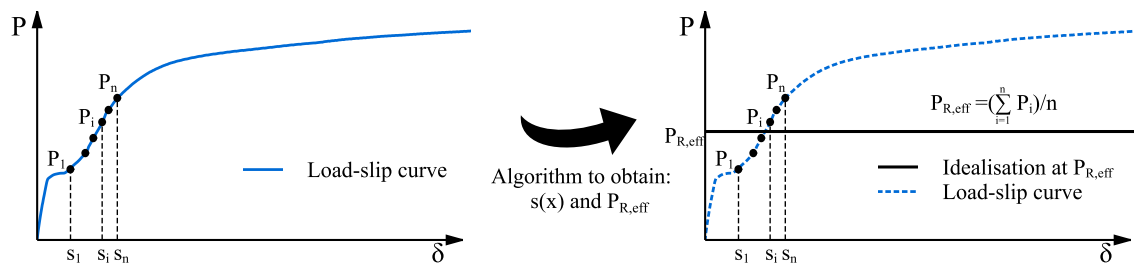


Figure 8.9: Schematic representation of the algorithm's objective: transform a load-slip curve into a perfectly-plastic idealisation at $P_{R, eff}$.

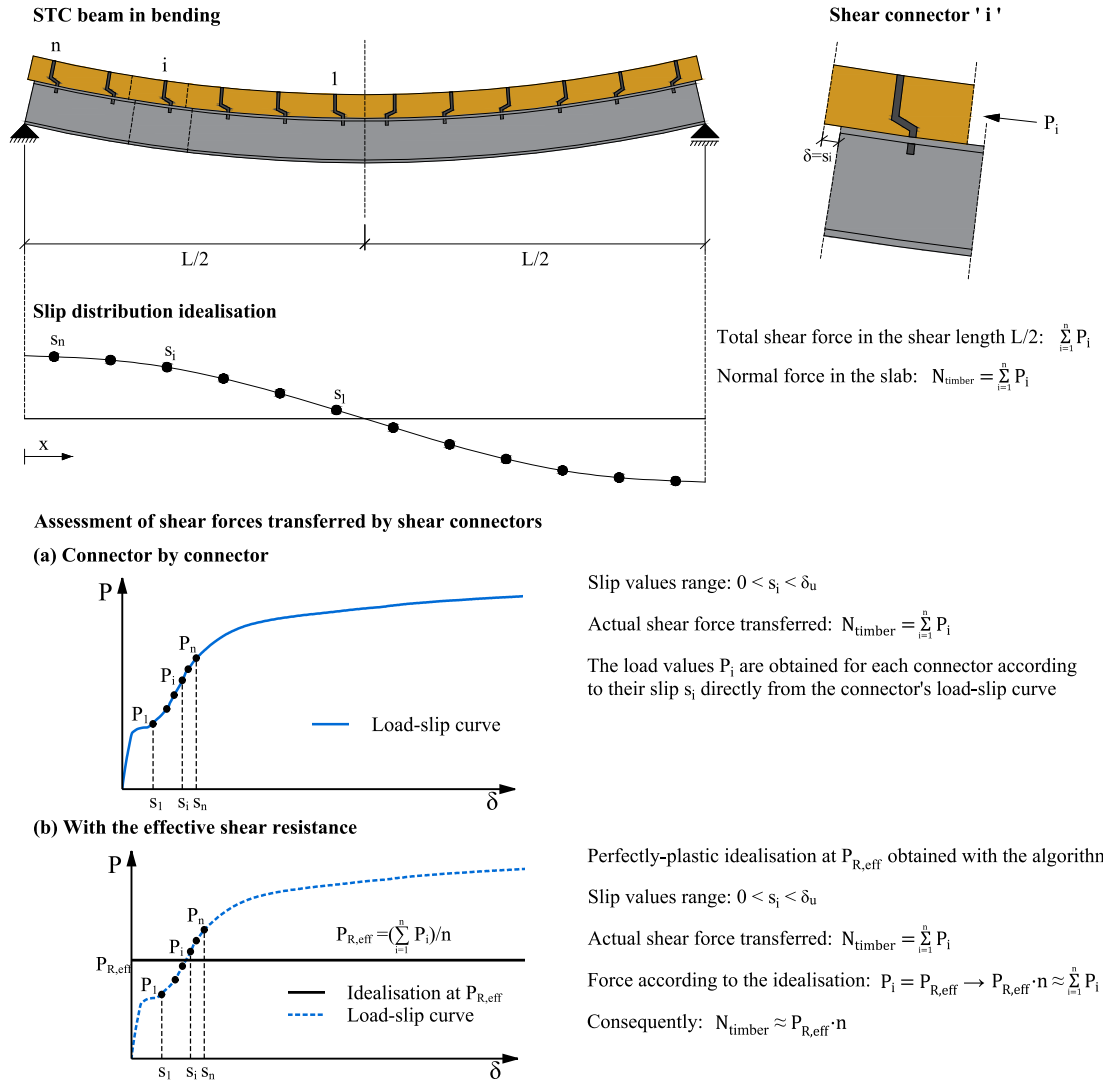


Figure 8.10: Schematic representation of two possibilities to evaluate the shear forces transferred by shear connectors that cannot be directly idealised as perfectly-plastic.

With the introduction of the effective shear resistance $P_{R,eff}$, there is an additional possibility to assess the shear forces transferred by the shear connectors in an STC beam when they cannot be directly idealised as perfectly-plastic (see Figure 8.10). The two main possibilities to assess the shear forces transferred by the shear connectors are as follows:

- (a) **Connector by connector:** The forces are estimated individually for every shear connector. The slip distribution ($s(x)$) of the beam is obtained through testing, numerically or approximated by a mathematical function. Then, with the slip values corresponding to each shear connection (s_i) the shear forces transferred by each connector (P_i) are obtained from the load slip curve specific for the connector. The sum of these forces is the total shear force transferred in the connectors ($\sum_{i=1}^n P_i$), and it is equal to the normal force that can be developed in the timber slab at the critical section (i.e. $N_{timber} = \sum_{i=1}^n P_i$).

- (b) **With the effective shear resistance, $P_{R, eff}$:** The effective shear resistance of a given connector has to be previously estimated with the algorithm proposed in this study (see Section 8.8.3). The evaluation of the transferred shear forces is straightforward in this case, as it is based on the idealisation of the connector as perfectly-plastic, thus it is assumed that every connector transfers a constant shear force equal to the effective shear resistance of the connectors (i.e. $P_i = P_{R, eff}$). Therefore, the total shear force is calculated as the multiplication of the number of connectors and its effective shear resistance (i.e. $\sum_{i=1}^n P_i = P_{R, eff} \cdot n$). This force is equal to the normal force that can be developed in the timber slab at the critical section (i.e. $N_{timber} = P_{R, eff} \cdot n$).

8.8.2. CONSIDERATIONS FOR THE ALGORITHM

The algorithm presented here is an effective analytical tool to determine the average shear force transferred by shear connectors placed within the shear length of a composite beam, it relies on the following considerations:

- i. **Slip distribution along the composite beam:** the slip distribution $s(x)$ is approximated by a mathematical function.
- ii. **Load-slip curve of the shear connector:** the load-slip response of the connector is well defined and known from experimental tests (e.g. push-out tests).
- iii. **Shear connectors arrangement:** six equidistant connectors are considered within the shear length of the beam, the connectors' arrangement is symmetrical with respect to the midspan.
- iv. **The effective shear resistance:** this resistance value estimated through the proposed algorithm is specific to the shear connector and highly depends on both the assumed slip function ($s(x)$) and the end-slip value.

The algorithm was developed for simply supported beams under sagging bending, thus, the slip distribution ($s(x)$) along the beam can be approximated by the cosine function presented in Equation 8.7, as shown by Aribert [150] for SCC beams and by Kozma et al. [151] for demountable SCC beams. For the STC beams tested in this investigation, this seems to be a reasonable approximation as shown in Figure 8.11. This function is dependent on the end-slip, which is an assumed value based on experimental and numerical observations.

$$s(x) = s_1 \cos \frac{\pi \cdot x}{L} \quad (8.7)$$

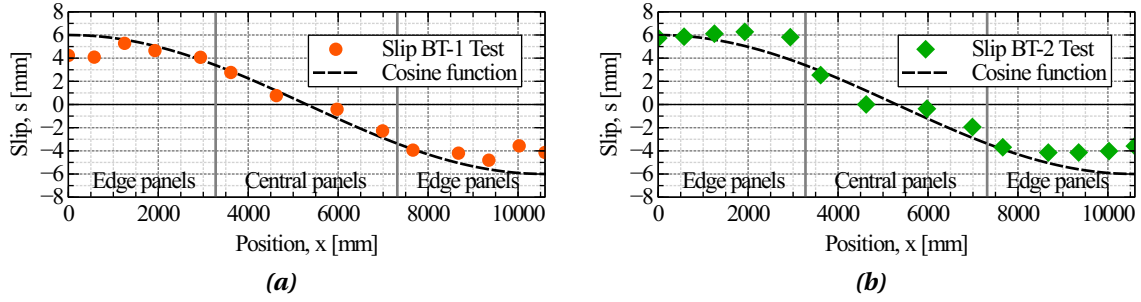


Figure 8.11: Comparison of the slip measurements from the full-scale beam tests and the proposed cosine slip function $s(x)$ for: (a) BT-1 and BT-2.

According to Eurocode 4 [94], ductile shear connectors for SCC beams are able to develop slip values of at least 6 mm, this means that at ultimate limit state the expected maximum slip is at least 6 mm. This implies a correlation between slip and ultimate capacity, in which an end-slip of at least 6 mm is implicitly linked to the ultimate capacity of SCC beams. For STC beams there is not enough data to associate an end-slip value to their ultimate capacity. However, based on the results of this investigation, 6 mm is also a reasonable end-slip value for the STC beams developed and tested in this study. Therefore, this value might be cautiously adjusted for different connections and STC systems as the effective shear resistance ($P_{R, eff}$) is highly influenced by this assumption.

In the proposed algorithm, the effective shear resistance ($P_{R, eff}$) of the connectors is obtained as the average shear force developed at the n rows of connectors placed within the shear length of the beam (see Equation 8.8). For the sake of simplicity, it is proposed to use $n = 6$, since it has been demonstrated that the value of the effective shear resistance ($P_{R, eff}$) does not vary considerably for $n > 6$ [7]. Additionally, the shear connectors are distributed equidistantly through the beam.

$$P_{R, eff} = \frac{\sum_{i=1}^n P_i}{n} \quad (8.8)$$

8.8.3. ALGORITHM'S STEPS

The end-slip value considered to define the slip function $s(x)$, must be carefully chosen, its value corresponds to the end-slip expected at ultimate state when analysing the ultimate capacity of STC beams. Here, an end-slip of 6 mm is proposed for the analyses of the tested STC beams. However, it may be a different value for different conditions (e.g. different shear connection). Considering that an end-slip of 6 mm is reached at ultimate limit state of the STC beams subject of this investigation, the algorithm to determine the effective shear resistance of steel-to-timber connections, such as the connections presented in this contribution, the effective shear resistance of the connectors can be estimated as follows:

1. Six rows of shear connectors are evenly spaced along the beam's shear length.
2. The slip distribution is defined as a cosine function according to Equation 8.7.

3. The slip of the first row of connectors (s_1), the end-slip, is taken as 6 mm. Nevertheless, the suitability of this value for different conditions and shear connections is to be assessed.
4. The slip values of the connector rows 2 to 6 (i.e. s_2 to s_6) are calculated.
5. With the slip values s_i , the shear forces P_i are obtained from the load-slip curve specific for the connector.
6. Estimate the effective shear resistance $P_{R, eff}$ according to Equation 8.8.

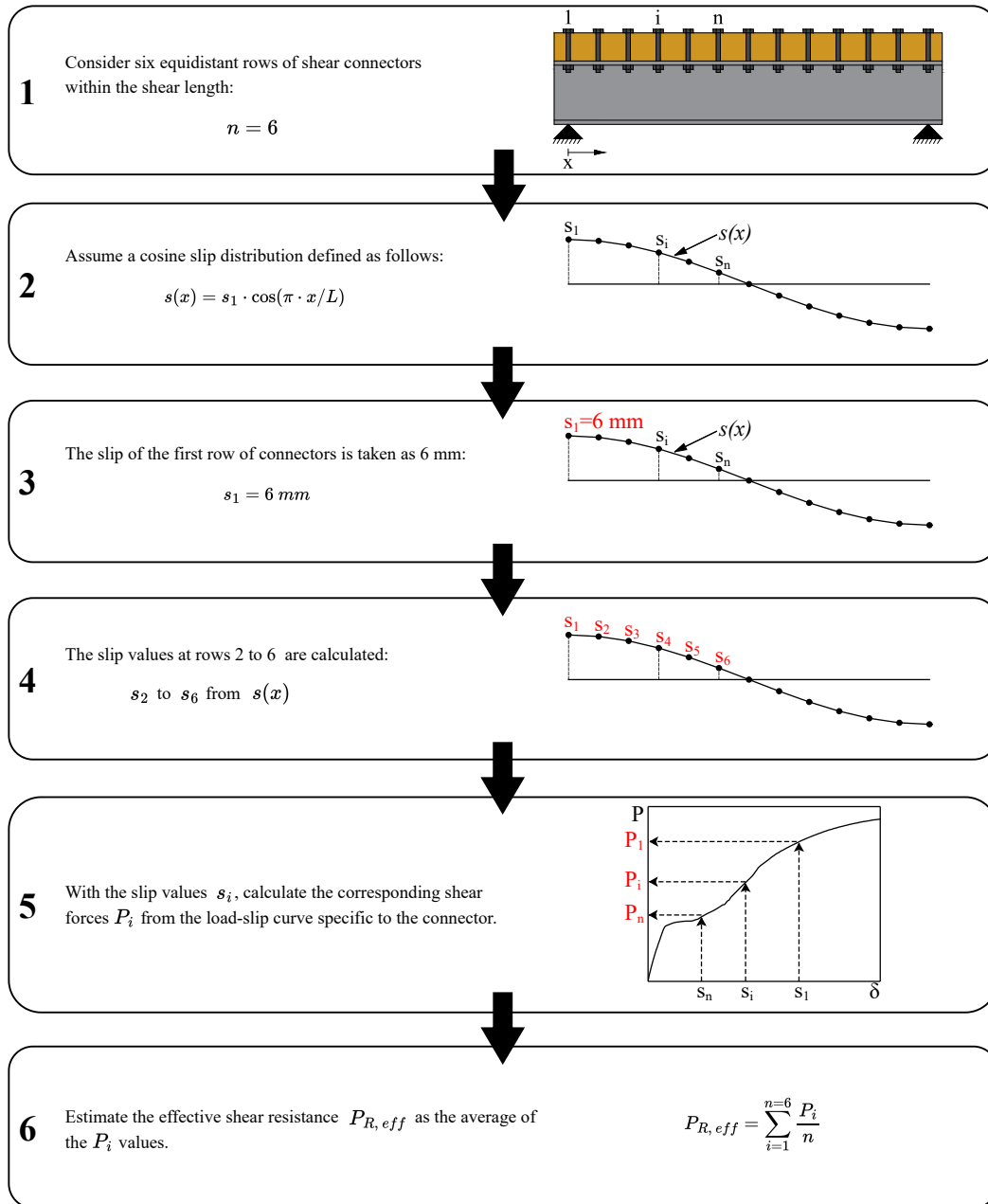


Figure 8.12: Flow-chart of the algorithm's steps.

8.9. ESTIMATION OF THE BENDING CAPACITY OF STC BEAMS CONSIDERING THE SECTION'S RESISTANCE AND THE EFFECTIVE SHEAR RESISTANCE OF THE CONNECTORS

The stress-strain-based approach presented in Section 8.3 allows to determine the resistance of an STC cross-section with specific geometry and material properties. When the moment resistance values for different degrees of shear connection are computed, the resulting values can be used to construct an M_R vs. η curve. Once this curve and the degree of shear connection are established, the moment resistance can be directly obtained from the curve (see Figure 8.13).

The procedure to determine the M_R vs. η curve and the moment resistance of a beam with a particular degree of shear connection involves the following steps:

1. Estimate the upper bound of the M_R vs. η curve (i.e. moment resistance for full-rigid shear connection).
2. Estimate the lower bound of the M_R vs. η curve (i.e. moment resistance for no shear connection).
3. Calculate intermediate values (i.e. moment resistance for partial shear connection cases).
4. Build the M_R vs. η curve with the previously estimated values.
5. Compute the degree of shear connection (η) of the STC beam.
6. Determine the resistance of a beam with a particular degree of shear connection from the M_R vs. η curve.

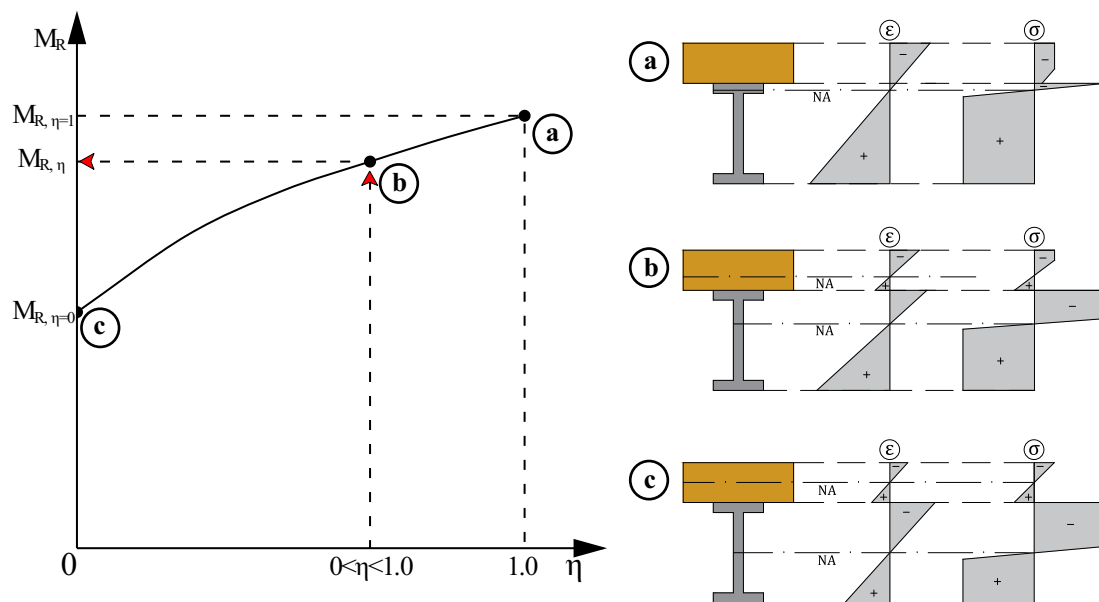


Figure 8.13: Relation between moment resistance and degree of shear connection (M_R vs. η curve) and cases considered in the analysis of STC cross-sections: (a) rigid shear connection; (b) partial shear connection; and (c) no shear connection.

These steps can be grouped in three main procedures (see Figure 8.14):

- I. **Cross-section resistance:** Estimation of the cross-section resistance values for different degrees of shear connection and construction of the M_R vs. η curve.
- II. **Degree of shear connection:** Calculation of the degree of shear connection with consideration of: (i) the effective shear resistance of the shear connectors according to the approach presented in Section 8.8, and (ii) the amount of connectors placed within the shear length in the actual STC beam configuration.
- III. **Bending capacity of the STC beam:** The moment resistance ($M_{R, \eta}$) can be directly obtained from the M_R vs. η curve with the known η value.

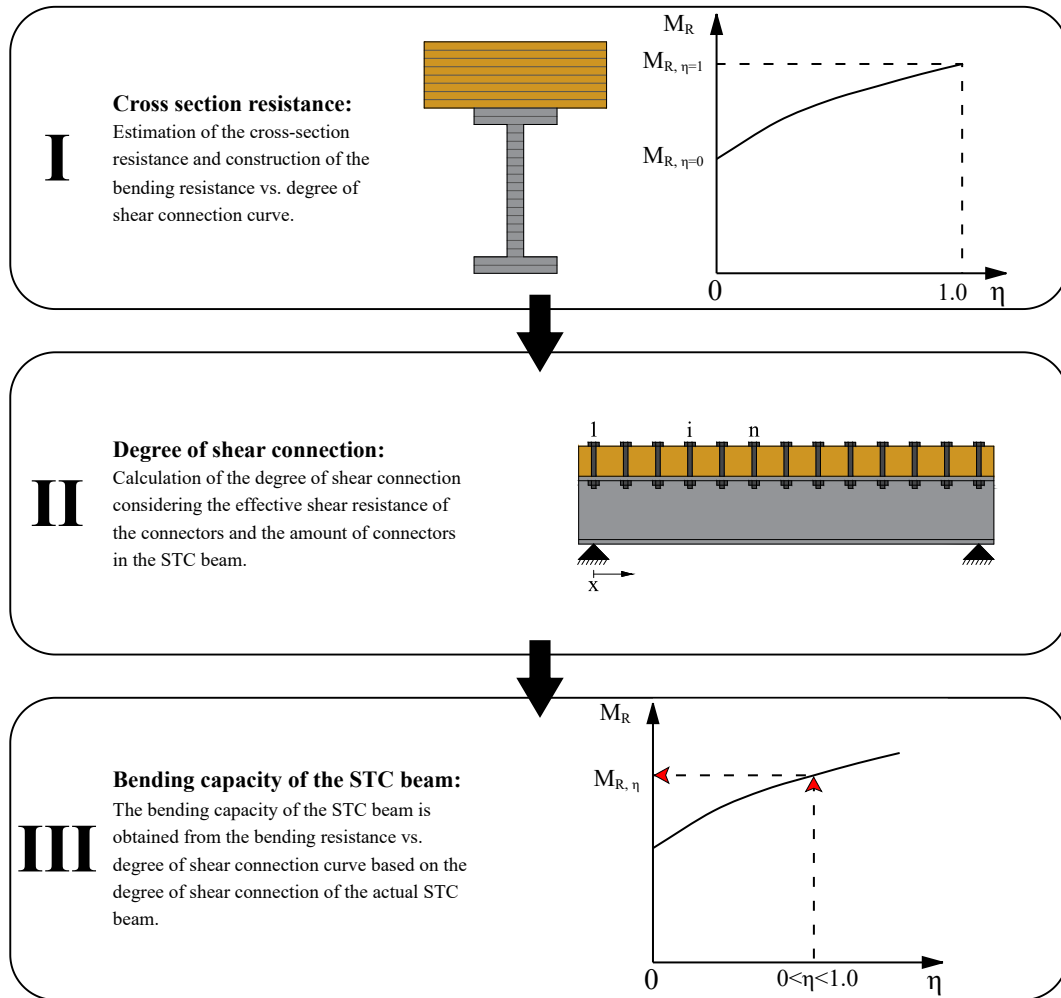


Figure 8.14: Recapitulation of the procedures to estimate the bending capacity of STC beams.

8.10. COMPARISON OF EXPERIMENTAL RESULTS AND STRAIN-BASED MOMENT RESISTANCE VALUES

8.10.1. GENERAL

The strain-based approach was implemented in a MATLAB script to build the M_R vs. η curve for the cross-section of the STC beams tested in this investigation (see Chapter 6). Examples of the implementation of the strain-based procedure have been presented by Rugova [152], Pelivani [153], and Akhigbe [154]. The effective shear resistance ($P_{R, eff}$) of SCT-1, SCT-2, and SCT-3 was obtained considering an end-slip of 6 mm, obtaining the values of 73.9 kN, 76.3 kN, and 88.7 kN, respectively.

Due to the shear lag effects observed in the experimental investigations the effective width estimated according to strain measurements in the timber slabs was $L/5.5$ as presented in Section 6.8.4. Therefore, this effective width was considered in the geometry definition of the STC cross-section for the analytical computations presented in this section.

In the analytical computations, the radius of the hot-rolled sections was neglected. Different M_R vs. η curves were obtained considering different assumptions for the materials' stress-strain relationships, then, the M_R, η values for the tested STC beams were estimated from the M_R vs. η curves. The parameters of the material constitutive laws for steel and timber are illustrated in Figure 8.15, and Table 8.1 summarizes the different steel and timber material parameters considered for the comparisons of experimental and analytical results.

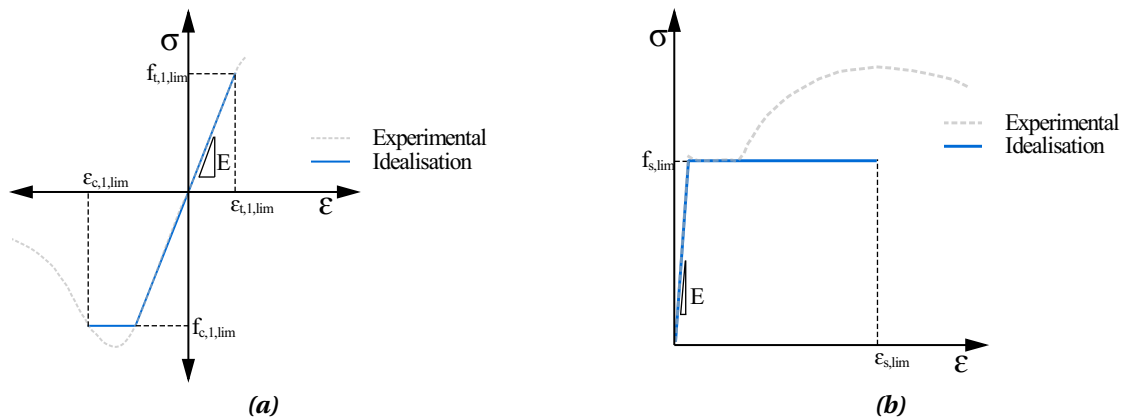


Figure 8.15: Schematic representation of the material constitutive laws implemented in the analytical calculations for: (a) steel; and (b) timber (LVL).

Table 8.1: Properties of steel and timber considered in the analytical calculations.

Property	Units	Steel material model		Property	Units	Timber material model	
		S-1	S-2			T-1	T-2
E	[MPa]	207 000	207 000	E	[MPa]	7 920	7 920
$f_{s,lim}$	[MPa]	399	399	$f_{c,1,lim}$	[MPa]	40.4	34.3
$\epsilon_{s,lim}$	[‰]	150	1.9	$f_{t,1,lim}$	[MPa]	40.4	34.3
				$\epsilon_{c,1,lim}$	[‰]	5.1	8.6
				$\epsilon_{t,1,lim}$	[‰]	5.1	4.3

Since the objective is to estimate the capacity of the tested STC beams, elasticity modulus, as well as the limit stresses and strains were defined according to the results obtained experimentally. The material constitutive laws implemented in the strain-based procedure consider that both, tension and compression can be developed in timber. An overview of the material models and the moment resistances considered is presented below.

Steel material models:

- i. **S-1:** The steel material model S-1 is defined by a linear elastic perfectly-plastic stress-strain relationship, implemented to estimate the ultimate capacity of the STC beams post-yielding of the steel profile.
- ii. **S-2:** The steel material model S-2 consists of linear elastic stress-strain relationship, implemented to estimate the capacity of the STC beams in the elastic range.

Timber material models:

- i. **T-1:** The timber material model T-1 implements a linear elastic stress-strain relationship considering identical elasticity modulus and limit stresses in both compression and tension. It is used with steel material model S-1 to estimate the ultimate capacity of the STC beams and with S-2 to estimate the capacity of the STC beams within the elastic range.
- ii. **T-2:** The timber material model T-2 implements a linear elastic perfectly-plastic stress-strain relationship in compression and a linear elastic stress-strain relationship in tension, with identical elasticity modulus and limit stresses in both compression and tension. However, the limit strain is larger in compression allowing for the plastic plateau after the proportional limit in compression. The proportional limit was defined as 85% of the compressive strength in compression obtained experimentally (i.e. $0.85f_{c,1}$). This material model is used with steel material model S-1 to estimate the ultimate bending capacity of the STC beams.

According to this, the moment resistance values that have been estimated and compared with the experimentally obtained moment vs. midspan deflection curves of BT-1 and BT-2 are as follows:

- i. Elastic moment resistance, $M_{R,el}$: the material models for timber and steel (i.e. T-1 and S-2) consist of linear elastic stress-strain relationships. Thus, the material models considered are: T-1 and S-2.
- ii. Ultimate moment resistance, $M_{R,\eta}(T-1)$: considering (i) plasticity can be developed in steel (i.e. S-1) and (ii) only the elastic range in timber (i.e. T-1), both assumptions in line with the observations of the full-scale beam tests presented in Chapter 6. In this case the material models considered are: T-1 and S-1.
- iii. Ultimate moment resistance, $M_{R,\eta}(T-2)$: considering (i) plasticity can be developed in steel (i.e. S-1) and (ii) plasticity development in timber (i.e. T-2), both assumptions in line with the observations of the full-scale beam tests presented in Chapter 6. Hence, the

material models considered are: T-2 and S-1.

8.10.2. COMPARISON OF RESULTS

The moment resistance values have been compared with the moment vs. midspan deflection curves obtained experimentally and numerically, the results are presented in Figure 8.16a for BT-1 and in Figure 8.16b for BT-2. In the experimentally obtained moment vs. midspan deflection curves, the moment due to self weight and the corresponding deflection were not considered. To account for their effect in the estimations of the bending capacity, the moment due to self-weight (i.e. $M_{sw} = 38 \text{ kN}\cdot\text{m}$) was subtracted. Therefore the horizontal lines represent the moment resistance estimated analytically minus the moment due to self-weight of the specimens (i.e. $M_R - M_{sw}$).

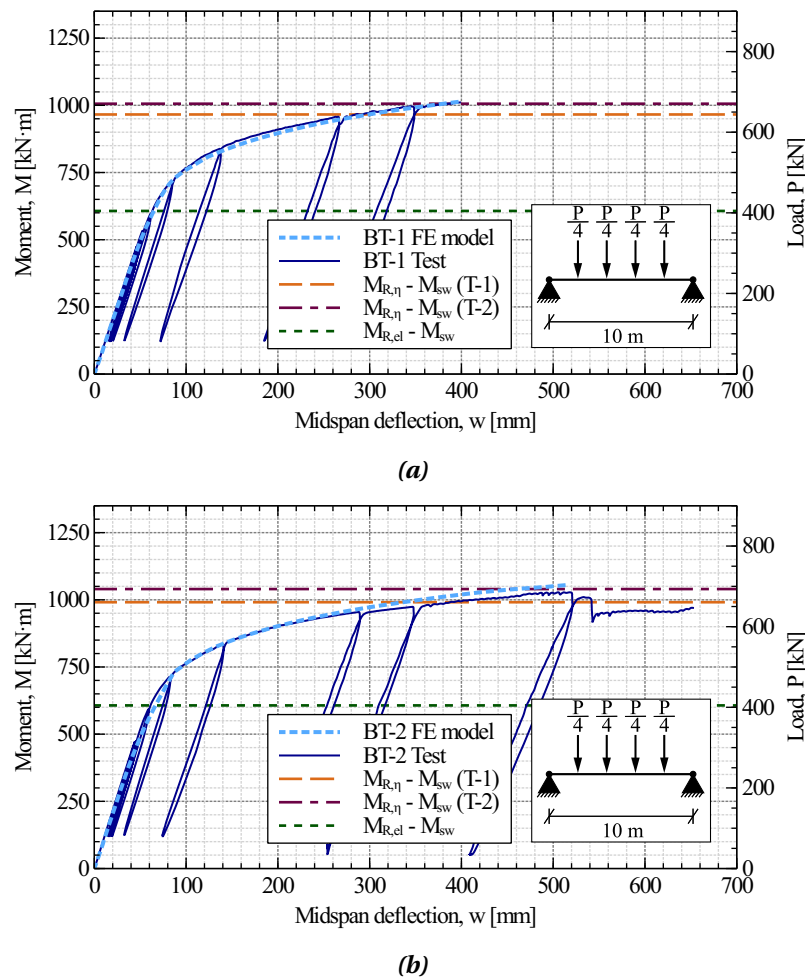


Figure 8.16: Moment vs. midspan deflection curve and analytically estimated moment resistance values for: (a) BT-1; and (b) BT-2.

According to the results presented in Figure 8.16 the following conclusions can be made:

- i. $M_{R,\eta}(T-1)$: Considering timber as fully elastic with identical elasticity modulus in tension and compression and equal compressive and tensile strength (i.e. timber material

model T-1), in combination with steel linear elastic perfectly-plastic (i.e. steel material model S-1) leads to a slight underestimation of the maximum bending moment observed in the experimental investigations, which is on the safety side.

- ii. $M_{R,\eta}(T-2)$: When a linear elastic perfectly-plastic stress-strain relationship is considered for timber (i.e. timber material model T-2), in combination with steel linear elastic perfectly-plastic (i.e. steel material model S-1), the resistance is closer to the maximum bending moment observed in the tests, but in the case of BT-2 it slightly overestimates the capacity of the STC beam, which may be a non-conservative estimation of the bending capacity.
- iii. $M_{R,el}$: The implementation of elastic stress-strain relationships for both timber and steel led to moment resistance values that lay close to the limit of the elastic branch of the moment vs. midspan deflection curves.
- iv. b_{eff} : Considering the effective width as $L/5.5$ (see Section 6.8.4) leads to reasonable moment resistance values that are in good agreement with the experimental observations.

8.11. SIMPLIFIED ANALYTICAL PROCEDURE

8.11.1. GENERAL

The strain-based approach is a robust analytical tool to predict the moment resistance of STC cross-sections at different states of stresses that are controlled by imposing strain limits for the materials, however, its implementation can be challenging. When the objective is to determine the capacity of STC beams at the ultimate limit state, the procedure can be simplified using straightforward analytical equations with particular assumptions about the materials.

In Section 8.10, the ultimate capacity of the beam was estimated using the strain-based procedure. This procedure considered two cases: (i) a linear elastic idealisation for timber (i.e. timber material model T-1) and a linear elastic perfectly-plastic idealisation for steel (i.e. steel material model S-1), and (ii) a linear elastic perfectly-plastic idealisation for both timber and steel (i.e. steel S-1 and timber T-1). The predictions of the bending capacity, which implemented properties with ultimate strain and strength values, yielded reasonable results in both cases.

In the strain-based calculations, the assumption that timber remains fully elastic at the ultimate state yielded conservative results. Furthermore, this assumption aligns closely with both experimental and numerical observations, where the steel beam exhibited extensive plasticisation while the timber remained fully elastic. Based on this, a set of assumptions has been proposed to simplify the computation of the bending capacity of STC beams to a straightforward stress analysis of the cross-section. Therefore, the simplified analytical procedure to determine the capacity of STC beams at the ultimate limit state is based on the following material considerations:

- i. **Steel material:** The material constitutive law of steel is idealised as perfectly-plastic. This is an usual assumption for the estimation of the ultimate capacity of steel and steel com-

posite members.

ii. **Timber material:** Two cases have to be considered:

- (a) The timber has both compression and tension stresses: These cases may appear for any degree of shear connection. In such cases, the material constitutive law of timber is represented by a linear-elastic stress-strain relationship, where the compressive strength and the moduli of elasticity are equal for both tension and compression. This is the customary material idealisation of timber at ultimate limit state.
- (b) The timber has only compression stresses: These cases only occur for full-rigid shear connection in which the neutral axis is in the steel beam. In these cases the material constitutive law of timber is idealised as perfectly-plastic.

These assumptions simplify the computations as the stress analyses are straightforward for rectangular stress blocks and linear stress distributions. The unknowns of the system can be determined for the stress distribution fulfilling the equilibrium condition without the need to carry out iterations or complex scripting.

8.11.2. MATERIAL ASSUMPTIONS

STEEL

To simplify the computation of the stress distribution in the steel beam, it is proposed to idealise the steel as perfectly-plastic for both tension and compression (see Figure 8.17). In the proposed idealisation the stress at ultimate limit state ($f_{s,lim}$) is associated to the yielding stress (f_y).

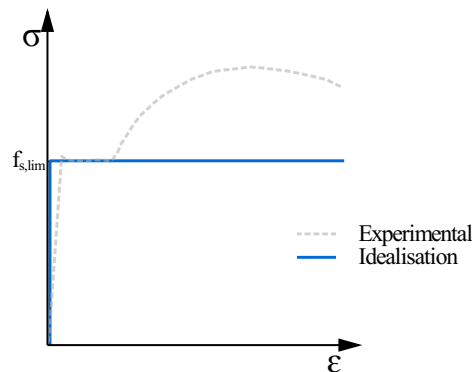


Figure 8.17: Idealisation of the stress-strain relationship of steel for the simplified analytical procedure.

This idealisation is common in the stress analyses of steel and steel composite beams. It simplifies the ultimate state analyses as it allows to consider rectangular stress distributions instead of triangular and/or trapezoidal stress distributions in the section. With this idealisation it is possible to obtain accurate approximations to the actual capacity of the member and close to the solution that considers the actual non-linear stress-strain material constitutive law of steel. Additionally, this assumption is consistent with the experimental and numerical ob-

servations of the STC beams tested in this investigation, in which the steel beams plasticised to a large extent.

TIMBER

For ultimate limit state analyses, the stresses in timber cross-sections are typically idealised as linear-elastic, meaning that only the elastic range is considered. Additionally, the same elastic moduli and strength is considered for both, tension and compression. For members in bending, this assumption is consistent with their actual response, as they fail once the most stressed fibre in tension reaches its strength, while little or no plasticity is observed in compression. The objective of this assumption is to avoid timber's brittle failure in tension, and overestimation of the bending capacity by considering additional compressive stresses taken by timber post-proportional limit.

According to the measurements of the full-scale bending tests, timber remained within its elastic range, even at very large deformations. Therefore, the idealisation of timber as linear elastic is reasonable for the cases where timber undergoes tensile and compressive stresses. This idealisation is shown in Figure 8.18a, where the compressive and tensile strength correspond to the strength in compression.

When analysing the ideal case of full-rigid connection, there is only one neutral axis, which can be positioned in the timber slab or in the steel beam at the equilibrium state. When the neutral axis is in the timber slab, the timber undergoes both tension and compression while the steel section is fully in tension, and when the neutral axis is in the steel beam, the timber is fully in compression while the steel beam has both compression and tensile stresses. When timber is fully compressed it can take loads beyond its proportional limit, as demonstrated by the material tests carried-out in this investigation and presented in Chapter 4. Thus, for ultimate limit state analyses it is reasonable to idealise timber as perfectly-plastic when it is only under compression stresses (see Figure 8.18b).

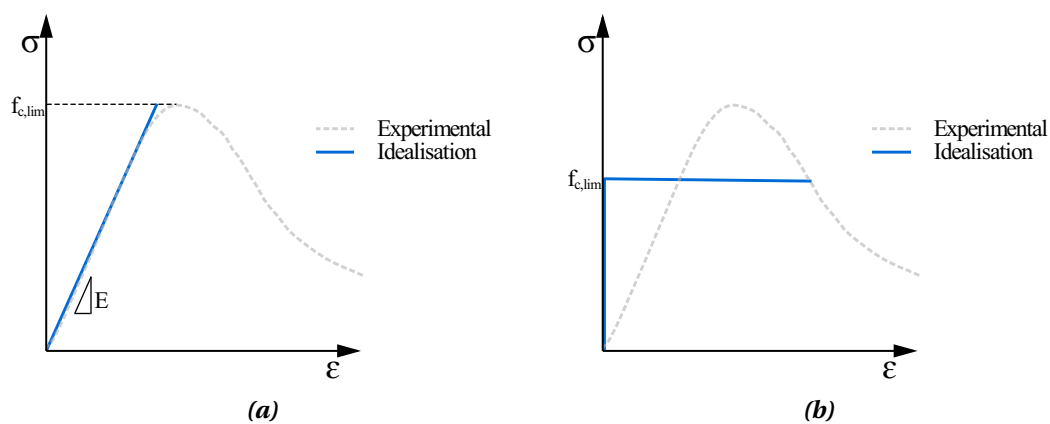


Figure 8.18: Idealisation of the stress-strain relationship of timber (a) linear elastic; and (b) perfectly-plastic.

In the proposed demountable STC flooring system, there are gaps between adjacent panels. This discontinuity generates an additional critical section which capacity must be also consid-

ered. The gaps are to be filled with mortar to ensure compressive forces are transferred from the central panels to the edge panels and thus the connectors are activated. However, tensile forces are not transferred. For this section, it is proposed to neglect the contribution of timber in tension, and consider an idealisation of the timber material as perfectly-plastic.

In summary, for timber it is proposed to consider two idealisations that apply for different cases:

1. Linear elastic idealisation: This idealisation applies for any degree of shear connection when the timber exhibits both tension and compression.
2. perfectly-plastic idealisation: This idealisation is implemented only for cross-sections at the gaps, and for the case of full-rigid shear connection when the neutral axis is located in the steel beam, meaning that the timber is fully under compression.

When timber is idealised as perfectly-plastic, the strength $f_{c,lim}$ is defined as shown in Equation 8.9. In this case β is a factor that gives an area below the line $\sigma = \beta \cdot f_{c,1}$ in the range $0 \leq \varepsilon \leq \varepsilon_{c,lim}$, equal to the area below the curve $\sigma(\varepsilon)$ corresponding to the stress-strain relationship obtained in the material tests, as shown in Equation 8.10 (see Figure 8.19). Consequently, the factor β is determined as established in Equation 8.11.

$$f_{c,lim} = \beta \cdot f_{c,1} \quad (8.9)$$

$$\int_0^{\varepsilon_u} \beta \cdot f_{c,1} d\varepsilon = \int_0^{\varepsilon_{c,lim}} \sigma(\varepsilon) d\varepsilon \quad (8.10)$$

$$\beta = \frac{\int_0^{\varepsilon_u} \sigma(\varepsilon) d\varepsilon}{f_{c,1} \cdot \varepsilon_u} \quad (8.11)$$

The value of this factor is dependent on the stress-strain relationship of the material obtained through tests, for the LVL tested in this investigation a value of $\beta = 0.70$ has been obtained considering the mean stress-strain relationship from the compression tests in the longitudinal direction (i.e. grain direction).

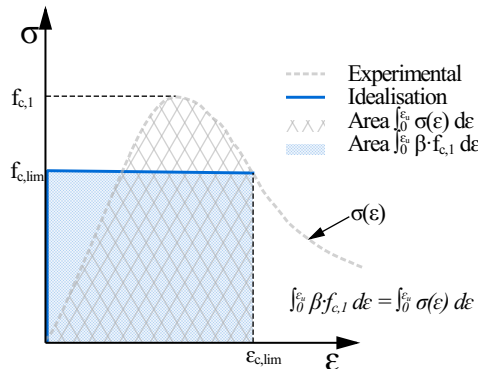


Figure 8.19: Areas considered for the determination of the factor β .

8.11.3. OVERVIEW OF CASES CONSIDERED

According to the degree of shear connection in a composite cross-section, three cases can be distinguished: (i) full-rigid shear connection, (ii) no shear connection, and partial shear connection. When the bending capacity of the cross-sections is determined through stress analysis is important to consider that for each of these cases the position of the neutral axes at the equilibrium state has different implications for the material assumptions, furthermore, different formulations apply to determine the stresses distributions. Thus, the possibilities for the position of the neutral axes for each of these shear connection cases is as follows:

1. **Full-rigid shear connection:** For full-rigid shear connection, there is only one neutral axis and there are three main possibilities for its location at equilibrium state: (i) at the timber slab, (ii) at the top flange of the beam, and (iii) at the web of the beam.
2. **No shear connection:** In the case of no shear connection at all, there are two neutral axis, one in the timber slab and one in the steel beam at the web.
3. **Partial shear connection:** For partial shear connection cases there are two neutral axes one at the timber slab and one at the steel beam. The neutral axis of the steel beam can be either: (i) at the top flange, or (ii) at the web of the steel beam.

Table 8.2: Overview of the cases considered and their material idealisations.

Shear connection case	Neutral axis location	Material idealisation	
		Steel	Timber
Full-rigid shear connection	Timber slab	Perfectly-plastic	Elastic ^a
	Steel beam's top flange	Perfectly-plastic	Perfectly-plastic
	Steel beam's web	Perfectly-plastic	Perfectly-plastic
No shear connection	Timber slab and steel beam	Perfectly-plastic	Elastic
Partial shear connection	Timber slab and steel beam's top flange	Perfectly-plastic	Elastic ¹
	Timber slab and steel beam's web	Perfectly-plastic	Elastic ¹

^a Perfectly-plastic in compression with tension neglected when analysing a cross-section located at a gap.

8.11.4. BENDING CAPACITY OF STC BEAMS WITH FULL-RIGID SHEAR CONNECTION

NEUTRAL AXIS IN THE TIMBER SLAB

Figure 8.20 shows the stress distribution in a steel-timber cross-section in which the neutral axis is located in the timber slab. The neutral axis is in the timber slab when the ratio of the magnitude of maximum normal force in the steel section to the normal force in the timber slab when it is in full compression with a linear stress distribution from 0 at the bottom fibre to $f_{c,lim}$ at the top fibre is smaller than 1, this condition is shown in Equation 8.12.

$$\frac{f_{s,lim} \cdot A_2}{0.5 \cdot f_{c,lim} \cdot A_1} < 1 \quad (8.12)$$

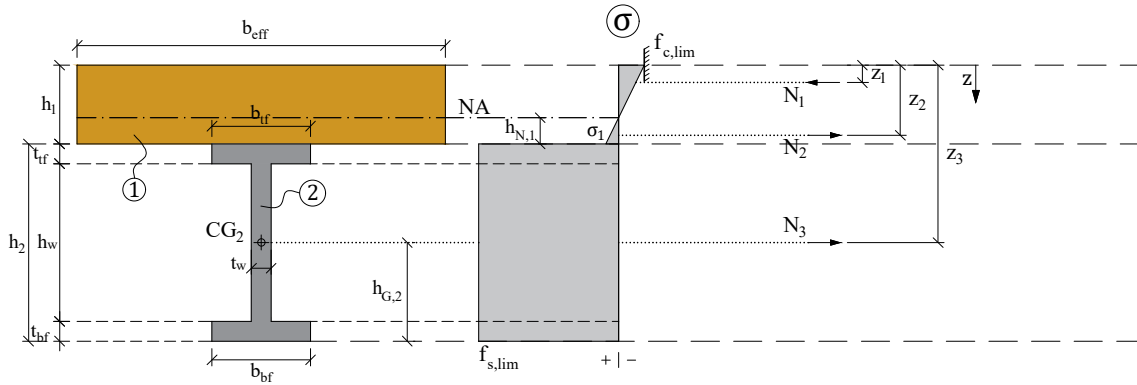


Figure 8.20: Stress distribution for full-rigid shear connection with neutral axis in the timber.

The unknowns of this system are the stress at the bottom fibre of timber (σ_1) and the location of the neutral axis, which position is defined by its distance from the bottom fibre of the timber slab ($h_{N,1}$). The stress σ_1 can be obtained from the relationships between the stress at the top fibre and the heights of the stress distributions in compression and tension in the timber slab as shown in Equation 8.13.

$$\sigma_1 = \frac{h_{N,1} \cdot f_{c,lim}}{h_1 - h_{N,1}} \quad (8.13)$$

The sum of normal forces (N_i) for the equilibrium state must be equal to zero (Equation 8.14):

$$\sum_{i=1}^n N_i = N_1 + N_2 + N_3 = 0 \quad (8.14)$$

Where the normal forces N_i are calculated according to Equations 8.15 to 8.17:

$$N_1 = -0.5 \cdot f_{c,lim} \cdot b_{eff} \cdot (h_1 - h_{N,1}) \quad (8.15)$$

$$N_2 = 0.5 \cdot \sigma_1 \cdot h_{N,1} \cdot b_{eff} \quad (8.16)$$

$$N_3 = f_{s,lim} \cdot A_2 \quad (8.17)$$

Substituting Equations 8.13 and 8.15 to 8.17 in Equation 8.14, and solving for the position of the neutral axis measured from the bottom fibre of the timber slab $h_{N,1}$ gives Equation 8.18:

$$h_{N,1} = \frac{h_1 \cdot (b_{eff} \cdot f_{c,lim} \cdot h_1 - 2 \cdot N_3)}{2 \cdot (b_{eff} \cdot f_{c,lim} - N_3)} \quad (8.18)$$

With this value is possible to obtain σ_1 in Equation 8.13. Hence, the unknowns of the system are now well defined and it is possible to proceed to determine the moment resistance of the cross-section, which is calculated as the product of the normal forces N_i and the respective lever arm z_i , and considering as a reference the top fibre of the timber slab (see Equation 8.19). This results in Equation 8.20 when substituting the values of the forces N_i and the lever arms z_i .

$$M_R = \sum_{i=1}^n N_i \cdot z_i \quad (8.19)$$

$$M_R = f_{s,lim} \cdot A_1 \cdot (h_1 + h_2 - h_{G,2}) + \left(\frac{f_{c,lim} \cdot b_{eff} \cdot h_{N,1}^2}{2 \cdot (h_1 - h_{N,1})} \right) \cdot \left(h_1 - \frac{h_{N,1}}{3} \right) - \frac{f_{c,lim} \cdot b_{eff} \cdot (h_1 - h_{N,1})^2}{6} \quad (8.20)$$

NEUTRAL AXIS IN THE TOP FLANGE

Figure 8.21, shows the stress distribution of a steel-timber section with the neutral axis in the top flange. When the timber slab is fully compressed and the resultant forces are not sufficient to balance the tensile forces of a hypothetically tensioned steel beam, the steel beam must take on some compression stresses either in the top flange or in a portion of the web. Consequently, the neutral axis is located in the steel beam when the ratio of the magnitudes of the normal force in the fully compressed timber slab to the normal force in the fully tensioned steel beam is smaller than 1, as shown in Equation 8.21.

$$\frac{f_{c,lim} \cdot A_1}{f_{s,lim} \cdot A_2} < 1 \quad (8.21)$$

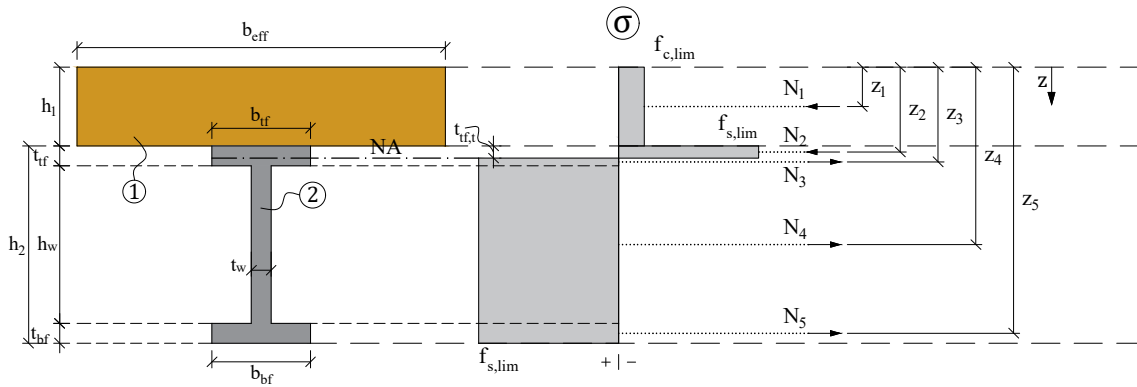


Figure 8.21: Stress distribution for full-rigid shear connection with neutral axis in the top flange of the steel beam.

In order to determine whether the neutral axis is in the top flange, it must be checked if the magnitude of the compressive normal forces in the timber slab, plus the forces in the top flange in the hypothetical case of full compression, are sufficient to balance the normal tensile forces in the web and the bottom flange. After verifying Equation 8.21, this is evaluated with the expression in Equation 8.22. If this expression holds true, the neutral axis is located in the top flange of the beam.

$$\frac{f_{s,lim} \cdot (A_2 - b_{tf} \cdot t_{tf})}{f_{c,lim} \cdot A_1 + f_{s,lim} \cdot b_{tf} \cdot t_{tf}} < 1 \quad (8.22)$$

Where $f_{c,lim}$ is estimated according to Equation 8.9. At the equilibrium state the sum of the normal forces N_i is equal to zero (see Equation 8.23), which values are calculated according to Equations 8.24 to 8.28.

$$\sum_{i=1}^n N_i = N_1 + N_2 + N_3 + N_4 + N_5 = 0 \quad (8.23)$$

$$N_1 = -f_{c,lim} \cdot b_{eff} \cdot h_1 \quad (8.24)$$

$$N_2 = -f_{s,lim} \cdot b_{tf} \cdot t_{tf,t} \quad (8.25)$$

$$N_3 = f_{s,lim} \cdot b_{tf} \cdot (t_{tf} - t_{tf,t}) \quad (8.26)$$

$$N_4 = f_{s,lim} \cdot h_w \cdot t_w \quad (8.27)$$

$$N_5 = f_{s,lim} \cdot b_{bf} \cdot t_{bf} \quad (8.28)$$

The objective is to find the position of the neutral axis which is defined by the thickness of the portion of the top flange in compression ($t_{tf,t}$). It can be determined when substituting the values of the normal forces N_i in Equation 8.23 and solving for $t_{tf,t}$ as shown in Equation 8.29.

$$t_{tf,t} = \frac{1}{2 \cdot b_{tf}} \cdot \left(h_w \cdot t_w + b_{bf} \cdot t_{bf} - \frac{f_{c,lim} \cdot b_{eff} \cdot h_1}{f_{s,lim}} \right) + 0.5 \cdot t_{tf} \quad (8.29)$$

The moment resistance of the cross-section is then estimated as the sum of the normal forces N_i multiplied by their lever arm z_i (see Equation 8.30). After substituting Equations 8.24 to 8.28 and the values of the lever arms in Equation 8.30, Equation 8.31 is obtained.

$$M_R = \sum_{i=1}^n N_i \cdot z_i \quad (8.30)$$

$$\begin{aligned}
M_R = & f_{s,lim} \cdot b_{tf} \cdot (t_{tf} - t_{tf,t}) \cdot (h_1 + 0.5 \cdot t_{tf,t} + 0.5 \cdot t_{tf}) + f_{s,lim} \cdot h_w \cdot t_w \cdot (h_1 + t_{tf} + 0.5 \cdot h_w) \\
& + f_{s,lim} \cdot b_{bf} \cdot t_{bf} \cdot (h_1 + h_2 + 0.5 \cdot t_{bf}) - 0.5 \cdot f_{c,lim} \cdot b_{eff} \cdot h_1^2 - f_{s,lim} \cdot b_{tf} \cdot t_{tf,t} \cdot (h_1 + 0.5 \cdot t_{tf,t})
\end{aligned} \quad (8.31)$$

NEUTRAL AXIS IN THE WEB

The neutral axis is in the web in the case of full-rigid shear connection (see Figure 8.22) when the ratio of the magnitudes of the sum of the normal forces of the timber and the top flange in compression to the sum of the normal forces in the web and the bottom flange in tension is smaller than 1 as shown in Equation 8.32.

$$\frac{f_{c,lim} \cdot A_1 + f_{s,lim} \cdot b_{tf} \cdot t_{tf}}{f_{s,lim} \cdot (A_2 - b_{tf} \cdot t_{tf})} < 1 \quad (8.32)$$

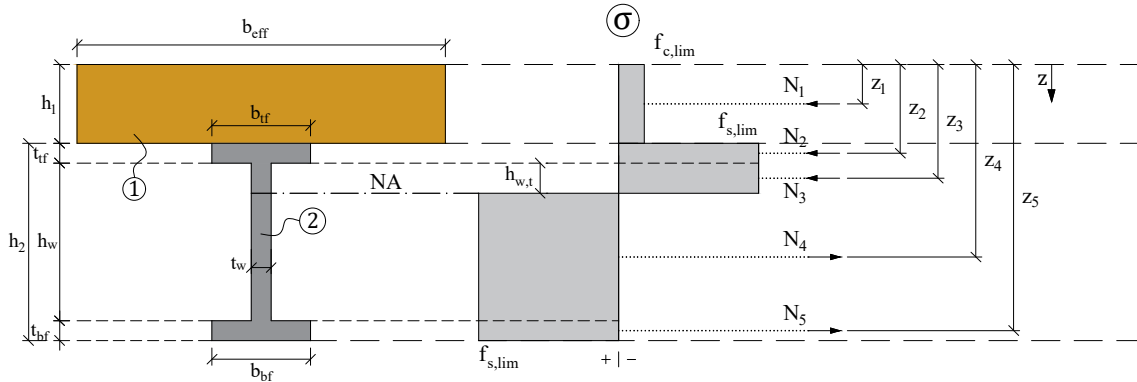


Figure 8.22: Stress distribution for full-rigid shear connection with neutral axis in the web of the steel beam.

The position of the neutral axis is defined in this case by the height of the portion of the web in compression ($h_{w,t}$) as shown in Figure 8.22. The sum of the normal forces (N_i) must be equal to zero at the equilibrium state (see Equation 8.33). The normal forces N_i are calculated according to Equations 8.34 to 8.38.

$$\sum_{i=1}^n N_i = N_1 + N_2 + N_3 + N_4 + N_5 = 0 \quad (8.33)$$

$$N_1 = -f_{c,lim} \cdot b_{eff} \cdot h_1 \quad (8.34)$$

$$N_2 = -f_{s,lim} \cdot b_{tf} \cdot t_{tf} \quad (8.35)$$

$$N_3 = -f_{s,lim} \cdot h_{w,t} \cdot t_w \quad (8.36)$$

$$N_4 = f_{s,lim} \cdot (h_w - h_{w,t}) \cdot t_w \quad (8.37)$$

$$N_5 = f_{s,lim} \cdot b_{bf} \cdot t_{bf} \quad (8.38)$$

When Equations 8.34 to 8.38, are substituted in Equation 8.33 and it is solved for $h_{w,t}$, the result is Equation 8.39.

$$h_{w,t} = \frac{b_{bf} \cdot t_{bf} - b_{tf} \cdot t_{tf}}{2 \cdot t_w} - \frac{f_{c,lim} \cdot b_{eff} \cdot h_1}{2 \cdot f_{s,lim} \cdot t_w} + 0.5 \cdot h_w \quad (8.39)$$

The moment resistance (M_R) of the section is given by the product of the normal forces N_i and the respective lever arms z_i , considering as reference the top fibre of the timber slab (see Equation 8.40). Therefore, the moment resistance M_R is estimated according to Equation 8.41.

$$M_R = \sum_{i=1}^n N_i \cdot z_i \quad (8.40)$$

$$M_R = f_{s,lim} \cdot t_w \cdot (h_w - h_{w,t}) \cdot (h_1 + t_{tf} + 0.5 \cdot h_w + 0.5 \cdot h_{w,t}) + f_{s,lim} \cdot b_{bf} \cdot t_{bf} \cdot (h_1 + h_2 - 0.5 \cdot t_{bf}) - 0.5 \cdot f_{c,lim} \cdot b_{eff} \cdot h_1^2 - f_{s,lim} \cdot b_{tf} \cdot t_{tf} \cdot (h_1 + 0.5 \cdot t_{tf}) - f_{s,lim} \cdot h_{w,t} \cdot t_w \cdot (h_1 + t_{tf} + 0.5 \cdot h_{w,t}) \quad (8.41)$$

8.11.5. BENDING CAPACITY OF STC BEAMS WITH NO SHEAR CONNECTION

In the case of no shear connection at all between the timber slab and the steel beam it is assumed that no vertical separation of the element occurs, meaning that there is no uplift of the timber slab. Additionally, it is assumed that timber fails upon reaching its proportional limit and at this point, the steel beam is fully plasticised. Figure 8.23 shows the stress distribution of the cross-section with this assumptions.

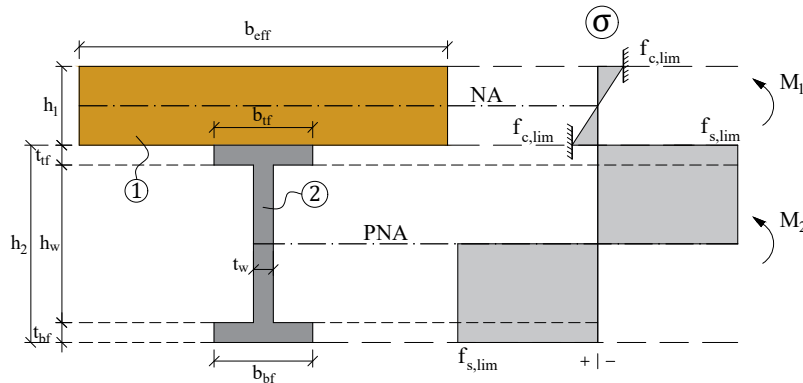


Figure 8.23: Stress distribution for the case of no shear connection.

Under these assumptions, the calculation of the bending capacity is straightforward, it is the sum of the bending capacity of the timber slab (M_1) and the bending capacity of the steel

beam (M_2) (see Equation 8.42).

$$M_R = M_1 + M_2 \quad (8.42)$$

The bending capacity of the timber slab M_1 is calculated as the product of the strength limit of timber ($f_{c,lim}$) and the elastic section modulus of the timber slab ($W_{1,el}$) as shown in Equation 8.43.

$$M_1 = f_{c,lim} \cdot W_{1,el} \quad (8.43)$$

The bending capacity of the steel beam (M_2) is estimated as the product of the strength limit of steel ($f_{s,lim}$) and the plastic section modulus of the steel beam ($W_{2,pl}$) as shown in Equation 8.44.

$$M_2 = f_{s,lim} \cdot W_{2,pl} \quad (8.44)$$

Therefore, the moment resistance of a steel-timber cross-section with no shear connection at all is calculated according to Equation 8.42.

$$M_R = f_{c,lim} \cdot W_{1,el} + f_{s,lim} \cdot W_{2,pl} \quad (8.45)$$

8

8.11.6. BENDING CAPACITY OF STC BEAMS WITH PARTIAL SHEAR CONNECTION

GENERAL

In a composite beam, there is partial shear connection when the shear connectors cannot transfer the forces to achieve full shear connection. This means that the resultant normal force in the timber slab (N_{timber}) at the critical section is smaller than the normal force that can be developed in the case of full-rigid shear connection ($N_{timber,\eta=1}$) (see Equation 8.46). According to the definition of degree of shear connection provided in Chapter 8.6 in Equation 8.4, the resultant normal force in N_{timber} is directly proportional to the degree of shear connection (η) and the the normal force $N_{timber,\eta=1}$, as shown in Equation 8.47.

$$|N_{timber}| < |N_{timber,\eta=1}| \quad (8.46)$$

$$N_{timber} = \eta \cdot N_{timber,\eta=1} \quad (8.47)$$

The resultant normal force in the timber slab in the critical section N_{timber} is equal to the sum of shear forces P_i transferred by the n shear connectors installed within the shear length (see Equation 8.48).

$$N_{timber} = \sum_{i=1}^n P_i \quad (8.48)$$

When the connectors developed in this research project are idealised as rigid-ductile (i.e.

perfectly-plastic), the normal force N_{timber} is estimated as the product of the number of connectors (n) and their effective shear resistance ($P_{R, eff}$) (see Equation 8.49).

$$N_{timber} = n \cdot P_{R, eff} \quad (8.49)$$

NEUTRAL AXIS OF THE STEEL BEAM IN THE TOP FLANGE

In the case of partial shear connection there are two neutral axes: one in the timber slab and one in the steel beam, the stress distribution is as shown in Figure 8.24. It is assumed that the stress distribution in the timber slab remains within its elastic range and the steel beam is fully plasticised. The neutral axis in the steel beam is located in the top flange when the ratio of the sum of the normal force in the timber slab N_{timber} and the normal force in the hypothetical case of the top flange being fully compressed to the sum of the normal forces in the web and bottom flange of the beam when they are in tension is greater than 1 (see Equation 8.50).

$$\frac{|N_{timber}| + f_{s,lim} \cdot b_{tf} \cdot t_{tf}}{f_{s,lim}(A_2 - b_{tf} \cdot t_{tf})} > 1 \quad (8.50)$$

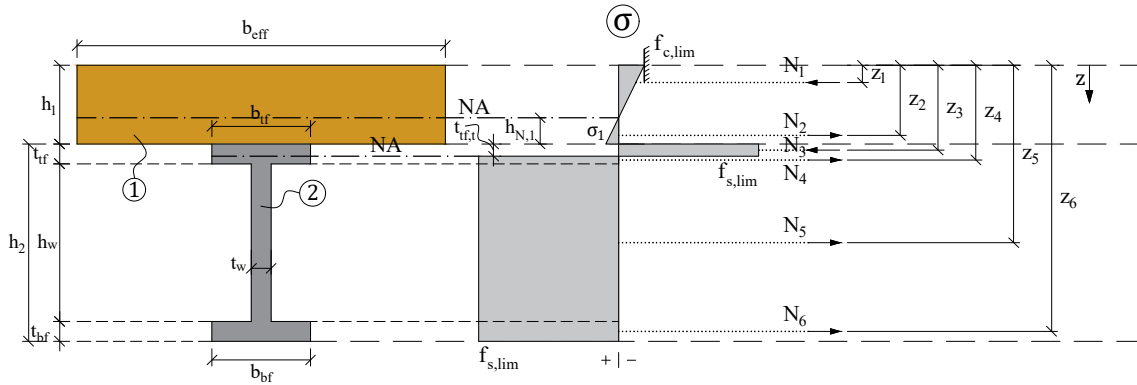


Figure 8.24: Stress distribution for partial shear connection with neutral axis in the top flange of the steel beam.

In this system the unknowns are the stress at the bottom fibre of the timber slab (σ_1), and the positions of the neutral axes, which are defined by their distance from the bottom fibre of the timber slab (i.e. $h_{N,1}$ and $t_{tf,t}$). The relationship between stresses in the top and bottom fibres of the timber slab and the height of the stresses in compression and tension can be established by triangles similarities according to Equation 8.51. Thus, the stress in the bottom fibre of the timber slab (σ_1) can be expressed in terms of the limiting stress in timber, the position of the neutral axis and the height of the timber slab as shown in Equation 8.52.

$$\frac{\sigma_1}{f_{c,lim}} = \frac{h_{N,1}}{h_1 - h_{N,1}} \quad (8.51)$$

$$\sigma_1 = \frac{f_{c,lim} \cdot h_{N,1}}{h_1 - h_{N,1}} \quad (8.52)$$

The resultant normal force in the timber slab N_{timber} is equal to the sum of the normal forces in compression N_1 and tension N_2 , as shown in Equation 8.53.

$$N_{timber} = N_1 + N_2 \quad (8.53)$$

Where the normal forces N_1 and N_2 are calculated according to Equations 8.54 and 8.55:

$$N_1 = -0.5 \cdot f_{c,lim} \cdot b_{eff} \cdot (h_1 - h_{N,1}) \quad (8.54)$$

$$N_2 = 0.5 \cdot \sigma_1 \cdot b_{eff} \cdot h_{N,1} = \frac{0.5 \cdot f_{c,lim} \cdot b_{eff} \cdot h_{N,1}^2}{h_1 - h_{N,1}} \quad (8.55)$$

Substituting Equations 8.54 and 8.55 in Equation 8.53 and solving for $h_{N,1}$ gives Equation 8.56:

$$h_{N,1} = \frac{h_1 \cdot (f_{c,lim} \cdot b_{eff} \cdot h_1 - 2 \cdot N_{timber})}{2 \cdot (f_{c,lim} \cdot b_{eff} \cdot h_1 - N_{timber})} \quad (8.56)$$

The resultant normal forces in the timber slab (N_{timber}) and in the steel beam (N_{steel}) have the same magnitude (see Equation 8.57).

$$-N_{timber} = N_{steel} \quad (8.57)$$

The resultant normal force N_{steel} is the sum of the forces N_3 to N_6 (see Equation 8.58). Where the normal forces N_3 to N_6 are calculated as shown in Equations 8.59 to 8.62.

$$N_{steel} = -N_{timber} = N_3 + N_4 + N_5 + N_6 \quad (8.58)$$

$$N_3 = -f_{s,lim} \cdot b_{tf} \cdot t_{tf,t} \quad (8.59)$$

$$N_4 = f_{s,lim} \cdot b_{tf} \cdot (t_{tf} - t_{tf,t}) \quad (8.60)$$

$$N_5 = f_{s,lim} \cdot h_w \cdot t_w \quad (8.61)$$

$$N_6 = f_{s,lim} \cdot b_{bf} \cdot t_{bf} \quad (8.62)$$

When substituting the values of Equations 8.59 to 8.62 in Equation 8.58, and solving for the thickness of the top part of the flange in compression ($t_{tf,t}$) Equation 8.63 is obtained.

$$t_{tf,t} = \frac{A_2}{2 \cdot b_{tf}} + \frac{N_{timber}}{2 \cdot f_{s,lim} \cdot b_{tf}} \quad (8.63)$$

Finally, the moment resistance of the section (M_R) is calculated as the sum of the product of the normal forces and their respective lever arms (z_i) (see Equations 8.64 and 8.65).

$$M_R = \sum_{i=1}^n N_i \cdot z_i \quad (8.64)$$

$$M_R = -\frac{0.5 \cdot f_{c,lim} \cdot b_{eff} \cdot (h_1 - d_{N,1})^2}{3} + 0.5 \cdot \sigma_1 \cdot b_{eff} \cdot d_{N,1} \cdot \left(h_1 - \frac{h_{N,1}}{3} \right) \\ - f_{s,lim} \cdot b_{tf} \cdot t_{tf,t} \cdot (h_1 + 0.5 \cdot t_{tf,t}) + f_{s,lim} \cdot b_{tf} \cdot (t_{tf} - t_{tf,t}) \cdot (h_1 + 0.5 \cdot t_{tf} + 0.5 \cdot t_{tf,t}) \\ + f_{s,lim} \cdot h_w \cdot t_w \cdot (h_1 + t_{tf} + 0.5 \cdot h_w) + f_{s,lim} \cdot b_{bf} \cdot t_{bf} \cdot (h_1 + h_2 - 0.5 \cdot t_{bf}) \quad (8.65)$$

NEUTRAL AXIS OF THE STEEL BEAM IN THE WEB

The neutral axis is in the web of the steel beam when the ratio of the sum of the normal force in the timber slab N_{timber} and the normal force in the hypothetical case of the top flange being fully compressed to the sum of the normal forces in the web and bottom flange of the beam when they are in tension is smaller than 1 (see Equation 8.66).

$$\frac{|N_{timber}| + f_{s,lim} \cdot b_{tf} \cdot t_{tf}}{f_{s,lim} (A_2 - b_{tf} \cdot t_{tf})} < 1 \quad (8.66)$$

The stress distribution for this case is shown in Figure 8.25. The unknowns of the system are the stress at the bottom fibre of the timber slab (σ_1), and the positions of the neutral axes. The position of the neutral axis in the timber is defined by its distance from the bottom fibre of the slab ($h_{N,1}$), and the position of the neutral axis in web is defined by its distance from the bottom fibre of the top flange ($h_{w,t}$). The relationships between the stresses of the top and the bottom fibre in the timber slab and the height of the stresses in compression and tension in timber are similar to those established for the case of neutral axis in the top flange. Therefore, Equations 8.51 to 8.56 apply for this case, the stress σ_1 can be calculated according to Equation 8.52, and the position of the neutral axis in the timber slab $h_{N,1}$ can be determined according to Equation 8.56.

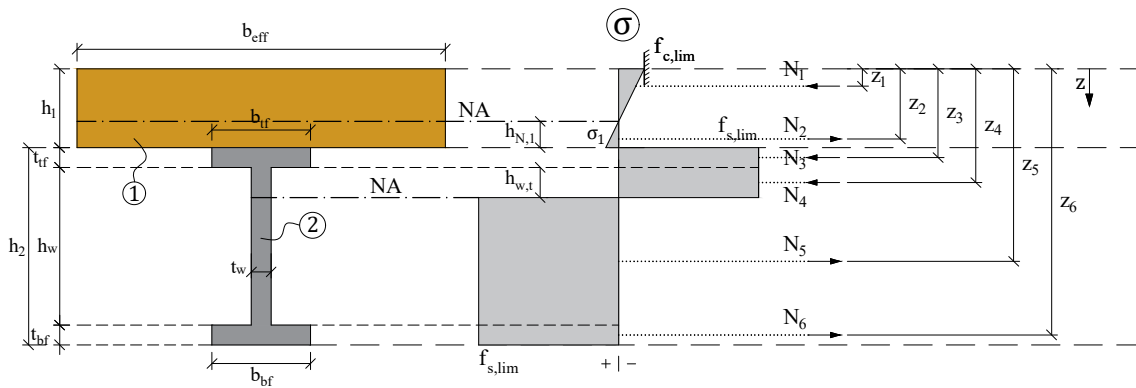


Figure 8.25: Stress distribution for partial shear connection with neutral axis in the web of the steel beam.

The resultant normal forces in the timber slab (N_{timber}) and in the steel beam (N_{steel}) have the same magnitude (see Equation 8.67).

$$-N_{timber} = N_{steel} \quad (8.67)$$

The resultant normal force N_{steel} is the sum of the forces N_3 to N_6 (see Equation 8.68). Where the normal forces N_3 to N_6 are calculated as shown in Equations 8.69 to 8.72.

$$N_{steel} = -N_{timber} = N_3 + N_4 + N_5 + N_6 \quad (8.68)$$

$$N_3 = -f_{s,lim} \cdot b_{tf} \cdot t_{tf} \quad (8.69)$$

$$N_4 = -f_{s,lim} \cdot h_{w,t} \cdot t_w \quad (8.70)$$

$$N_5 = f_{s,lim} \cdot (h_w - h_{w,t}) \cdot t_w \quad (8.71)$$

$$N_6 = f_{s,lim} \cdot b_{bf} \cdot t_{bf} \quad (8.72)$$

When substituting the values of Equations 8.69 to 8.72 in Equation 8.68, and solving for the height of the top part of the web in compression ($h_{w,t}$) Equation 8.73 is obtained.

$$h_{w,t} = 0.5 \cdot h_w - \frac{b_{tf} \cdot t_{tf} + b_{bf} \cdot t_{bf}}{2 \cdot t_w} + \frac{N_{timber}}{2 \cdot f_{s,lim} \cdot t_w} \quad (8.73)$$

Finally, the moment resistance of the section (M_R) is calculated as the sum of the product of the normal forces and their respective lever arms (z_i) (see Equations 8.74 and 8.75).

$$M_R = \sum_{i=1}^n N_i \cdot z_i \quad (8.74)$$

$$\begin{aligned} M_R = & -\frac{0.5 \cdot f_{c,lim} \cdot b_{eff} \cdot (h_1 - d_{N,1})^2}{3} + 0.5 \cdot \sigma_1 \cdot b_{eff} \cdot d_{N,1} \cdot \left(h_1 - \frac{h_{N,1}}{3} \right) \\ & - f_{s,lim} \cdot b_{tf} \cdot t_{tf} \cdot (h_1 + 0.5 \cdot t_{tf}) - f_{s,lim} \cdot h_{w,t} \cdot t_w \cdot (h_1 + t_{tf} + 0.5 \cdot h_{w,t}) \\ & + f_{s,lim} \cdot (h_w - h_{w,t}) \cdot t_w \cdot (h_1 + t_{tf} + 0.5 \cdot h_w + 0.5 \cdot h_{w,t}) + f_{s,lim} \cdot b_{bf} \cdot t_{bf} \cdot (h_1 + h_2 - 0.5 \cdot t_{bf}) \end{aligned} \quad (8.75)$$

8.11.7. BENDING CAPACITY OF AN STC CROSS-SECTION AT A GAP

GENERAL

When there are transversal discontinuities in the slab (e.g. transversal gaps filled with mortar) of STC beams, it is important to check the capacity of the cross-section at those locations. Due to the discontinuity, only compressive forces are transferred, which could reduce the capacity of the cross-section. Therefore, the sections at the gaps are critical sections that must be checked. For analyses at ultimate limit state, it is proposed to idealise the timber material as

perfectly-plastic in compression while neglecting tension. Two cases are considered depending on the position of the neutral axis of the steel beam: (i) neutral axis in the top flange, (ii) neutral axis in the web, and (iii) one neutral axis in the timber slab.

NEUTRAL AXIS OF THE STEEL BEAM IN THE TOP FLANGE

Figure 8.26 shows the stress distribution of an STC cross-section at a gap, where tensile forces in the timber are neglected. The normal force in the timber slab N_{timber} is equal to the normal force N_1 , this force must be known and is calculated as the sum of the shear forces of the connectors placed from the nearest support up to the section at the gap being analysed. The neutral axis is in the top flange when the ratio of the sum of the normal force in the timber and the normal force of the top flange, when fully compressed, to the sum of the normal tensile forces of the web and the bottom flange is greater than 1 (see Equation 8.76)

$$\frac{|N_{timber}| + f_{s,lim} \cdot b_{tf} \cdot t_{tf}}{f_{s,lim} \cdot (A_2 - b_{tf} \cdot t_{tf})} > 1 \quad (8.76)$$

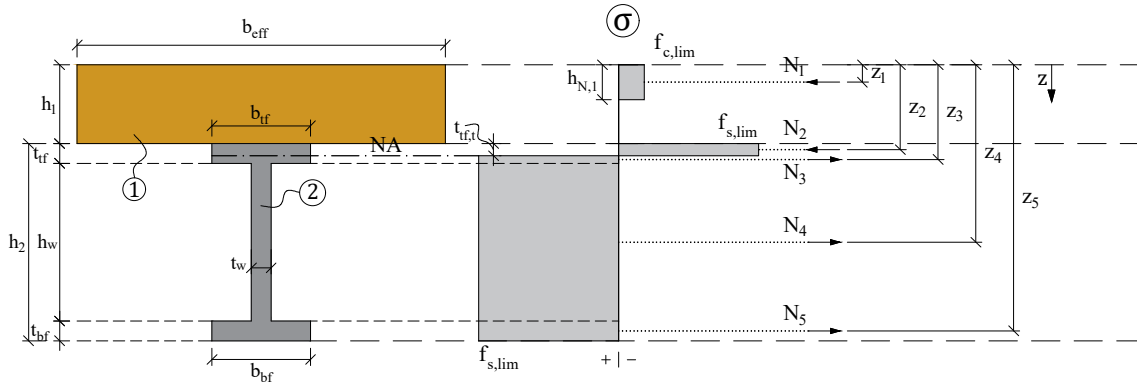


Figure 8.26: Stress distribution for a cross-section at a gap with neutral axis in the top flange of the steel beam.

The unknowns of this system are the height of the compression zones in the timber ($h_{N,1}$) and in the top flange of the beam ($t_{tf,t}$). The compressive force in the timber slab is a known value that can be estimated according to Equation 8.77, solving this equation for $h_{N,1}$ gives Equation 8.78.

$$N_{timber} = -f_{c,lim} \cdot b_{eff} \cdot h_{N,1} \quad (8.77)$$

$$h_{N,1} = -\frac{N_{timber}}{f_{c,lim} \cdot b_{eff}} \quad (8.78)$$

The resultant normal forces in the timber slab (N_{timber}) and in the steel beam (N_{steel}) have the same magnitude, and the normal force in the steel beam can be calculated as shown in Equation 8.79, solving this equation for $t_{tf,t}$, gives Equation 8.80.

$$N_{steel} = -N_{timber} = f_{s,lim} \cdot (A_2 - b_{tf} \cdot t_{tf,t}) \quad (8.79)$$

$$t_{tf,t} = \frac{N_{timber} + f_{s,lim} \cdot A_2}{f_{s,lim} \cdot b_{tf}} \quad (8.80)$$

The moment resistance of this section is given by the sum of the product of the normal forces N_i and the lever arms z_i (see Equation 8.81). The normal forces N_i can be calculated according to Equations 8.82 to 8.86. Thus, substituting Equations 8.82 to 8.86 in Equation 8.81 gives Equation 8.87.

$$M_R = \sum_{i=1}^n N_i \cdot z_i \quad (8.81)$$

$$N_1 = N_{timber} = -f_{c,lim} \cdot b_{tf} \cdot h_{N,1} \quad (8.82)$$

$$N_2 = -f_{s,lim} \cdot b_{eff} \cdot t_{tf,t} \quad (8.83)$$

$$N_3 = f_{s,lim} \cdot b_{tf} \cdot (t_{tf} - t_{tf,t}) \quad (8.84)$$

$$N_4 = f_{s,lim} \cdot h_w \cdot t_w \quad (8.85)$$

$$N_5 = f_{s,lim} \cdot b_{bf} \cdot t_{bf} \quad (8.86)$$

$$\begin{aligned} M_R = & -0.5 \cdot f_{c,lim} \cdot b_{eff} \cdot h_{N,1}^2 - f_{s,lim} \cdot b_{tf} \cdot t_{tf,t} \cdot (h_1 + 0.5 \cdot t_{tf,t}) \\ & + f_{s,lim} \cdot b_{tf} \cdot (t_{tf} - t_{tf,t}) \cdot (h_1 + 0.5 \cdot t_{tf} + 0.5 \cdot t_{tf,t}) + f_{s,lim} \cdot h_w \cdot t_w \cdot (h_1 + t_{tf} + 0.5 \cdot h_w) \\ & + f_{s,lim} \cdot b_{bf} \cdot t_{bf} \cdot (h_1 + h_2 - 0.5 \cdot t_{bf}) \end{aligned} \quad (8.87)$$

NEUTRAL AXIS OF THE STEEL BEAM IN THE WEB

Figure 8.27 shows the stress distribution of an STC cross-section at a gap with the neutral axis in the web of the steel beam. The neutral axis is located in the web when the ratio of the sum of the normal force in the timber and the normal force of the top flange, when fully compressed, to the sum of the normal tensile forces of the web and the bottom flange is smaller than 1 (see Equation 8.88).

$$\frac{|N_{timber}| + f_{s,lim} \cdot b_{tf} \cdot t_{tf}}{f_{s,lim} \cdot (A_2 - b_{tf} \cdot t_{tf})} < 1 \quad (8.88)$$

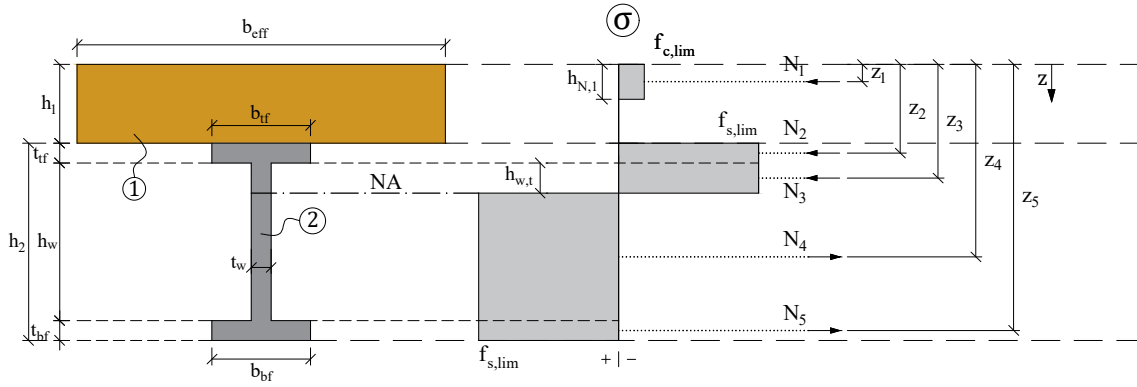


Figure 8.27: Stress distribution in a cross-section at a gap when the neutral axis is in the web of the steel beam.

Similar to the case when neutral axis is in the top flange, the resultant normal force in the timber slab (N_{timber}) is a known value. The unknowns of the system are the height of the compression zones in the timber slab ($h_{N,1}$) and in the web of the beam ($h_{w,t}$). The height of the slab in compression $h_{N,1}$, can be calculated according to Equation 8.78.

The resultant normal forces in the timber slab (N_{timber}) and in the steel beam (N_{steel}) have the same magnitude, and the normal force in the steel beam can be calculated as shown in Equation 8.89, solving this equation for $h_{w,t}$, gives Equation 8.90.

$$N_{steel} = -N_{timber} = f_{s,lim} \cdot (A_2 - b_{tf} \cdot t_{tf} - h_{w,t} \cdot t_w) \quad (8.89)$$

$$h_{w,t} = \frac{N_{timber}}{f_{s,lim} \cdot t_w} + \frac{A_2 - b_{tf} \cdot t_{tf}}{t_w} \quad (8.90)$$

The moment resistance of the cross-section is given by the sum of the product of the normal forces N_i and the respective lever arms z_i (see Equation 8.91). The normal forces N_i can be calculated according to Equations 8.92 to 8.96. Thus, substituting Equations 8.92 to 8.96 in Equation 8.91 gives Equation 8.97.

$$M_R = \sum_{i=1}^n N_i \cdot z_i \quad (8.91)$$

$$N_1 = N_{timber} = -f_{c,lim} \cdot b_{eff} \cdot h_{N,1} \quad (8.92)$$

$$N_2 = -f_{s,lim} \cdot b_{tf} \cdot t_{tf} \quad (8.93)$$

$$N_3 = -f_{s,lim} \cdot h_{w,t} \cdot t_w \quad (8.94)$$

$$N_4 = f_{s,lim} \cdot (h_w - h_{w,t}) \cdot t_w \quad (8.95)$$

$$N_5 = f_{s,lim} \cdot b_{bf} \cdot t_{bf} \quad (8.96)$$

$$\begin{aligned} M_R = & -0.5 \cdot f_{c,lim} \cdot b_{eff} \cdot h_{N,1}^2 - f_{s,lim} \cdot b_{tf} \cdot t_{tf} \cdot (h_1 + 0.5 \cdot t_{tf}) \\ & - f_{s,lim} \cdot h_{w,t} \cdot t_w \cdot (h_1 + t_{tf} + 0.5 \cdot h_{w,t}) + f_{s,lim} \cdot (h_w - h_{w,t}) \cdot t_w \cdot (h_1 + t_{tf} + 0.5 \cdot h_w + 0.5 \cdot h_{w,t}) \\ & + f_{s,lim} \cdot b_{bf} \cdot t_{bf} \cdot (h_1 + h_2 - 0.5 \cdot t_{bf}) \end{aligned} \quad (8.97)$$

NEUTRAL AXIS IN THE TIMBER SLAB

When the sum of the forces transferred by the shear connectors placed within the gap section and the nearest support are equal or larger than the normal force that can be developed in the steel section when it is fully in tension, then the maximum compressive normal force that can be developed in the slab is equal to the full tensile capacity of the steel section (see Equation 8.98 and 8.99).

$$-N_{timber} = N_{steel} \quad (8.98)$$

$$f_{c,lim} \cdot b_{eff} \cdot h_{N,1} = f_{s,lim} \cdot A_2 \quad (8.99)$$

The stress distribution in this case is illustrated in Figure 8.28. It is shown, that the steel section is fully in tension while only one portion of the timber slab is compressed.

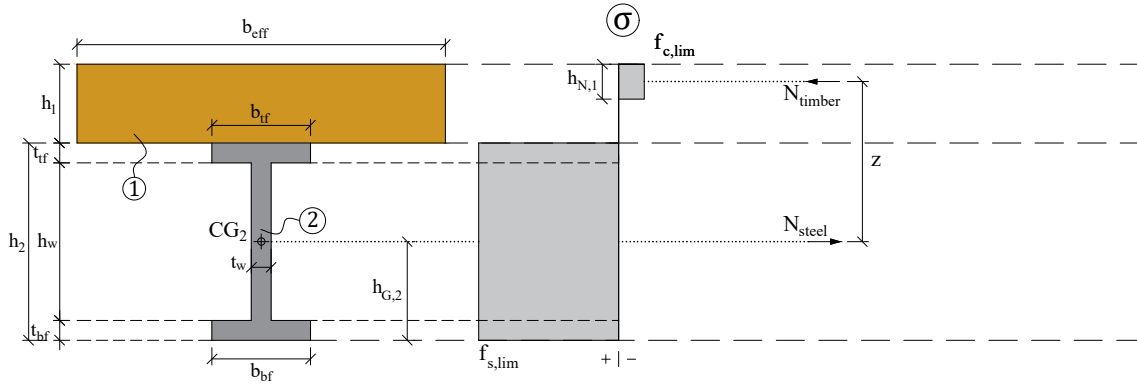


Figure 8.28: Stress distribution in a cross-section at a gap with one neutral axis in the timber slab.

The unknown of this system is the height of the compression zone in the timber slab ($h_{N,1}$), which can be obtained by solving Equation 8.99 for $h_{N,1}$ (see Equation 8.100).

$$h_{N,1} = \frac{f_{s,lim} \cdot A_2}{f_{c,lim} \cdot h_{N,1}} \quad (8.100)$$

The moment resistance of this section is calculated as the product of the resultant normal force and the lever arm (see Equation 8.101).

$$M_R = N_{steel} \cdot z = f_{s,lim} \cdot A_1 \cdot (h_1 - 0.5 \cdot h_{N,1} + h_2 - h_{G,2}) \quad (8.101)$$

8.11.8. COMPARISON OF RESULTS

The comparison of the Moment vs. midspan deflection curve and the moment resistance of the cross-section at midspan for the two full-scale beam tests is shown in Figure 8.29a for BT-1 and in Figure 8.29b for BT-2. The bending capacities were obtained considering the effective width b_{eff} of the timber slab as $L/5.5$ and the effective shear resistance $P_{R, eff}$ of the connectors as 73.9 kN for SCT-1 and 88.7 kN for SCT-3, which were estimated as established in Section 8.8 assuming an end-slip of 6 mm to define the cosine slip function $s(x)$.

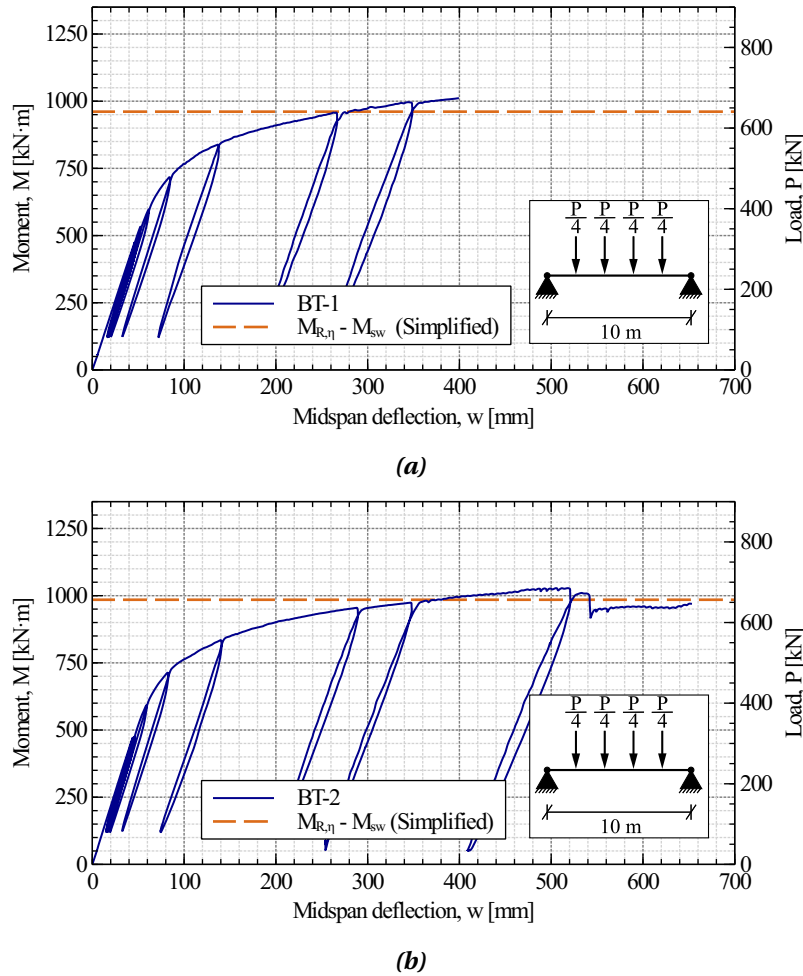


Figure 8.29: Moment vs. midspan deflection curve and analytically estimated moment resistance values for: (a) BT-1; and (b) BT-2.

The degree of shear connection (η) was 0.69 for BT-1 and 0.85 for BT-2. Additionally, the moment resistance of the section was estimated for different degrees of shear connection (η) from 0 to 1, in steps of 0.05 (i.e. 0.0, 0.05, 0.10, ..., 0.95, 1.0), with the two proposed analytical procedures, the strain-based procedure and the simplified analytical procedure. Figure 8.30 shows a comparison of the M vs. η curves obtained with the two approaches. The root mean

square error (RMSE) was calculated to assess the accuracy of the simplified method to obtain the results given by the strain-based procedure. An RMSE of 1.4 was obtained, which indicates that the deviation between the results obtained with the strain-based procedure and the simplified analytical procedure is very small. These results indicate that the proposed simplified method is an effective straightforward analytical approach that gives a good estimation of the ultimate bending capacity of STC beams.

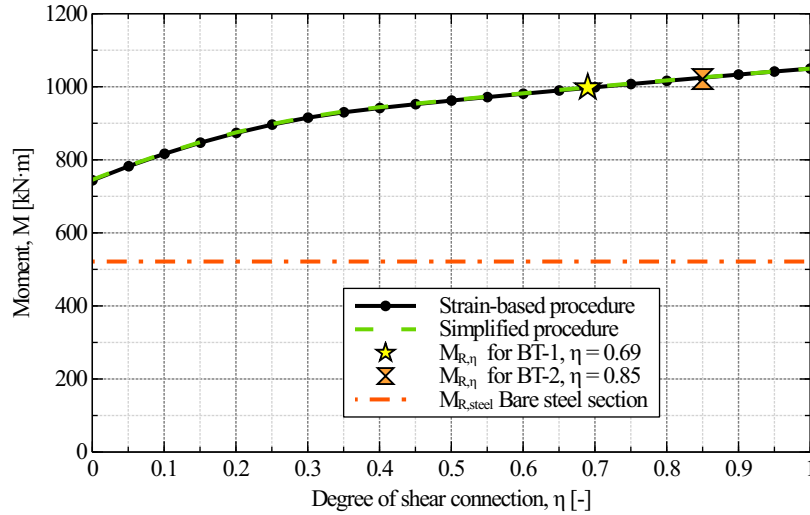


Figure 8.30: Comparison of the M vs. η curve obtained with the the strain-based procedure and the simplified analytical procedure for the cross-section of the beams tested in the full-scale tests.

8

8.12. PROCEDURE TO ESTIMATE THE BENDING CAPACITY OF STC BEAMS IN THE ELASTIC RANGE

8.12.1. GENERAL

In Chapter 6 in Section 6.8.7 it was demonstrated that the γ -method established in Eurocode 5 [69] can be used to estimate the effective bending stiffness $((EI)_{ef})$ of the STC beams. Thus, it is also feasible to calculate the stresses in the cross-section and the bending capacity of STC beams with this approach when the materials remain within the elastic range. Figure 8.31 shows the stress distribution in the cross-section and the parameters considered.

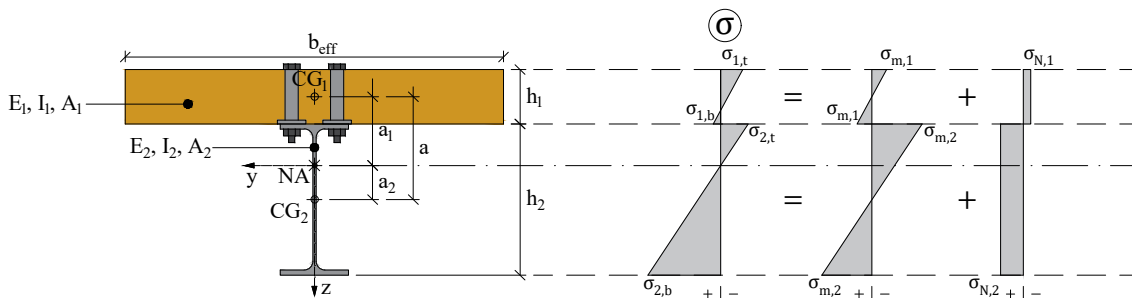


Figure 8.31: Stress distribution in a steel-timber cross-section when the stresses remain within the elastic range of the timber slab and the steel beam.

8.12.2. STRESSES IN THE CROSS-SECTION IN THE ELASTIC RANGE

With the γ -method [69] it is possible to estimate the stresses in a cross-section while considering the effects of composite action. The stress distribution in the cross-section consists of two components: bending stresses ($\sigma_{m,i}$) and normal stresses ($\sigma_{N,i}$). For a given moment (M) that exerts stresses within the elastic range of the timber slab and the steel beam, these components of the stresses are estimated according to Equations 8.102 and 8.103, where the parameters γ_i and a_i are estimated according to Equations 6.8 to 6.10.

$$\sigma_{m,i} = \frac{0.5 \cdot E_i \cdot h_i \cdot M}{(EI)_{ef}} \quad (8.102)$$

$$\sigma_{N,i} = \frac{\gamma_i \cdot E_i \cdot a_i \cdot M}{(EI)_{ef}} \quad (8.103)$$

In the case of sagging bending, due to the composite action, in the timber slab the compressive bending stresses are increased by the compressive normal stresses while the bending tensile stresses are reduced in the same proportion. In the steel section occurs the opposite, the bending stresses in compression are reduced by the tensile normal stresses while the bending tensile stresses are increased in the same proportion. Therefore, the stresses in the top and bottom fibres of the timber are estimated according to Equations 8.104 and 8.105 and the stresses in the steel beam are calculated according to Equations 8.106 and 8.107.

$$\sigma_{1,t} = -\sigma_{m,1} - \sigma_{N,1} = \frac{M \cdot E_1}{(EI)_{ef}} \cdot (-0.5 \cdot h_1 - \gamma_1 \cdot a_1) \quad (8.104)$$

$$\sigma_{1,b} = \sigma_{m,1} - \sigma_{N,1} = \frac{M \cdot E_1}{(EI)_{ef}} \cdot (0.5 \cdot h_1 - \gamma_1 \cdot a_1) \quad (8.105)$$

$$\sigma_{2,t} = -\sigma_{m,2} + \sigma_{N,2} = \frac{M \cdot E_2}{(EI)_{ef}} \cdot (-0.5 \cdot h_2 + \gamma_2 \cdot a_2) \quad (8.106)$$

$$\sigma_{2,b} = \sigma_{m,2} + \sigma_{N,2} = \frac{M \cdot E_2}{(EI)_{ef}} \cdot (0.5 \cdot h_2 + \gamma_2 \cdot a_2) \quad (8.107)$$

8.12.3. BENDING CAPACITY IN THE ELASTIC RANGE

The elastic bending capacity of STC beams is reached when the timber slab or the steel beam reach their proportional limit. Since the experimental and numerical observations have shown that the timber remains in the elastic range up to the ultimate limit state, it is assumed that steel reaches its proportional limit while timber is still elastic and only this case is considered in this study.

In the case of sagging bending of an STC beam, the most stressed fibre of the steel beam is at the bottom of the section in the bottom flange. The target is to find the moment resistance ($M_{R,el}$) of the STC beam for the state in which the stress at the bottom fibre of the steel section ($\sigma_{2,b}$) is equal to the yielding strength of the steel (f_y). Equation 8.107 relates the bending

moment (M) and the stress at the bottom fibre of the steel beam ($\sigma_{2,b}$). Therefore, the moment resistance can be determined from this equation when solving for M (see Equation 8.108).

$$M = \frac{\sigma_{2,b} \cdot (EI)_{ef}}{E_2 \cdot (0.5 \cdot h_2 + \gamma_2 \cdot a_2)} \quad (8.108)$$

After substituting M with $M_{R,el}$ and $\sigma_{2,b}$ with f_y in Equation 8.107, it becomes Equation 8.109. Thus, the elastic moment resistance $M_{R,el}$ is estimated according to Equation 8.109.

$$M_{R,el} = \frac{f_y \cdot (EI)_{ef}}{E_2 \cdot (0.5 \cdot h_2 + \gamma_2 \cdot a_2)} \quad (8.109)$$

8.12.4. COMPARISON OF RESULTS

Figure 8.32 shows the comparison of the moment vs. midspan deflection curves obtained in the full-scale beam tests BT-1 and BT-2, and the elastic moment resistance obtained with the proposed procedure.

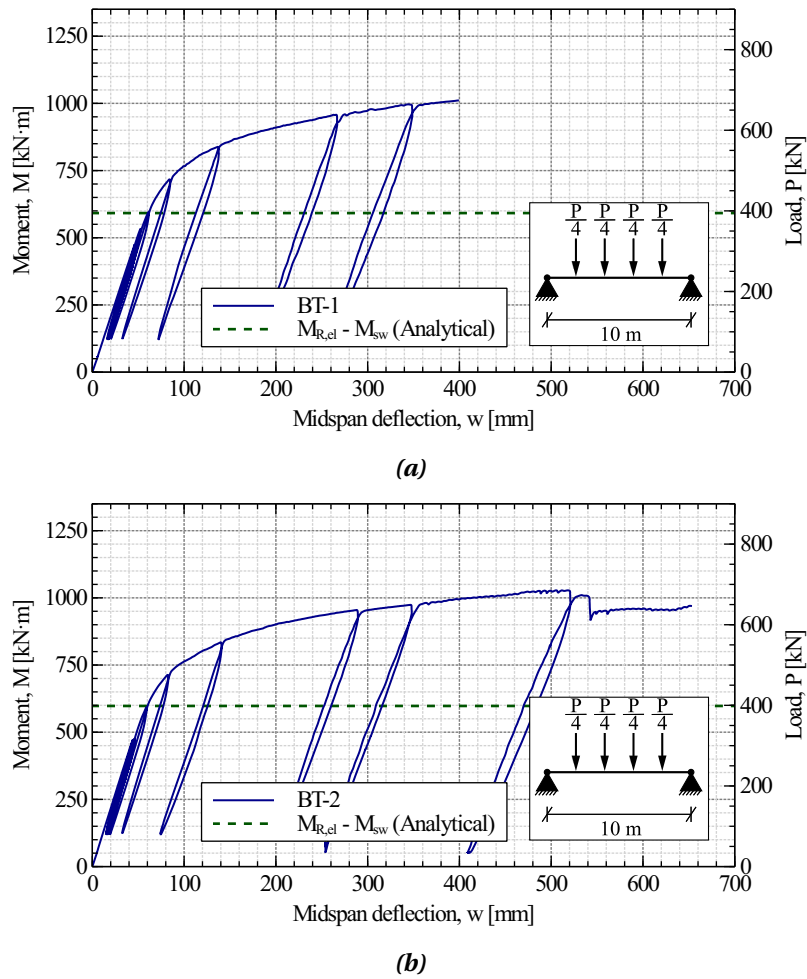


Figure 8.32: Moment vs. midspan deflection curve and analytically estimated elastic moment resistance values for: (a) BT-1; and (b) BT-2.

8.13. SUMMARY OF PROPOSED ANALYTICAL PROCEDURES AND THEIR EFFECTIVENESS

8.13.1. PROPOSED ANALYTICAL PROCEDURES

In this investigation analytical procedures have been proposed to predict parameters of the STC beam that are relevant for design at serviceability limit state (SLS) and at ultimate limit state (ULS). These parameters and the proposed procedures are summarized below:

- **Ultimate bending capacity (strain-based procedure):** Strain-based procedures are robust analytical tools that allow to predict the moment resistance of cross-sections considering non-linear material constitutive laws and the strain distributions for full shear connection, partial shear connection and no shear connection cases. This procedure was discussed in Section 8.3 and 8.9.
- **Ultimate bending capacity (simplified procedure):** It has been demonstrated that with certain assumptions for the materials it is possible to simplify the calculation of the moment resistance of STC cross-sections for different shear connection cases. Based on results of this study, it is proposed to consider that (i) at ULS the steel beam is fully plasticised and (ii) the capacity of the STC beam is reached when the stresses in the timber reach their proportional limit in the top fibre of the timber slab. The formulations of this procedure have been discussed in Section 8.11.
- **Elastic bending capacity:** A procedure based on the γ -method has been proposed in this study to predict the elastic bending capacity of STC beams. The γ -method was originally conceived by Möhler [93] for timber-timber composite sections and it is included in Eurocode 5 [69] for such cases. However, it is also used to determine the capacity of timber-concrete composite beams. Therefore, its applicability has been extended to STC beams. This approach has been introduced in Section 8.12.
- **Effective bending stiffness:** The estimation of this parameter was discussed in Chapter 6, Section 6.8.7. According to the results of this investigation and the results presented by Loss et al. [85] this is a suitable method to estimate the effective bending stiffness of STC beams. With this parameter it is possible to predict the deflection of the STC beams within the elastic range for various loading conditions.

The procedures to estimate the ultimate bending capacity of STC beams are coupled with the procedure that allows the idealisation of the connectors as rigid-ductile (i.e. perfectly-plastic). This procedure has been discussed in Section 8.8 and was used to obtain the shear forces transferred by the connectors at ULS.

8.13.2. EFFECTIVENESS OF THE PROPOSED ANALYTICAL PROCEDURES

For the STC beams tested in this investigation, the following parameters were obtained analytically through the proposed analytical procedures and compared with the experimentally obtained results:

- Ultimate bending capacity with the strain-based procedure with steel considered as linear elastic perfectly-plastic and timber as linear elastic ($M_{R,\eta}$ (T-1)).
- Ultimate bending capacity with the strain-based procedure with steel and timber considered as linear elastic perfectly-plastic ($M_{R,\eta}$ (T-2)).
- Ultimate bending capacity with the simplified procedure ($M_{R,\eta}$).
- Elastic bending capacity with the γ -method ($M_{R,el}$).
- Initial bending stiffness with the γ -method ($(EI)_{ef}$).

Table 8.3 presents the parameters obtained analytically and experimentally, and the deviation of the analytical calculations. The self-weight was not considered in the loads and moment calculations of the experimentally obtained values. To account for this, the moment due to self-weight (M_{sw}) was subtracted from the analytically obtained values. Thus, the analytically obtained values presented in the table have been already reduced by $M_{sw} = 38 \text{ kN} \cdot \text{m}$.

Table 8.3: Summary of parameters from the tests, the analytical estimations with the proposed procedures and their respective deviation.

Parameter	$M_{max,exp}$ [kN·m]	$M_{R,\eta}$ (T-1) [kN·m]	$M_{R,\eta}$ (T-2) [kN·m]	$M_{R,\eta}$ [kN·m]	$M_{el,exp}$ [kN·m]	$M_{R,el}$ [kN·m]	$(EI)_{exp}$ [kN·m ²]	$(EI)_{ef}$ [kN·m ²]
BT-1 Value	1 010	966	1 006	961	615	592	107 552	108 536
Deviation [%]	—	4.4	0.4	4.9	—	3.7	—	0.9
BT-2 Value	1029	991	1 040	985	609	598	112 305	112 237
Deviation [%]	—	3.7	1.1	4.3	—	1.8	—	0.1

From these results, the following can be concluded:

- $M_{R,\eta}$ (T-1) : The strain-based approach that considers the material constitutive law of steel as elastic perfectly-plastic and for timber elastic, had deviations of 4.4% for BT-1 and 3.7% for BT-2, in both cases the estimations were conservative.
- $M_{R,\eta}$ (T-2) : The strain-based approach that considers the material constitutive laws of steel and timber as elastic perfectly-plastic, exhibited deviations of 0.4% for B-1 and 1.1% for BT-2, these were the estimations closest to the experimental values. However, the prediction of the bending capacity for BT-1 was conservative while in the case of BT-2 it was overestimated.
- $M_{R,\eta}$: The proposed simplified analytical procedure gave results which are comparable to those observed in the strain-based approach when timber is considered to behave only within its elastic range. The deviations were 4.9% for BT-1 and 4.3% for BT-2, for both cases the estimations were conservative.

- $M_{R,el}$: The predictions of the elastic moment resistance with the γ -method showed deviations of 3.7% for BT-1 and 1.8% for BT-2, the predicted values were on the safety side.
- $(EI)_{ef}$: The initial bending stiffness calculated with the γ -method had deviations of 0.9% for BT-1 and 0.1% for BT-2.

These results indicate that the proposed procedures are effective in predicting the moment resistance values and the effective bending stiffness of the tested STC beams, demonstrating good potential for use in the design of STC beams. Nevertheless, their effectiveness must be assessed for more cases.

9

VIBRATION TESTS

9.1. INTRODUCTION

Flooring systems must ensure structural integrity while also adhering to comfort and serviceability standards. These requirements demand that floors are designed to withstand specified loads safely, constrain deformations within acceptable limits, and exhibit satisfactory vibration performance. Particularly for long-span lightweight flooring systems, achieving satisfactory vibration performance is challenging due to their tendency towards low natural frequencies and reduced damping.

Vibration in flooring systems is predominantly a serviceability issue, often associated with discomfort for the occupants. However, it can also have more severe implications, such as inducing fatigue or overstressing structural members. Common sources of vibration in floors include pedestrian traffic and synchronized crowd activities, which can generate periodic forces that excite the flooring system.

The occurrence of vibrations becomes critical when the frequency of the excitations coincides with one of the natural frequencies of the flooring system, leading to resonance. This can result in significant accelerations and deformations, thereby impacting both the structural integrity and the comfort of the occupants. Hence, designing floors to ensure their natural frequencies do not align with typical excitation frequencies (e.g., 1.8 Hz to 2.2 Hz for pedestrian traffic [155] and 1.5 Hz to 3.5 Hz for crowd activities [156]) is crucial.

Perceived discomfort from floor vibrations is subjective and varies from person to person, making it challenging to establish universal criteria to avoid adverse comments from the occupants. While current standards provide guidelines to minimize the likelihood of negative feedback, ensuring the comfort of all occupants remains a complex task.

Given the difficulty in modifying an existing floor to mitigate vibration issues post-construction, it is fundamental to address these concerns during the conceptual design phase. This is particularly relevant for the STC flooring system developed in this investigation, which is lighter than conventional SCC floors due to the implementation of LVL slabs.

To assess the vibration response of the newly developed STC flooring system, experimental modal analyses (EMA) were conducted. These analyses aimed to determine the natural fre-

quencies, mode shapes, and modal damping of the STC beams. The experiments consisted of EMA on two full-scale STC beam specimens, accelerometers were installed in the specimen and a modal hammer was used to induce transient excitations.

The data collected from these tests were used to compute frequency response functions (FRF) and extract the natural frequencies and mode shapes. Additionally, FE simulations were done to validate the experimental findings and compare them with analytical predictions.

This chapter presents the methodology and results of the vibration tests conducted on the STC flooring system. Experimental, numerical, and analytical results were compared to validate the numerical models' responses and evaluate the effectiveness of the analytical predictions. This study offers valuable insights into the suitability and vibration behavior of the STC floor, and it serves as a foundational basis for more detailed and comprehensive investigations. Vibration of floors is a complex phenomenon influenced by various factors, including the specific flooring system, its grid, the loads acting on the floor, the presence of partition walls, among others.

9.2. EXPERIMENTAL TESTS

9.2.1. GENERAL

The two full-scale STC beam specimens (i.e. BT-1 and BT-2) that were assembled for the bending tests were used to carry-out the vibration tests before the beam tests were conducted. The beams were tested in simply supported conditions. Accelerometers were installed in the test specimens and the specimens were excited with a modal hammer. The roving hammer technique was used in these tests, it involves systematically moving an impact hammer to various points on the structure to excite different modes of vibration, while keeping the response measurement sensors (i.e. accelerometers) fixed to gather comprehensive modal data.

The two beam specimens were instrumented and tested in the same manner. The input excitation and the output accelerations were recorded and the data was post-processed to obtain the FRFs, the natural frequencies, the mode shapes and the modal damping ratios associated to each mode.

9.2.2. STC BEAM SPECIMENS

The specifics of the components and geometry of the two STC beam specimens are described in Chapter 6, Section 6.4. Both beams were identical in terms of geometry, materials, and shear connection distribution (see Figure 6.1). The only difference between the specimens was the type of shear connection: BT-1 implemented SCT-1, while BT-2 implemented SCT-3. Each beam had a total length of 10.6 m, a slab width of 2.51 m, and a span of 10 m. The mass of the beam specimens was estimated to be approximately 3 220 kg for BT-1 and 3 280 for BT-2.

9.2.3. TEST SETUP AND INSTRUMENTATION

The test setup and instrumentation for the two specimens were identical. The beams were simply supported at two points, resulting in a span of 10 m. The rover hammer approach was used in these tests: the sensors were fixed at predefined locations throughout the entire test, while the beams were excited at different locations with a modal hammer.

Accelerations were recorded using piezoelectric accelerometers. Fifteen accelerometers were installed on each specimen at the locations indicated in Figure 9.1. These locations were arranged to form a regular grid. Sensors near the supports were not aligned with the supports because vertical accelerations at those points might be negligible, potentially yielding insufficient data for modal analyses. Figure 9.2 shows the instrumentation of an STC beam with accelerometers for the vibration test.

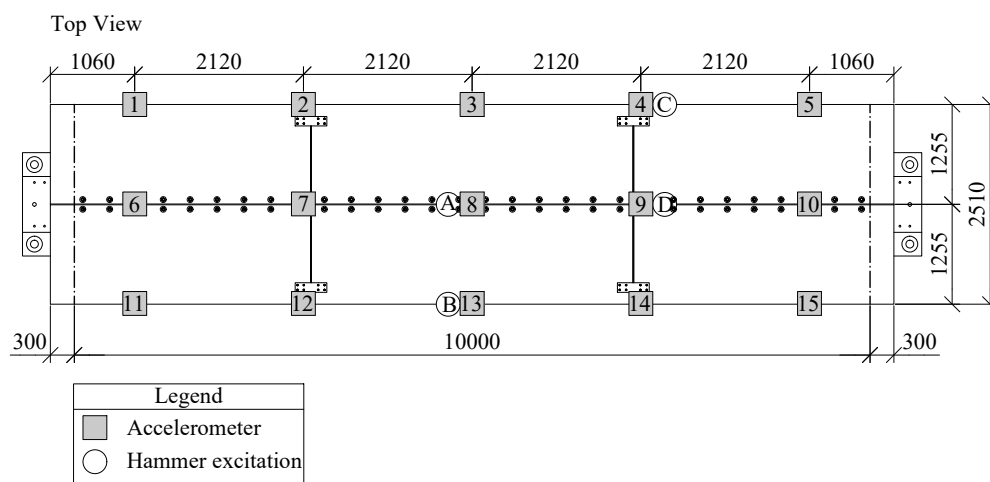


Figure 9.1: Positions of the accelerometers and the excitation points in the STC beams for the vibration tests.



Figure 9.2: Instrumentation of the STC beam with accelerometers for the vibration test.

Two types of single-axis accelerometers from PCB Piezotronics were used (see Figure 9.3a). The model 352C33, with a measurement range of ± 50 g pk, was used at the excitation point, while the model 393B04, with a measurement range of ± 5 g pk, was used at the other points. This setup prevented overshooting the sensors with a lower measurement range and ensured that accelerations were recorded at all points. The single-axis accelerometers were oriented to measure vertical accelerations and were fixed to the timber slab with strong double-sided adhesive tape.

The beams were excited at the four locations indicated in Figure 9.1 using a modal hammer with an in-built load sensor. This modal hammer, from Endevco (see Figure 9.3b), weighs 1362 g. The tip with medium stiffness was used to generate the impacts.

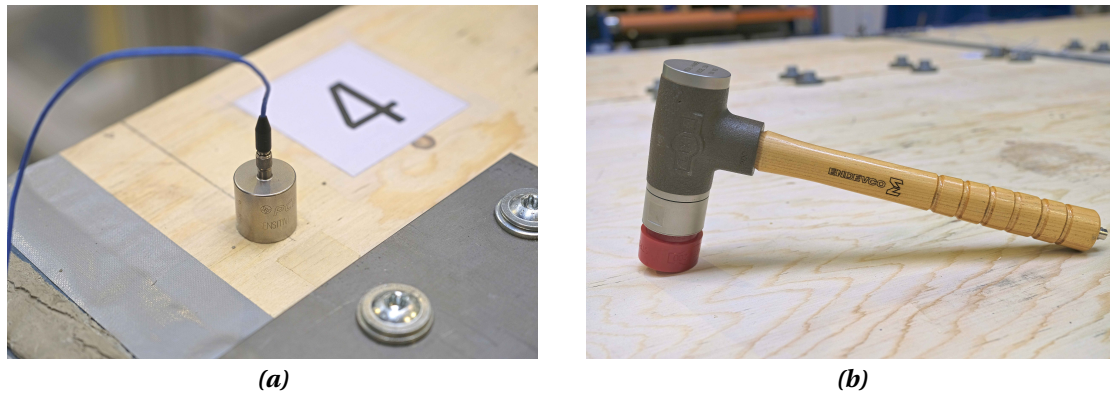


Figure 9.3: Devices used to measure accelerations and to excite the structure: (a) piezoelectric accelerometer; and (b) modal hammer with load sensor.

9

9.2.4. TESTING PROCEDURE

The beams were excited with the modal hammer at four points as indicated in Figure 9.1 with labels A, B, C, and D. The impacts at A and D had the objective to activate bending modes whereas the impacts at B and C had the objective to activate torsional modes. At each excitation point the beam was hit five times at the soffit of the slab as shown in Figure 9.4.



Figure 9.4: Excitation with hammer hit at the soffit of the LVL slab.

The impact and the accelerations were recorded for approximately 10 seconds at a rate of 5000 Hz. Figure 9.5a shows an example of one of the recorded impacts, and Figure 9.5b displays the corresponding accelerations recorded by one of the accelerometers, both in the time domain. The latter figure shows that the accelerations decay to zero within the first 2 seconds, a trend observed in most sensors for all impacts. However, the measurements were recorded over 10 seconds to minimize the risk of leakage due to signal truncation in any of the sensors.

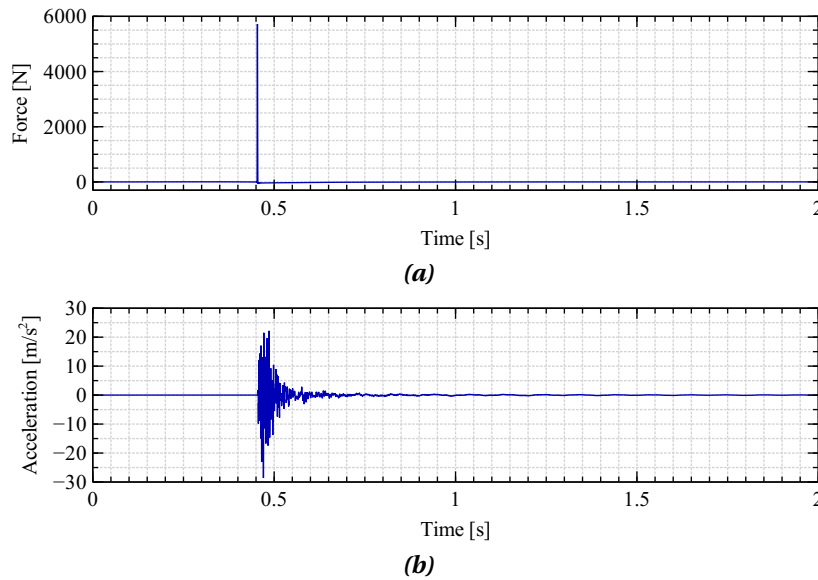


Figure 9.5: Examples of the (a) input impact force with the modal hammer and (b) the accelerations, both recorded in the time domain.

9.2.5. RESULTS

The signals recorded in the tests were post-processed to generate the FRFs. The recorded accelerations were transformed from the time domain to the frequency domain with the fast Fourier transform (FFT). The FRFs were used to identify the natural frequencies of the STC beams. Additionally, the data was processed to obtain the mode shapes of the STC beams. Figure 9.6 shows the FRFs obtained for specimens BT-1 and BT-2.

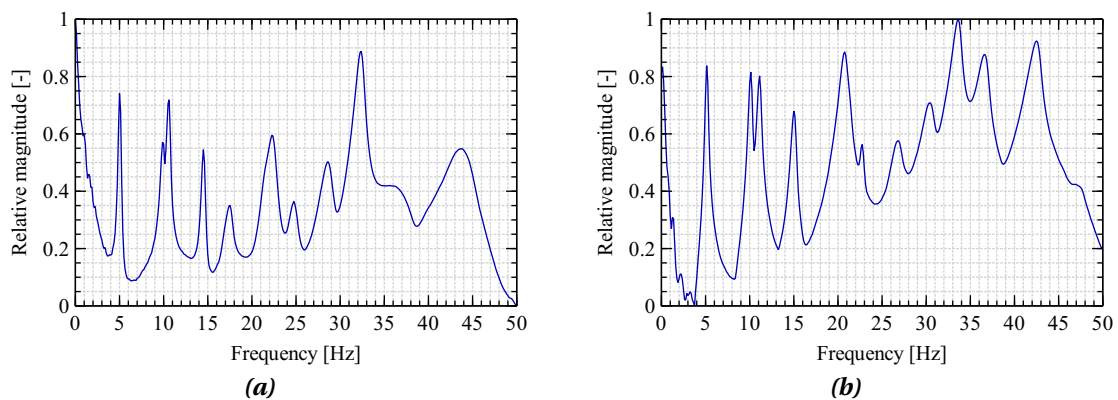


Figure 9.6: Frequency response functions for: (a) BT-1 and (b) BT-2.

The first four natural frequencies (f_i) and their corresponding modal damping ratios (ξ_i) are presented in Table 9.1. The mode shapes of the two STC beam specimens are displayed in Figure 9.7. The second mode of these specimens corresponds to their first bending mode, which is typically the most relevant for floor vibrations. This frequency is far from the excitation frequencies associated with the walking pace, which range from 1.8 Hz to 2.2 Hz [155], and for crowd activities, which range from 1.5 Hz to 3.5 Hz [156]. These results indicate that the risk of resonance is low.

Table 9.1: Natural frequencies and modal damping ratios obtained experimentally.

Specimen	Mode No.	f_i [Hz]	ξ_i [%]
BT-1	1	5.02	1.30
	2	9.87	0.87
	3	10.54	1.34
	4	14.48	0.88
BT-2	1	5.15	2.07
	2	10.10	0.73
	3	11.09	1.10
	4	14.99	1.08

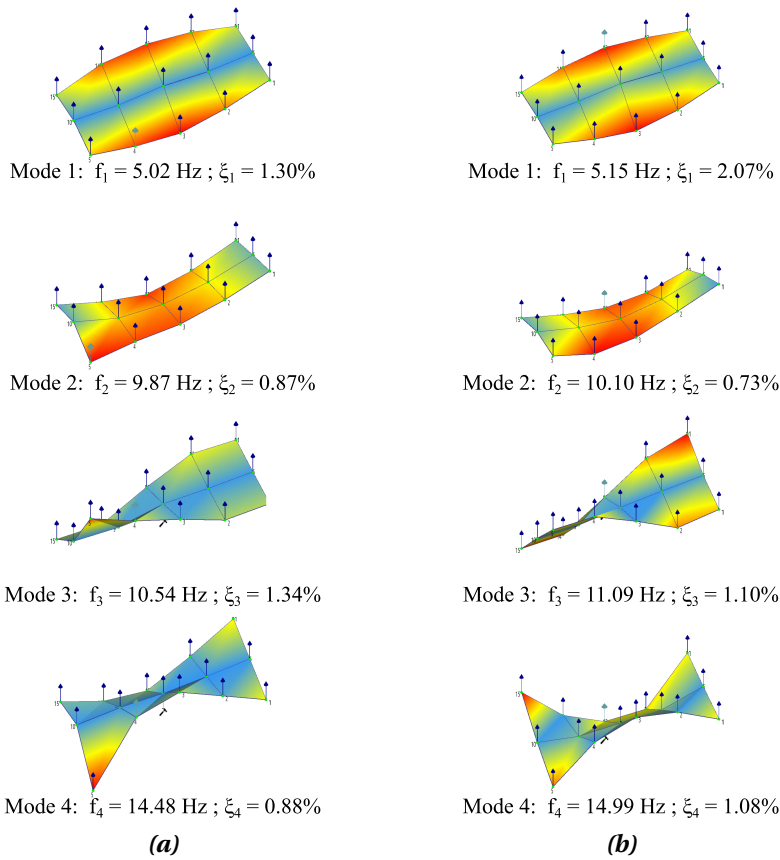


Figure 9.7: Mode shapes for: (a) BT-1 and (b) BT-2.

9.3. ANALYTICAL ESTIMATION OF THE NATURAL FREQUENCY OF STC BEAMS

9.3.1. ANALYTICAL FORMULATION

The behaviour of a beam in bending is governed by Equation 9.1, which relates the response in terms of displacement, velocity and acceleration at a certain position and time to the mass and stiffness of the system and an initial force.

$$m \frac{\partial^2 w}{\partial t^2} + EI \frac{\partial^4 w}{\partial x^4} = F(x, t) \quad (9.1)$$

In this equation m is the mass of the composite beam, w is the deflection of the beam, t is the time, EI is the bending stiffness, x is the position along the beam, and $F(x, t)$ is the force function. The natural frequencies can be derived from this equation by setting the force function ($F(x, t)$) to zero and applying appropriate boundary conditions.

The first bending mode of vibration is the most relevant to determine the dynamic response of a floor. For free elastic vibration of a simply supported beam, the fundamental frequency corresponding to the first bending mode of vibration (f_n) is given by solving Equation 9.1, which results in Equation 9.2.

$$f_n = \frac{\pi}{2} \sqrt{\frac{EI}{m \cdot L^4}} \quad (9.2)$$

9.3.2. COMPARISON OF EXPERIMENTAL RESULTS AND ANALYTICAL PREDICTIONS

The frequency of the first bending mode of vibration was estimated for the two beams with Equation 9.2. The bending stiffness of the STC beams considered in these analytical calculations was estimated from the tests for a load corresponding to loading stage I, following the procedure presented in Chapter 6, Section 6.8.7, the stiffness values have been presented in Table 6.3.

Table 9.2 presents a comparison of the frequency of the first bending mode of vibration obtained experimentally ($f_{n,exp}$) and analytically (f_n). These results show that there is a deviation of approximately 8% and 9% between the experimental and the analytical predictions. In a similar investigation, Chiniforush et al. [113], determined experimentally and analytically the natural frequency corresponding to the first bending mode of vibration of STC beams, finding similar deviations. This analytical equation gives, nevertheless, a good conservative approximation of the actual natural frequency corresponding to the first bending mode of vibration of the STC beams.

Table 9.2: Experimental and analytical frequencies for the first bending mode of vibration.

Specimen	$f_{n,exp}$ [Hz]	f_n [Hz]	Deviation [%]
BT-1	9.87	9.08	8.0
BT-2	10.10	9.19	9.0

9.4. ESTIMATION OF THE NATURAL FREQUENCIES AND MODE SHAPES WITH NUMERICAL MODELS

9.4.1. GENERAL

The 3D continuum FE model developed in ABAQUS [142] for the numerical investigations presented in Chapter 7 was used to do modal analyses to determine the natural frequencies and the mode shapes of the tested specimens. The frequency procedure with the Lanczos solver was used to extract the natural frequencies and the mode shapes.

The geometry of the simply supported beams is illustrated in Figure 9.8. It consists of the steel beam, six timber panels, and the mortar filling the two transversal gaps. The total length of the STC beams was 10.6 m with a distance between the supports of 10 m, and an overall slab width of 2.51 m. The steel beams were modelled as IPE 400 profiles made of steel grade S355. The six LVL panels were modelled using the properties of Kerto-Q LVL, and the 10 mm gaps between them were considered. The full set of properties has been presented in Chapter 7 in Section 7.2.2. The steel beam, the slabs, and the mortar filling the transversal gaps were modelled with 8-node brick elements with reduced integration (C3D8R). The LVL slabs were connected to the beams with mesh independent fasteners, and their load slip behaviour was defined using the experimentally obtained mean load slip curves from the push-out tests. Boundary conditions corresponding to a simply supported beam were defined (see Figure 9.8).

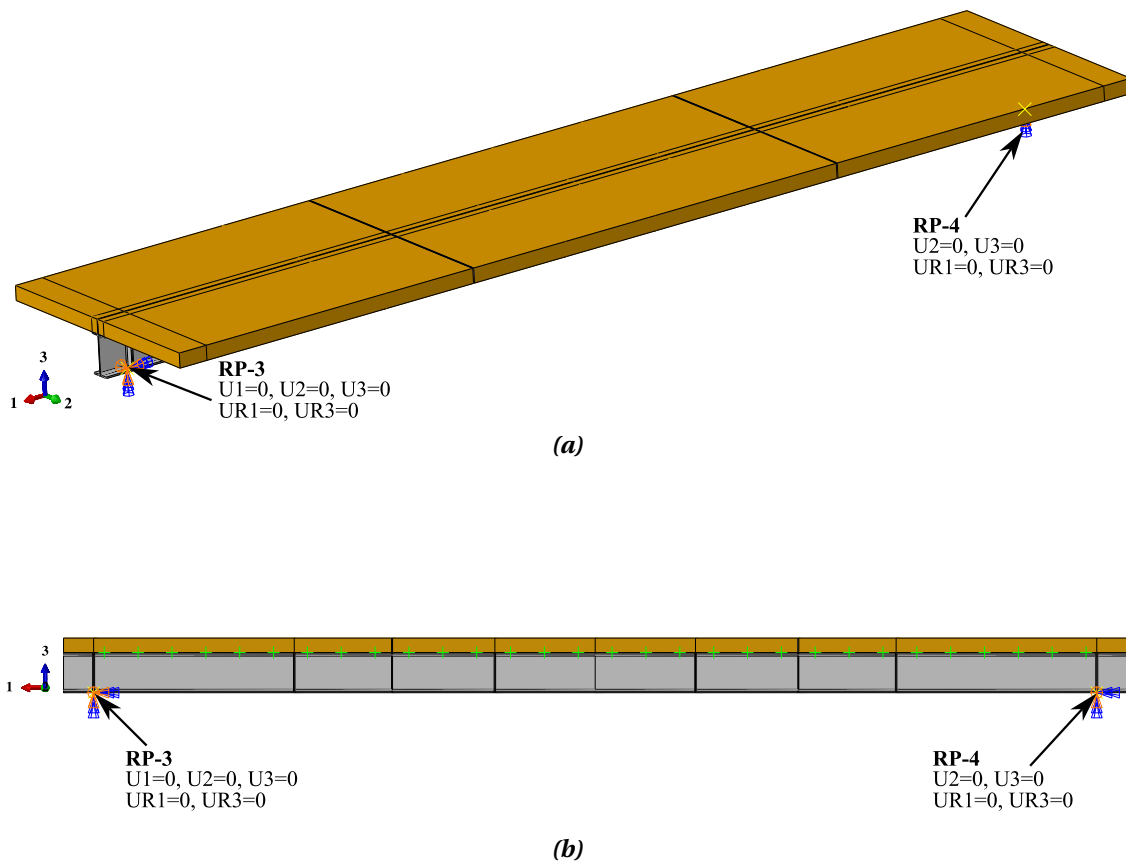


Figure 9.8: Boundary conditions of the FE model: (a) isometric view; and (b) elevation view.

9.4.2. COMPARISON OF EXPERIMENTAL AND NUMERICAL RESULTS

The first four natural frequencies of the STC beam obtained from the FE model ($f_{i,FE}$) are presented in Table 9.3, along with the experimentally obtained frequencies ($f_{i,exp}$). Figure 9.9 displays the mode shapes of the modes of vibration obtained numerically and experimentally. The results suggest that while the numerical model can predict the mode shapes and natural frequencies, the predicted natural frequencies are conservative and show some deviations.

Table 9.3: Natural frequencies and modal damping ratios obtained experimentally.

Specimen	Mode No.	$f_{i,exp}$ [Hz]	$f_{i,FE}$ [Hz]	Deviation [%]
BT-1	1	5.02	4.71	6.2
	2	9.87	8.40	14.9
	3	10.54	10.14	3.8
	4	14.48	15.27	5.5
BT-2	1	5.15	4.71	8.5
	2	10.10	8.40	16.8
	3	11.09	10.14	8.6
	4	14.99	15.27	1.9

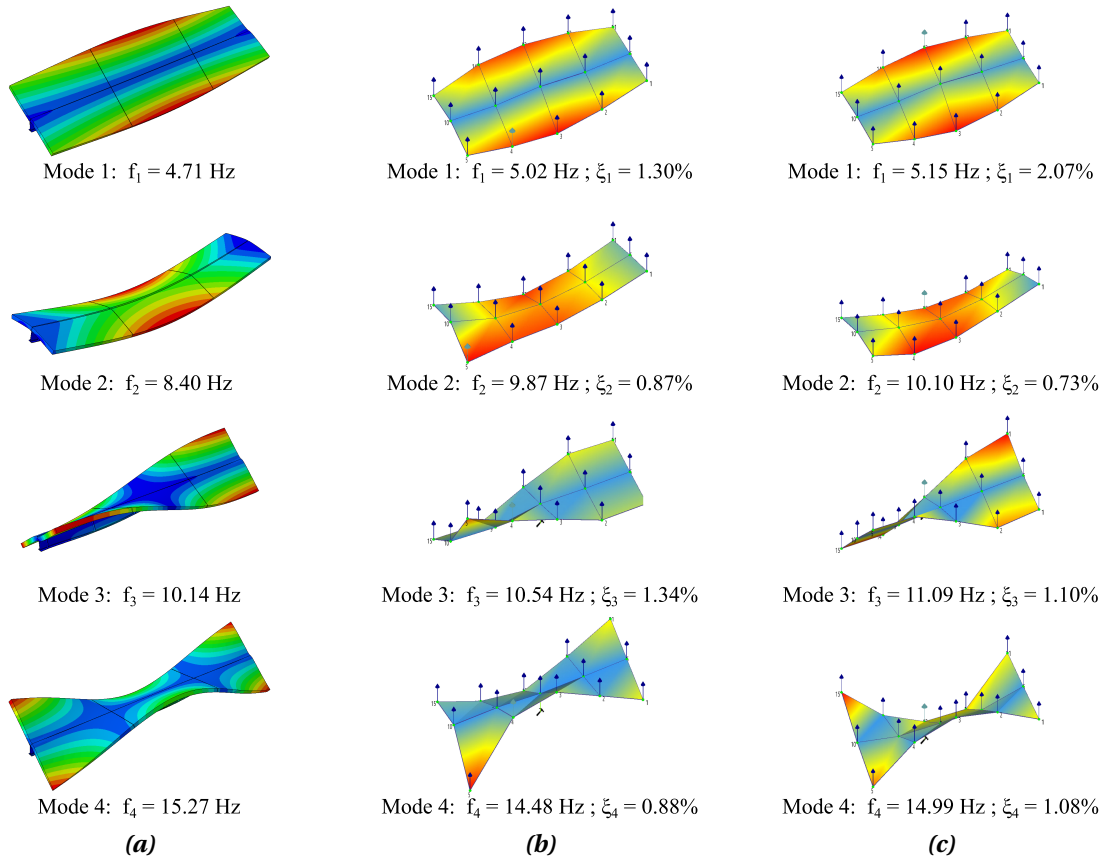


Figure 9.9: Mode shapes obtained (a) numerically; and experimentally for (b) BT-1, and (c) BT-2.

10

DESIGN CONSIDERATIONS

10.1. INTRODUCTION

Currently, there is no standard, code, or technical guide addressing the design aspects of STC beams with LVL slabs. Therefore, preliminary design considerations are fundamental in the development of the demountable and reusable steel-timber composite flooring system studied in this investigation. These considerations can facilitate its implementation in real-world applications by enabling the investigation of possibilities and limitations of specific cases. The preliminary design considerations presented in this chapter aim to be a basis for further research on the design aspects of STC beams and flooring systems. The design considerations presented here are based on the experimental findings of this investigation and the analytical procedures presented in Chapter 6, Chapter 8, and Chapter 9.

The design considerations are for short term behaviour as this study only included experiments investigating the bending capacity of simply supported beams subjected to point loads. Additionally, the tests were carried out under ambient temperature and dry indoor conditions. The design considerations for cross-section moment resistance calculations apply for sections which sufficient rotation capacity in bending that can develop their plastic moment resistance with no local effects (e.g. local buckling) affecting the attainment of the full plastic state, for instance the structural sections classified as Class 1 and Class 2 according to Eurocode 3 [147].

10.2. MATERIALS

10.2.1. STEEL

In the investigations presented in this thesis, hot-rolled sections made of structural steel were considered. Therefore, the provisions of Eurocodes for the determination of design material property values for structural steel can be applied for this application. The design considerations for cross-section resistance presented here apply to steel cross-sections classified as Class 1 and Class 2 according to Eurocode 3 [147].

Eurocode 3 [147] establishes the design values of material coefficients (i.e. modulus of elasticity, Poisson's ratio, shear modulus) and the nominal values of yield strength (f_y) and ultimate

tensile strength for structural steels (f_u). The modulus of elasticity (E) for design is $E = 210\,000$ MPa and the design strength for cross-section resistance calculations is given by Equation 10.1, where the partial safety factor (γ_{M0}) is taken as $\gamma_{M0} = 1.00$.

$$f_{y,d} = \frac{f_y}{\gamma_{M0}} \quad (10.1)$$

10.2.2. TIMBER

Design provisions from Eurocode 5 [69] along with the technical specification of the LVL manufacturer (i.e. Kerto-Q [16]) can be adopted to define the mechanical properties for the estimation of the cross-section resistance of STC beams. The design value f_d of a strength parameter f is determined from Equation 10.2. To estimate the cross-section resistance, the design compressive strength of timber has to be defined, thus, Equation 10.2 becomes Equation 10.3 when the grain direction of the timber is aligned with the longitudinal direction of the STC beam.

$$f_d = k_{mod} \frac{f_k}{\gamma_M} \quad (10.2)$$

$$f_{c,0,d} = k_{mod} \frac{f_{c,0,k}}{\gamma_M} \quad (10.3)$$

In these equations, the factor k_{mod} which takes into consideration the service class and the load duration is $k_{mod} = 0.8$ for service class 1 and medium term load duration. The partial safety factor for LVL is considered as $\gamma_M = 1.20$. For LVL and GLVL crafted from Kerto-Q panels, the characteristic strength in compression parallel to the grain is $f_{c,0,k} = 26$ MPa [16]. The modulus of elasticity parallel to the grain according to the technical specification of Kerto-Q panels [16] is $E_{0,mean} = 10\,500$ MPa.

10

10.3. SHEAR CONNECTION

10.3.1. SHEAR CONNECTION RESISTANCE

The resistance of the shear connections developed in this research project can be estimated following a procedure similar to that established in Eurocode 4 [94] in Annex B, clause B.2.5. Hence, to determine the shear resistance of the connectors, three nominally identical specimens have to be tested. From these tests, the characteristic load-slip curve corresponds to the lower bound of the load slip curves reduced by 10%. This curve can be used to obtain the characteristic shear resistance of the connection (P_{Rk}) following the procedure proposed in Chapter 8 in Section 8.8, which enables the idealisation of the shear connector as perfectly-plastic. The design resistance of the connector (P_{Rd}) should be calculated according to Equation 10.4, where the value for the partial safety factor is $\gamma_V = 1.25$.

$$P_{Rd} = \frac{P_{Rk}}{\gamma_V} \quad (10.4)$$

10.3.2. SHEAR CONNECTION STIFFNESS

According to the results of this investigation, the use of the mean initial stiffness (K_1) of the shear connections for calculations within the elastic range that require the effective bending stiffness of the composite beam (EI_{ef}) yields good approximation to the experimental observations. Thus, the mean initial stiffness K_1 obtained in Chapter 5 in Section 5.8.1 can be used for SLS calculations (see Equation 10.5).

$$K_{SLS} = K_1 \quad (10.5)$$

10.4. CROSS-SECTION RESISTANCE

10.4.1. GENERAL

In Chapter 8, two analytical procedures were proposed to predict the bending capacity of the STC beams: (i) a strain-based procedure, and (ii) a simplified procedure. The formulations presented considered mean experimental mechanical properties to compare the analytical results with the experimental observations. For design calculations, the design strength values have to be considered. Therefore, the strength of steel denoted in Chapter 8 as $f_{s,lim}$ becomes $f_{y,d}$, and the strength of timber in compression parallel to the grain denoted in Chapter 8 as $f_{c,lim}$ becomes $f_{c,0,d}$. In the calculations, the effective width of the slab has to be considered, according to the findings of this investigation, the effective width can be taken as $b_{eff} = L/5.5$. For ULS the design cross-section moment resistance (M_{Rd}) shall be always greater than the design moment (M_{Ed}) acting on the considered STC beam, thus, Equation 10.6 shall be satisfied.

$$\frac{M_{Ed}}{M_{Rd}} < 1 \quad (10.6)$$

10.4.2. CRITICAL CROSS-SECTIONS

In the STC flooring system developed in this investigation there are cross-sections where the stress concentrations may govern the failure. In simply supported beams (see Figure 10.1) the section at midspan is where the maximum bending moment is expected (cross-section I), additionally, the presence of transversal gaps creates two potential weak cross-sections (cross-section II). Therefore, the resistance of these sections must be calculated and compared with the design bending moment acting on the beam to ensure that the beam has sufficient capacity.

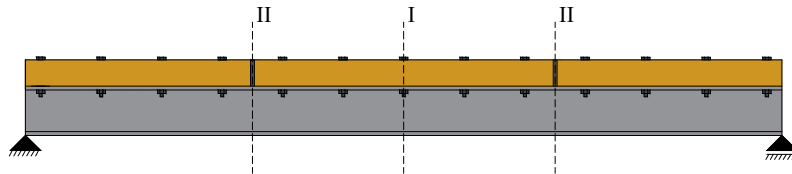


Figure 10.1: cross-sections that may be critical for failure: (I) midspan cross-section and (II) cross-section at transversal gap.

10.4.3. ANALYTICAL ESTIMATION OF THE CROSS-SECTION'S MOMENT RESISTANCE

For ULS, the design moment resistances (M_{Rd}) of the critical cross-sections can be calculated analytically as follows:

- I. Cross-section at midspan: it can be calculated according to the strain-based procedure introduced in Chapter 8 in Section 8.3 and Section 8.9. Alternatively, the simplified analytical procedure introduced in Chapter 8 in Section 8.11 can be implemented.
- II. Cross-section at the gap: it can be estimated analytically through the procedure introduced in Chapter 8 in Section 8.11.7.

For fully elastic analyses, the design elastic moment resistance ($M_{Rd,el}$) of the cross-section can be calculated through the γ -method adapted for STC beams as shown in Chapter 8 in Section 8.12.

10.5. BENDING STIFFNESS AND DEFLECTIONS

10.5.1. BENDING STIFFNESS

The effective bending stiffness of the STC beams that takes into account the shear connections' stiffness ($(EI)_{ef}$) can be calculated according to the γ -method adapted for STC beams as shown in Chapter 6 in Section 6.8.7. In this case, the section properties have to be calculated considering the effective width $b_{eff} = L/5.5$ of the timber slab and the mean moduli of elasticity for steel and LVL.

10.5.2. DEFLECTIONS

With the effective bending stiffness $(EI)_{ef}$ of the STC beam cross-section calculated according to the method proposed in this investigation, it is possible to estimate the deflections within the elastic range as demonstrated in Chapter 6 in Section 6.8.7. The deflection limits are typically defined specifically for each project, however, a typical limit deflection value for floors in general is $w_{lim} = L/250$.

10.6. VIBRATION

10.6.1. FUNDAMENTAL FREQUENCY

The fundamental bending frequency (f_n) can be estimated analytically according to the formulation presented in Chapter 9 in Section 9.3. For practical applications, that formula has been simplified and given in terms of the deflection (w) as shown in Equation 10.7, in which w is expressed in mm.

$$f_n = \frac{17.8}{\sqrt{w}} \approx \frac{18}{\sqrt{w}} \quad (10.7)$$

However, this frequency corresponds only to the STC beam alone. The composite beams are typically not isolated and are part of a flooring system, they are connected to a system of primary and secondary beams which also contribute to the vibration performance of the floor-

ing system, therefore, this has to be considered when analysing the vibration of an STC flooring system. It has been demonstrated that the sum of the deflections of each of the structural components (i.e. STC beam, primary and secondary beams) can be used in Equation 10.7 to give a good approximation of the fundamental frequency of the flooring system [157]. Nevertheless, FE analysis of the actual flooring system may be used to compare the analytically estimated values and to gain more knowledge on its vibration response.

10.6.2. VIBRATION ASSESSMENT AND ACCEPTANCE CRITERIA

Human-induced vibrations on floors caused by people walking or rhythmic activities can result in perception of these vibrations by the occupants, leading to discomfort. To reduce the likelihood of discomfort and negative perceptions from the occupants this aspect has to be appropriately addressed in design.

Several factors contribute to the adequacy of a structural system for vibration performance, this includes understanding the planned use of the space and the expected levels of vibration from its occupants. The vibration behaviour of a flooring system depends on its weight or mass, damping, and stiffness. These factors govern the dynamic performance of a system, hence, through modifications to these factors, the vibration performance of a structural system may be improved.

The footfall vibration occurs between excitation frequencies of 1.8 Hz to 2.2 Hz [155], and the excitation due to crowd activities occurs typically between excitation frequencies of 1.5 Hz to 3.5 Hz [156]. Therefore, it is recommended that the flooring systems have modal frequencies over 8 Hz to ensure the floor is not susceptible to the fundamental or harmonic frequencies of excitation. However, this is only one part of the vibration assessment of the flooring systems, depending on the standard, additional parameters may be evaluated to ensure that the floor fulfils code-defined vibration thresholds, which are in general, given in terms of accelerations.

The modal parameters can be estimated through FE models or through simplified analytical procedures, the assessment may be done applying concepts and procedures established in existing guidelines for instance Feldmann et al. [158], Smith et al. [157], AISC Design Guide 11 [159], and WoodWorks' Vibration Design Guide [160]. The acceptance criteria may be established according to the relevant standards, for instance Eurocodes [69, 94], ISO [161, 162, 163], DIN [164], BSI [165], ANSI [166].

11

CONCLUSIONS AND OUTLOOK

11.1. INTRODUCTION

This chapter synthesizes the key findings and conclusions of the research presented in this contribution. It also outlines directions for future research to further advance the application of STC systems in real-world construction practices. The overarching goal of the "Prefa-SeTi" research project is to provide a sustainable alternative to conventional flooring systems by exploring an innovative STC solution that aligns with the principles of the circular economy. To achieve this, a demountable and reusable STC flooring system was developed and assessed, along with novel shear connections that enable the demountability and reuse of structural components. Additionally, analytical procedures to calculate the bending stiffness, elastic and ultimate bending capacity, and vibration parameters of the STC beams have been proposed. The conclusions drawn from the experimental, numerical, and analytical investigations offer a comprehensive understanding of the behaviour and performance of STC beams. According to the results of this investigation, the analytical procedures have potential for implementation in the design of STC beams.

11.2. CONCLUSIONS

11.2.1. EXPERIMENTAL INVESTIGATIONS ON LVL

These investigations aimed to fill a significant knowledge gap by providing comprehensive information about the mechanical properties of LVL made from Scandinavian Spruce wood. The investigation included the determination of strength, moduli of elasticity, and shear moduli through a series of tests, including compression, tension, shear, and bending. Additionally, the testing procedures, load-deformation responses and descriptions of observed failure modes have been presented.

The mechanical properties obtained in these experimental investigations are crucial for analyzing the load-deformation behaviour and capacity of the STC beams subject of this research. These properties can be employed in analytical calculations and incorporated into FE models, to explore the deformation and failure of structural members.

In addition to the property values, stress-strain responses, and load-deformation behaviour, which have been summarized in Chapter 4, the key findings of this study are as follows:

- In compression and tension tests, the longitudinal direction exhibits the highest strength and stiffness, followed by the tangential and radial directions.
- Stress-strain responses in compression differ among the three directions, with the longitudinal direction showing softening after reaching the peak, the tangential direction exhibiting hardening after the proportional limit, and the radial direction demonstrating significant deformation capacity and a hardening branch after the proportional limit.
- Tension tests shows a sharp transition in which the load starts to decrease, this happens when the fibres in the matrix of the specimen fail in tension, however, the failure in some cases is not sudden as the failure is not localized at a specific section but rather in an irregular pattern and friction remains within the fractured veneers.
- Shear tests S-3 to S-6 exhibit a near-brittle post-peak response, marked by sudden load drops after reaching the peak. In contrast, shear tests S-1 and S-2 show a post-peak behaviour with a gradual load decrease due to ongoing inter-layer friction.
- Bending tests reveal that failure occurs at the soffit. Gradual failure at a layer-by-layer basis is observed, with load drops occurring when the most stressed layers of the soffit fail. Ultimately, a final sudden load drop is associated with the fracture of the matrix.

These findings contribute valuable insights into the mechanical behaviour of LVL crafted with Scandinavian Spruce Wood, enhancing its applicability in STC beams and other engineering contexts.

11.2.2. NOVEL SHEAR CONNECTIONS FOR DEMOUNTABLE STC BEAMS

In composite construction the shear connections are key to ensure the transfer of shear forces and the attainment of composite action. Shear connections specifically designed to enable demountability and reuse of STC beams do not exist. This research project addressed this by proposing three novel connections that enable demountability and reuse of STC beams and flooring systems. This study was focused on connections implementing bolts with a diameter of 20 mm and a steel grade of 10.9, which were installed in LVL panels 144 mm thick. The mechanical performance of these connections was studied through push-out tests. This contribution presented the details of the connections, the testing procedures and the results of the tests. The key findings and conclusions of this experimental investigation can be summarized as follows:

- The shear connections introduced in this study offer ease of installation and facilitate the assembly and disassembly of components. These characteristics align with the principles of the circular economy.
- The shear connection devices protect the timber and facilitate the attainment of the required preload for high-strength bolts, preventing timber crushing in the radial direction.

- Preload calibration tests demonstrated a weak correlation (70.4%) between force and torque, whereas force and nut rotation exhibited a strong correlation (92.9%). Hence, a combined method involving torque and nut rotation is preferred to achieve the minimum preload. It is important to note that the rotation values obtained in this study were significantly influenced by the use of the DTI in the connection assembly, since the protrusions compress significantly, it has an important influence on the rotation of the nut. Therefore, if the DTI is removed from the assembly a new calibration of the required rotation to attain the minimum preload is needed.
- All three connection types exhibited a nonlinear load-slip response. While there were differences in terms of the loads, stiffness, and post-peak behaviour, they shared a similar load-slip pattern.
- The clearance between the bolt and the holes in the flanges and the shear connection devices significantly impacts the initial slip of the connection, determining when the bolt starts to work in bearing and shear.
- In terms of stiffness of the bearing branch, SCT-1 exhibited the lowest stiffness (16.4 kN/mm) while SCT-2 and SCT-3 performed better (20.4 kN/mm and 23.5 kN/mm, respectively).
- At a slip of 15 mm, the load-slip curves of each test series reach similar values, this was demonstrated by the low coefficient of variation observed in the three specimens of each test series. At this point, SCT-1 and SCT-2 reached a load P_{15mm} of approximately 124 kN, while SCT-3 reached 149.1 kN.
- The connectors exhibited a load bearing capacity per shear connector at a 6 mm slip of 95.7 kN, 104.4 kN, and 120.2 kN for SCT-1, SCT-2, and SCT-3, respectively. The peak loads for SCT-1 and SCT-3 were within the same order of magnitude, at 161.4 kN and 163.8 kN, respectively, whereas SCT-2 outperformed both with a peak load of 173.1 kN.
- The higher stiffness and loads reached by SCT-3 at early loading stages (e.g. $\delta < 40$ mm) can be attributed to their reinforcement provided by inclined screws, which contribute with their withdrawal and bearing capacities.
- All three connection types displayed a significant deformation capacity (greater than 40 mm slip), attributed to the high compressibility of timber, and the strength of both the bolts and the shear connection devices.
- The three connection types exhibited a similar failure mode. There was timber crushing due to embedment of the shear connection device and one plastic hinge developed in the steel components at the steel-timber interface.
- The three connection types reached a maximum load value, followed by rupture of bolts in the case of SCT-1 and softening for SCT-2 and SCT-3 without rupture of the bolts.
- Only SCT-1 exhibited rupture of the bolts, the failure of the first bolt occurred at a slip of 65-75 mm, SCT-2 and SCT-3 were able to reach the maximum available deformation

of the testing setup which was approximately 140 mm, at this deformation the push-out tests of SCT-1 and SCT-3 were stopped and no rupture of the connections was observed.

11.2.3. FULL-SCALE STC BEAM TESTS

The flexural behaviour of the demountable and reusable STC beams developed in this research project was studied through full-scale six-point bending tests on two beams with a span of 10 m and an overall slab width of 2.51 m. Each of the specimens implemented one type of shear connection, BT-1 implemented SCT-1 whereas BT-2 implemented SCT-3. The findings from the experimental six-point bending tests on STC beams with newly developed shear connections have yielded several key insights, leading to the following conclusions:

- The beams demonstrated substantial load-bearing and deformation capabilities. The tests were stopped due to the specimens reaching the maximum deformation given by the testing setup, nevertheless, the deformations reached in BT-1 and BT-2 were quite large, approximately 400 mm and 650 mm, respectively, and the maximum recorded loads were 674 kN (bending moment of 1011 kN·m) for BT-1, and 686 kN (bending moment of 1029 kN·m) for BT-2.
- The elastic limit of the two STC beams was reached at a load of approximately 400 kN (bending moment of 600 kN·m) and a midspan deflection of 60 mm.
- The efficiency of the composite action was assessed in terms of their bending stiffness. Their actual bending stiffness and the bending stiffness of identical beams with full-rigid shear connection and with no shear connection were considered to estimate the enhancement in stiffness. The efficiency of the composite action (η_{EI}) of BT-1 was 76.1% and 82.6% for BT-2, indicating that the bending stiffness improved significantly with the composite action provided by the shear connections.
- In the STC beams tested in this investigation the maximum bending moment was reached at large deformations, approximately $L/20$, indicating that these beams have good ductility.
- The shear connectors exhibited slip values smaller than 1 mm, for loads within the elastic range of the STC beams. This indicates that when loads remain within the elastic range (e.g. service conditions) it is possible to reuse the LVL panels.
- Maximum slip values of 5.3 mm and 6.6 mm were recorded for BT-1 and BT-2, respectively. Larger slip values were recorded in BT-2 because it was subjected to larger deformations. In BT-1 the test was stopped due to the jack reaching its maximum travel and the lack of an extension arm for the hydraulic jack to continue with the application of load. This issue was addressed in BT-2, and therefore it was possible to reach larger deformations.
- At the end of the test, the most stressed connections were cut longitudinally to assess the damages and nearly no damage was observed, only slight embedment of the shear

connection devices in the timber with a permanent deformation of approximately 1 mm, additionally, no deformations or damages were observed in the bolts and the holes of the flange of the steel beam.

- The steel beams in both specimens exhibited plasticization and underwent large deformations, yet without local damages or fracture. In BT-1 the largest recorded tensile strains in the bottom flange of the steel beams was at the midspan section. In BT-2 the steel beam exhibited a redistribution of stresses, the most stressed region was initially at midspan, from a certain loading stage little increase of strains was observed in the bottom flange of the steel beam in the midspan section whereas in the region near the transversal gap, the strains increased to larger values. Thus, showing that the regions of the steel beam near the transversal gap plasticized to a larger extent than the midspan section, which is typically the most stressed in simply supported beams in sagging bending.
- The strength and failure of the STC beams was in both cases governed by the yielding and ultimate strength of the steel beam. This means that, increasing the steel grade can enhance the utilization of the LVL slab and shift the yielding of the steel beam in the critical regions, increasing the moment at yielding and the moment capacity of the STC beams.
- The strains recorded in the timber remained within the elastic range, furthermore, the strain distribution through the width of the slab was not uniform, which indicates that the shear lag effects are to be considered. The effective width at midspan, estimated at the last loading stage was 1881 mm for BT-1 and 1771 mm for BT-2, corresponding to an effective width of approximately $L/5.5$.
- The use of high strength mortar to fill the transversal gaps was effective to transfer compression forces from the central panels to the edge panels, hence, the shear connectors of the edge panels were activated. Moreover, the mortar showed minimal damage despite significant deformations, in both tests it remained undamaged up to the loading stage VIII.
- BT-2 exhibited mortar crushing and LVL delamination near the transversal gaps after loading stage VIII, indicating that at large deformations these regions become potential points of failure. However, the segmentation of the slabs along the longitudinal directions and having gaps between them is needed as it provides tolerances and facilitates transport and assembly / disassembly, which can be critical for long spans.

11.2.4. NUMERICAL INVESTIGATIONS ON STC BEAMS

Nonlinear 3D FE models of the testes STC beams were developed in ABAQUS [142] to extend the findings of the full-scale bending tests. A modelling strategy has been presented and the numerical models were validated with the results of the experimental tests. With the validated models the influence of certain parameters on the response of the STC beams was investigated.

The parameters investigated were (i) the steel grade of the steel beam, (ii) the presence or absence of transversal gaps and the effect of filling them, and (iii) the connectors' spacing and the degree of shear connection. These investigations allowed to draw the following conclusions:

- The numerical models developed to simulate the tests are in good agreement with the experimental results in terms of load-displacement and can be used to study the influence of certain parameters on the response of the STC beams.
- The influence of the steel grade on the STC beams was studied by changing the properties to structural steel grade S460. Using this steel grade increased the yielding of the STC beams by approximately 30% and the bending capacity by about 25% compared to the tested beams with IPE 400 profiles made of steel grade S355.
- The tested beams had transversal gaps of 10 mm filled with mortar. The FE models without gaps showed that the presence of the gap had little influence on the initial elastic branch. However, after yielding, the beams without transversal gaps exhibited higher stiffness, which resulted in an increased bending capacity.
- Not filling the gap has a significant impact on the response of the STC beams. Beams with transversal gaps but without mortar filling exhibited significantly lower stiffness and reduced bending capacity, highlighting the importance of filling the transversal gaps with mortar. This ensures the transfer of compression from the central panels to the edge panels at all loading stages and the activation of the shear connectors installed in the edge panels.
- When comparing the tested beams with identical beams having full-rigid shear connection and no shear connection, it is evident that the tested beams have an initial bending stiffness similar to the beam with full-rigid shear connection. In contrast, the difference in stiffness and capacity between the tested beams and the beam with no shear connection is quite large, there is an enhancement of the bending stiffness of approximately 80% and an enhancement of bending capacity of at least 40%, highlighting the significance of the composite action.
- The tested beams had shear connections with spacing of 337.5 mm. The influence of the degree of shear connection was studied by varying the shear connectors' spacing, beams with shear connectors' spacing of 515 mm, 650 mm and 1225 mm were analysed. The results showed that the reduction of the number of connectors decreases significantly the bending stiffness of the STC beams but the impact on the bending capacity is not as significant.
- In the STC beams, fewer connectors (i.e. larger connectors spacing) result in larger slip values. However, due to the particular load-slip response of the developed connectors, they can transfer larger shear forces at larger slips. Consequently, even with fewer connectors, large shear forces can be transferred, and significant compressive forces can be developed in the slab due to the connectors' large deformation capacity and the high

loads they can transfer at large deformations.

- The presence of more connectors is associated with increased initial bending stiffness and lower slip values. However, when connectors reach low slip values, they transfer fewer shear forces. As a result, the increase in ultimate bending capacity achieved by adding more connectors is not as significant as the improvement in initial bending stiffness and the reduction in slip.

11.2.5. ANALYTICAL DETERMINATION OF THE BENDING CAPACITY OF STC BEAMS

In this research project, two procedures to determine the bending capacity of the STC beams have been proposed: (i) a strain-based procedure and (ii) a simplified analytical procedure. Additionally, the γ -method has been adapted for STC beams and has been used to calculate the bending stiffness and the elastic moment resistance of the STC beams, taking into consideration the stiffness of the shear connectors. Furthermore, an algorithm to transform the load-slip response into a perfectly-plastic idealisation. The analytically obtained results have been compared with the experimental observations. These investigations allow us to conclude the following:

- An algorithm has been proposed to transform the load-slip curves into an effective shear resistance, enabling the idealization of the shear connectors as perfectly plastic. This simplifies the calculation of the shear forces transferred by the shear connectors and the compressive force that can be developed in the STC beams.
- The strain-based procedure is a robust analytical tool that allows to estimate the moment resistance of STC cross-sections at different states. Its effectiveness in providing close approximations to the actual ultimate capacity has been proven.
- An alternative simplified analytical procedure suitable for practical applications has been proposed to estimate the bending capacity of STC beams at the ultimate limit state. In this procedure, the assumption that at ULS the timber remains in its elastic range while the steel is fully plasticized yielded results that are consistent with the experimental observations.
- The γ -method applied to STC beams yields results for the bending stiffness and the elastic moment resistance that are in good agreement with the experimental observations.
- The proposed analytical procedures are effective in predicting the elastic and ultimate moment resistance of the STC beams, as well as their effective bending stiffness, demonstrating good potential for their use in the design of STC beams. However, their effectiveness needs to be verified for more configurations.

11.2.6. VIBRATION BEHAVIOUR OF STC BEAMS

Floors are subject to excitations that cause vibrations, primarily due to people walking and crowd activities. These vibrations may be perceived by the occupants, causing discomfort or an impression that the floor is not safe. In this study, vibration tests were carried out on two

full-scale STC beam specimens. Their natural frequencies, mode shapes, and modal damping ratios were obtained. The experimentally obtained values were then compared with analytical and numerical estimations. These investigations lead to the following conclusions:

- The experimental vibration tests showed that both specimens had similar natural frequencies, mode shapes and modal damping ratios. The first bending frequency for BT-1 was 9.87 Hz and for BT-2 was 10.10 Hz, with damping ratios of 0.87% and 0.73% respectively.
- An analytical formulation to estimate the first bending frequency of simply supported beams is presented and used to calculate the first bending frequency of the two tested beams. The analytically obtained values provide a conservative estimation of the first bending frequency with deviations of 8.0% for BT-1 and 9.0% for BT-2.
- The FE models were able to predict the mode shapes observed in the experimental tests, however, the natural frequencies were in general underestimated.
- The first bending mode is the most relevant for the assessment of the vibration performance of floors subjected to human-induced vibrations which are typically in the range of 1.8 Hz to 2.2 Hz for pedestrian traffic and 1.5 Hz to 3.5 Hz for crowd activities. Since the first bending frequency of the tested beams was approximately 10 Hz, the risk of resonance is low.
- The results and procedures presented in this study are intended to serve as a basis for more detailed analyses required in design. Although the results suggest that resonance may not be an issue, detailed analyses must be conducted considering imposed loads and the influence of the primary and secondary beams. This will provide a better approximation of the actual response of the flooring system and allow for an assessment of its performance according to established standards.

11.3. OUTLOOK

This research provides valuable insights into the mechanical behaviour of an innovative demountable and reusable STC flooring system, highlighting its potential as a sustainable alternative to conventional flooring systems. The study has demonstrated the feasibility and potential of the STC system, particularly in terms of structural performance, and alignment with the principles of the circular economy. However, further research is essential to address the limitations of this research project and to facilitate its applicability in diverse scenarios.

Steel-timber composite structures represent a relatively new structural system, and as such, there is limited research available in the literature. Currently, there are no established codes or guidelines specifically addressing the design and implementation of STC beams and flooring systems. This study has achieved significant progress in developing and assessing an STC flooring system and its shear connections. The assessment, however, was constrained to short-term behaviour and specific configurations and materials.

Despite the promising findings of this contribution and the potential of STC flooring sys-

tems, there are several avenues for future research that would further solidify the application and effectiveness of STC systems. Addressing the limitations and exploring new aspects will provide a more comprehensive understanding and broader applicability of STC beams in diverse scenarios.

Based on the findings and limitations of this study, potential directions for future work and research include:

1. Material Variations:

- Investigate the performance of different types of engineered timber, such as Cross-Laminated Timber (CLT) and other variants of Laminated Veneer Lumber (LVL), to understand their behaviour in STC systems.
- Explore the impact of different timber species and varying thicknesses on the mechanical properties and overall performance of the STC beams.
- Study the influence of different steel grades and steel profiles on the mechanical behaviour

2. Connection Variations:

- Assess the performance of different bolt sizes, grades, and configurations to optimize the shear connections for various applications.
- Develop and test new types of shear connectors to further enhance the demountability and reuse potential of the STC beams.

3. Structural Configurations:

- Extend the study to include different support and loading conditions, such as fixed-end, actual connections to primary beams, and varying span lengths to comprehensively understand the flexural behaviour of STC systems.
- Test beams varying the spacing of the shear connectors to better understand the influence of the degree of shear connection.
- Test a full-scale flooring unit under various loading conditions.

4. Dynamic Performance:

- Conduct more detailed vibration analyses considering various imposed loads, different boundary conditions, and the influence of primary and secondary beams to better assess the flooring system's performance under human-induced vibrations.
- Study the vibration response of a full-scale flooring unit with actual imposed loads, partition walls, furniture, etc.

5. Long-term Performance and Durability:

- Investigate the long-term performance of the STC flooring systems under different

loading conditions, including creep effects, the effects of environmental conditions such as humidity, temperature variations, and potential biological degradation.

- Perform cyclic tests on the shear connections and full-scale beams to evaluate the performance and reliability of the shear connections and the overall STC system under cyclic loading conditions.

6. Analytical methods:

- Investigate the effectiveness of the strain-based and the simplified procedures in more cases to ensure its applicability for diverse configurations.

7. Design:

- Develop comprehensive design guidelines for STC systems, incorporating findings from experimental, numerical, and analytical studies.
- Integrate STC systems into building codes and standards to facilitate widespread implementation.

8. Life Cycle Assessment:

- Conduct lifecycle assessments to quantify the environmental benefits of STC systems compared to conventional flooring systems, including embodied energy, carbon footprint, and potential for material reuse.
- Evaluate the economic feasibility and cost-benefit analysis of implementing STC systems in various construction projects.

LIST OF PUBLICATIONS

JOURNAL PAPERS

- J.3. **Alfredo Romero** and Christoph Odenbreit. “Innovative Demountable Steel-Timber Composite (STC) Beams: Experimental Full-Scale Bending Tests”. In: *Engineering Structures* 318 (2024), p. 118599. ISSN: 01410296. DOI: [10.1016/j.engstruct.2024.118599](https://doi.org/10.1016/j.engstruct.2024.118599)
- J.2. **Alfredo Romero** and Christoph Odenbreit. “Experimental Investigation on Novel Shear Connections for Demountable Steel-Timber Composite (STC) Beams and Flooring Systems”. In: *Engineering Structures* 304 (2024), p. 117620. ISSN: 01410296. DOI: [10.1016/j.engstruct.2024.117620](https://doi.org/10.1016/j.engstruct.2024.117620)
- J.1. **Alfredo Romero** and Christoph Odenbreit. “Experimental Investigation on Strength and Stiffness Properties of Laminated Veneer Lumber (LVL)”. In: *Materials* 16.22 (2023), p. 7194. ISSN: 1996-1944. DOI: [10.3390/ma16227194](https://doi.org/10.3390/ma16227194)

CONFERENCE PAPERS

- C.4. Christoph Odenbreit, **Alfredo Romero**, and András Kozma. “A novel shear connection and analysing algorithm to allow for circular economy in steel-concrete and steel-timber composite construction”. In: *Proceedings of the 10th International Conference on Steel and Aluminium Structures (ICSAS24)*. Rio de Janeiro, Brazil, 2024, pp. 741–753.
- C.3. **Alfredo Romero**, Jie Yang, and Christoph Odenbreit. “Bending Resistance of Steel-timber Composite (STC) Beams: Analytical vs. Numerical Investigations”. In: *Proceedings of Eurosteel 2023*. Amsterdam, Netherlands, 2023, pp. 59–64. ISSN: 2509-7075. DOI: [10.1002/cepa.2417](https://doi.org/10.1002/cepa.2417)
- C.2. **Alfredo Romero**, Jie Yang, François Hanus, Hervé Degée, and Christoph Odenbreit. “Push-out tests on connections for demountable and reusable steel-timber composite beam and flooring systems”. In: *Proceedings of the World Conference on Timber Engineering (WCTE 2023)*. Oslo, Norway, 2023, pp. 3568–3574. ISBN: 978-1-71387-327-3. DOI: [10.52202/069179-0464](https://doi.org/10.52202/069179-0464)
- C.1. **Alfredo Romero**, Jie Yang, François Hanus, and Christoph Odenbreit. “Numerical Investigation of Steel-LVL Timber Composite Beams”. In: *Proceedings of the XIII Conference on Steel and Composite Construction*. Portugal, 2021, pp. 21–30. ISSN: 2509-7075. DOI: [10.1002/cepa.1694](https://doi.org/10.1002/cepa.1694)

BIBLIOGRAPHY

- [1] REN21 Secretariat. *2020 Global Status Report for Buildings and Construction Towards a Zero-Emissions, Efficient and Resilient Buildings and Construction Sector*. Tech. rep. 2020.
- [2] Eleni Iacovidou and Phil Purnell. “Mining the Physical Infrastructure: Opportunities, Barriers and Interventions in Promoting Structural Components Reuse”. In: *Science of the Total Environment* 557–558 (2016), pp. 791–807. ISSN: 18791026. DOI: [10.1016/j.scitotenv.2016.03.098](https://doi.org/10.1016/j.scitotenv.2016.03.098).
- [3] Patrizia Ghisellini, Maddalena Ripa, and Sergio Ulgiati. “Exploring Environmental and Economic Costs and Benefits of a Circular Economy Approach to the Construction and Demolition Sector. A Literature Review”. In: *Journal of Cleaner Production* (2018). ISSN: 09596526. DOI: [10.1016/j.jclepro.2017.11.207](https://doi.org/10.1016/j.jclepro.2017.11.207).
- [4] European Commission. Directorate General for Communication. *European Green Deal: Delivering on Our Targets*. LU: Publications Office, 2021. (Visited on 11/17/2023).
- [5] United Nations. *Resolution Adopted by the General Assembly on 25 September 2015, Transforming Our World: The 2030 Agenda for Sustainable Development, UN Document: A/RES/70/1*. New York City, USA, 2015.
- [6] *World Population Prospects 2019: Highlights*. New York: United Nations, 2019. ISBN: 978-92-1-148316-1.
- [7] András Kozma. “Demountable Composite Beams: Analytical Calculation Approaches for Shear Connections with Multilinear Load-Slip Behaviour”. Doctoral Thesis. University of Luxembourg, 2020.
- [8] Isidora Jakovljević, Milan Spremić, and Zlatko Marković. “Demountable Composite Steel-Concrete Floors: A State-of-the-Art Review”. In: *Gradjevinar* 73.3 (2021). ISSN: 13339095. DOI: [10.14256/JCE.2932.2020](https://doi.org/10.14256/JCE.2932.2020).
- [9] Galina Churkina et al. “Buildings as a Global Carbon Sink”. In: *Nature Sustainability* 3.4 (Jan. 2020), pp. 269–276. ISSN: 2398-9629. DOI: [10.1038/s41893-019-0462-4](https://doi.org/10.1038/s41893-019-0462-4).
- [10] Bernardino D’Amico, Francesco Pomponi, and Jim Hart. “Global Potential for Material Substitution in Building Construction: The Case of Cross Laminated Timber”. In: *Journal of Cleaner Production* 279 (Jan. 2021), p. 123487. ISSN: 09596526. DOI: [10.1016/j.jclepro.2020.123487](https://doi.org/10.1016/j.jclepro.2020.123487).
- [11] M. Sansom et al. *Reuse and Demountability Using Steel Structures and the Circular Economy (REDUCE)*. Tech. rep. European Commission, Directorate-General for Research and Innovation. Brussels, Belgium, 2020.

- [12] Finish Woodworking Industries. *Laminated Veneer Lumber (LVL) Bulletin*. Helsinki, Finland, 2019.
- [13] Finnish Woodworking Industries. *LVL Handbook*. Helsinki, Finland: Federation of the Finish Woodworking Industries, 2019. ISBN: 978-952-94-2346-0.
- [14] E. L. Schaffer et al. "Feasibility of Producing High-Yield Laminated Structural Product: General Summary". In: *U.S.D.A. Forest Service Research Paper FPL 175* (1972), p. 18.
- [15] Theodore Laufenberg. "Exposure Effects upon Performance of Laminated Veneer Lumber and Glulam Materials". In: *Forest Products Journal* 32.5 (1982), pp. 42–48.
- [16] Metsä Wood. *Kerto LVL - Mechanical Properties*. Tech. rep. Espoo, Finland: Metsä Wood, 2021.
- [17] OECD. *Global Material Resources Outlook to 2060: Economic Drivers and Environmental Consequences*. OECD, Feb. 2019. ISBN: 978-92-64-30744-5. DOI: [10.1787/9789264307452-en](https://doi.org/10.1787/9789264307452-en).
- [18] Bernardino D'Amico, Francesco Pomponi, and Jim Hart. "Global Potential for Material Substitution in Building Construction: The Case of Cross Laminated Timber". In: *Journal of Cleaner Production* 279 (2021), p. 123487. ISSN: 09596526. DOI: [10.1016/j.jclepro.2020.123487](https://doi.org/10.1016/j.jclepro.2020.123487).
- [19] Ivana Kuzmanovska et al. "Tall Timber Buildings: Emerging Trends and Typologies". In: *WCTE 2018 - World Conference on Timber Engineering*. 2018.
- [20] Alireza A. Chiniforush et al. "Energy Implications of Using Steel-Timber Composite (STC) Elements in Buildings". In: *Energy and Buildings* (2018). ISSN: 03787788. DOI: [10.1016/j.enbuild.2018.07.038](https://doi.org/10.1016/j.enbuild.2018.07.038).
- [21] Osama A.B. Hassan, Fredrik Öberg, and Emil Gezelius. "Cross-Laminated Timber Flooring and Concrete Slab Flooring: A Comparative Study of Structural Design, Economic and Environmental Consequences". In: *Journal of Building Engineering* (2019). ISSN: 23527102. DOI: [10.1016/j.jobbe.2019.100881](https://doi.org/10.1016/j.jobbe.2019.100881).
- [22] A. Hassanieh, H. R. Valipour, and M. A. Bradford. "Experimental and Analytical Behaviour of Steel-Timber Composite Connections". In: *Construction and Building Materials* 118 (2016). ISSN: 09500618. DOI: [10.1016/j.conbuildmat.2016.05.052](https://doi.org/10.1016/j.conbuildmat.2016.05.052).
- [23] A. Hassanieh, H. R. Valipour, and M. A. Bradford. "Experimental and Numerical Study of Steel-Timber Composite (STC) Beams". In: *Journal of Constructional Steel Research* 122 (2016), pp. 367–378. ISSN: 0143974X. DOI: [10.1016/j.jcsr.2016.04.005](https://doi.org/10.1016/j.jcsr.2016.04.005).
- [24] Alfredo Romero et al. "Numerical Investigation of Steel-LVL Timber Composite Beams". In: *ce/papers* 5.2 (Apr. 2022), pp. 21–30. ISSN: 2509-7075, 2509-7075. DOI: [10.1002/cepa.1694](https://doi.org/10.1002/cepa.1694).
- [25] Alfredo Romero, Jie Yang, and Christoph Odenbreit. "Bending Resistance of Steel-timber Composite (STC) Beams: Analytical vs. Numerical Investigations". In: *ce/papers* 6.3-4 (Sept. 2023), pp. 59–64. ISSN: 2509-7075, 2509-7075. DOI: [10.1002/cepa.2417](https://doi.org/10.1002/cepa.2417).

- [26] Forest Products Laboratory - USDA. "Wood Handbook: Wood as an Engineering Material". In: *USDA - General Technical Report* General Te (2010). ISSN: 03781127.
- [27] R. C. Moody et al. "Press-Lam: Progress in Technical Development of Laminated Veneer Structural Products". In: *U.S.D.A. Forest Service Research Paper FPL 279* (1977), p. 26.
- [28] Ayhan Özçifçi. "Effects of Scarf Joints on Bending Strength and Modulus of Elasticity to Laminated Veneer Lumber (LVL)". In: *Building and Environment* 42.3 (Mar. 2007), pp. 1510–1514. ISSN: 03601323. DOI: [10.1016/j.buildenv.2005.12.024](https://doi.org/10.1016/j.buildenv.2005.12.024).
- [29] Istie Rahayu et al. "Ten New Poplar Cultivars Provide Laminated Veneer Lumber for Structural Application". In: *Annals of Forest Science* 72.6 (Sept. 2015), pp. 705–715. ISSN: 1286-4560, 1297-966X. DOI: [10.1007/s13595-014-0422-0](https://doi.org/10.1007/s13595-014-0422-0).
- [30] Stéphane Girardon et al. "Modelling the Effects of Wood Cambial Age on the Effective Modulus of Elasticity of Poplar Laminated Veneer Lumber". In: *Annals of Forest Science* 73.3 (Sept. 2016), pp. 615–624. ISSN: 1286-4560, 1297-966X. DOI: [10.1007/s13595-016-0569-y](https://doi.org/10.1007/s13595-016-0569-y).
- [31] Istie Rahayu et al. "The Effect of Juvenility and Veneer Thickness on Bending Strength of Douglas-fir Laminated Veneer Lumber". In: *Journal of the Indian Academy of Wood Science* 13.1 (June 2016), pp. 64–72. ISSN: 0972-172X, 0976-8432. DOI: [10.1007/s13196-016-0167-5](https://doi.org/10.1007/s13196-016-0167-5).
- [32] Rafael Rodolfo De Melo and Cláudio Henrique Soares Del Menezzi. "Influence of Veneer Thickness on the Properties of LVL from Paricá (*Schizolobium Amazonicum*) Plantation Trees". In: *European Journal of Wood and Wood Products* 72.2 (Mar. 2014), pp. 191–198. ISSN: 0018-3768, 1436-736X. DOI: [10.1007/s00107-013-0770-8](https://doi.org/10.1007/s00107-013-0770-8).
- [33] Citra Yanto Ciki Purba et al. "The Influence of Veneer Thickness and Knot Proportion on the Mechanical Properties of Laminated Veneer Lumber (LVL) Made from Secondary Quality Hardwood". In: *European Journal of Wood and Wood Products* 77.3 (May 2019), pp. 393–404. ISSN: 0018-3768, 1436-736X. DOI: [10.1007/s00107-019-01400-3](https://doi.org/10.1007/s00107-019-01400-3).
- [34] Erol Burdurlu et al. "The Effects of Ply Organization and Loading Direction on Bending Strength and Modulus of Elasticity in Laminated Veneer Lumber (LVL) Obtained from Beech (*Fagus Orientalis* L.) and Lombardy Poplar (*Populus Nigra* L.)" In: *Construction and Building Materials* 21.8 (2007). ISSN: 09500618. DOI: [10.1016/j.conbuildmat.2005.05.002](https://doi.org/10.1016/j.conbuildmat.2005.05.002).
- [35] S. R. Shukla and D. Pascal Kamdem. "Properties of Laboratory Made Yellow Poplar (*Liriodendron Tulipifera*) Laminated Veneer Lumber: Effect of the Adhesives". In: *European Journal of Wood and Wood Products* 67.4 (Nov. 2009), p. 397. ISSN: 0018-3768, 1436-736X. DOI: [10.1007/s00107-009-0333-1](https://doi.org/10.1007/s00107-009-0333-1).

- [36] Bekir Cihad Bal and İbrahim Bektaş. "The Effects of Wood Species, Load Direction, and Adhesives on Bending Properties of Laminated Veneer Lumber". In: *BioResources* 7.3 (May 2012), pp. 3104–3112. ISSN: 19302126, 19302126. DOI: [10.15376/biores.7.3.3104-3112](https://doi.org/10.15376/biores.7.3.3104-3112).
- [37] Semra Çolak, Gürsel Çolakoğlu, and Ismail Aydın. "Effects of Logs Steaming, Veneer Drying and Aging on the Mechanical Properties of Laminated Veneer Lumber (LVL)". In: *Building and Environment* 42.1 (Jan. 2007), pp. 93–98. ISSN: 03601323. DOI: [10.1016/j.buildenv.2005.08.008](https://doi.org/10.1016/j.buildenv.2005.08.008).
- [38] Abdelhakim Daoui et al. "Influence of Veneer Quality on Beech LVL Mechanical Properties". In: *Maderas. Ciencia y tecnología* 13.1 (2011), pp. 69–83. ISSN: 0718-221X. DOI: [10.4067/S0718-221X2011000100007](https://doi.org/10.4067/S0718-221X2011000100007).
- [39] Guillaume Pot, Louis-Etienne Denaud, and Robert Collet. "Numerical Study of the Influence of Veneer Lathe Checks on the Elastic Mechanical Properties of Laminated Veneer Lumber (LVL) Made of Beech". In: *Holzforschung* 69.3 (Apr. 2015), pp. 337–345. ISSN: 1437-434X, 0018-3830. DOI: [10.1515/hf-2014-0011](https://doi.org/10.1515/hf-2014-0011).
- [40] Wayan Darmawan et al. "Lathe Check Characteristics of Fast Growing Sengon Veneers and Their Effect on LVL Glue-Bond and Bending Strength". In: *Journal of Materials Processing Technology* 215 (Jan. 2015), pp. 181–188. ISSN: 09240136. DOI: [10.1016/j.jmatprotec.2014.08.015](https://doi.org/10.1016/j.jmatprotec.2014.08.015).
- [41] Wanzhao Li et al. "The Effect of Structural Changes on the Compressive Strength of LVL". In: *Wood Science and Technology* 54.5 (Sept. 2020), pp. 1253–1267. ISSN: 0043-7719, 1432-5225. DOI: [10.1007/s00226-020-01205-1](https://doi.org/10.1007/s00226-020-01205-1).
- [42] Wanzhao Li et al. "The Effect of Lathe Checks on the Mechanical Performance of LVL". In: *European Journal of Wood and Wood Products* 78.3 (May 2020), pp. 545–554. ISSN: 0018-3768, 1436-736X. DOI: [10.1007/s00107-020-01526-9](https://doi.org/10.1007/s00107-020-01526-9).
- [43] Gürsel Colakoglu et al. "Effect of Boric Acid Treatment on Mechanical Properties of Laminated Beech Veneer Lumber". In: *Silva Fennica* 37.4 (2003). ISSN: 22424075. DOI: [10.14214/sf.488](https://doi.org/10.14214/sf.488).
- [44] Ayhan Özçifçi, Yalçın Örs, and Burhanettin Uysal. "Determination of Some Physical and Mechanical Properties of Laminated Veneer Lumber Impregnated with Boron Compounds". In: *Journal of Applied Polymer Science* 105.4 (Aug. 2007), pp. 2218–2224. ISSN: 0021-8995, 1097-4628. DOI: [10.1002/app.26217](https://doi.org/10.1002/app.26217).
- [45] Brad Jianhe Wang and Chunping Dai. "Hot-Pressing Stress Graded Aspen Veneer for Laminated Veneer Lumber (LVL)". In: *Holzforschung* 59.1 (Jan. 2005), pp. 10–17. ISSN: 0018-3830, 1437-434X. DOI: [10.1515/HF.2005.002](https://doi.org/10.1515/HF.2005.002).

- [46] S. R. Shukla and D. Pascal Kamdem. "Properties of Laminated Veneer Lumber (LVL) Made with Low Density Hardwood Species: Effect of the Pressure Duration". In: *Holz als Roh- und Werkstoff* 66.2 (Apr. 2008), pp. 119–127. ISSN: 0018-3768, 1436-736X. DOI: [10.1007/s00107-007-0209-1](https://doi.org/10.1007/s00107-007-0209-1).
- [47] Ramazan Kurt et al. "Effect of Pressure Duration on Physical, Mechanical, and Combustibility Characteristics of Laminated Veneer Lumber (LVL) Made with Hybrid Poplar Clones". In: *BioResources* 6.4 (Oct. 2011), pp. 4886–4894. ISSN: 19302126, 19302126. DOI: [10.15376/biores.6.4.4886-4894](https://doi.org/10.15376/biores.6.4.4886-4894).
- [48] Ramazan Kurt and Muhammet Cil. "EFFECTS OF PRESS PRESSURES ON GLUE LINE THICKNESS AND PROPERTIES OF LAMINATED VENEER LUMBER GLUED WITH PHENOL FORMALDEHYDE ADHESIVE". In: *BioResources* 7.4 (Sept. 2012), pp. 5346–5354. ISSN: 1930-2126. DOI: [10.15376/biores.7.4.5346-5354](https://doi.org/10.15376/biores.7.4.5346-5354).
- [49] RISE Research Institute of Sweden. *The CLT Handbook*. Stockholm, Sweden: Swedish wood, 2019.
- [50] Marcin Chybiński and Łukasz Polus. "Experimental and Numerical Investigations of Laminated Veneer Lumber Panels". In: *Archives of Civil Engineering; 2021; vol. 67; No 3; 351-372* (2021). ISSN: 2300-3103. DOI: [10.24425/ace.2021.138060](https://doi.org/10.24425/ace.2021.138060).
- [51] WA van Beerschoten. "Structural Performance of Post-tensioned Timber Frames under Gravity Loading". PhD thesis. PhD Thesis, University of Canterbury, 2013.
- [52] Manoochehr Ardalany. "Analysis and Design of Laminated Veneer Lumber Beams with Holes". PhD thesis. PhD Thesis, University of Canterbury, 2012.
- [53] M. Ardalany et al. "Tension Perpendicular to Grain Strength of Wood, Laminated Veneer Lumber (LVL), and Cross-Banded LVL (LVL-C)". In: *Incorporating Sustainable Practice in Mechanics of Structures and Materials - Proceedings of the 21st Australian Conference on the Mechanics of Structures and Materials*. 2011. DOI: [10.1201/b10571-162](https://doi.org/10.1201/b10571-162).
- [54] Bettina Franke and Pierre Quenneville. "Analysis of the Fracture Behavior of Radiata Pine Timber and Laminated Veneer Lumber". In: *Engineering Fracture Mechanics* 116 (Jan. 2014), pp. 1–12. ISSN: 00137944. DOI: [10.1016/j.engfracmech.2013.12.004](https://doi.org/10.1016/j.engfracmech.2013.12.004).
- [55] Bekir Cihad Bal. "Some Physical and Mechanical Properties of Reinforced Laminated Veneer Lumber". In: *Construction and Building Materials* 68 (Oct. 2014), pp. 120–126. ISSN: 09500618. DOI: [10.1016/j.conbuildmat.2014.06.042](https://doi.org/10.1016/j.conbuildmat.2014.06.042).
- [56] Neda M. Sokolović et al. "Flexural Properties in Edgewise Bending of LVL Reinforced with Woven Carbon Fibers". In: *Materials* 16.9 (Apr. 2023), p. 3346. ISSN: 1996-1944. DOI: [10.3390/ma16093346](https://doi.org/10.3390/ma16093346).
- [57] Michał Marcin Bakalarz and Paweł Grzegorz Kossakowski. "Strengthening of Full-Scale Laminated Veneer Lumber Beams with CFRP Sheets". In: *Materials* 15.19 (Sept. 2022), p. 6526. ISSN: 1996-1944. DOI: [10.3390/ma15196526](https://doi.org/10.3390/ma15196526).

- [58] M. Moore. "Scotia Place – 12 Story Apartment Building A Case Study of High-Rise Construction Using Wood and Steel – WCTE 2000". In: 2000.
- [59] Andi Asiz and Ian Smith. "Connection System of Massive Timber Elements Used in Horizontal Slabs of Hybrid Tall Buildings". In: *Journal of Structural Engineering* 137.11 (2011). ISSN: 0733-9445. DOI: [10.1061/\(asce\)st.1943-541x.0000363](https://doi.org/10.1061/(asce)st.1943-541x.0000363).
- [60] Cristiano Loss, Maurizio Piazza, and Riccardo Zandonini. "Connections for Steel–Timber Hybrid Prefabricated Buildings. Part I: Experimental Tests". In: *Construction and Building Materials* 122 (2016). ISSN: 09500618. DOI: [10.1016/j.conbuildmat.2015.12.002](https://doi.org/10.1016/j.conbuildmat.2015.12.002).
- [61] Cristiano Loss, Maurizio Piazza, and Riccardo Zandonini. "Connections for Steel–Timber Hybrid Prefabricated Buildings. Part II: Innovative Modular Structures". In: *Construction and Building Materials* 122 (2016). ISSN: 09500618. DOI: [10.1016/j.conbuildmat.2015.12.001](https://doi.org/10.1016/j.conbuildmat.2015.12.001).
- [62] A. Hassanieh, H. R. Valipour, and M. A. Bradford. "Load-Slip Behaviour of Steel-Cross Laminated Timber (CLT) Composite Connections". In: *Journal of Constructional Steel Research* 122 (2016). ISSN: 0143974X. DOI: [10.1016/j.jcsr.2016.03.008](https://doi.org/10.1016/j.jcsr.2016.03.008).
- [63] A. Hassanieh, H. R. Valipour, and M. A. Bradford. "Composite Connections between CLT Slab and Steel Beam: Experiments and Empirical Models". In: *Journal of Constructional Steel Research* 138 (2017). ISSN: 0143974X. DOI: [10.1016/j.jcsr.2017.09.002](https://doi.org/10.1016/j.jcsr.2017.09.002).
- [64] A. Hassanieh et al. "Modelling of Steel-Timber Composite Connections: Validation of Finite Element Model and Parametric Study". In: *Engineering Structures* 138 (2017), pp. 35–49. ISSN: 18737323. DOI: [10.1016/j.engstruct.2017.02.016](https://doi.org/10.1016/j.engstruct.2017.02.016).
- [65] A. Hassanieh, H. R. Valipour, and M. A. Bradford. "Bolt Shear Connectors in Grout Pockets: Finite Element Modelling and Parametric Study". In: *Construction and Building Materials* 176 (2018). ISSN: 09500618. DOI: [10.1016/j.conbuildmat.2018.05.029](https://doi.org/10.1016/j.conbuildmat.2018.05.029).
- [66] Ruyuan Yang et al. "Mechanical Behaviour of Steel Timber Composite Shear Connections". In: *Construction and Building Materials* 258 (2020). ISSN: 09500618. DOI: [10.1016/j.conbuildmat.2020.119605](https://doi.org/10.1016/j.conbuildmat.2020.119605).
- [67] China's Ministry of Housing and Urban-Rural Development. *GB/T 50005-2017 Standard for Design of Timber Structures*. 2017.
- [68] American Wood Council. *National Design Specification (NDS) for Wood Construction 2018 Edition*. 2017. DOI: [978-1-940383-42-2](https://doi.org/10.1016/j.jcsr.2017.09.002).
- [69] European Committee for Standardisation CEN. *EN 1995-1-1:2004 - Eurocode 5: Design of Timber Structures - Part 1-1: General - Common Rules and Rules for Buildings*. 2004.
- [70] Chun Lin Wang et al. "Experimental Investigation of the Shear Characteristics of Steel-to-Timber Composite Joints with Inclined Self-Tapping Screws". In: *Engineering Structures* 215 (2020). ISSN: 18737323. DOI: [10.1016/j.engstruct.2020.110683](https://doi.org/10.1016/j.engstruct.2020.110683).

- [71] Yong Zhao et al. "Experimental Study on Shear Performance of Steel-Timber Screw Connectors with Grout Pockets". In: *Engineering Structures* 266 (Sept. 2022), p. 114535. ISSN: 0141-0296. DOI: [10.1016/J.ENGSTRUCT.2022.114535](https://doi.org/10.1016/J.ENGSTRUCT.2022.114535).
- [72] Ying Gao et al. "Experimental and Numerical Study on the Lateral Torsional Buckling of Full-Scale Steel-Timber Composite Beams". In: *Advances in Structural Engineering* 25.3 (Feb. 2022), pp. 522–540. ISSN: 1369-4332, 2048-4011. DOI: [10.1177/13694332211057263](https://doi.org/10.1177/13694332211057263).
- [73] Fabiana Yukiko Moritani et al. "ANALYTICAL AND EXPERIMENTAL STUDY ON REVERSIBLE STEEL-TIMBER COMPOSITE CONNECTION SYSTEMS". In: *World Conference on Timber Engineering (WCTE 2023)*. Oslo, Norway: World Conference on Timber Engineering (WCTE 2023), 2023, pp. 3364–3372. ISBN: 978-1-71387-329-7. DOI: [10.52202/069179-0438](https://doi.org/10.52202/069179-0438).
- [74] Marcin Chybiński and Łukasz Polus. "Experimental and Numerical Investigations of Aluminium-Timber Composite Beams with Bolted Connections". In: *Structures* 34 (Dec. 2021), pp. 1942–1960. ISSN: 23520124. DOI: [10.1016/j.istruc.2021.08.111](https://doi.org/10.1016/j.istruc.2021.08.111).
- [75] Marcin Chybiński and Łukasz Polus. "Mechanical Behaviour of Aluminium-Timber Composite Connections with Screws and Toothed Plates". In: *Materials* 15.1 (Dec. 2021), p. 68. ISSN: 1996-1944. DOI: [10.3390/ma15010068](https://doi.org/10.3390/ma15010068).
- [76] Yongfeng Zhou et al. "Experimental Study of the Shear Performance of H-shaped Aluminum-Timber Composite Connections". In: *Construction and Building Materials* 334 (June 2022), p. 127421. ISSN: 09500618. DOI: [10.1016/j.conbuildmat.2022.127421](https://doi.org/10.1016/j.conbuildmat.2022.127421).
- [77] Henan Zhang and Zhibin Ling. "Finite Element Modeling on Shear Performance of Grouted Stud Connectors for Steel-Timber Composite Beams". In: *Materials* 15.3 (Feb. 2022), p. 1196. ISSN: 1996-1944. DOI: [10.3390/ma15031196](https://doi.org/10.3390/ma15031196).
- [78] Noah Böhm, Achim Vogelsberg, and Bertram Kühn. "Investigations of the Shear Connectors and the Load-bearing Behaviour of Steel Cross-laminated Timber Composite Beams". In: *ce/papers* 6.3-4 (Sept. 2023), pp. 78–83. ISSN: 2509-7075, 2509-7075. DOI: [10.1002/cepa.2379](https://doi.org/10.1002/cepa.2379).
- [79] A. Ataei et al. "Cyclic Behaviour of Bolt and Screw Shear Connectors in Steel-Timber Composite (STC) Beams". In: *Journal of Constructional Steel Research* 161 (2019). ISSN: 0143974X. DOI: [10.1016/j.jcsr.2019.05.048](https://doi.org/10.1016/j.jcsr.2019.05.048).
- [80] A. Ataei et al. "Behaviour of Embedded Bolted Shear Connectors in Steel-Timber Composite Beams Subjected to Cyclic Loading". In: *Journal of Building Engineering* 54 (Aug. 2022), p. 104581. ISSN: 23527102. DOI: [10.1016/j.jobbe.2022.104581](https://doi.org/10.1016/j.jobbe.2022.104581).
- [81] European Committee for Standardisation CEN. *EN 1998-1:2004 - Eurocode 8: Design of Structures for Earthquake Resistance - Part 1: General Rules, Seismic Actions and Rules for Buildings*. 2004.

- [82] A. A. Chiniforush et al. "Long-Term Behaviour of Steel-Timber Composite (STC) Shear Connections". In: *Engineering Structures* 196 (2019). ISSN: 18737323. DOI: [10.1016/j.engstruct.2019.109356](https://doi.org/10.1016/j.engstruct.2019.109356).
- [83] Andi Asiz and Ian Smith. "Demands Placed on Steel Frameworks of Tall Buildings Having Reinforced Concrete or Massive Wood Horizontal Slabs". In: *Structural Engineering International* 19.4 (Nov. 2009), pp. 395–403. ISSN: 1016-8664, 1683-0350. DOI: [10.2749/101686609789847000](https://doi.org/10.2749/101686609789847000).
- [84] A. Hassanieh, H. R. Valipour, and M. A. Bradford. "Experimental and Numerical Investigation of Short-Term Behaviour of CLT-steel Composite Beams". In: *Engineering Structures* 144 (2017). ISSN: 18737323. DOI: [10.1016/j.engstruct.2017.04.052](https://doi.org/10.1016/j.engstruct.2017.04.052).
- [85] Cristiano Loss and Buick Davison. "Innovative Composite Steel-Timber Floors with Prefabricated Modular Components". In: *Engineering Structures* 132 (2017). ISSN: 18737323. DOI: [10.1016/j.engstruct.2016.11.062](https://doi.org/10.1016/j.engstruct.2016.11.062).
- [86] David Owolabi and Cristiano Loss. "Experimental and Numerical Study on the Bending Response of a Prefabricated Composite CLT-steel Floor Module". In: *Engineering Structures* 260 (June 2022), p. 114278. ISSN: 01410296. DOI: [10.1016/j.engstruct.2022.114278](https://doi.org/10.1016/j.engstruct.2022.114278).
- [87] Yong Zhao et al. "Experimental and Finite Element Analysis of Flexural Performance of Steel-Timber Composite Beams Connected by Hybrid-Anchored Screws". In: *Engineering Structures* 292 (Oct. 2023), p. 116503. ISSN: 01410296. DOI: [10.1016/j.engstruct.2023.116503](https://doi.org/10.1016/j.engstruct.2023.116503).
- [88] Noah Böhm, Achim Vogelsberg, and Bertram Kühn. "Bending and Vibration Behaviour of CLT-Steel Composite Beams". In: *Journal of Sustainable Architecture and Civil Engineering* 34.1 (Feb. 2024), pp. 75–88. ISSN: 2335-2000, 2029-9990. DOI: [10.5755/j01.sace.34.1.35467](https://doi.org/10.5755/j01.sace.34.1.35467).
- [89] Nicka Keipour, Hamid R. Valipour, and Mark A. Bradford. "Steel-Timber versus Steel-Concrete Composite Floors: A Numerical Study". In: *WCTE 2016 - World Conference on Timber Engineering*. 2016.
- [90] Markku Heinisuo et al. "NEW STEEL-TIMBER COMPOSITE BEAM, NORDIC SYSTEM". In: *ce/papers* 3.5-6 (2019). ISSN: 2509-7075. DOI: [10.1002/cepa.1194](https://doi.org/10.1002/cepa.1194).
- [91] Aku Aspila et al. "Elastic Design of Steel-Timber Composite Beams". In: *Wood Material Science & Engineering* 17.4 (July 2022), pp. 243–252. ISSN: 1748-0272, 1748-0280. DOI: [10.1080/17480272.2022.2093128](https://doi.org/10.1080/17480272.2022.2093128).
- [92] Julia Strzelecka, Łukasz Polus, and Marcin Chybiński. "Theoretical and Numerical Analyses of Steel-timber Composite Beams with LVL Slabs". In: *Civil and Environmental Engineering Reports* 33.2 (Sept. 2023), pp. 64–84. ISSN: 2080-5187, 2450-8594. DOI: [10.59440/ceer/172510](https://doi.org/10.59440/ceer/172510).

- [93] Karl Möhler. "Über Das Tragverhalten von Biegeträgern Und Druckstäben Mit Zusammengesetzten Querschnitten Und Nachgiebigen Verbindungsmitteln". PhD thesis. 1956.
- [94] European Committee for Standardisation CEN. *EN 1994-1-1:2004 - Design of Composite Steel and Concrete Structures - Part 1-1: General Rules and Rules for Buildings*. 2004.
- [95] N. Keipour, H. R. Valipour, and M. A. Bradford. "Steel-Timber Composite Beam-to-Column Joints: Effect of Connections between Timber Slabs". In: *Journal of Constructional Steel Research* 151 (2018). ISSN: 0143974X. DOI: [10.1016/j.jcsr.2018.09.019](https://doi.org/10.1016/j.jcsr.2018.09.019).
- [96] Shahryar Qazizadeh, S.K. Hashemi, and H.R. Valipour. "Numerical Investigation of Steel-Timber Composite Floors with Flush End-Plate Connection". In: *Structures* 56 (2023), p. 104892. ISSN: 23520124. DOI: [10.1016/j.istruc.2023.104892](https://doi.org/10.1016/j.istruc.2023.104892).
- [97] N. Keipour, H. R. Valipour, and M. A. Bradford. "Experimental Study of Steel-Timber Composite (STC) Beam to Steel Column Joints Having a Flush End-Plate". In: *Engineering Structures* 174 (2018). ISSN: 18737323. DOI: [10.1016/j.engstruct.2018.08.009](https://doi.org/10.1016/j.engstruct.2018.08.009).
- [98] Farshid Nouri, Mark Bradford, and Hamid Valipour. "Steel-Timber Composite Beam-to-Column Connections with Shear Tab". In: *Journal of Structural Engineering* 145.3 (2019). ISSN: 0733-9445. DOI: [10.1061/\(asce\)st.1943-541x.0002274](https://doi.org/10.1061/(asce)st.1943-541x.0002274).
- [99] Abdolreza Ataei et al. "Experimental Study of Steel-Timber Composite Beam-to-Column Joints with Extended End Plates". In: *Construction and Building Materials* 226 (2019). ISSN: 09500618. DOI: [10.1016/j.conbuildmat.2019.07.154](https://doi.org/10.1016/j.conbuildmat.2019.07.154).
- [100] F. Nouri and H. R. Valipour. "Semi-Rigid Partial-Strength Steel-Timber Composite (STC) Connections with Mechanically Anchored Steel Rods". In: *Journal of Constructional Steel Research* 158 (2019). ISSN: 0143974X. DOI: [10.1016/j.jcsr.2019.04.017](https://doi.org/10.1016/j.jcsr.2019.04.017).
- [101] F. Nouri, H. R. Valipour, and M. A. Bradford. "Finite Element Modelling of Steel-Timber Composite Beam-to-Column Joints with Nominally Pinned Connections". In: *Engineering Structures* 201 (2019). ISSN: 18737323. DOI: [10.1016/j.engstruct.2019.109854](https://doi.org/10.1016/j.engstruct.2019.109854).
- [102] F. Nouri, H. R. Valipour, and M. A. Bradford. "Structural Behaviour of Steel-Timber Composite (STC) Beam-to-Column Connections with Double Angle Web Cleats Subjected to Hogging Bending Moment". In: *Engineering Structures* 192 (2019). ISSN: 18737323. DOI: [10.1016/j.engstruct.2019.04.092](https://doi.org/10.1016/j.engstruct.2019.04.092).
- [103] F. Nouri and H. R. Valipour. "Moment-Rotation Model for Steel-Timber Composite Connections with Slab Continuity Steel Rods". In: *Journal of Constructional Steel Research* 173 (2020). ISSN: 0143974X. DOI: [10.1016/j.jcsr.2020.106257](https://doi.org/10.1016/j.jcsr.2020.106257).
- [104] Nicka Keipour, Hamid R. Valipour, and Mark A. Bradford. "Structural Behaviour of Steel-Timber versus Steel-Concrete Composite Joints with Flush End Plate". In: *Construction and Building Materials* 262 (2020). ISSN: 09500618. DOI: [10.1016/j.conbuildmat.2020.120885](https://doi.org/10.1016/j.conbuildmat.2020.120885).

- [105] Alireza A. Chiniforush et al. "Steel-timber Composite (STC) Beams: Numerical Simulation of Long-term Behaviour". In: *ce/papers* 1.2-3 (Sept. 2017), pp. 2051–2059. ISSN: 2509-7075, 2509-7075. DOI: [10.1002/cepa.250](https://doi.org/10.1002/cepa.250).
- [106] Alireza A. Chiniforush, Ali Akbarnezhad, and Sardar Malek. "Time-Dependent Deflection Measurement for Steel-Timber Composite (STC) Flooring System". In: *International Conference on Advances in Experimental Structural Engineering*. Vol. 2020-February. 2020.
- [107] A.A. Chiniforush et al. "Experimental and Theoretical Investigation of Long-Term Performance of Steel-Timber Composite Beams". In: *Engineering Structures* 249 (Dec. 2021), p. 113314. ISSN: 01410296. DOI: [10.1016/j.engstruct.2021.113314](https://doi.org/10.1016/j.engstruct.2021.113314).
- [108] A.A. Chiniforush, H.R. Valipour, and A. Akbarnezhad. "Long-Term Coupled Analysis of Steel-Timber Composite (STC) Beams". In: *Construction and Building Materials* 278 (Apr. 2021), p. 122348. ISSN: 09500618. DOI: [10.1016/j.conbuildmat.2021.122348](https://doi.org/10.1016/j.conbuildmat.2021.122348).
- [109] Angelo Aloisio et al. "Vibration Serviceability of Hybrid CLT-steel Composite Floors Based on Experimental and Numerical Investigations Using Random Walk Models". In: *Engineering Structures* 304 (Apr. 2024), p. 117600. ISSN: 01410296. DOI: [10.1016/j.engstruct.2024.117600](https://doi.org/10.1016/j.engstruct.2024.117600). (Visited on 06/13/2024).
- [110] David Owolabi and Cristiano Loss. "EXPERIMENTAL STUDY ON THE VIBRATION CHARACTERISTICS OF A PREFABRICATED CROSS-LAMINATED TIMBER-STEEL COMPOSITE FLOOR". In: *World Conference on Timber Engineering (WCTE 2023)*. Oslo, Norway: World Conference on Timber Engineering (WCTE 2023), 2023, pp. 1880–1887. ISBN: 978-1-71387-329-7. DOI: [10.52202/069179-0248](https://doi.org/10.52202/069179-0248).
- [111] David Owolabi, Cristiano Loss, and Jianhui Zhou. "Vibration Properties and Serviceability Performance of a Modular Cross-Laminated Timber-Steel Composite Floor System". In: *Journal of Structural Engineering* 149.12 (Dec. 2023), p. 04023171. ISSN: 0733-9445, 1943-541X. DOI: [10.1061/JSENDH.STENG-12587](https://doi.org/10.1061/JSENDH.STENG-12587).
- [112] A. A. Chiniforush et al. "DYNAMIC RESPONSE OF STEEL-TIMBER COMPOSITE (STC) BEAMS". In: *Proceedings of the 24th International Congress on Sound and Vibration*. London, UK, 2017.
- [113] A. A. Chiniforush et al. "Vibration Behaviour of Steel-Timber Composite Floors, Part (1): Experimental & Numerical Investigation". In: *Journal of Constructional Steel Research* 161 (2019). ISSN: 0143974X. DOI: [10.1016/j.jcsr.2019.07.007](https://doi.org/10.1016/j.jcsr.2019.07.007).
- [114] A. Hassanieh et al. "Vibration Behaviour of Steel-Timber Composite Floors, Part (2): Evaluation of Human-Induced Vibrations". In: *Journal of Constructional Steel Research* 158 (2019). ISSN: 0143974X. DOI: [10.1016/j.jcsr.2019.03.026](https://doi.org/10.1016/j.jcsr.2019.03.026).

- [115] Haoyu Huang, Yan Gao, and Wen-Shao Chang. “Human-Induced Vibration of Cross-Laminated Timber (CLT) Floor under Different Boundary Conditions”. In: *Engineering Structures* 204 (Feb. 2020), p. 110016. ISSN: 01410296. DOI: [10.1016/j.engstruct.2019.110016](https://doi.org/10.1016/j.engstruct.2019.110016).
- [116] Chang Wang et al. “Predicting the Human-Induced Vibration of Cross Laminated Timber Floor under Multi-Person Loadings”. In: *Structures* 29 (Feb. 2021), pp. 65–78. ISSN: 23520124. DOI: [10.1016/j.istruc.2020.10.074](https://doi.org/10.1016/j.istruc.2020.10.074).
- [117] Najmeh Cheraghi-Shirazi, Keith Crews, and Sardar Malek. “Review of Vibration Assessment Methods for Steel-Timber Composite Floors”. In: *Buildings* 12.12 (Nov. 2022), p. 2061. ISSN: 2075-5309. DOI: [10.3390/buildings12122061](https://doi.org/10.3390/buildings12122061).
- [118] Hassan Karampour et al. “Vibration of Timber and Hybrid Floors: A Review of Methods of Measurement, Analysis, and Design”. In: *Buildings* 13.7 (July 2023), p. 1756. ISSN: 2075-5309. DOI: [10.3390/buildings13071756](https://doi.org/10.3390/buildings13071756).
- [119] Zheng Li et al. “In-Plane Behavior of Timber-Steel Hybrid Floor Diaphragms: Experimental Testing and Numerical Simulation”. In: *Journal of Structural Engineering* 142.12 (Dec. 2016), p. 04016119. ISSN: 0733-9445, 1943-541X. DOI: [10.1061/\(ASCE\)ST.1943-541X.0001601](https://doi.org/10.1061/(ASCE)ST.1943-541X.0001601).
- [120] Cristiano Loss and Andrea Frangi. “Experimental Investigation on In-Plane Stiffness and Strength of Innovative Steel-Timber Hybrid Floor Diaphragms”. In: *Engineering Structures* 138 (May 2017), pp. 229–244. ISSN: 01410296. DOI: [10.1016/j.engstruct.2017.02.032](https://doi.org/10.1016/j.engstruct.2017.02.032).
- [121] Cristiano Loss, Stefano Rossi, and Thomas Tannert. “In-Plane Stiffness of Hybrid Steel–Cross-Laminated Timber Floor Diaphragms”. In: *Journal of Structural Engineering* 144.8 (Aug. 2018), p. 04018128. ISSN: 0733-9445, 1943-541X. DOI: [10.1061/\(ASCE\)ST.1943-541X.0002105](https://doi.org/10.1061/(ASCE)ST.1943-541X.0002105).
- [122] Metsä Wood. *Kerto LVL*. 2020.
- [123] Marcin Chybiński and Łukasz Polus. “Experimental Study of Aluminium-Timber Composite Bolted Connections Strengthened with Toothed Plates”. In: *Materials* 15.15 (July 2022), p. 5271. ISSN: 1996-1944. DOI: [10.3390/MA15155271](https://doi.org/10.3390/MA15155271).
- [124] ArcelorMittal. *XCarb - Towards Carbon Neutral Steel*.
- [125] European Committee for Standardisation CEN. *EN 10025 - Hot Rolled Products for Structural Steels*. Brussels, Belgium, 2004.
- [126] European Committee for Standardisation CEN. *EN 912 - Timber Fasteners - Specifications for Connectors for Timbers*. Brussels, Belgium, 2011.
- [127] DIBt. *ETA-11/0190 - European Technical Assessment of Würth Self-Tapping Screws*. 2018.
- [128] European Committee for Standardisation CEN. *EN 14399 - High-strength Structural Bolt-ing Assemblies for Preloading*. Brussels, Belgium, 2015.

- [129] European Committee for Standardisation CEN. *EN 1993-1-8:2005 - Eurocode 3: Design of Steel Structures - Part 1-8: Design of Joints*. 2005.
- [130] European Committee for Standardisation CEN. *EN 1090-2- Execution of Steel Structures and Aluminium Structures - Part 2: Technical Requirements for Steel Structures*. Brussels, Belgium, 2018.
- [131] European Committee for Standardisation CEN. *EN 408:2010 - Timber Structures - Structural Timber and Glued Laminated Timber - Determination of Some Physical and Mechanical Properties*. 2012.
- [132] European Committee for Standardisation CEN. *EN 789 - Timber Structures - Test Methods - Determination of Mechanical Properties of Wood Based Panels*. 2014.
- [133] European Committee for Standardisation CEN. *EN 14358 - Timber Structures - Calculation and Verification of Characteristic Values*. 2015.
- [134] Metsä Wood. *Kerto® LVL Q-panel*. Finland, 2022.
- [135] European Committee for Standardisation CEN. *EN ISO 6892-1 Metallic Materials - Tensile Testing (Part 1: Method of Test at Room Temperature)*. Brussels, Belgium, 2016.
- [136] European Committee for Standardisation CEN. *EN 26891 - Timber Structures - Joints Made with Mechanical Fasteners - General Principles for the Determination of Strength and Deformation Characteristics*. Switzerland.
- [137] PAGEL. *Pagel Super High Strength Grout C100/115 (Technical Data Sheet)*. 2021.
- [138] Reza Masoudnia, Ashkan Hashemi, and Pierre Quenneville. "Predicting the Effective Flange Width of a CLT Slab in Timber Composite Beams". In: *Journal of Structural Engineering* 144.7 (July 2018), p. 04018084. ISSN: 0733-9445, 1943-541X. DOI: [10.1061/\(ASCE\)ST.1943-541X.0001979](https://doi.org/10.1061/(ASCE)ST.1943-541X.0001979).
- [139] Miriam Kleinhenz et al. "DETERMINATION OF THE EFFECTIVE WIDTH OF CROSS-LAMINATED TIMBER RIB PANELS USING DIGITAL IMAGE CORRELATION". In: *World Conference on Timber Engineering (WCTE 2023)*. Oslo, Norway: World Conference on Timber Engineering (WCTE 2023), 2023, pp. 2416–2425. DOI: [10.52202/069179-0319](https://doi.org/10.52202/069179-0319).
- [140] Andrea Frangi and Mario Fontana. "Elasto-Plastic Model for Timber-Concrete Composite Beams with Ductile Connection". In: *Structural Engineering International* 13.1 (Feb. 2003), pp. 47–57. ISSN: 1016-8664. DOI: [10.2749/101686603777964856](https://doi.org/10.2749/101686603777964856).
- [141] L. Bathon and N. Graf. "A Continuous Wood-Concrete-Composite System". In: *Proceedings WCTE 2000*. Whistler, BC., 2000.
- [142] Dassault Systèmes Simulia Corp. *Abaqus/CAE*. Providence, RI, USA, 2021.
- [143] Xiang Yun and Leroy Gardner. "Stress-Strain Curves for Hot-Rolled Steels". In: *Journal of Constructional Steel Research* 133 (2017). ISSN: 0143974X. DOI: [10.1016/j.jcsr.2017.01.024](https://doi.org/10.1016/j.jcsr.2017.01.024).

- [144] Klara Winter, Roland Maderebner, and Philipp Dietsch. "A NEW APPROACH TO DETERMINE AND EVALUATE THE POISSON'S RATIO OF WOOD". In: *World Conference on Timber Engineering (WCTE 2023)*. Oslo, Norway: World Conference on Timber Engineering (WCTE 2023), 2023, pp. 366–375. ISBN: 978-1-71387-329-7. DOI: [10.52202/069179-0050](https://doi.org/10.52202/069179-0050).
- [145] Rodney Hill. *The Mathematical Theory of Plasticity*. The Oxford Engineering Science Series 11. Oxford: Clarendon Press, 2009. ISBN: 978-0-19-850367-5.
- [146] ABAQUS. *Abaqus User's Manual Version 2019*. 2019.
- [147] European Committee for Standardisation CEN. *EN 1993-1-1:2005 - Eurocode 3: Design of Steel Structures - Part 1-1: General Rules and Rules for Buildings*. 2005.
- [148] Christoph Odenbreit, Andras Kozma, and Alfredo Romero. "Discussion of an Algorithm to Transfer Arbitrary Shear Connector Load-Slip Curves into an Effective Shear Resistance". In: *23. DAST-Forschungskolloquium*. Dortmund: Deutscher Ausschuss für Stahlbau, Feb. 2022, pp. 93–96.
- [149] András Kozma et al. "A New Concept and Algorithm to Transfer Brittle and Arbitrary Load-Slip Curves into an Effective Shear Resistance Suitable for Eurocode 4". In: *Journal of Theoretical and Applied Mechanics* (2022). ISSN: 1429-2955. DOI: [10.15632/jtam-pl/156164](https://doi.org/10.15632/jtam-pl/156164).
- [150] Jean-Marie Aribert. "Analyse et Formulation Pratique de l'influence de La Nuance de l'acier Du Profilé Sur Le Degré Minimum de Connection Partielle d'une Poutre Mixte". In: *Construction Métallique* 3–1997 (1997).
- [151] Andras Kozma, Jie Yang, and Christoph Odenbreit. "Effective Resistance of Demountable Shear Connectors". In: *Proceedings of the 14th International Conference on Metal Structures - ICMS 2021* (2021).
- [152] Lorik Rugova. "Finite Element Simulation of Load Bearing Behaviour of Steel-Timber Composite Beams". M.S. Thesis. Luxembourg: University of Luxembourg, 2021.
- [153] Melis Pelivani. "Strain Controlled Bending Capacity of Composite Steel-Timber Sections". M.S. Thesis. Luxembourg: University of Luxembourg, 2022.
- [154] Paulinus Akhigbe. "Strain Controlled Bending Resistance of Steel-Timber Composite Sections with Non-Linear Material Behavior". M.S. Thesis. Luxembourg: University of Luxembourg, 2023.
- [155] Aikaterini Pachi and Tianjian Ji. "Frequency and Velocity of People Walking". In: *The Structural Engineer* 83.3 (2005).
- [156] T. Ji and B.R. Ellis. "Floor Vibration Induced by Dance-Type Loads: Theory". In: *The Structural Engineer* 72.3 (1994).
- [157] A. L. Smith, S. J. Hicks, and P. J. Devine. *Design of Floors for Vibration: A New Approach*. Ascot: Steel Construction Institute, 2009. ISBN: 978-1-85942-176-5.

- [158] European Commission - Directorate General for Research. *Human-Induced Vibration of Steel Structures (Hivoss)*. Luxembourg: Publications Office, 2010.
- [159] American Institute of Steel Construction. *AISC Design Guide 11: Vibrations of Steel-Framed Structural Systems Due to Human Activity*. 2016.
- [160] WoodWorks - Wood Products Council. *Mass Timber Floor Vibration Design Guide*. United States, 2023.
- [161] International Organisation for Standardisation. *ISO 10137:2007 Bases for Design of Structures - Serviceability of Buildings and Walkways against Vibrations*. 2007.
- [162] International Organisation for Standardisation. *ISO 2631-1:1997 Mechanical Vibration and Shock - Evaluation of Human Exposure to Whole-Body Vibration*. 1997.
- [163] International Organisation for Standardisation. *ISO 2631-2:2003 Mechanical Vibration and Shock - Evaluation of Human Exposure to Whole-Body Vibration*. 2003.
- [164] German Institute for Standardisation. *DIN 4150-2:2023 Vibrations in Buildings - Part 2: Effects on People in Buildings*. 2023.
- [165] British Standard Institution. *BS 6472-1:2008 Guide to Evaluation of Human Exposure to Vibration in Buildings - Vibration Sources Other than Blasting*. 2008.
- [166] American National Standards Institute. *ANSI S3.29-1983: Guide to Evaluation of Human Exposure to Vibration in Buildings*. 1983.

ANNEX

A

ANALYTICAL STRAIN-BASED PROCEDURE

A.1. MOMENT RESISTANCE FOR FULL-RIGID SHEAR CONNECTION

The procedure to estimate the moment resistance for rigid shear connection is as follows:

1. Define the amount n of layers through the cross-section of the STC beam.
2. Establish the material constitutive laws for the timber slab and the steel beam.
3. Define the strain limits for tension and compression for both materials.
4. Set the initial strain distribution, fixed at the bottom fibre of the steel section at the strain limit in tension, and at the top fibre of timber with a small compressive strain value equal to the incremental strain step ($\Delta\epsilon$) as shown in Figure A.1a. It must be checked that the strain distribution does not exceed the imposed strain limits of timber in tension, when the limits are exceeded in this initial strain distribution, the tensile strain at the bottom fibre of the steel beam must be reduced until the strain limits are not exceeded (see Figure A.1b).

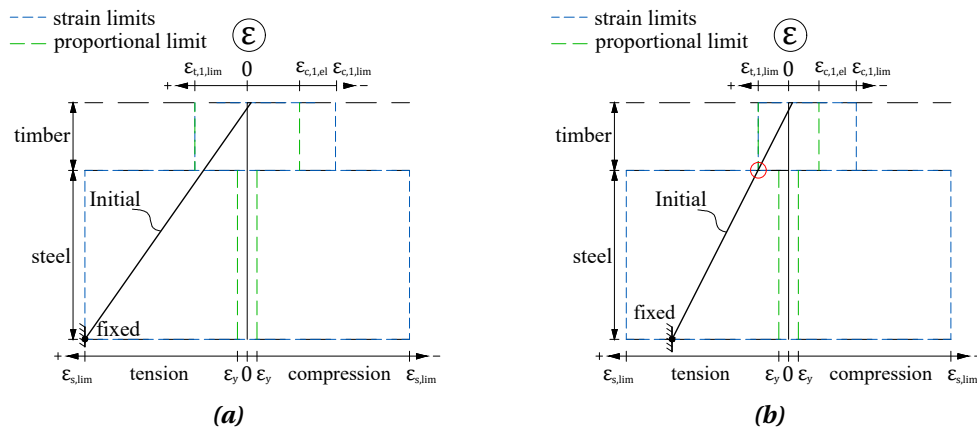


Figure A.1: Possible initial strain distributions: (a) fixed at the bottom fibre of the steel section at the strain limit in tension; and (b) constrained by the strain limit in tension of the timber slab and fixed at the maximum possible strain in tension at the bottom fibre of the steel section.

5. The average strains and stresses are obtained at each layer based on the material constitutive laws.
6. The internal normal forces at every layer are computed and equilibrium in the cross-section is checked.
7. If equilibrium is not reached a new strain distribution is set, keeping the strain at the bottom fibre of the steel beam fixed, the strain at the top fibre of the timber is increased by the incremental strain step $\Delta\epsilon$ (see Figure A.2). Then, steps 5 to 7 are repeated until equilibrium is reached.

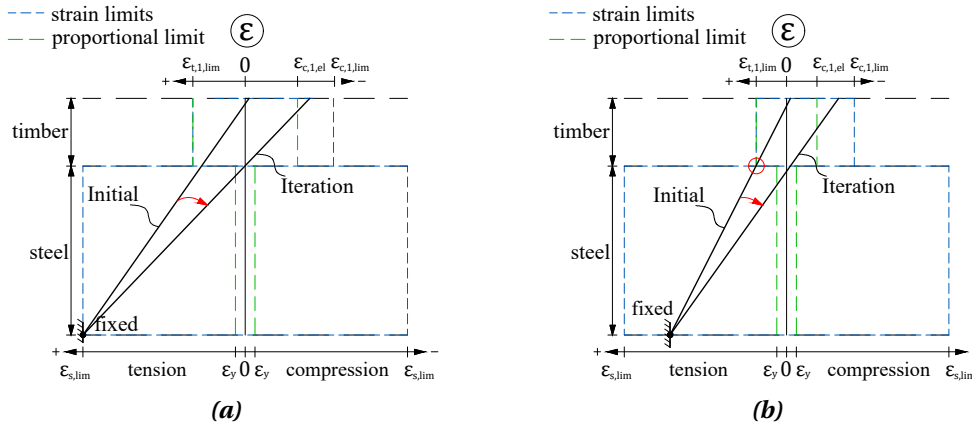


Figure A.2: Illustration of the strain distributions at iteration steps for the two cases considered: (a) strain at the bottom fibre of the steel section fixed at the strain limit in tension and increments at the top fibre of the timber slab; and (b) initial strain constrained by the strain limit of the bottom fibre of the timber slab.

8. There is a possibility that equilibrium is not achieved upon reaching the limit compressive strain at the top fibre of the timber slab. In such case, the tensile forces have to be reduced by the incremental step $\Delta\epsilon$ while fixing the strain at the top fibre of the timber in every iteration as shown in Figure A.3. Thus, steps 5, 6 and 8 are repeated until equilibrium has been reached.

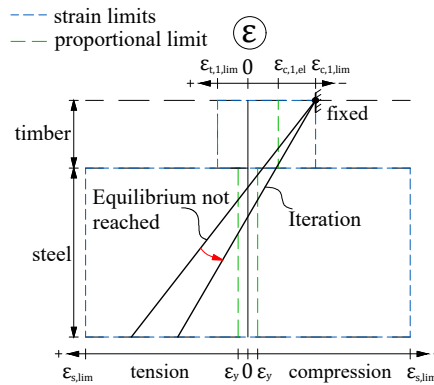


Figure A.3: Strain distribution fixed at the top fibre of the timber slab at the strain limit in compression.

9. The moment resistance is calculated considering the normal forces of the layers at the equilibrium state and their lever arms with respect to a reference in the section (e.g. the top fibre of the cross-section).
10. The resultant normal force in the timber slab is calculated considering the forces of the layers within the timber slab.

A.2. MOMENT RESISTANCE FOR NO SHEAR CONNECTION

The procedure to estimate the moment resistance for the case of no shear connection is as follows:

1. Define the amount n of layers through the cross-section of the STC beam.
2. Establish the material constitutive laws for the timber slab and the steel beam.
3. Define the strain limits in tension and compression for both materials.
4. Set the initial strain distribution, fixed at the bottom fibre of the timber section at the strain limit in tension, and at the top fibre of timber with a small strain value equal to the incremental strain step $\Delta\epsilon$ (see Figure A.4).

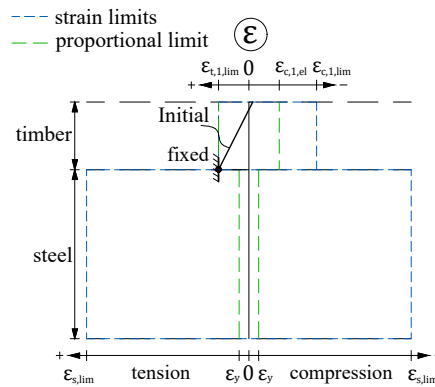
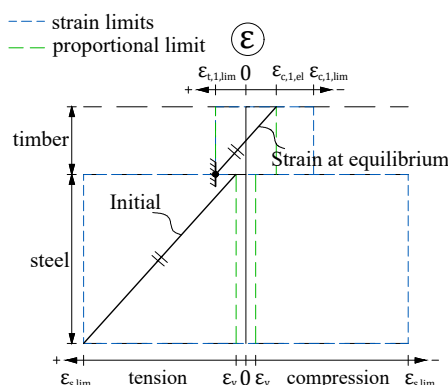


Figure A.4: Initial strain distribution in the timber slab.

5. The average strains and stresses are obtained at each layer based on the material constitutive law.
6. The internal normal forces at every layer of the timber slab are computed and equilibrium in the timber cross-section is checked.
7. If equilibrium is not reached a new strain distribution is set, keeping the strain at the bottom fibre of the timber slab fixed, the strain at the top fibre of the timber is increased by the incremental strain step $\Delta\epsilon$ (see Figure A.5). Then, steps 5 to 7 are repeated until equilibrium is reached.

8. The slope of the strain distribution of the timber slab at the equilibrium state is calculated.
9. Set the initial strain distribution in the steel section with the same slope (i.e. the strain distributions of timber and steel must be parallel to ensure compatibility of deformations) of the strain distribution in the timber slab calculated in step 4, with the strain at the bottom fibre equal to the limit strain in tension (see Figure A.6).



10. The average strains and stresses are obtained at each layer based on the material constitutive law.
11. The internal normal forces at every layer are computed and equilibrium in the cross-section is checked.
12. If equilibrium is not reached a new strain distribution is set, the new strain distribution is a parallel line at a distance $\Delta \epsilon$ of the previous strain distribution. This means that the slope of the strain distribution is kept in every iteration, and the strain distribution in the steel section moves towards the compression zone in each iteration (see Figure A.7). Steps 11 to 13 are repeated until equilibrium in the steel section is reached.

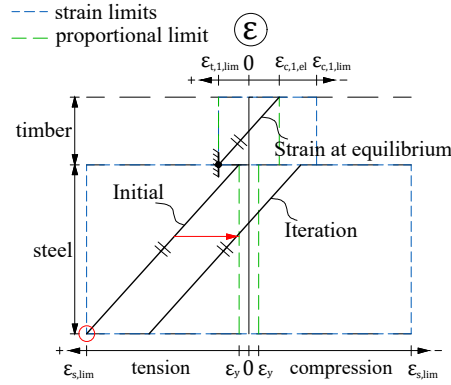


Figure A.7: Strain distribution in the steel beam at an iteration, it must be parallel to the strain distribution in the timber slab.

13. The moment resistance is calculated considering the normal forces of the layers at the equilibrium state and their lever arms with respect to a reference in the section (e.g. the top fibre of the cross-section).

A.3. MOMENT RESISTANCE FOR PARTIAL SHEAR CONNECTION

The calculation of the moment resistance for partial shear connection cases is only possible after estimating the moment resistance of the cross-section for the cases of full-rigid shear connection and no shear connection, this is because the strain distributions of these cases are used as boundaries. The procedure to estimate the moment resistance for the case of partial shear connection is as follows:

1. Define the amount n of layers through the cross-section of the STC beam.
2. Establish the material constitutive laws for the timber slab and the steel beam.
3. Define the strain limits in tension and compression for both materials.
4. Set two reference points in the timber slab, one at the top fibre of the timber slab at the intersection with the strain distribution for full-rigid shear connection (point A) and another point at the bottom fibre of the timber slab at the intersection with the strain distribution for no shear connection (point B) as shown in Figure A.8.
5. Define the strain distributions to be considered for the calculation of multiple moment resistance values within the upper and lower bounds determined previously. To do so, consider the strain distributions for the cases of full-rigid shear connection and no shear connection and divide the bottom and the top fibre of the timber slab by equally spaced points (see Figure A.8).
6. Link the points defined in the previous step to the reference points A and B, these links would be the reference strain distributions. The point A will be linked to the points defined in the bottom fibre of the timber slab and the point B will be linked to the points defined in the top fibre of the timber slab as shown in Figure A.9.

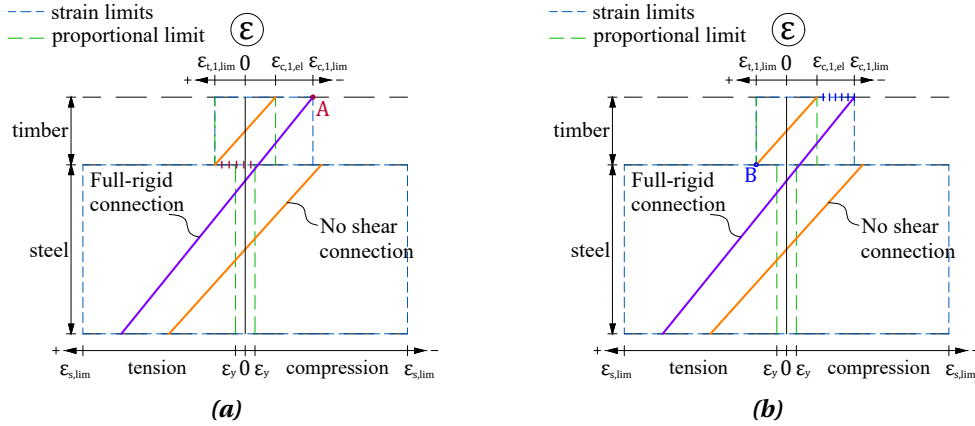


Figure A.8: Illustration of the reference points (a) at the top fibre of the timber slab (point A) with its corresponding segments at the bottom fibre; and (b) at the bottom fibre of the timber slab (point B) with its corresponding segments at the top fibre.

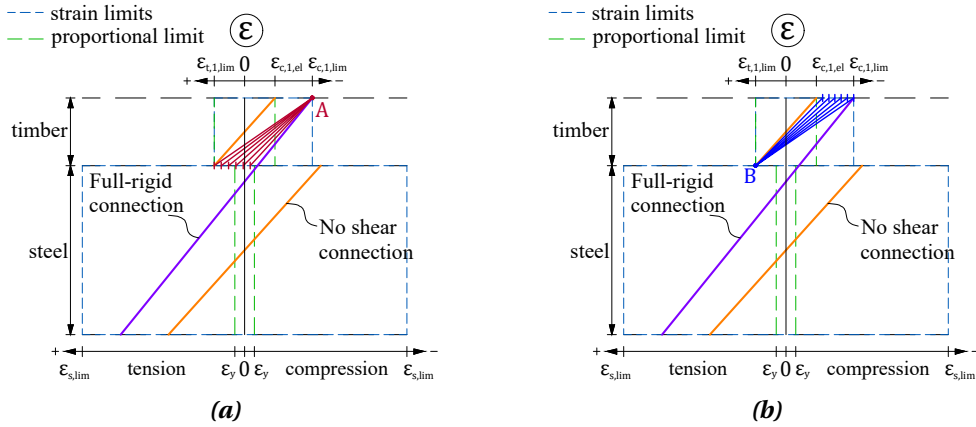


Figure A.9: Illustration of the links between reference points and their corresponding segments (i.e. strain distributions) (a) at the top fibre of the timber slab (point A) with its corresponding segments at the bottom fibre; and (b) at the bottom fibre of the timber slab (point B) with its corresponding segments at the top fibre.

7. Calculate the slope of the strain distributions in the timber defined in 6.
8. For each one of the strain distributions set the initial strain distribution in the steel section with the same slope of the strain distribution in the timber slab calculated in step 7, and with the strain at the bottom fibre equal to the limit strain in tension. An example is shown in Figure A.10.
9. The average strains and stresses are obtained at each layer based on the material constitutive laws.
10. The internal normal forces at every layer are computed and equilibrium in the cross-section is checked.
11. If equilibrium is not reached a new strain distribution in the steel section is set, the new strain distribution is a parallel line at a distance $\Delta\epsilon$ of the previous strain distribution

(see Figure A.11). This means that the slope of the strain distribution is kept in every iteration, and the strain distribution in the steel section moves towards the compression zone in each iteration. Steps 9 to 11 are repeated until equilibrium in the steel section is reached.

12. The moment resistance is calculated considering the normal forces of the layers at the equilibrium state.

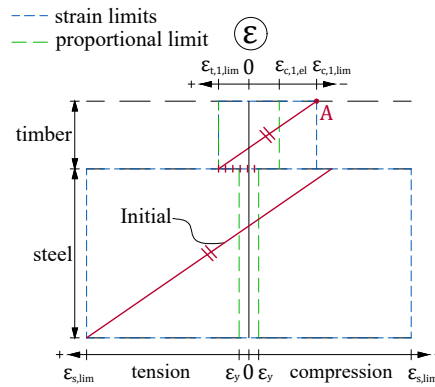


Figure A.10: Example of a strain distribution in the timber slab linked to point A and an initial strain distribution in the steel beam.

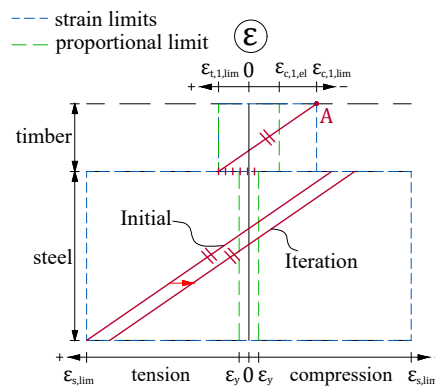


Figure A.11: Example of a strain distribution in the timber slab linked to point A and a strain distribution in the steel beam at an iteration step.